UNIVERSIDADE FEDERAL DO PARÁ
INSTITUTO DE GEOCIÊNCIAS
PROGRAMA DE PÓS-GRADUAÇÃO EM GEOLOGIA E GEOQUÍMICA

TESE DE DOUTORADO Nº 143

PALEOAMBIENTE E PALEOCLIMA DA FORMAÇÃO PEDRA DE FOGO DA BACIA DO PARNAÍBA E SUA CORRELAÇÃO COM OS EVENTOS GLOBAIS DE SILICIFICAÇÃO DO PERMIANO

Tese apresentada por:

LUIZ SATURNINO ANDRADE
Orientador: Prof. Dr. Afonso César Rodrigues Nogueira (UFPA)

BELÉM- PARÁ
2019

Dados Internacionais de Catalogação na Publicação (CIP) de acordo com ISBD
Sistema de Bibliotecas da Universidade Federal do Pará

Gerada automaticamente pelo módulo Ficat, mediante os dados fornecidos pelo(a) autor(a)

A553p Andrade, Luiz Saturnino de Andrade

Paleoambiente e paleoclima da Formação Pedra de Fogo da Bacia do Parnaíba e sua correlação com os eventos globais de silicificação do Permiano / Luiz Saturnino de Andrade. — 2019.

xxv, 176 f. : il. color.

Orientador(a): Prof. Dr. Afonso César Rodrigues Nogueira Nogueira

Tese (Doutorado) – Programa de Pós-Graduação em Geologia e Geoquímica, Instituto de Geociências, Universidade Federal do Pará, Belém, 2019.

1. Rochas Sedimentares. 2. Geologia estratigráfica - Permiano. 3. Paleoclima - Silicificação. 4. Bacia Sedimentares. 5. Pangea (Supercontinente). I. Título.

CDD 552.50981

UNIVERSIDADE FEDERAL DO PARÁ
PROGRAMA DE PÓS-GRADUAÇÃO EM GEOLOGIA E GEOQUÍMICA
TESE APROVADA COM DISTINÇÃO
Instituto de Geociências

Universidade Federal do Pará
Instituto de Geociências
Programa de Pós-Graduação em Geologia e Geoquímica

PALEOAMBIENTE E PALEOCLIMA DA FORMAÇÃO PEDRA DE FOGO DA BACIA DO PARNAÍBA E SUA CORRELAÇÃO COM OS EVENTOS GLOBAIS DE SILICIFICAÇÃO

TESE APRESENTADA POR:

LUIZ SATURNINO DE ANDRADE

Como requisito parcial à obtenção do Grau de Doutor na Área de GEOLOGIA, Linha de Pesquisa ANÁLISE DE BACIAS SEDIMENTARES

Data de Aprovação: 02 / 09 / 2019

Banca Examinadora:

Prof. Dr. Afonso César Rodrigues Nogueira
(Orientador - UFPA)

Profª. Drª Ana Maria Goes
(Membro - USP)

Prof. Dr. Gelson Luis Fambrini
(Membro - UFPE)

Prof. Dr. José Bandeira Cavalcante da Silva Júnior
(Membro – UFPA)

Prof. Dr. Werner Truckenbrodt
(Membro - UFPA)

Aos meus pais

AGRADECIMENTOS

Ao Programa de Pós-Graduação do Instituto de Geociências e Universidade Federal do Pará (UFPA) pela infraestrutura disponível e apoio financeiro.

À Coordenação de Aperfeiçoamento de Pessoal de Nível Superior (CAPES, código de financiamento 001), e Conselho Nacional de Pesquisa (CNPq no.141968/2016-8) pela concessão da bolsa de doutorado.

Ao meu orientador, Prof. Dr. Afonso César Rodrigues Nogueira, por sua amizade, oportunidades, confiança, paciência, apoio e incentivo, principalmente nos momentos finais para a entrega desta Tese. Agradeço também pelas discussões, questionamentos e ensinamentos científicos ao longo de todos esses anos de amizade. Muito obrigado por tudo.

Ao Laboratório de Caracterização Mineral (LCM) Setor Raios-X nas pessoas da Profª Drª Simone Paz, Andréia Oliveira e Bruna Gomes, pela disposição e auxílio nas análises de Fluorescência de Raios-X.

Ao técnico do Laboratório de Difração de Raios-X (DRX) do Instituto de Geociências da Universidade Federal do Pará, Aldemir Sotero, pela disponibilidade e auxílio nas análises e interpretações dos resultados.

Ao Laboratório de Microanálises do Instituto de Geociências da Universidade Federal do Pará, nas pessoas do Prof. Dr. Cláudio Nery Lamarão, Msc. Gisele Tavares Marques, e a Ana Paula Corrêa pela disposição, gentileza e auxílio na obtenção de imagens no Microscópio Eletrônico de Varredura (MEV).

Ao Laboratório de Catodoluminescência do PPGG-UFPA, na pessoa do Dr. Hudson Santos pela disponibilidade e auxílio na obtenção e interpretação das imagens de catodoluminescência.

Ao técnico do Laboratório de Sedimentologia do Instituto de Geociências da Universidade Federal do Pará, Everaldo Cunha, pelo seu auxílio e disposição no tratamento das amostras.

À Joelma Lobo e Bruno Veras, do Laboratório de Laminação do Instituto de Geociências da Universidade Federal do Pará, pela confecção das lâminas delgadas e polidas. Incansáveis, simpáticos e atenciosos em todas as vezes que os procurei.

Aos colegas do Grupo de Sedimentologia da UFPA (GSED): Dr. Hudson Santos, Dr. Pedro Augusto, Msc. (quase doutor) Cleber Rabelo, aos mestrandos e doutorandos Renato Sol, Renan Fernandes, Walmir Lima, Lucas Cunha, Ivan Romero, Alexandre Ribeiro e Msc. Mateus Xavier, pela amizade, críticas, sugestões e trocas de conhecimento durante esses anos de aprendizado.

Aos amigos Profª Drª Kamilla Borges, Msc. Franco Felipe, Dr. Francisco Abrantes Jr., doutorando (USP) John Afonso, e Dr. Isaac Salém, pelas discussões geológicas e momentos de descontração.

Ao Prof. Dr. José Bandeira Cavalcante (JB), pela amizade, discussões científicas, simpatia e muita boa vontade em me ajudar sempre.

À Profª Drª Andressa Nogueira, pela amizade e atenção recebida.

Aos professores Dr. Joelson Soares, Dr. Arnaldo de Queiroz, Dr. Vladimir Távora, Msc. Vânia Barriga, Drª. Rosemery Nascimento, Dr. Maurício Borges, pela amizade e atenção.

Ao Prof. Dr. “Ícone da Geologia do Brasil” Roberto Vizeu, pela amizade, companheirismo, ensinamentos, e principalmente, pelos grandes momentos de relaxamento durante os exercícios (TORA-TORA) em “nosso circuito particular”, livres da algazarra urbana. Uma grande amizade que levarei por toda a vida.

Ao Prof. Dr. Fábio Fernandes, pela grande amizade, e pelos momentos de brutalidade nos treinos de corrida.

Ao Dr. Guilherme Raffaeli, pela amizade, discussões científicas e revisão crítica de um dos artigos com importantes recomendações para a melhoria do trabalho.

Ao Dr. Cléber Calça, pela elaboração das lâminas de microbialitos, discussões e sua valiosa interpretação.

Ao Prof. Dr. Juan Carlos Cisneros, da Universidade Federal do Piauí, por sua importante ajuda na realização dos campos, e obtenção das amostras do sílex Pedra de Fogo.

Ao Prof. Dr. Roberto Iannuzzi, da Universidade Federal do Rio Grande do Sul, pelas discussões sobre as particularidades da paleoflora permiana.

À Doutoranda (UFRGS) Domingas Maria da Conceição, pelas discussões sobre a paleoflora permiana.

Às Secretárias Cleida Freitas e Joanicy Lopes, pela gentileza, atenção e simpatia.

À mestranda Beatriz Oliveira pelo essencial auxílio na tradução de um dos artigos, e também pelas deliciosas trufas.

Aos amigos Afonso Quaresma, Ivaldo Belém, Afonso Ferreira, Francisco Nascimento (Naná), Nazareno, Walter Pinheiro (Waltinho), Lourivaldo Costa (Hulk) pela amizade.

À amiga de longa data, doutoranda Vanisse Rodrigues, pela amizade e momentos de descontração.

Agradeço especialmente à amiga mestranda Amanda Suany, pela amizade, atenção, gentileza, questionamentos filosóficos, e especialmente, por seu essencial esforço e dedicação na formatação desta Tese. Sua ajuda foi importantíssima. Muitíssimo obrigado.

Agradeço especialmente à minha esposa doutoranda Renata Veras, que sempre esteve ao meu lado, apoiando com palavras de incentivo, amor, carinho, atenção e paciência, principalmente nos muitos momentos de estresse e tensão, durante as várias madrugas despertas para o fechamento desta Tese. Obrigado pela elaboração dos mapas e da minuciosa formatação desta Tese. Jamais teria conseguido sem a sua incansável ajuda. Muitíssimo obrigado. Te amo!

Aos meus pais, por seus esforços na minha criação e educação, pelos valores passados e ensinamentos transmitidos. Nunca tiveram as oportunidades que eu tenho, mas sempre se mantiveram ao meu lado, independente da distância e dos muitos momentos de ausência ao longo desses anos de dedicação a Geologia. O amor que sinto por vocês é indescritível. Aos meus irmãos pela atenção, respeito e carinho.

Enfim, a todas as pessoas que direta ou indiretamente, contribuíram de alguma forma para a realização deste estudo.

Tudo tem suas maravilhas,
até mesmo a escuridão e o silêncio...
e eu aprendi que em qualquer estado que esteja,
estarei contente"

(Helen Keller)

RESUMO

A Formação Pedra de Fogo da Bacia do Parnaíba, localizada no Nordeste do Brasil, constitui uma unidade sedimentar que possui um dos mais importantes registros sedimentares do início do Permiano (Cisuraliano), caracterizada principalmente por intensa silicificação. Embora muitos trabalhos tenham contribuído para o entendimento do paleoambiente desta unidade, importantes lacunas quanto às condições sedimentológicas e paleoclimáticas que favoreceram a grande concentração e preservação da sílica, mediante as mudanças globais ocorridas no início e ao longo do Permiano, ainda permanecem inconclusivas. Apesar de notório que as fontes de sílica contribuíram para o expressivo conteúdo de *chert*, estas nunca foram satisfatoriamente explicadas. Não se tem referências sobre as origens orgânica e/ou inorgânica, bem como, pouco se sabe a respeito das condições e processos que conduziram à preservação dos depósitos e concreções silicosas, bem como a gênese da conhecida ocorrência de carbonatos. No intuito de preencher estas lacunas, e/ou contribuir para o melhor entendimento dos processos deposicionais na Formação Pedra de Fogo. Este estudo fez análises de fácies e estratigrafia, e petrografia, complementadas por imagens de catodoluminescência, análise de DRX e MEV-EDS nos depósitos permianos expostos nas porções leste, sul e oeste da Bacia do Parnaíba. As principais fácies sedimentares foram agrupadas em associações de fácies representativas de um sistema fluvial entrelaçado e eólico, posicionados no topo da Formação Piauí (Carbonífero). Esses depósitos são sobreposto por um sistema lacustre-s*abkha* da Formação Pedra de Fogo, dominado por ondas de tempestades, e alimentado por uma rede de fluviais efêmeros. De uma forma geral, a Formação Pedra de Fogo representa um sistema lacustre de clima árido, endorréico, frequentemente afetado por regimes de tempestades e alimentado por fluviais efêmeros, na sua maioria não-canalizados. Embora caracteristicamente de clima árido, este sistema mantinha, pelo menos sazonalmente, teores relativamente elevados de umidade suficiente para manutenção e proliferação de sua pujante tafoflora, formada principalmente por samambaias e gimnospermas. Essa flora colonizava as margens desses lagos, tanto nos períodos relativamente úmidos, quanto nos períodos relativamente secos, como forma de compensar a reduzida umidade do macroambiente. As variações entre o posicionamento estratigráfico dos registros de estruturas organossedimentares (tapetes microbianos e estromatólitos estratiformes) e caules de gimnospermas em posição de vida, foram interpretadas como variações recorrentes da linha de costa lacustre, em resposta as fases de expansão e contração desses lagos, desencadeadas por sazonalidades climáticas que prevalecia na porção ocidental sul do Pangeia.

Provavelmente, a flora da Formação Pedra de Fogo constituiu importante catalizador da expressiva silicificação que caracteriza esta unidade. Esta silicificação é predominantemente sindeposicional/eodiagenética, formada amplamente por microquartzo, sob condições de supersaturação em sílica suficientemente alta para preservar delicados filamentos de cianobactérias, bem como pínulas de samambaias e caules de gimnospermas em posição de vida. A oclusão de fraturas e vazios de dissolução (poros secundários) por mosaico de cristais de megaquartzo, esferulitos de calcedônia e duas gerações de calcedônia fibrosa (*chalcedonic overlay*), além de grandes cristais (mm) em drusa de calcita espática, são indicativos de silicificação policíclica e posterior circulação de fluidos carbonáticos até zonas mesogenéticas. A presença da microtextura *gridwork*, indica que a gêneses da silicificação é similar ao chert-tipo Magadi (*Rift Valley* no Quênia), porém de fontes distintas, dada a inexistência, pelo menos até o momento, de fontes vulcânicas associadas aos depósitos do Pedra de Fogo.

Palavras-chave: Permiano. Paleoclima. Silicificação. Lacustre. Sabkha

ABSTRACT

The Pedra de Fogo Formation of the Parnaíba Basin, Northern Brasil is a sedimentary unit that has one of the most important sedimentary records of the early Permian (Cisuralian), characterized mainly by intense silicification. Although previous works have contributed to the understanding of its paleoenvironment, important gaps regarding the sedimentary and paleoclimatic conditions that favored the great concentration and preservation of silica, due to the global changes occurred at the beginning and along of the Permian, still remain inconclusive. Problems as to which sources of silica contributed most to the expressive chert content were never satisfactorily explained. There is no reference to the organic and/or inorganic origins, nor is little known about the conditions and processes that led to the preservation of silica deposits and concretions, as well as the genesis of the known occurrence of carbonates. In order to fill these gaps and/or contribute to a better understanding of the depositional processes in the Pedra de Fogo Formation. This study made facies and stratigraphic analysis, and petrography, complemented by cathodoluminescence image, XRD and SEM-EDS analysis of the permian deposits exposed in the east and southeast portions of the Parnaíba Basin. The main sedimentary facies were grouped into facies associations representative of braided fluvial-aeolian systems from the top Piauí Formation (Carboniferous). This deposits are overlain by lacustrine-sabkha system, wave-dominated nearshore-lacustrine and ephemeral streamsdeposits of the Permian Pedra de Fogo Formation. In general, this unit was deposited in an arid, endorheic lacustrine system, often affected by storm regimes and fed by unconfined flows. Although the arid climate was predominant, this system keeps seasonally, relatively high levels of moisture sufficient to maintain and proliferate its thriving taphoflora, formed mainly by Ferns and Gymnosperms tree. This flora colonized the lakeshore, both in relatively wet and dry periods, as a way to compensate for the low humidity in macroenvironmental. Cyclic variations between the records of organosedimentary structures (microbial mats and stratiform stromatolites) and gymnosperm stem in life position were interpreted as the recurrent migration of the lacustrine shoreline, in response to the expansion and contraction phases of these lakes, triggered by climatic seasonality in the southwestern portion of Pangea. Probably, the flora of the Pedra de Fogo Formation was an important catalyst for the expressive silicification that characterizes this predominantly syndepositional / eodiagenetic unit. This silicification is formed largely by microquartz, under conditions of supersaturation in silica, high enough to preserve the

delicate cyanobacteria filaments, as well as pinnules ferns and gymnosperm stems in life position. The occlusion of fractures and dissolution voids (secondary pores), by mosaic megaquartz mosaic, chalcedony spherulites and two generations of chalcedonic overlays, in addition to large crystals (mm) in coarse mosaic calcspar are indicative of polycyclic silicification and circulation of carbonate fluids to mesogenetic zones. The presence of gridwork microtexture indicates that the genesis of silicification is similar to the Magadi chert-type (Rift Valley of Kenya), but from distinct sources, given the absence of volcanic sources associated with Pedra de Fogo deposits.

Key words: Permian. Paleoclimate. Silicification. Lacustrine. Sabkha

LISTA DE ILUSTRAÇÕES

CAPÍTULO 1

Figura 1- Mapa do norte da América do Sul mostrando a localização da Bacia do Parnaíba. A) Mapa da Bacia do Parnaiba. B) Mapa geológico simplificado da região estudada, mostrado a distribuição das principais unidades geológicas.....7

Figura 2-Carta estratigráfica da Bacia do Parnaíba com a disposição cronoestratigráfica das cinco sequências deposicionais. Este trabalho irá investigar a Formação Pedra de Fogo, dentro do contexto da Sequência Neocarbonífera-Eotriássica. Fonte: Modificado de (Vaz *et al*. 2007).....9

CAPÍTULO 4

Figura 1-Mapa geológico e de localização da área de estudo. A) Mapa geológico simplificado da Bacia do Parnaíba. O retângulo preto indica a posição da área de estudo. Fonte: Modificado de (Schobbenhaus *et al*. 1984). B) Disposição espacial das principais unidades geológicas presentes na área de estudo, com destaque para as formações Piauí e Pedra de Fogo.....18

Figura 2- Coluna estratigráfica das principais unidades sedimentares aflorantes ao longo da sucessão estudada nas bordas leste, sul e oeste da Bacia do Parnaíba. Destaque para a Formação Pedra de Fogo.....23

Figura 3-Figura 5-Perfis litoestratigráficos da sucessão estudada. Os depósitos da Formação Pedra de Fogo representam múltiplos ciclos formados pela intercalação entre camadas de arenito com geometria tabular/em lençol de fluviais efêmeros na sua maior parte não-confinados com pelitos pouco espessos do lacustre raso-sabkha. Note que tanto a frequência de eventos de rápida inundação (FC/FN) bem como eventos de tempestades (LT) são frequentes na parte inferior da sucessão, e tendem a se extinguir o reduzir para o todo. A parte superior consiste basicamente de pacotes mais espessos de pelito da porção central do sistema lacustre intercalados com delgadas camadas de arenito muito fino das porções distais dos eventos de inundação. O quadro no canto superior esquerdo da figura posiciona de forma aproximada cada perfil em suas unidades sedimentares correspondentes.....25

Figura 4- Característica geral da AF1. A-B) Delgadas camadas tabulares de arenito fino maciço (Aom) intercalada com pelito (fácies Pm) avermelhado igualmente maciço. Parte inferior da Formação Pedra de Fogo em contato com a Formação Piauí. "afloramento Morro da Pandora", região de Duque Bacelar-MA.....28

Figura 5- Característica geral da AF1 com camadas disposta em padrão *flat-lying*. A) Intercalação arenito muito fino (Aom)/pelito (fácies Pm/Pwl) com 32 ciclos centimétricos. B-B') Geometria fortemente tabular da fácies Aom. C-C') Detalhe dos ciclos Aom/Pm/Pwl. Notar a base plana da fácies Aom. D) Detalhe da fácies Pm/Pwl com acamamento *wave-linsen*. E) Lateralmente podem ocorrer laminações cruzadas (tracejado preto). F-F') Arenito com estratificação cruzada sigmoidal (As). Afloramento as margens da BR-153 em Frente a Santo Antônio, próximo a Colinas do Tocantins-TO.....29

Figura 6- Característica geral da AF1. A) Ciclos gronodecrescentes ascendentes decimétricos (setas na porção esquerda superior da foto), formados por camadas tabulares (*flat-lying*) de arenitos fino a médio intercalados (fácies Aom e Aa) por pelitos da fácies Pm. B-B') Arenito fino a médio com estratificação cruzada acanalada (fácies Aa). C-C') Níveis de clastos de quartzo na base em padrão gronocrescente ascendente. D-E) Escamas fósseis de peixes desarticulados (espécie não-identificada) ocorre na base da fácies Pm. Afloramento no leito do riacho Pedra de Fogo, região de Nova Iorque-Pastos Bons-MA. F) Segundo nível de gretas de dissecação associada. Diferencia-se do primeiro nível pela ausência de evaporitos, e as dimensões centimétricas dos polígonos. H, G) Primeiro nível de gretas de dissecação com nódulos evaporíticos entre os polígonos. Observar as dimensões decimetricas dos polígonos.....30

Figura 7- Característica geral da AF1. A-B) Fácies Cm com seixos de quartzo, eventualmente *cherts*. C-D) Caules de samambaia silicificados. A, B, C) Afloramento próximo a Bielândia-TO. D) Afloramento na MA-034 próximo a Duque Bacelar-MA..... 32

Figura 8- Gretas de dissecação e estruturas *tepees* ocorrem comumente na AF1. A) Gretas decimétrica associadas à fácies Pm. Nódulos evaporíticos ocorrem nos polígonos. B) Gretas associadas ao pelito/arenito muito fino, maciço. Os polígonos são marcados por relevos negativos. C-D) Gretas decimétricas com polígonos em relevo positivo. Cimento carbonático ocorre nos polígonos. E) Estrutura *tepees* centimétrica marcada por clastos silicificados tabulares arqueados. F) Estrutura *tepees* decimétrica marcada pelo arqueamento das camadas de arenito fino. Canalizações se desenvolvem associadas a estes *tepees.* A, B) Afloramento próximo a Monsenhor Gil-PI. C-E) Afloramento próximo a Bielândia-TO. F) Afloramento na rodovia estadual PI-130, próximo a Palmeirais-PI.....33

Figura 9-Caules silicificados de Gimnospermas e Samambaias da AF1. A-B) Caules silicificados de Gimnospermas em posição de vida. C-F) Caules de gimnospermas rolados. D) Observar o alargamento em uma das extremidades do tronco adernado (setas amarelas), indicativo de sua base. G) Caules de gimnosperma semi-adernado (setas amarelas). H) Caules silicificados de Samambaias. Observar a estruturação interna preservada, núcleo e casa. A-F) Afloramentos na região de Duque Bacelar-MA. G) Afloramento no Parque Floresta Fóssil, margem direita do rio Poti, Teresina-PI.....34

Figura 10- Fotomicrografias do quartzo arenito representativo da AF2. A-B) Aspecto geral do arcabouço formado predominantemente por grãos de quartzo monocristalinos (Qm) e grãos detríticos de chert (Ch-seta amarela). Grãos mal a moderadamente selecionados, muito angulosos a subarredondados, esfericidade alta. Predomínio da granulometria entre areia fina e média, esporadicamente areia grossa. Observar o predomínio de contatos restos (setas vermelhas), e secundariamente côncavo-convexos (setas brancas). C) Grão detrítico de chert. O aspecto fibroso (seta amarela) indica provavelmente calcedônia. D) Muscovita parcialmente rompida pelo efeito da compactação mecânica (setas amarelas). E-F) Grãos de quartzo monocristalino (Qm), com fraca extinção ondulante (seta vermelha). Observar os aspectos morfológicos dos grãos desde muito angulosos (seta branca), com formas irregulares (tracejado amarelo) e esfericidade baixa, até muito arredondados (seta azul). Comumente os grãos de quartzo apresentam bordas profundamente corroídas (setas amarelas). G) Pseudomatriz (Pm) na forma de grãos de argila esmagados (setas amarelas). H) Imagem de MEV (elétrons secundários) mostrando grão de quartzo em contato concâvo-convexo com provável grão detrítico de feldspato (Fk), alterando para caulinita (K) (retângulo amarelo). I) Imagem de MEV (elétrons secundários) mostrando cristais pseudohexagonais de caulinita arranjados sob forma de livretos.....37

Figura 11- Depósitos representativos da AF2. A ocorrência de estratificação cruzada hummocky é relativamente comum na AF2. A-A') Estratificação cruzada *hummocky* anisotrópica mostrando uma nítida simetria entre a superfície basal escavada e um bem definido antiforme ou *hummock*, truncando laminações internas características dessas estruturas. B-B') Estratificação cruzada *hummocky* com suave superfície de escavação truncada lateralmente por superfície antiforme. C-C') Estratificação cruzada *hummocky* isotrópica (seta). D-D') Estratificação cruzada *hummocky* mostrando suavizado antiforme excepcionalmente claro (centro) truncando lateralmente pronunciada superfície de escavação.....38

Figura 12- Seção mostrando o aspecto geral da Associação AF3 – Lacustre central recobrindo a Associação AF1. Notar as espessas camadas de pelito avermelhado e maciço, intercalados com delgadas camadas tabulares de arenito muito fino. Afloramento no km 39 da rodovia TO-222, próximo ao município de Araguaína-TO.....40

Figura 13-Seção estratigráfica simplificada da sucessão sedimentar da Formação Pedra de Fogo, que recobre discordantemente os arenitos Fúlvio-eólicos da Formação Piauí ao longo das bordas leste, sul e oeste da Bacia do Parnaíba.....42

CAPÍTULO 5

Figure 1- Lithostratigraphic chart of the Pedra de Fogo Formation, showing its comparative chronostratigraphic differences by different works. Also note the paleoenvironmental and lithological diversification of this unit. Detailed explanations are in the text…...59

Figure 2-Simplified geologic map of the Parnaíba Basin in Northern Brazil and geographic distribution of the Permian Pedra de Fogo Formation in the eastern portion of the basin (Modified from Góes 1995).....60

Figure 3- Lithostratigraphic section of the studied areas in the regions of Coelho Neto, Duque Bacelar and Nova Iorque in the state of Maranhão, and Teresina and Altos in the state of Piauí (see the location of this section in Figure 2). The frame in the upper right corner shows the profiles according to their current dimensions. The vertical exaggeration between the profiles, especially between 5 and 6, is due to the out-of-scale horizontal distance.....62

Figure 4- A) Overview of FA1 association in the region of Coelho Neto-MA. Note the irregularity in the basal parts of the chert layers (black arrows). B, C) Detail of the strong irregularity of the lower part of the chert levels. Although layers of massive chert predominate, nodular chert occurs frequently throughout the section. D) Coalesced nodules "sunk" in the mudrock. E) Chert nodules aligned (arrows), with oblate spheroid shapes with main axis consistent with the bedding. Dimension of main axis (horizontal) varies between 14 and 25 cm. Layer thickness ranges between 6-15 cm.....66

Figure 5- Registered occurrences at the basis of the studied succession. A, B) Intraformational Chert "Breccia" with oblate clasts up to 4 cm long on its largest axis. C) Silicified trunk of gymnosperm in life position. Arrows indicate circular features within the trunks associated with the growth rings. D) Gymnosperm rolled trunk. Although listed, these fossils are "autochthonous" because they have not been under significant transportation, only rolled from the hillsides as a result of the current erosion (Duque Bacelar / Coelho Neto-MA region). E) Partially reconstituted (dashed) fern wood (Nova Iorque-MA region)…….....67

Figure 6- A, B) Columnar-laminated microbialitic complex with sub-millimeter bimodal lamination alternating between a thicker light colored lamination and a thinner dark lamination. The lower portion (a) has stratiform lamination, moderately convex with high laminar inheritance and dome synoptic relief. In the middle portion (b) there are cylindrical columnar microbialites with vertical growth vector, contiguous structures and asymmetric parabolic lamination with high degree of laminar inheritance. The top (c) columnar portion branches (arrows) with horizontal beta-like shape that maintain the same characteristics as the median portion.....71

Figure 7- General aspect of the FA2 association (Nearshore wave and storm dominated). A-D) Very fine sandstone/siltstone with horizontal lamination (Shl) and wave-formed ripples (Sw). Arrows indicate micro-hummocky surfaces. E) Two generations of symmetrical wavy ripples (Sw) in plan view. 1-ripples with a rounded shape and weakly sinuous 3D crest and tuning fork bifurcations. Note that the ripple lee-side slope is directed towards SSE. Oscillatory flow direction is N010°. 2-ripples with a rounded shape. Note that the ripple lee-side slope is directed towards ESE. First generation of wavy ripple in profile view. Note the symmetric and rounded shape. C, D) pocket knife measures 9 cm. E, F) pencil measures 15 cm.....72

Figure 8-Fine Sandstone hummocky cross-stratification (Shs facies). The circle shows the low dip angle of the lenses (~ 11º), the arrows indicate the aggradation part of the structure or hummock.....73

Figure 9- Architectural elements and facies observed for the Terminal Splays deposit (FA3). According to the geometry of the elements, they were grouped into four representative distinct types of; G1-distal sheet-splay geometry; G2-intermediatery steady splay-geometry; G3-Amalgamated complexes splays geometry; and G4-Proximal channel-fill splay geometry. 76

Figure 10- Overview of the FA3 association. A) Tabular layer of fine to coarse massive sandstone (Sm facies) with tabular geometry with silicified wood. Fine sandstone lenses (lower dotted), equally massive inside the sandstone with wave-formed ripples (Sw facies). B) Detail of silicified fern stem (sfs) (~ 60 cm long) strongly amalgamated because of compaction. Chert detrital nodules (Chn) (arrows). C, D) Thin, massive sandstone layer about 30 cm thick, flat top and bottom, with no apparent variation in grain size. Chert fragments about 5 cm in diameter occur at the contact between the Sm and Mm facies (black arrows).....77

Figure 11- Overview of the FA4 Association. A, B) Tabular cross-stratified sandstone with tangential base (St) and thinning-upward of the sets, containing horizontal stratification (Sh). C, D) Fine to medium sandstone with horizontal stratification (Sh). E, F) Tabular cross-stratification sets (St), sectioned by levels with sandstone supercritically climbing ripples cross-lamination (Scs). Arrows indicate reactivation surfaces.....79

Figure 12- Occurrences distribution of fossil woods in the Pedra de Fogo Formation. 1, 2, 3, 4, 5) In this study; 1) Conceição *et al*. (2016); 2) Caldas *et al.* (1989); 5) Iannuzzi & Langer (2014); 6) Röβler & Galtier (2002a, 2002b, 2003). 83

Figure 13- Suggested climate regime for the Pedra de Fogo Formation based on the found facies associations, modified from Cecil (1990)…….....…...85

Figure 14- Paleoenvironmental model for the studied succession. Under a climate seasonality regime, the “Pedra de Fogo Lacustrine System” (SLPF) had periodic fluctuations in its level, with consequent expansion and contraction of its margins, in response to climatic conditions: wetter (A) and more arid (B), respectively. Similarly, taphoflora was suppressed in the driest periods (B), and proliferated in the wettest periods (A), where the greater frequency and intensity of flash flood events reactivated ephemeral fluvial systems that supplied these lake basins. In the upper right corner, the red square places the SLPF in the paleogeographic and paleoclimatic context of the Early Permian. Paleogeographic map modified from Warren (2017)…….....86

CAPÍTULO 6

Figure 1-Simplified map of the Parnaíba Basin in Northern Brazil and geographic distribution of the Permian Pedra de Fogo Formation in the eastern portion of the basin (Modified from Góes 1995).....104

Figure 2-Stratigraphic logs representative of the Permian chert-bearing succession of the Parnaíba Basin. The contact between FA1 and FA2 is interpreted as a regional unconformity (Supersuface-Ss). See local sites in figure 1……..…….....108

Figure 3-Faciological aspects of PF-chert succession in the Parnaiba Basin. A) Panoramic section of outcrop near of Amarantes region, showing in the base the aeolian dune field deposits of Piauí Formation (AF1) overlaid by centimetric- to decimetric-scale cycles of mudstone interbedded with sandstone of the Pedra de Fogo Formation (AF2) forming a flat-lying geometry. B) Aspects of the flat contact (Ss) between AF1 and AF2. C) Tangential cross-stratification sets separated by layers with adhesion ripple lamination (adl); yellow dashed lines indicate reactivation surfaces, and black dashed indicate foresets. D) and E) Foresets with asymptotic base and frequent reactivation surfaces (yellow dashed). F) Cross-strata in plan-view exhibiting ‘zigzag’ pattern. G) Grainflow laminae in cross-lamination (arrows). H) and H’) Compound cross-strata overlain by even parallel stratified sandstone with thinning upward tendency. I) General aspect of massive/bioturbated mudstone (facies Mb) layer inside in the interdune deposits. J) Plan view of bioturbation (bt-black arrows) of the facies Mb attributable to the Scoyenia *ichnofacies*. K, L) Evaporitic adhesion (Eas) and adhesion warts (Aw) features (black arrows). Note the typical dome-shaped (red arrows) microtopography, characteristic from evaporitic-adhesion structures.....111

Figure 4- The shallow lacustrine-sabkha deposits exposed in the upper portion of the outcrop near of Amarantes region, the eastern Parnaiba Basin. A) An interpretative drawing showing the general arrangement in flat-lying beds constituted by centimeter-scale cycles of mudstone and sandstone with chert nodules and layers (black color) concentrated in the base and top of the outcrop marked also by convolute bedding. B) General view of the sheet-like cycle geometry. C, D) Very fine-grained sandstone with wavy bedding. E) Subcritical and supercritical climbing-ripple cross lamination; white arrows and dashed lines indicate the crest line; red and yellow lines mark respectively, the stoss-side and lee-side laminae; the continuous and undulated white lines in the uppermost part mark predominance of supercritically climbing ripples. F) Hummocky cross-lamination (yellow arrows). G) Truncated lamination of hummock (yellow arrows) and swale (white arrows) morphology. H) Small-scale shallow channels on the collapsed tepee (T/c). I) irregular silicified evaporitic nodules interbedded with chert beds. J) Wavy bedding with small-scale folds and flame structures in sandstone and chert beds considered as an evaporitic pseudomorph. K) Centimetric desiccation cracks (white arrows). L) Convolute lamination. M) Rip-up mud clasts (black arrows). The location of figures B-M is indicated in the section shown in A…….. 115

Figure 5- General view showing the stratiform PF-cherts in outcrops near to Coelho Netro and Duque Bacelar towns, the eastern Parnaiba Basin. A) Cherts layers (Ch) forming massive bodies and nodules interbedded in massive mudstone (Md). B) Contorted bed of chert. C) Nodular internal features in chert (black arrows). D) Chert oblate spheroid with its major axis lying on the bedding plane (“cucumber” shape). Nodular chert in high relief on the outcrop, due its resistance to the weathering in comparision with the host mudstone. D) and E) Isolated nodule ranging up to 25 cm in size. G) Chert layer showing breccia-like texture. H) Tabular chert fragments under microscope constituted of microquartz and are cemented also by microquartz. 119

Figure 6- Geometry, textural aspects and features in PF-chert. A) and B) The laterally continuous chert layers locally interrupted and with irregular and undulated (deformed) bed limits. C) and D) Breccia with chert fragments with a fitting aspect inserted in a siliciclastic matrix displaying deformed lamination. E) and F) Thin chert laminae interbedded with siltstone with undulated lamination and ball-and pillow structure.....120

Figure 7- Microbial mats from the Pedra de Fogo Formation. A, B) Centimetre-thick beds of chert with microbial laminites. C, D) Photomicrographs showing putative morphology colony of unicellular and filamentous of microbial communities (arrows)…… 122

Figure 8- Petrified fossil plants from the Pedra de Fogo Formation. A, B) Gymnosperm silicified woods in life-position. B) Black arrows indicate growth ring-like structures. C) Gymnosperm silicified trunks showing flattened to elliptical form axes indicative of compaction by burial. D) Fern silicified pinnules *Buritiranopteris costata*; E) Detail from silicified pinnules partially cover trunk fragment (black arrows), indicate a very fast sin-depositional/early diagenetic silicification process. F) Detail of two ferns silicified fóssil from family *Psaroniaceae*, with well preserved internal structures (*Psaronius sp.* on the left and *Tietea singularis sp.* on the right)…….. 123

Figure 9-Composition of PF-chert. A) X-ray diffractograms from PF-cherts showing the high intensity of quartz peaks, indicative from well-crystallized quartz. B) EDS spectra demonstrating the Si-rich composition typical of PF-chert. 125

Figure 10- Photomicrographs comparing two groundmass textures in chert between crossed polarizers with gypsum plate inserted. A) Groundmass chert with randomly oriented quartz crystals with "pinpoint" extinction. B) Groundmass chert displaying a reticular or gridwork extinction pattern. Note the alignment of blue and yellow stringers parallel to diagonal white arrows. C-D) Groundmass displays gridwork extinction formed by the aggregation of minute quartzine spherules. Note the schematic drawing of spherulites (right corner), with a range size up to 30 µm. E, F) Scanning electron photomicrographs of the groundmass showing interlocking of minute quartzine spherules. All photomicrographs are a cross-polarized light. A, B and C are with gypsum plate inserted. 126

Figure 11- Photomicrographs of chicken-wire chert texture. A-D) Microcrystalline quartz groundmass mimics the chicken-wire appearance of anhydrite nodules. Note some remaining cavities occluded by mosaic quartz (yellow arrows). All photomicrographs are a cross-polarized light. 127

Figure 12- Photomicrographs of length-slow chalcedony and megaquartz growing into internal voids. A) Aggregates of spherulitic chalcedony (sch) that subtend angles of 90° or more; some of the aggregates in center of void subtend a full 360°. Note development of microflamboyant quartz (mfq) inside and between spherulites. B) Cavity filled by spherulitic chalcedony (sch), are lined with a chalcedonic overlay (ch1; ch2). C) Spherulites of length-slow quartzine (sch) rimmed by chalcedonic overlays (ch1; ch2). Note the positive optical sign, in consequence of the elongation of the fibers, is parallel to 129

Figure 13-Photomicrographs of filling phases of calcite spar, “chert breccia” and flow structures; crossed polarizers. A) Coarse mosaic calcspar felling cavity. Note a characteristic increasing crystal size away from the substrate towards the cavity center. B) Same field of view under cathodoluminescence image showing growth zones of bladed-prismatic calcite (black arrows). C-D) Rounded large…….....132

Figure 14- Paleoenvironmental and Paleoclimate Evolution of the Late Carboniferous to Permian deposits in the Parnaiba Basin, Western Gondwana. A) Stage 1- the Pennsylvanian desert system dominated by dune fields (Piauí Formation) was a dry setting bordering a narrow epicontinental sea in the center-western Gondwana. B) Stage 2 – the increase of the humidity conditions in this desert allowed a relative water saturation of the water table generating the development of interdune ponds rapidly colonized by organisms. C) Stage 3 - the elevation of e local base level controlled by rising groundwater led the development of deflation horizon or supersurface, culminating in the interruption of the aeolian deposition marking the end of the carboniferous desert (Piauí Formation), and the beginning of the Permian Pedra de Fogo Formation. D) Stage 4. The expressive evaporites precipitation and siliciclastic inflow characterize the definitive implantation of an arid lacustrine and sabkha system of the Permian Pedra de Fogo Formation.....135

Figure 15-Morphology, genesis and diagenetic stages of silica fabrics of PF-chert. Each category is explained more fully in the text. Modified from Wilson (1966).....139

Figure 16-Photomicrographs of groundmass with a gridwork extinction. Cross-polarized light and gypsum plate inserted. A) Groundmass chertdisplaing a mosaic of minute spherulites of length-slow quartzine describe a regular gridwork pattern (white arrows).....145

Figure 17-The paleoenvironmental and paleoclimate evolution of the cyclic sedimentation of the shallow lacustrine-sabkha influenced by expansion and contraction stages, conditioned by climatic seasonality regime during the Early Permian in the Parnaiba Basin, Western Gondwana. A) Under wet climate stage. High local base level rise controlled by groundwater elevation. The high volume of precipitation triggered frequents inundations of the lake by ephemeral streams with development of buoyant plumes. Predominance of physical sedimentary process with waves reworking and siliciclastic preferential deposition. B) Under arid climate stage. Low local base level controlled by groundwater fall. The high evaporation rate leads contraction of lake and increasing salinity. The shrinking of lake expor the lacustrine plain where salts crystallize at the surface as efflorescent crusts. The predominance of chemical process leads to synsedimentary formation of the nodular and anhydrite laminae (perhaps after gypsum?) within mud in a very shallow lacustrine. Still on synsedimentary stage the silica cementation with began with replacement and void filling. The process commences about the margins of a nodule with a volume for volume replacement of anhydrite by microcrystalline quartz. The void filling began with chalcedonic overlays rimmed the vug pororosity, and then continue with the growth of spherulitic chalcedonic. It generally ends with the growth of euhedral drusy megaquartz crystals into a central vug. Eventually fractures are equally occlude by drusy megaquartz. This edge inward evolution of the or nodule fill is typified by a variety of textural styles. This edge inward evolution of the or nodule fill is typified by a variety of silica textural styles as showing in this paper.....148

Figure 18- Circulation of dissolved and solid silica phases in the water systems (Modified from Laschet 1984)…….....150

LISTA DE TABELAS

CAPÍTULO IV

Tabela 1-Sumário dos principais trabalhos realizados na Formação Pedra de Fogo 21
Tabela 2- Principais fácies e processos deposicionais da Formação Pedra de Fogo.....26
Tabela 3-Resumo das associações de fácies e fácies da Formação Pedra de Fogo.....27

CAPÍTULO V

Table 1- Facies and depositional processes of the succession studied on the east-southeast edges of the Parnaíba Basin.....63
Table 2- Facies association of Pedra de Fogo and Piauí Formation, Parnaíba Basin.....65

SUMÁRIO

DEDICATÓRIA.....**iv**
AGRADECIMENTOS.....**v**
EPÍGRAFE.....**vii**
RESUMO.....**viii**
ABSTRACT.....**x**
LISTA DE ILUSTRAÇÕES.....**xii**
LISTA DE TABELAS.....**xxiii**
1 INTRODUÇÃO 1
1.1 APRESENTAÇÃO 1
2 MATERIAIS E MÉTODOS 3
2.1 ANÁLISE DE FÁCIES 3
2.2 ANÁLISE ESTRATIGRÁFICA 3
2.3 CATODOLUMINESCÊNCIA 4
2.4 DRX – DIFRATOMETRIA DE RAIOS-X 4
2.5 MICROSCOSCOPIA ELETRÔNICA DE VARREDURA 5
3 BACIA DO PARNAÍBA, E ARCABOUÇO LITOESTRATIGRÁFICO DO GRUPO BALSAS 6
3.1 BACIA DO PARNAÍBA 6
3.1.1 Aspectos gerais 6
3.1.2 Arcabouço litoestratigráfico 7
3.1.2.1 Sequência Neocarbonífera – Eotriássica (Grupo Balsas) 9
3.1.2.1.1 Formação Piauí *9*
3.1.2.1.2 Formação Pedra de Fogo *9*
3.1.2.2 Formação Motuca 12
3.1.2.2.1 Formação Sambaíba *13*
4 SISTEMA LACUSTRE ÁRIDO DO INÍCIO DO PERMIANO (CISURALIANO): UM REGISTRO NA BACIA DO PARNAÍBA 14
5 THE EVOLUTION OF CISURALIAN DEPOSITS IN THE EASTERN PARNAÍBA BASIN, BRAZIL: UNRAVELLING THE FLOURISHING OF THE EQUATORIAL FOREST IN THE WESTERN GONDWANA 55
FACIES 63
6 THE PERMIAN CONTINENTAL CHERTS FROM THE PARNAIBA BASIN: ORIGIN AND GLOBAL CORRELATION THROUGOUT THE WEST GONDWANA 102

7 CONCLUSÔES E CONSIDERAÇÕES FINAIS 167
REFERÊNCIAS 171

1 INTRODUÇÃO

1.1 APRESENTAÇÃO

O Período Permiano (298 – 251 Ma) é marcado por condições de aquecimento e aridez (Bucout *et al*. 2013, Rees 1999, Rees *et al*. 2002). As colisões continentais iniciadas no Devoniano-Carbonífero resultaram na formação do supercontinente Pangeia no final do Carbonífero e início do Permiano (Blakey 2008). A formação de cinturões montanhosos resultantes dessas colisões entre massas continentais interferiu no regime de circulação dos ventos, e intensificou condições de aridez em quase todo o Pangeia. (Chumakov & Zharkov 2003, Courtillot & Renne 2003, Scotese *et al.* 1999). Soma-se a isto as grandes dimensões do Pangeia, que reduzia e/ou impossibilitava o transporte de significativa umidade para porções interiores deste supercontinente (uma escala ampliada do atual Deserto de Gobi), além de baixos valores do albedo da Terra e flutuações atmosféricas de CO_2. Todos estes fatores condicionaram um progressivo aumento das temperaturas globais durante o Permiano, e foram intensificadas com as volumosas erupções vulcânicas das "Armadilhas Siberianas" resultando nas condições de superaquecimento ou "*Super Hot-House*" no final do Permiano (Scotese *et al*. 1999, Chumakov & Zharkov 2003, Courtillot & Renne 2003).

Condições de extrema aridez em grande parte do interior do Pangeia foram acompanhadas de sucessivas regressões de mares epicontinentais, desaparecimento de áreas com sedimentação glacial e instalação de sistemas desérticos em diversas bacias sedimentares do globo (Zharkov & Chumakov 2001). Um forte regime de sazonalidade climática e a prevalência de eventos de megamonções influenciaram significativamente sistemas sedimentares desenvolvidos no interior do supercontinente Pangeia (Kutzbach & Gallimore 1989, Parrish 1993). A distribuição espacial das precipitações era principalmente controlada pela circulação de monções (Roscher *et al.* 2011). Na região tropical ocidental no sul da América do Norte e norte da América do Sul, os alísios equatoriais (*equatorial easterlies*) mudaram sua direção para os ventos de oeste já no início do Permiano (Tabor & Montañez 2002). Ao lado do equador, chovia durante todo o ano, enquanto mais ao norte e ao sul a precipitação era fortemente sazonal (Roscher *et al.* 2011).

Na Bacia do Parnaíba, esses eventos paleogeográficos e paleoclimáticos são registrados pela sucessão sedimentar do Grupo Balsas, que marca o início da continentalização e progressiva desertificação na bacia. A Formação Pedra de Fogo, relacionada ao início do Permiano (Cisuraliano), parece especialmente registrar as oscilações paleoclimáticas entre os estágios mais úmidos e secos sazonais. A característica ciclicidade e multiplicidade lito-

faciológica é aqui diretamente relacionadas ao regime de sazonalidade climática dominante por todo o Período Permiano.

O principal objetivo desse trabalho é propor as condições paleoclimáticas e paleogeográficas que favoreceram e/ou possibilitaram a grande concentração e preservação da sílica na Formação Pedra de Fogo mediante as oscilações regionais e globais no nível de base ocorridas no Cisuraliano da Bacia do Parnaíba.

O corpo desta tese é constituído por três artigos, sendo dois em inglês submetidos a revistas internacionais, e um em português que está em via de submissão. Além dos artigos, esta tese é constituída por: um capítulo referente à metodologia empregada na construção da tese; um capíulo referente ao levantamento bibliográfico acerca do arcabouço litoestratigráfico do Grupo Balsas; conclusões e as referências bibliográficas utilizadas nestes capítulos.

2 MATERIAIS E MÉTODOS

2.1 ANÁLISE DE FÁCIES

A análise de fácies foi auxiliada por perfis colunares e estratigráficos e seguiu o método proposto por Walker (1992) em afloramentos que envolve: i) o reconhecimento de fácies sedimentares, caracterizando a composição, geometria, texturas, estruturas sedimentares e padrões de paleocorrentes; ii) compreensão dos processos sedimen-tares que geram as determinadas fácies e; iii) fácies cogenéticas e contemporâneas agrupadas em associações de fácies que refletem os diferentes ambientes e subambientes sedimentares.

A descrição de fácies, na escala de afloramentos, foi auxiliada por perfis colunares e seções panorâmicas, estas últimas obtidas por meio de fotomosaicos de afloramentos seguindo o procedimento de Arnot *et al.* (1997). Coletas sistemáticas de amostras em função das diferentes fácies (marinhas e transicionais) auxiliaram na melhor caracterização dos litotipos. As seções delgadas foram avaliadas sob microscópio óptico apenas para a classificação petrográfica dos arenitos conforme Folk (1974) e Pettijohn (1975). A descrição foi composta de: i) descrição dos constituintes de cada rocha: matriz, cimento, aloquímicos e grãos siliciclásticos e os processos diagenéticos para determinar o nome da rocha; ii) impregnação das rochas com epóxi azul, para a visualização e contagem dos tipos de poros, e assim determinar suas origens; iii) contagem de 300 pontos em cada lâmina para a determinação da porcentagem dos constituintes de cada rocha, tipos de contatos e o grau de empacotamento; iv) tingimento com alizarina vermelho-S, para a distinção mineralógica entre calcita e dolomita (Tucker 2001).

2.2 ANÁLISE ESTRATIGRÁFICA

A análise de fácies foi utilizada em conjunto com os conceitos da estratigrafia de sequências (Catuneanu 2006, Schumm 1993, Shanley & McCabe 1993, 1994). Este método favorece a reconstituição dos processos controladores da sedimentação local como o nível de base estratigráfico, através do entendimento das variações do perfil de equilíbrio ao longo da deposição da sucessão, e sua relação com a formação de diferentes componentes tais como: sequências, tratos de sistemas, superfícies de parassequências, tipos de ciclos e os tipos de superfícies limitantes (discordância subaérea, superfícies de ravinamento e superfície transgressiva máxima). A terminologia de “ordens” (i.e. terceira, quarta, quinta) é usada com restrições devido à arbitrariedade dos limites de tempo separando as várias escalas dos ciclos/parassequências e o controle de idade relativamente pobre nas rochas estudadas.

2.3 CATODOLUMINESCÊNCIA

As imagens de catodoluminescência servem como guia indicativo a cerca das diferentes gerações de cimento carbonático. Através deste método pode-se associar a cimentação aos diferentes ambientes diagenéticos (freático, marinho e grau de soterramento), investigar as diferentes gerações de cimento e em quais estágios diagenéticos ocorreu à redução de porosidade carbonática (quando ocorrer), qual tipo de calcita seria o principal agente redutor de porosidade, se ferrosa ou magnesiana e estimar o tempo de cimentação (Fernandes Neto 2010, Flügel 2004, Witkowski *et al.* 2000).

As imagens de Catodoluminescência apresentadas nesta tese foram obtidas utilizando um microscópio óptico Leica, modelo DM 4500 P LED acoplado ao aparelho Optical cathodoluminescence CL 8200 MK5-2.s do Laboratório de Catodoluminescência do Instituto de Geociências (UFPA).

2.4 DRX – DIFRATOMETRIA DE RAIOS-X

A análise por Difração de Raios-x (DRX) possibilitou a identificação de potenciais fases minerais existentes no sílex. Foram analisadas quinze amostras do sílex da Formação Pedra de Fogo, de diferentes pontos da Bacia do Parnaíba, correspondente aos munícipios de: Nova Iorque, Coelho Neto e Duque Bacelar-MA; Teresina e Altos-PI. Para análise por DRX as amostras foram inicialmente pulverizadas (Método do Pó) na Oficina de Preparação de Amostras do Instituto de Geociências-UFPA.

Depois de pulverizadas, as amostras foram homogeneizadas pelo método da pilha alongada. O procedimento consistiu em distribuir as amostras uniformemente em uma pilha alongada. Posteriormente foram separadas as extremidades das pilhas e então redistribuídas ao longo da pilha novamente. Após a repetição desse procedimento por três vezes, foi retirada uma alíquota de 160g do centro da pilha para análise. As análises por DRX foram realizadas no Difratômetro de Raios-X (DXR) modelo Empyrean da PANalytical, tubos de raios-X cerâmico de anodo de Co ($K_{\alpha 1}$= 1,789010 Å), foco fino longo, filtro K_{β} de Fe, detector PIXCEL3D-Medpix3 1x1, no modo *scanning*, com voltagem de 40 kV, corrente de 35mA, tamanho do passo 0,0263° em 2θ, varredura de 3° a 85° em 2θ, tempo/passo de 30,6s, fenda divergente: 1/4° e anti-espalhamento: 1/2°, máscara: 10 mm.

2.5 MICROSCOSCOPIA ELETRÔNICA DE VARREDURA

Foram feitas análises de Elétrons Secundários, Retroespalhados e EDS nas amostras do sílex da Formação Pedra de Fogo para melhor visualização das relações texturais e mineralógica das fases de cimentação da sílica. As amostras foram metalizadas com ouro durante 1,5 minutos (aprox. 15 nm), ou carbono, com 5 pulsos de 2 segundos (aprox. 20 nm), e analisadas no Laboratório de Microanálises do Instituto de Geociências (IG) da UFPA. O equipamento utilizado foi um MEV Zeiss modelo SIGMAVP pertencente ao Instituto Tecnológico Vale (ITV), cedido em contrato de comodato para a UFPA. Para elétrons secundários as condições de análises foram: corrente do feixe de elétrons = 80 μA, voltagem de aceleração constante = 10 kv, distância de trabalho = 8,5 mm. Para elétrons retroespalhados as condições de análises foram: corrente do feixe de elétrons = 80 μA, voltagem de aceleração constante = 20 kv, distância de trabalho = 8,5 mm.

As análises por EDS foram realizadas no MEV Zeiss modelo SIGMA-VP com EDS IXRF modelo Sedona-SD acoplado, pertencente ao Instituto Tecnológico Vale (ITV), cedido em contrato de comodato para a UFPA. As condições de operação foram: corrente do feixe de elétrons = 80 μA, voltagem de aceleração constante = 20 kv, distância de trabalho = 8,5 mm, tempo de contagem para análise dos elementos = 30 s.

3 BACIA DO PARNAÍBA, E ARCABOUÇO LITOESTRATIGRÁFICO DO GRUPO BALSAS

3.1 BACIA DO PARNAÍBA

3.1.1 Aspectos gerais

A Bacia do Parnaíba, localizada na porção norte-nordeste ocidental do Brasil, constitui uma das quatro bacias sedimentares intracratônicas do território brasileiro. Esta bacia estende-se sobre os estados do Maranhão, Piauí, e parte dos estados do Pará, Tocantins, Ceará e Bahia, cobrindo uma área de aproximadamente 600.000 km^2, com cerca de 3.5 km de rochas sedimentares no seu depocentro (Góes & Feijó 1994, Vaz *et al.* 2007). É limitada ao norte pelo Arco Ferrer-Urbano Santos, a noroeste pelo Arco Capim ou Tocantins, a leste pela Falha de Tauá, a sudeste pelo Lineamento Senador Pompeu, e a oeste pelo Lineamento Tocantins-Araguaia (Figura 1A) (Cordani *et al.* 1984, Góes 1995, Rezende & Pamplona 1970). Seu embasamento constitui rochas do cinturão Araguaia-Tocantins, da Faixa Gurupi, dos crátons Amazônico e São Francisco, e da Província Borborema (Cunha 1986). Conforme Góes (1995) e Vaz *et al*. (2007), a Formação Riachão e o Grupo Jaibaras representam o embasamento sedimentar da bacia. Segundo Castro *et al*. (2014), seu preenchimento sedimentar foi precedido por dois estágios de rifteamentos, de idades Neoproterozoica-Eopaleozoica e Cambro-ordoviciana, com direções gerais N-S/NE-SW e NE-SW, respectivamente. Vaz *et al*. (2007) correlacionam esses riftes precursores aos grábens Jaibaras, Jaguarapi, Cococi e São Julião (Província Borborema), gerados em sistemas de riftes entre o final do Proterozoico e início do Paleozoico.

Conforme Figueiredo & Raja Gabaglia (1986), a grande extensão da Bacia do Parnaíba, combinada com suas características sedimentares e pequena espessura (*sag basin*), indica lenta subsidência termal flexural durante sua evolução paleozoica.

A Bacia do Parnaíba foi redefinida por Góes (1995) em Província Sedimentar do Meio Norte, subdividindo-a em quatro bacias menores com gêneses, estilos tectônicos, preenchimentos sedimentares e idades distintas, denominadas de: Bacia do Parnaíba (Siluriano-Triássico), Anfíclise das Alpercatas (Jurássico-Eocretáceo), Bacia do Grajaú (Cretáceo) e Bacia do Espigão Mestre (Cretáceo). De acordo com Cunha (1986) os limites atuais da Bacia do Parnaíba demarcam depósitos paleozoicos remanescentes de bacias afro-brasileiras paleozoicas. Para Caputo *et al*. (2006), a erosão durante e após a ruptura do

Gondwana, reduziu progressivamente as dimensões originais desta bacia com o recuo de suas escarpas.

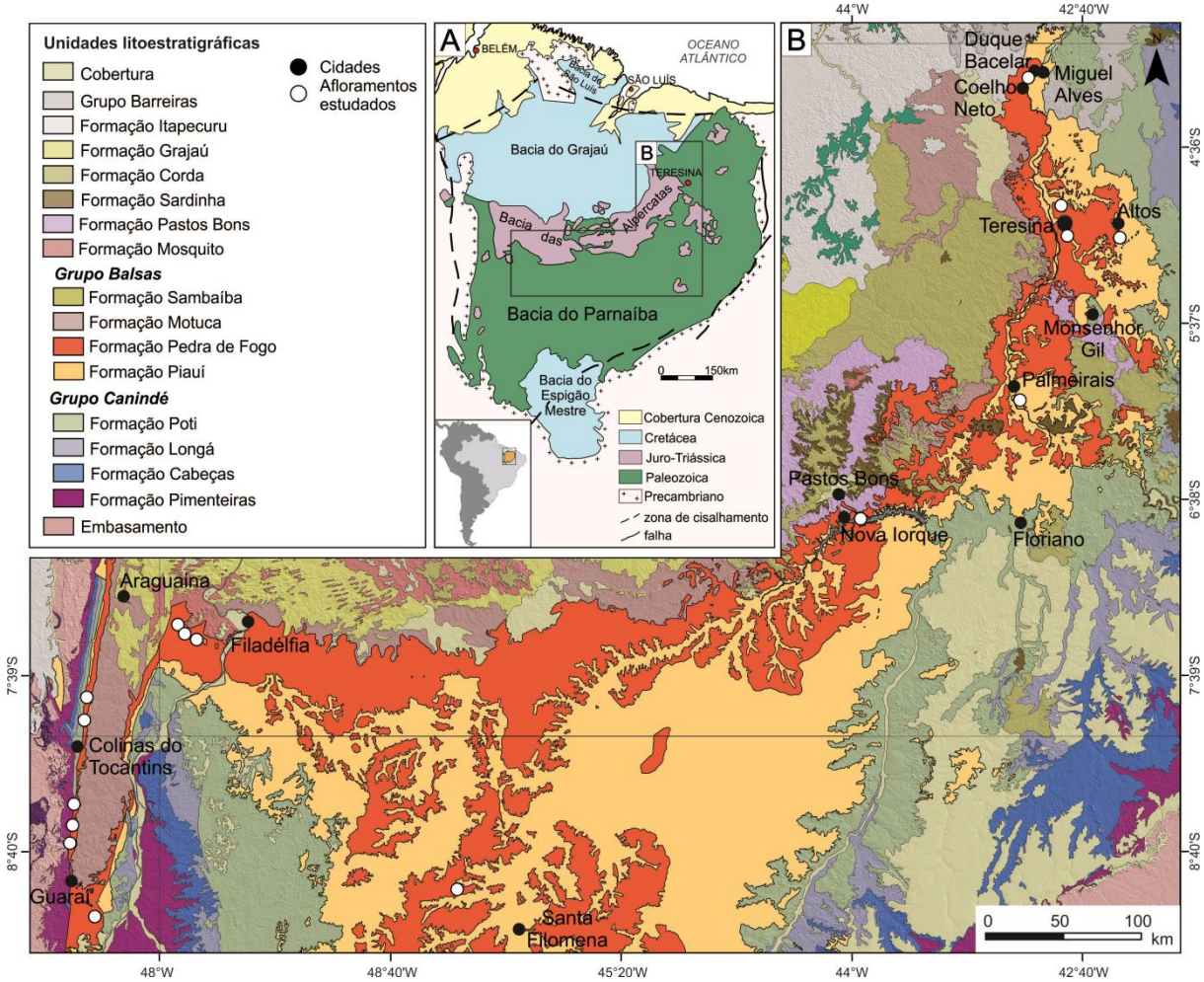

Figura 1- Mapa do norte da América do Sul mostrando a localização da Bacia do Parnaíba. **A)** Mapa da Bacia do Parnaíba. **B)** Mapa geológico simplificado da região estudada, mostrado a distribuição das principais unidades geológicas.

3.1.2 Arcabouço litoestratigráfico

O preenchimento litoestratigráfico da Bacia do Parnaíba é subdivido por Vaz *et al*. (2007) em cinco sequências deposicionais denominadas: siluriana, mesodevoniana-eocarbonífera, neocarbonífera-eotriássica, jurássica e cretácea, delimitadas por importantes discordâncias que se estendem por toda a bacia (Figura 2). A Formação Pedra de Fogo, objeto deste estudo, está inserida na sequência neocarbonífera-eotriássica, registrada pela deposição do Grupo Balsas, iniciada no Pensilvaniano com a Formação Piauí, e encerrada no Eotriássico com a Formação Sambaíba (Vaz *et al*. 2007). Segundo Góes *et al*. (1990), o Grupo Balsas marca o início da continentalização na Bacia do Parnaíba, com progressiva desertificação e deslocamento de seu depocentro para sua parte central. Conforme Barbosa *et al*. (2016), a

Sequência Neocarbonífera-Eotriássica teve início com depósitos flúvio-eólicos, que foram posteriormente afogados por depósitos marinhos e costeiros, que por sua vez foram progressivamente substituídos por sistemas lacustres e desérticos, resultante de condições climáticas crescentemente árida a semiárida. O Grupo Balsas ocorre principalmente nas porções centro-sul e parte das regiões oeste e leste-nordeste da bacia, e é constituído da base para o topo pelas formações Piauí, Pedra de Fogo, Motuca e Sambaíba, as quais registram intensas e significativas mudanças estruturais e ambientais na bacia durante sua deposição (Góes & Feijó 1994, Vaz *et al*. 2007).

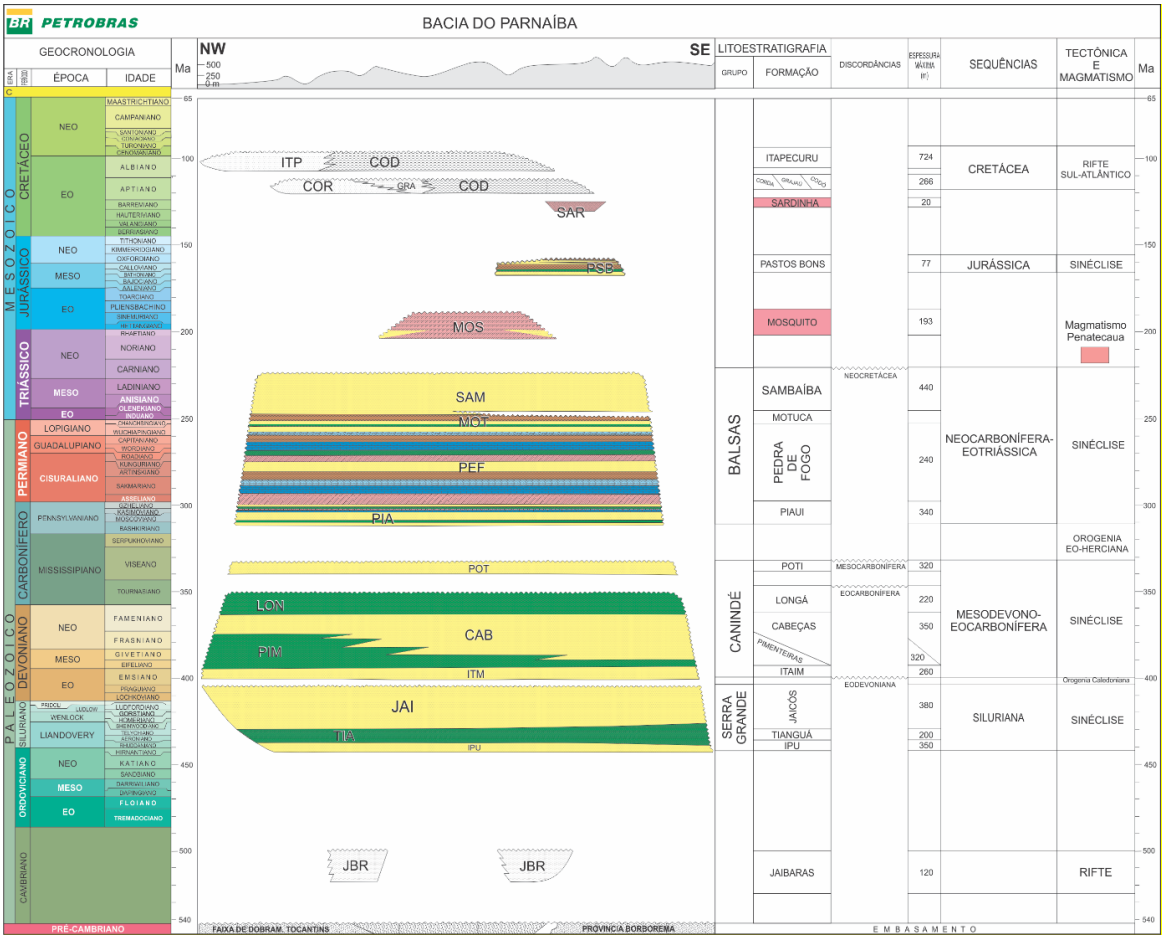

Figura 2-Carta estratigráfica da Bacia do Parnaíba com a disposição cronoestratigráfica das cinco sequências deposicionais. Este trabalho irá investigar a Formação Pedra de Fogo, dentro do contexto da Sequência Neocarbonífera-Eotriássica. Fonte: Modificado de (Vaz *et al*. 2007).

3.1.2.1 Sequência Neocarbonífera – Eotriássica (Grupo Balsas)

3.1.2.1.1 Formação Piauí

A Formação Piauí tem sua porção inferior caracterizada por arenitos médios com estratificação cruzada de grande porte, eventualmente maciços, intercalados por folhelhos vermelhos, enquanto a parte superior consiste de arenitos finos a médios, com intercalações de folhelhos vermelhos, calcários e finas camadas de *chert*, além de lentes conglomeráticas, geradas a partir de ambiente fluvial com contribuição eólica, e breves incursões marinhas em clima semi-árido a desértico (Lima & Leite 1978). Cronoestratigraficamente esta unidade é pensilvaniana (Melo *et al*. 1998).

3.1.2.1.2 Formação Pedra de Fogo

Sobreposta concordantemente a Formação Piauí ocorre a Formação Pedra de Fogo. Esta unidade aflora fundamentalmente na região central da Bacia do Parnaíba, ao longo de uma

extensa faixa com aproximadamente 600 km na direção leste-oeste, com largura média de 80 km, sendo também representativa em subsuperfície (Faria Jr. & Truckenbrodt 1980a, Pinto & Sad 1986).

Plummer (1946) denominou de Pedra de Fogo a sucessão de arenitos, folhelhos, calcários e principalmente *chert* com fragmentos de madeiras silicificadas que afloram nas margens do riacho Pedra de Fogo entre os municípios de Pastos Bons e Nova Iorque no Maranhão.

A formalização litoestratigráfica da unidade como Formação Pedra de Fogo foi feita por Aguiar (1971), caracterizada pela presença de sílex e calcário oolítico/pisolítico de coloração creme a esbranquiçado, eventualmente estromatolítico, intercalados com arenitos finos a médios, folhelhos cinza e anidrita.

Conforme Barbosa & Gomes (1957) a Formação Pedra de Fogo possui característica sedimentação cíclica, constituída da base para o topo por arenitos amarelados, siltitos, calcários oolíticos ou concrecionários e folhelhos esverdeados com fragmentos vegetais e lentes de calcário.

Baseado em aspectos litológicos, texturais e mineralógicos desta unidade, Faria Jr. (1979) subdividiu-a em três membros: i) O Membro *Sílex* Basal constituído por siltitos e folhelhos intercalados por bancos dolomíticos e concreções silicosas, com larga distribuição na bacia. ii) O Membro Médio, formado da base para o topo por arenitos e/ou siltitos, às vezes carbonáticos, estendendo-se até as intercalações de folhelhos com *chert*, além de eventuais horizontes silicificados com feições de algas estromatolíticas e/ou esteiras microbiais, sobrepostas a bancos carbonáticos com gretas de contração centimétricas, muitas vezes preenchidas por *chert* e calcita. Sua ocorrência é expressiva na parte central da bacia. iii) Membro Superior ou "Trisidela", caracterizado por bancos dolomíticos, intercalados por siltitos e folhelhos carbonáticos. Sua base é marcada por intercalações laminares de folhelhos cinza-esverdeados com níveis milimétricos e descontínuos de *chert*, bem como brechas intraformacionais. No topo ocorre abundante conteúdo de restos fósseis, níveis peletoidais e/ou silicificados, além de abundantes fragmentos de madeiras fósseis silicificadas, principalmente samambaias, em geral pertencentes ao gênero *Psaronius*, e com frequência associadas aos siltitos e arenitos finos imediatamente sotopostos aos "*red beds*" da Formação Motuca. Sua distribuição é principalmente na região central e oeste da bacia.

Pinto & Sad (1986) em revisão da estratigrafia da unidade, posicionaram os siltitos e arenitos com restos de madeiras silicificadas na porção inferior da Formação Motuca. Entretanto, esta proposta não foi considerada por trabalhos seguintes tais como: Abrantes Jr.

et al. (2016), Andrade (2012), Andrade *et al*. (2014), Araújo *et al*. (2016), Coimbra & Mussa (1984), Conceição *et al*. (2016a, b), Dino *et al.* (2002), Röβler & Galtier (2002a, b), Röβler & Galtier (2003), Santos & Carvalho (2009), Vaz *et al.* (2007). No entanto, Dias-Brito *et al*. (2007) retomaram o posicionamento estratigráfico dos litotipos portadores de madeiras silicificadas sugerido por Pinto & Sad (1986), e são seguidos por diferentes trabalhos de cunho paleontológicos/bioestratigráficos na borda oeste da Bacia do Parnaíba (Capretz 2010, Capretz & Rohn 2013, Benício *et al*. 2015, Kurzawe *et al*. 2013a, b, Matysová *et al.* 2010, Neregato *et al*. 2015, 2017, Tavares *et al*. 2014).

Recentemente, em trabalho na borda leste da Bacia do Parnaíba, Conceição *et al.* (2016a) registram um novo e importante conteúdo de floresta petrificada formada principalmente por troncos de gimnospermas de grande porte, muitos autóctones (em posição de vida) e com afinidade taxonômica com espécies identificadas na borda oeste da bacia. Esta assembleia fossilífera, estratigraficamente posicionada na parte inferior da Formação Pedra de Fogo, está em desacordo com os trabalhos previamente citados, que por sua vez têm atribuído a vasta ocorrência de troncos petrificados na borda oeste da bacia, exclusivamente para a Formação Motuca. Faz-se necessário o adensamento de trabalhos estratigráficos nas duas bordas da bacia para melhor resolver esta questão.

O conteúdo paleontológico da Formação Pedra de Fogo é vasto e diversificado, incluindo importantes descobertas recentes de novas espécies de tetrápodes (Cisneros *et al*. 2011, 2015), além de fragmentos de peixes e anfíbios (Figueroa & Gallo 2017, Santos 1994), até uma variedade de madeiras silicificadas (Coimbra & Mussa 1984, Conceição *et al*. 2016a, b, Martins 2000, Rößler & Galtier 2002a, b, Rößler & Galtier 2003, Rößler 2006, Santos & Carvalho 2009). Estes registros fósseis demonstram que a deposição desta unidade se deu em um período com abundante e variado número de organismos, tanto da fauna quanto da flora, além de fornecer importante suporte para o estabelecimento de idade da unidade.

Por diferentes métodos de investigação, autores diversos posicionam a Formação Pedra de Fogo ao longo do período Permiano. Price (1948) considerou-a como Eopermiano, enquanto Faria Jr. & Truckenbrodt (1980), Góes & Feijó (1994) e Lima & Leite (1978) situaram-na no intervalo eo-mesopermiano. Dino *et al*. (2002) identificaram similaridades palinológicas entre o Membro Superior "Trisidela" da Formação Pedra de Fogo, com a palinozona *Tornopollenites toreutos*, descrita por Playford & Dino (2000a, b) na Bacia do Amazonas, o que os levou a inferir idade Neopermiana para o topo desta unidade, além de correlacioná-la à parte superior da Formação Andirá – Permiano da Bacia do Amazonas. No entanto, Dino *et al*. (2002) indicam que esta idade poderia estar entre o Kunguriano

(Eopermiano tardio) e o Neopermiano, visto que o Membro Trisidela contém associação polínica fortemente similar à da Formação Flowerpot de Oklahoma. Com base nesse último aspecto, Dias-Brito *et al*. (2007) sugerem idade Kunguriana para a parte superior da Formação Pedra de Fogo, já que a formação estadunidense é posicionada neste andar. Por correlação bioestratigráfica com Floresta Petrificada de Chemnitz, Alemanha, Rößler (2006) considerou a Formação Pedra de Fogo também como de idade Kunguriana (Cisuraliano tardio). No entanto, conforme Rößler *et al*. (2012), a floresta fóssil daquele país foi rapidamente destruída, soterrada e fossilizada por vulcanismo piroclástico datado de cerca de 290,6 ± 1,8 M.a., obtida por SHRIMP em medições de U-Pb em zircões, o que automaticamente reposiciona a Formação Pedra de Fogo no Asseliano (Cisuraliano inicial).

O ambiente deposicional da Formação Pedra de Fogo tem sido historicamente descrito como de influência marinha, desde flúvio-deltaico a marinho raso (Aguiar 1964, Coimbra & Mussa 1984, Caldas *et al*. 1989, Dino *et al*. 2000, Faria Jr. 1979, Faria Jr. & Truckenbrodt 1980a, b, Lima & Leite 1978, Moore 1964), até planícies de *sabkha* sob eventuais influências de tempestades (Góes & Feijó 1994). Trabalhos recentes sugerem um ambiente fluvial (Rößler & Galtier 2002a, 2003, Rößler 2006). Conforme Andrade *et al*. (2014), esta unidade foi depositada em um sistema lacustre de clima árido, com rios efêmeros e *sabkhas* continentais, sob eventuais influências de tempestades. Estas conclusões são endossadas por Araújo *et al*. (2016) e Cisneros *et al.* (2015).

3.1.2.2 Formação Motuca

A Formação Motuca foi proposta por Plummer (1946) para os folhelhos avermelhados, com lentes delgadas de calcário e anidrita, sobrepostos a Formação Pedra de Fogo que afloram na Fazenda Motuca, entre São Domingos e Benedito Leite (MA). O contato inferior com a Formação Pedra de Fogo é geralmente concordante, podendo ser localmente brusco, enquanto o contato superior com a Formação Sambaíba é descrito como gradativo, e por vezes brusco e erosivo (Góes & Feijó 1994, Lima & Leite 1978). Conforme Abrantes Júnior & Nogueira (2013), esta unidade sedimentar é produto de um sistema lacustre raso com *mudflats* e *saline pans*, influenciado esporadicamente por influxos arenosos de rios efêmeros sob condições climáticas crescentemente áridas. Vaz *et al*. (2007) posicionam a Formação Motuca no Lopingiano (Permiano Superior).

3.1.2.2.1 Formação Sambaíba

A Formação Sambaíba foi definida por Plummer (1946) para designar os arenitos das mesetas observadas nos arredores do município homônimo, Estado do Maranhão. Segundo Aguiar (1971), essa unidade é constituída por arenitos de cor vermelha a creme esbranquiçado, finos a médios, com estratificações planares e principalmente cruzadas acanaladas de grande porte. O contato inferior é pontualmente discordante com as formações Piauí e Pedra de Fogo, e geralmente brusco com a Formação Motuca, enquanto o contato superior é discordante com os derrames básicos Eojurássico da Formação Mosquito (Góes & Feijó 1994, Lima & Leite 1978). O paleoambiente desta unidade é tido como um sistema desértico, com contribuições fluviais (Vaz *et al*. 2007). Conforme Abrantes Jr & Nogueira (2013), o deserto Sambaíba representa a intensa desertificação do supercontinente Pangea durante o Triássico.

4 SISTEMA LACUSTRE ÁRIDO DO INÍCIO DO PERMIANO (CISURALIANO): UM REGISTRO NA BACIA DO PARNAÍBA

Luiz Saturnino de Andrade[1,2*] & Afonso César Rodrigues Nogueira[2]

[1] Programa de Pós-Graduação em Geologia e Geoquímica-PPGG, Instituto de Geociências-IG, Universidade Federal do Pará-UFPA, 66075-110, Belém, Pará, Brasil.
E-mail: geoandrade.sl@gmail.com

[2] Grupo de Análise de Bacias Sedimentares da Amazônia, Universidade Federal do Pará-UFPA.
E-mail: afonsonogueir@gmail.com

*Corresponding author

RESUMO

Análise faciológica e estratigráfica realizada ao longo das bordas leste, sul e oeste da Bacia do Parnaíba, permitiu redefinir o paleoambiente da Formação Pedra de Fogo. Os depósitos estudados constituem uma sucessão de aproximadamente 100 m de espessura, predominantemente siliciclástica, com carbonatos e evaporitos subordinados. Dez fácies sedimentares principais, agrupadas em três associações de fácies (AF): AF1-Lacustre raso/*Sabkha*-com rios efêmeros; AF2-*Nearshore* lacustre dominado por ondas; AF3-Lacustre central. Estas associações indicam que a Formação Pedra de Fogo constitui majoritariamente uma sucessão continental representada por um sistema lacustre raso com fluviais efêmeros não-confinados e sob forte influência de tempestades. Estes fluviais efêmeros não-confinados adentravam estes lagos e podiam desenvolver lobos de suspensão e/ou fluxos em lençol que eventualmente alcançavam as regiões centrais do sistema lacustre, sítio de deposição pelítica. Suas porções periféricas eram sítios de deposição evaporítica com desenvolvimento de planícies de *sabkha* e/ou colonizadas por uma expressiva paleoflora. Os depósitos estudados indicam que a Formação Pedra de Fogo foi depositada sob influência de sazonalidade climática, com períodos quentes e áridos, representados pela ocorrência comum de evaporitos, intercalada por períodos de umidade relativa elevada, representada pelos registros de uma tafoflora de grande porte. Esta sucessão representa um importante registro das oscilações paleoclimática prevalecentes na porção oeste-central do Pangeia durante o início do Permiano (Cisuraliano).

Palavras-chave: Permiano; Cisuraliano; Bacia do Parnaíba; Formação Pedra de Fogo; Sistemas lacustres áridos.

ABSTRACT

Faciological and stratigraphic analysis carried out along the eastern, southern and western border of the Parnaíba Basin, allowed us to redefine the paleoenvironment of the Pedra de Fogo Formation. The studied deposits constitute a succession of approximately 100 m-thick, predominantly siliciclastic, with subordinate carbonates and evaporites. Ten main sedimentary facies were defined, grouped into three facies associations (FA): FA1-Shallow Lacustre / Sabkha-ephemeral streams; FA2- Lacustrine nearshore wave-dominated; FA3-Central Lacustrine. These facies associations indicate that the Pedra de Fogo Formation is mostly a continental succession represented by a shallow lacustrine system with unconfined flows and under strong storm events influence. These ephemeral streams entering these lakes could develop suspension lobes and/or sheet flows that eventually reached the central regions of the lacustrine system, mudrocks deposition site. Its peripheral basements were sites of evaporitic deposition with development of sabkha plains and/or colonized by an expressive paleoflora. The studied deposits indicate that the Pedra de Fogo Formation was deposited under the influence of climatic seasonality, with hot and arid periods, represented by the common occurrence of evaporites, interspersed with periods of relative high wet, represented by the records of a large taphoflora. This succession represents an important record of the paleoclimatic oscillations prevalent in the west-central portion of Pangea during the early Permian (Cisuralian).

Keywords: Permian; Cisuralian; Parnaíba Basin; Pedra de Fogo Formation; Arid lacustre systems

INTRODUÇÃO

A sedimentação permiana abrange depósitos das fases finais da glaciação carbonífero-permiana (Dickins 1996; Eyles et al. 1996; Santos et al. 1996; Visser 1997), que inclui planícies de *sabkhas* costeiras, *red beds*, sistemas aluviais e lacustres de clima árido adjacentes a extensos desertos no interior do Pangeia (Andrade et al. 2014; Abrantes Jr. & Nogueira 2013; Abrantes Jr. et al. 2016, 2019; Chumakov & Zharkov 2002). Colisões continentais iniciadas no Devoniano-Carbonífero resultaram na formação do supercontinente Pangeia no final do Pensilvaniano e início do Permiano (Blakey 2008). A formação de um extenso cinturão montanhoso na parte central do Pangeia, que se estendia do norte do México até o sudeste da Europa (Blakey 2008; Hatcher Jr. 2002), interferiu no regime de circulação dos ventos, intensificando condições de aridez em quase todo o interior do supercontinente. Intensas e volumosas erupções vulcânicas na região da atual Sibéria, conhecidas como

“Armadilhas Siberianas”, combinadas com baixos valores do albedo planetário, resultaram no superaquecimento no limite Permo-Triássico (Chumakov & Zharkov 2003; Courtillot & Renne 2003; Scotese et al. 1999).

No Brasil, a Formação Pedra de Fogo representa um dos mais significativos registros do período Permiano, caracterizada por expressiva silicificação em toda sua extensão dentro da parte central da Bacia do Parnaíba (Faria Jr. 1979; Plummer 1946). A multiplicidade litológica e fossilífera da Formação Pedra de Fogo, constitui um importante registro das variações paleoclimáticas, paleogeográficas e paleoambientais ocorridas na parte oeste-central do Pangeia durante o início do Permiano

Assim, este estudo apresenta o contexto estratigráfico geral da Formação Pedra de Fogo, ao longo uma extensa faixa descontínua de afloramentos nas bordas leste, sul e oeste da Bacia do Parnaíba (Figura 1). Ao longo desta ampla seção sedimentológica/estratigráfica pode-se visualizar a variação lateral e relações de contatos entre as associações de fácies individualizadas. Estas associações de fácies caracterizam um sistema lacustre árido frequentemente afetado por rios efêmeros e eventos de tempestades. Núcleos dispersos com densa ocorrência de caules silicificados evidenciam a colonização de porções periféricas destes lagos por uma pujante tafoflora Permiana.

CONTEXTO GEOLÓGICO

BACIA DO PARNAÍBA

A Bacia do Parnaíba está inserida na Província Parnaíba, porção leste da Plataforma Sul-Americana. Localiza-se na região norte-nordeste ocidental do Brasil, possui forma poligonal a levemente alongada na direção NE-SW, e extensão aproximada de 600.000 km^2, com cerca de 3.5 km de rochas sedimentares no seu depocentro (Góes & Feijó 1994). Trabalhos recentes com perfis de reflexão de sísmica profunda (até 1430 km de profundidade) mostram que a Bacia do Parnaíba está assentada sobre embasamento cristalino de rocha Neoproterozoicas da Província Borborema a leste, bloco Parnaíba no centro e Cráton Amazônico a oeste (Daly et al. 2014, 2018a, 2018b). Segundo Castro et al. (2014), seu preenchimento sedimentar foi precedido por dois estágios de rifteamentos de idades Neoproterozoica-Eopaleozoica e Cambro-ordoviciana, com direções gerais N-S/NE-SW e NE-SW, respectivamente.

A Bacia do Parnaíba foi redefinida por Góes (1995) em Província Sedimentar do Meio Norte, subdividida em quatro bacias menores com gêneses, estilos tectônicos, preenchimentos sedimentares e idades distintas, denominadas de: Bacia do Parnaíba (Siluriano-Triássico),

Anfíclise das Alpercatas (Jurássico-Eocretáceo), Bacia do Grajaú (Cretáceo) e Bacia do Espigão Mestre (Cretáceo).

O preenchimento litoestratigráfico da Bacia do Parnaíba é subdivido por Vaz et al. (2007) em cinco sequências deposicionais denominadas: siluriana, mesodevoniana-eocarbonífera, neocarbonífera-eotriássica, jurássica e cretácea, delimitadas por importantes discordâncias que se estendem por toda a bacia. A Formação Pedra de Fogo, objeto deste estudo, está inserida na sequência neocarbonífera-eotriássica, registrada pela deposição do Grupo Balsas, iniciada no Pensilvaniano com a Formação Piauí, e encerrada no Eotriássico com a Formação Sambaíba (Vaz et al. 2007).

Formação Pedra de Fogo

A Formação Pedra de Fogo sobrepõe a Formação Piauí e aflora fundamentalmente na região central da Bacia do Parnaíba, ao longo de uma extensa faixa com aproximadamente 600 km na direção leste-oeste, com largura média de 80 km, sendo também representativa em subsuperfície (Faria Jr. & Truckenbrodt 1980a; Pinto & Sad 1986). Esta unidade sedimentar foi formalizada por Plummer (1946), e é caracterizada por seu vasto conteúdo de chert, além de uma característica sedimentação cíclica constituída por evaporitos, carbonatos, pelitos (argillitos, folhelhos e siltitos) e arenitos (Barbosa & Gomes 1957; Faria Jr. & Truckenbrodt 1980a, 1980b; Melo & Prade 1968; Plummer 1946).

O conteúdo paleontológico da Formação Pedra de Fogo também é amplo e variado (Tabela 1), desde tetrápodes (Cisneros et al. 2011, 2015), peixes e anfíbios (Santos 1994; Figueroa & Gallo 2017), até uma variedade de madeiras silicificadas (Coimbra & Mussa 1984; Conceição et al. 2016a, 2016b; Iannuzzi et al. 2018; Martins 2000; Rößler & Galtier 2002a, 2002b e 2003; Rößler 2006; Santos & Carvalho 2009). Estes registros fósseis demonstram que o paleoambiente da Formação Pedra de Fogo abriga grande variedade faunística e florística, e os processos deposicionais devem ter sido excepcionalmente catastróficos para preservar essa ampla variedade de registro fóssil. Por bioestratigrafia, a sua idade foi recentemente sugerida como Cisuralina (Cisneros et al. 2015).

O ambiente deposicional da Formação Pedra de Fogo é historicamente considerado desde marinho raso a flúvio-deltaico (Aguiar 1964; Caldas et al. 1989; Coimbra & Mussa 1984; Dino et al. 2002; Faria Jr. 1979; Faria Jr. & Truckenbrodt 1980a;1980b; Lima & Leite 1978; Moore 1964), até planícies de *sabkha*, sob eventuais influências de tempestades (Góes & Feijó 1994). Trabalhos recentes sugerem um ambiente fluvial (Rößler & Galtier 2002a, 2003; Rößler 2006).

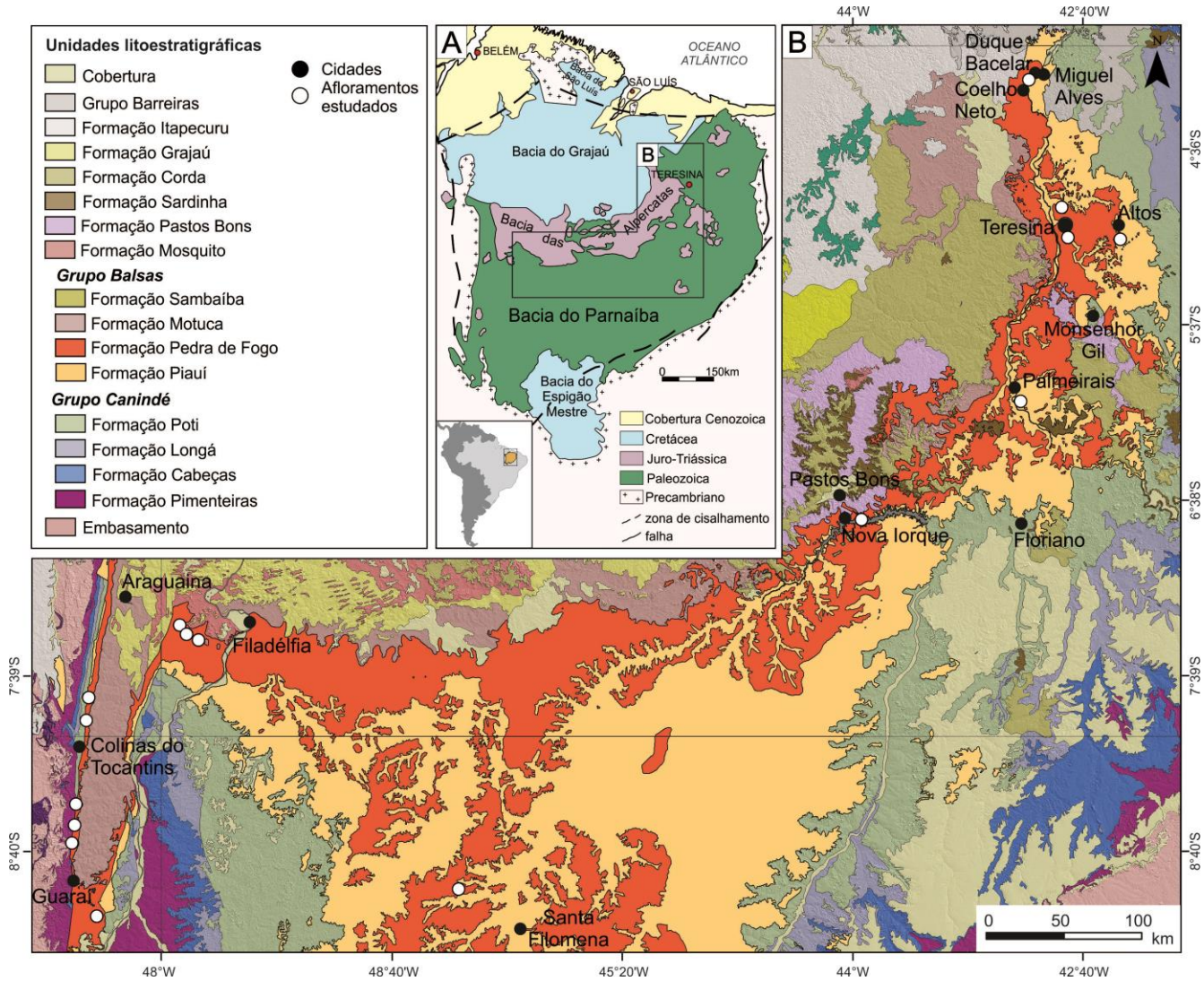

Figura 1-Mapa geológico e de localização da área de estudo. A) Mapa geológico simplificado da Bacia do Parnaíba. O retângulo preto indica a posição da área de estudo (Modificado de Schobbenhaus et al. 1984). B) Disposição espacial das principais unidades geológicas presentes na área de estudo, com destaque para as formações Piauí e Pedra de Fogo.

Em estudo na parte superior da unidade, borda oeste da Bacia do Parnaíba, Andrade et al. (2014) definiram aquela porção da unidade como sendo tipicamente formada por um sistema lacustre de clima árido, com rios efêmeros e *sabkha* continental, sob eventuais influências de tempestades. Posteriormente, o estudo na mesma região feito por Araújo et al. (2016) reforçou esta interpretação. Cisneros et al. (2015), em importante trabalho paleontológico na borda leste da bacia, na qual definiram duas novas espécies de tetrápodes (*Timonya anneae gen. et sp. nov.* e *Procuhy nazariensis gen. et sp. nov.*), associaram o paleoambiente dessas espécies análogo a associação de fácies AF2 de Andrade et al. (2014). Em recente trabalho na borda oeste da Bacia do Parnaíba, Abrantes Jr. et al. (2019) também definem esta poção da Formação Pedra de Fogo como lacustres efêmeros de clima árido sob efeito de sazonalidade climática. A tabela 1 mostra um sumário dos principais trabalhos realizados na Formação Pedra de Fogo. Esta variedade de ambientes deposicionais, bem como a diversidade fossilífera registrada na Formação Pedra de Fogo refletem a complexidade paleoambiental/paleoclimática, paleoecologica e paleogeográfica dessa unidade sedimentar (Tabelas 2 e 3).

MÉTODOS

Este estudo realizou análise de fácies e estratigráfica em dezoito perfis ao longo das bordas leste, sul e oeste da Bacia Parnaíba. Esta ampla sucessão estratigráfica exibe uma variação lateral e vertical das associações de fácies que caracterizam a Formação Pedra de Fogo (Figuras 2 e 3). O modelamento de fácies seguiu a proposta de Walker (1992, pg. 1-14), e Dalrymple (2010, pg. 3-18). Foram analisadas as características composicionais, estruturas sedimentares, texturas, padrões geométricos, conteúdo fossilífero e padrões de paleocorrentes. As fácies com similaridades cogenéticas e contemporâneas foram agrupadas em associações de fácies que permitem a interpretação do sistema deposicional

Complementarmente foi feito um estudo petrográfico. As imagens foram capturadas com a câmera Leica DFC310 FX, acoplada ao microscópio petrográfico da marca Leica DM4500 P Led com luz transmitida. Adicionalmente utilizou-se análise por Microscópio Eletrônico de Varredura (MEV) com sistema EDS integrado. As imagens de elétrons secundários foram obtidas no Laboratório de Microanálises do Instituto de Geociências (IG) da UFPA. O equipamento utilizado foi um MEV Zeiss modelo SIGMA-VP com EDS IXRF modelo Sedona-SD acoplado. As condições de operação foram: corrente do feixe de elétrons = 80 μA, voltagem de aceleração constante = 20 kv, distância de trabalho = 8,5 mm, tempo de contagem para análise dos elementos = 30 s.

RESULTADOS

ASSOCIAÇÃO DE FÁCIES

Aspectos gerais

Este estudo abrange exposições da Formação Pedra de Fogo nas bordas leste-sul e oeste da Bacia do Parnaíba, regiões dos municípios de Coelho Neto, Duque Bacelar e Nova Iorque no estado do Maranhão; União, Teresina, Altos, Palmeirais e Santa Filomena no estado do Piauí; Guaraí, Colinas do Tocantins, Bandeirante do Tocantins, Araguaina, e Filadélfia no estado do Tocantins (Figura 1).

A sucessão estudada aflora ao longo de rodovias estaduais e federais nos limites entre os estados do Piauí e Maranhão, margens dos rios Poti (Teresina-PI), Parnaíba (Represa da Boa Esperança-Nova Iorque-MA) e Tocantins (Filadélfia-TO e Carolina-MA).

Nas bordas leste e sul, a Formação Pedra de Fogo sobrepõe discordantemente arenitos flúvio-eólicos da Formação Piauí, e pontualmente é sobreposta de forma concordante por pelitos vermelhos e maciços da Formação Motuca, que também a recobre na borda oeste da bacia (Figura 2).

Tabela 1-Sumário dos principais trabalhos realizados na Formação Pedra de Fogo

Fósseis e dados químicos	Ambientes Deposicionais	Áreas	Idades	Temáticas	Referências
Anfíbios labirintodontes (*Prionosuchus*)					Price (1948)
Dernbachia brasiliensis gen. nov. et sp. nov e *Grammatopteris freitasii*		região de Filadélfia-TO	Eo-Permiano		Röβler & Galtier (2002a,b)
T*eresinonoxylon euzebioi* Mussa		região de Teresina-PI, nas margens do rio Poti,	Meso-Permiano	Bioestratigráfico	Caldas *et al.* (1989)
Psaronius brasilienis e *Tietea singularis*		região de Bielândia-TO	Neo-Permiano		Martins (2000)
	Nerítico raso a litorâneo com planícies de *sabkha*, sob eventuais influências de tempestades	Regional	Eo a Neo-Permiano		Góes & Feijó (1994)
Calamites	Transicional/flúvio-deltáico a marinho raso	região de Carolina-MA,	Meso-Carbonífero a Eo-Permiano		Coimbra & Mussa (1984)
		Regional	Eo a Meso-Permiano		Lima & Leite (1978)
Palinozona *Tornopollenites toreutos*	Marinho raso a costeiro, sob condições áridas a semi-áridas quentes	regiões de Carolina/ Mangabeiras-MA	Neo-Permiano	Palinológico	Dino *et al.* (2002)
	Deltáico	Regional		Paleontológico	Barbosa & Gomes (1957)
	Marinho a continental	região de Balsas-MA		Litológico	Moore (1964) Cunha (1964) Aguiar (1964)
B-V, Ga-B, B-K_2O, B-Ga-B e teor de B	Continental com eventuais invasões marinha	região de Carolina-MA/Filadélfia-TO		Geoquímico	Oliveira (1982)
	Marinho a continental lacustre			Litológico	Ojeda & Perillo (1967)
		Regional		Litológico/faunís-tico	Oliveira (1961)
	Marinho costeiro	região de Riachão-MA		Litológico	Ojeda & Bembom (1966)
Estromatólitos	Marinho raso a restrito, tipo epicontinental, variando de transicional, deltáico a nerítico	Toda extensão da Fm. Pedra de Fogo	Permiano	Sedimentológico /petrográfico	Faria Jr. (1979); Faria Jr. & Truckenbrodt (1980a,b)

Continuação

Microbialitos, microfósseis, ictiólitos, e caules de samambaias silicificados	Lacustre de clima árido, com rios efêmeros sob influência de tempestades	região de Filadélfia-TO	Permiano	Sedimentológico /Estratigráfico	Andrade *et al.* (2014)
Ttrápodes (*Rhinesuchidae , Timonya anneae gen. et sp. nov. e Procuhy nazariensis gen. et sp. nov*)	Lacustre de clima árido, com rios efêmeros	região de Timon-MA/Nazária-PI	Eo-Permiano (Cisuraliano)	Paleontológico/ Estratigráfico	Cisneros *et al.* (2015)
Ictiólitos, e caules de samambaias silicificados	Lacustre de clima árido	região de Filadélfia-TO/Nova Iorque-MA	Permiano	Sedimentológico /Estratigráfico	Araújo *et al.* (2016)
Lenhos de gimnospermas e caules de samambaias silicificados	Lacustre de clima árido, com rios efêmeros	região de Coelho Neto/Duque Bacelar-MA	Eo-Permiano (Cisuraliano)	Paleontológico/ Estratigráfico	Conceição *et al.*(2016)
Condríctios (*Rubencanthus diplotuberculatus; Sphenacanthus ignis* e *Bythiacanthus lopesi*)	Marinho (?)	região de Pastos Bons-MA	Eo-Permiano (Cisuraliano)	Paleontológico	Figueroa & Gallo (2017)
Microbialitos, verterbrados, folhas e lenhos de gimnospermas e caules de samambaias silicificados	Flúvio/lacustre de clima árido, com rios efêmeros	Em toda a extensão do Pedra de Fogo	Eo-Permiano (Cisuraliano)	Paleontológico/ Estratigráfico	Iannuzzi *et al*. (2108)
Microbialitos, microfósseis, ictiólitos, e caules de samambaias silicificados	Lacustre de clima árido, com rios efêmeros sob influência de tempestades		Meso-Permiano	Sedimentológico /Estratigráfico	Abrantes *et al*. (2019)

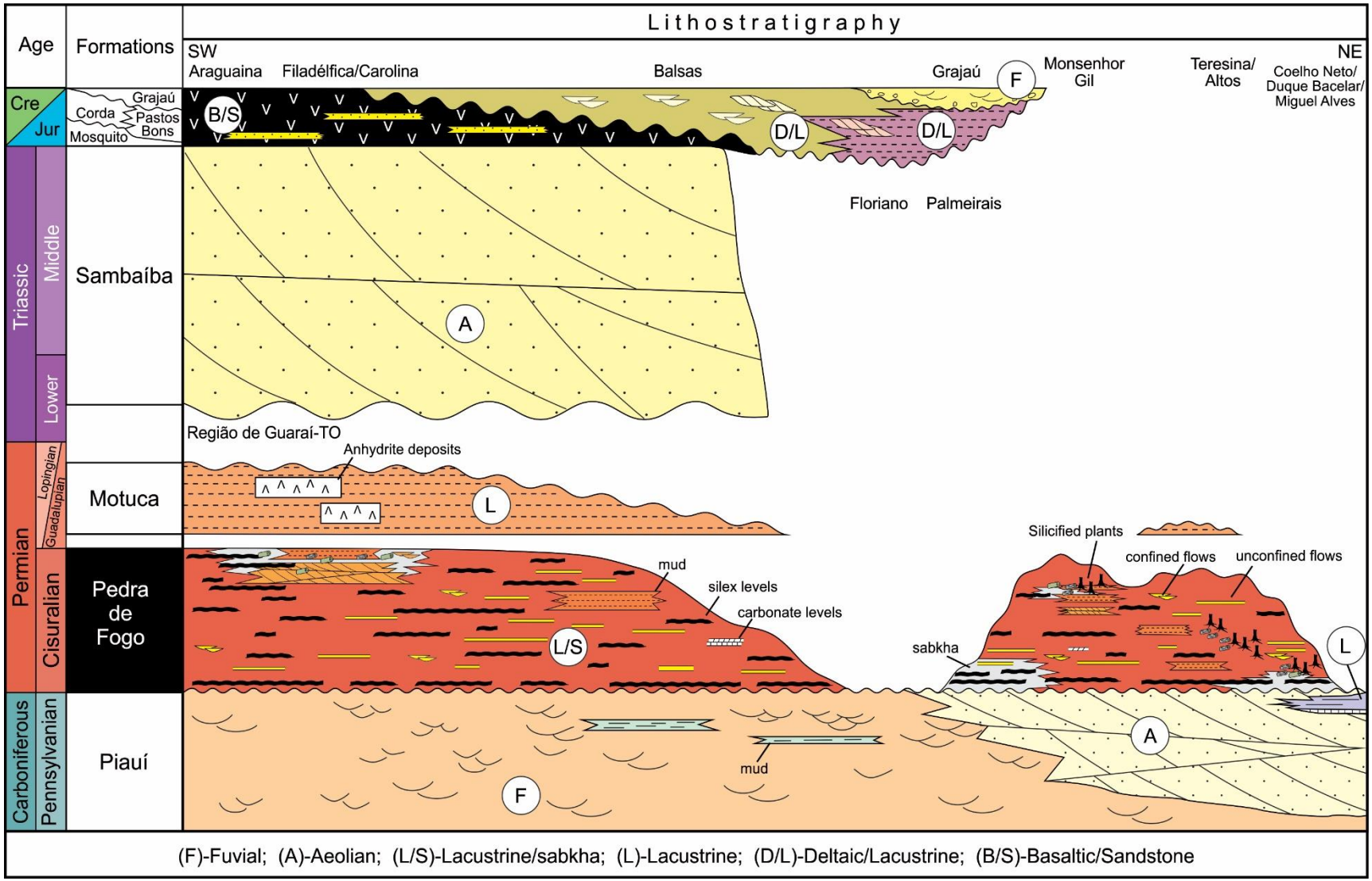

Figura 2- Coluna estratigráfica das principais unidades sedimentares aflorantes ao longo da sucessão estudada nas bordas leste, sul e oeste da Bacia do Parnaíba. Destaque para a Formação Pedra de Fogo.

Ao longo dos afloramentos estudados, a espessura total da Formação Pedra de Fogo, de forma descontínua é de até 100 m. As maiores espessuras estão concentradas na borda leste, no flanco de pequenos morros (até 70 m) e colinas (até 280 m).

Em geral, esta unidade é composta por pelitos de coloração vermelha a laranja claro, minoritariamente cinza a verde claro. Esses pelitos são predominantemente maciços, pontualmente possuem laminações plano-paralela a onduladas, simétricas e assimétricas, bem como laminações cruzadas cavalgantes. Os pelitos intercalam-se com camadas tabulares centimétricas a decimétricas de arenito amarelo claro, muito finos a finos, maciços, e com incipiente laminação plano-paralela. Eventualmente, a base dessas camadas de arenito é erosiva. A geometria tabular (em lençol) é característica desses arenitos. São extensos lateralmente com pouca variação nas espessuras das camadas. Eventualmente ocorrem arenitos vermelhos a laranja claros, com granulometria média a grossa, e estratificações cruzadas tabular a acanalada. Laminações cruzadas formadas por ondas, e estratificação cruzada *hummocky* são frequentes. Caules silicificados de samambaias e gimnospermas são característicos dessa unidade. Os caules silicificados de samambaias ocorrem fundamentalmente rolados, ou frequentemente imersos nos níveis pelíticos e/ou nas camadas tabulares de arenitos com *lag* conglomeráticos. Caules silicificados de gimnospermas em posição de vida são restritos a borda leste da bacia, nas regiões de Duque Bacelar/Coelho Neto-MA, Teresina, Altos e Monsenhor Gil-PI.

Níveis de brecha *chert*, nódulos silicificados e *cherts* maciços marcam a base da Formação Pedra de Fogo. Microbialitos, estratiformes e colunares são mais frequentes em sua parte inferior. Nódulos evaporíticos com formas e tamanhos são frequentes, assim como estruturas de exposição como *tepees* e gretas, bem como pontuais convoluções.

A análise sedimentológica/estratigráfica geral da Formação Pedra de Fogo definiu dez fácies principais, que foram agrupadas em três associações de fácies: Lacustre raso/*Sabkha* com rios efêmeros (AF1), *Nearshore* lacustre dominado por ondas (AF2), Lacustre central (AF3).

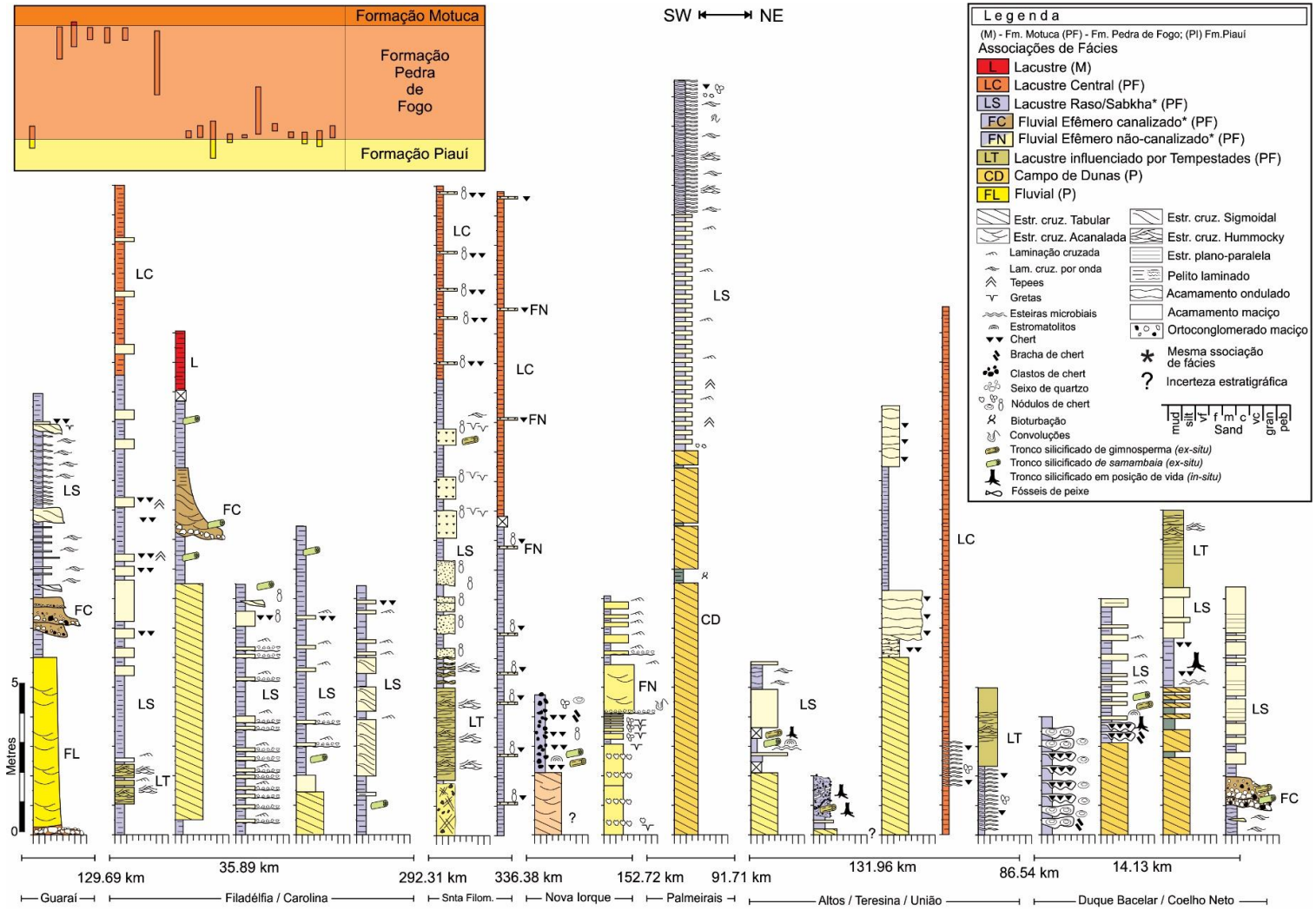

Figura 3-Perfis litoestratigráficos da sucessão estudada. Os depósitos da Formação Pedra de Fogo representam múltiplos ciclos formados pela intercalação entre camadas de arenito com geometria tabular/em lençol de fluviais efêmeros na sua maior parte não-confinados com pelitos pouco espessos do lacustre raso-sabkha. Note que tanto a frequência de eventos de rápida inundação (FC/FN) bem como eventos de tempestades (LT) são frequentes na parte inferior da sucessão, e tendem a se extinguir o reduzir para o todo. A parte superior consiste basicamente de pacotes mais espessos de pelito da porção central do sistema lacustre intercalados com delgadas camadas de arenito muito fino das porções distais dos eventos de inundação. O quadro no canto superior esquerdo da figura posiciona de forma aproximada cada perfil em suas unidades sedimentares correspondentes.

Tabela 2- Principais fácies e processos deposicionais da Formação Pedra de Fogo.

Fácies	Descrição	Interpretação
Chert (**Ch)**	Camadas tabulares com espessuras de até 20 cm e lateralmente contínuas. Chert nodular e brechas de chert são frequentes. Ocorre fundamentalmente associada a base da unidade. Apresenta concreções silicosas e feições de porosidade *vug*. Está associada a fácies **Plm**.	Silicificação sindeposicional a eodiagenética de carbonatos-evaporitos.
Pelito maciço (**Pm**)	Camadas tabulares com até 30 cm de espessura, lateralmente contínuas de pelito maciço, eventualmente laminado, vermelho a laranja esbranquiçado, frequentemente mosqueado. Comumente ocorrem abundantes nódulos e pseudonódulos evaporíticos silicificados. Caules silicificados de gimnospermas e samambaias ocorrem tanto na parte inferior, quanto na parte superior esta fácies. Apenas caules de gimnospermas ocorrem em posição de vida. Gretas, teepes e microbialitos ocorrem associados.	Deposição por decantação em ambiente de baixa energia. Processo de silicificação sindeposicional a eodiagenética dos vegetais. Exposição subaérea esporádica. Mineralização de tapetes microbianos bentônicos e/ou aprisionamento e ligação de partículas sedimentares
Pelito laminado a maciço (**Plm**)	Camadas tabulares com espessuras contínuas variando entre 1,7 e 18 m. São lateralmente contínuas por dezenas de quilômetros, formadas por pelitos laminado, por vezes maciço, vermelho a cinza-esbranquiçado. Caules silicificados dispostos horizontalmente ao acamamento. Camadas centimétricas tabulares de arenitos finos intercalam-se com os pelitos.	Deposição por decantação em ambiente de baixa energia. Processo de silicificação sindeposicional a eodiagenética da madeira.
Pelito com *wavy/linsen* (**Pwl**)	Alternância milimétrica entre arenitos finos e pelitos, creme-esbranquiçados a amarelo-claros, com esporádicas laminações cruzadas a onduladas. Presença de "*curled flakes*", por vezes ocorrem gretas associadas.	Alternância de tração e suspensão em ambiente subaquático. Posterior exposição subaérea.
Arenito com laminação truncada por onda (**Alo**)	Camadas tabulares centimétricas a decimétricas de coloração variando de vermelhas a branca, lateralmente contínuas, com arenito muito fino a silte com laminação truncada por onda.	Deposição por fluxo combinado dominantemente oscilatório a partir da ação de ondas de tempo bom.
Arenito com laminação ondulada a maciço (**Aom**)	Camadas tabulares com espessuras entre 0,15 e 1,3 m de arenito fino a síltico, amarelo esbranquiçado com grãos subarredondados maciço, por vezes com laminação cruzada incipiente a ondulada. Possui cimento carbonático. Eventualmente ocorrem níveis e *lags* de sílex, bem como caules silicificados em posição concordante ao acamamento.	Ação de correntes desconfinadas em leito plano com rápida deposição e consequente homogeneidade granulométrica. Igualmente possível é a deposição por decantação a partir de plumas em suspensão proveniente de fluxo hipopicnais. Eventuais retrabalhamentos por fluxo combinado.

Arenito fino com estratificação cruzada sigmoidal (**As**)	Arenitos finos a médios esbranquiçados. *Mud drapes* descontínuos recobrem os *foresets* sigmoidais. Lateralmente o *toe set* exibe laminações cruzadas cavalgante supercrítica e pontuais clastos tabulares de argila.	Migração de formas de leito sob fluxo unidirecional e rápida desaceleração. Deposição por tração e decantação com migração de marcas onduladas e retrabalhamento de planície de lama.
Arenito fino com estratificação (cruzada *hummocky* (**Ah**)	Camadas tabulares com até 0,6 m de espessura de arenito fino a médio, coloração creme-esbranquiçada, por vezes síltico, com grãos angulosos a subarredondado com estratificação cruzada *hummocky*.	Deposição por fluxo combinado dominantemente oscilatório por ação de ondas em períodos de tempestades.
Arenito com estratificação cruzada acanalada (**Aa**)	Arenitos médios a grossos, arranjados em *sets* de estratificação cruzada acanalada com até 0,7 m de espessura. Na base desta fácies escavações ocorrem fragmentos de troncos silicificados de até 0,3 m de diâmetro.	Migração de dunas 3D sob fluxo unidirecional em regime de fluxo inferior.
Conglomerado maciço (**Cm**)	Camadas centimétricas de ortoconglomerado polimítico, com seixos subangulosos a subarredondados com até 10 cm de diâmetro.	Depósitos em eixo de canal *(lags)* a partir de correntes unidirecionais de alta energia.

Tabela 3 – Resumo das associções de fácies e fácies da Formação de Pedra de Fogo.

Associações de Fácies	**Fácies**
Lacustre raso/*Sabkha*-com rios efêmeros (AF1)	Ch, Pm, Pwl, Aom, As, Aa, Cm
Nearshore lacustre dominado por ondas (AF2)	Alo, Aom, Ah
Lacustre central (AF3)	Am, Plm, Aom

Lacustre raso/*Sabkha*-com rios efêmeros (AF1)

A AF1 consiste em *Chert* (Ch), Argilito maciço (Am), Pelito maciço (Pm), Pelito com *wavy/linsen* (Pwl), Arenito com laminação ondulada a maciço (Aom), Arenito fino com estratificação cruzada sigmoidal (As), Arenito com estratificação cruzada acanalada (Aa), Conglomerado extraformacional maciço (Cm). Esta associação é mais frequente na parte inferior da unidade (Figura 2). A AF1 é caracterizada pela intercalação de ciclos centimétricos a decimétricos entre camadas de pelitos avermelhados, por vezes esbranquiçado, maciço, eventualmente laminados, recobertos por camadas tabulares de arenitos muito finos a finos, com laminação ondulada a maciço (Figuras 4, 5). Acamamento *wavy/linsen* ocorrem associados às fácies Am e Pm (Figuras 5C, D). Arenitos finos a médio com estratificação cruzada sigmoidal, por vezes estratificação cruzada acanalada, bem como níveis de conglomerados maciços com base erosiva marcada por *lags* de grânulos e seixos *chert* e

quartzo com até 3 cm de diâmetro ocorrem tanto no topo, quanto na base da sucessão (Figuras 5, 6, 7). Gretas e estruturas *tepees* também são relativamente comuns (Figura 8), e ocorrem associados a nódulos evaporíticossilicificado ("*pop-corns*") (Figuras 6H, G e 8A). Fragmentos silicificados de caules de samambaias com até 40 cm de comprimento são frequentes, bem como caules de gimnospermas em posição de vida (Figura 9). Esses caules ocorrem associados aos pelitos maciços, e são ausentes onde existem estruturas de exposição (e.g. gretas e *tepees*). Microbialitos estratiformes e colunares ocorrem tanto sobrepondo, como sendo sobrepostos por caules de gimnospermas em posição de vida. Camadas e níveis nodulares de *chert* (sílex) com até 20 cm de espessuras e lateralmente contínuas são comuns em toda esta associação. Brechas de *chert* ocorrem frequentemente na base da AF1.

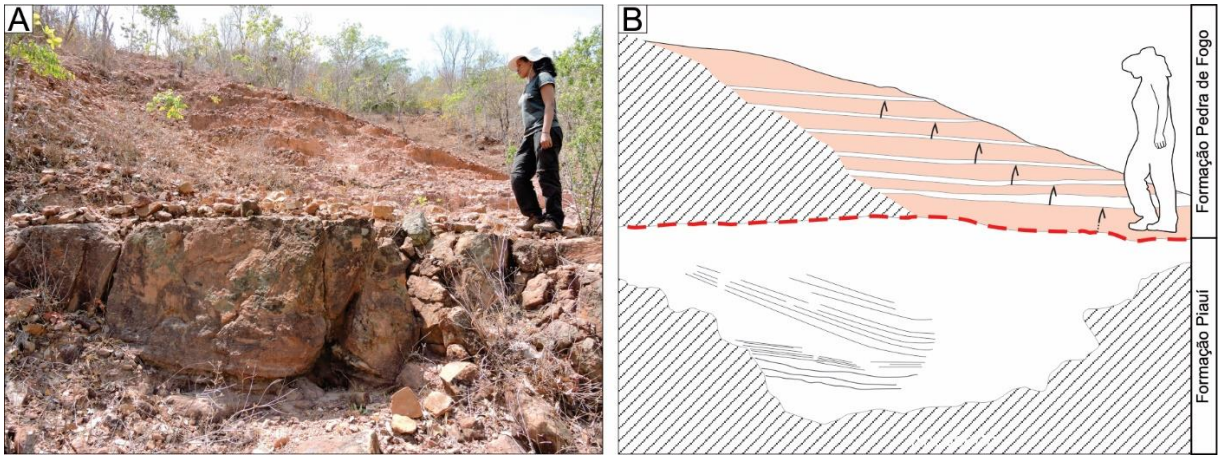

Figura 4-Característica geral da AF1. **A-B)** Delgadas camadas tabulares de arenito fino maciço (Aom) intercalada com pelito (fácies Pm) avermelhado igualmente maciço. Parte inferior da Formação Pedra de Fogo em contato com a Formação Piauí. "afloramento Morro da Pandora", região de Duque Bacelar-MA.

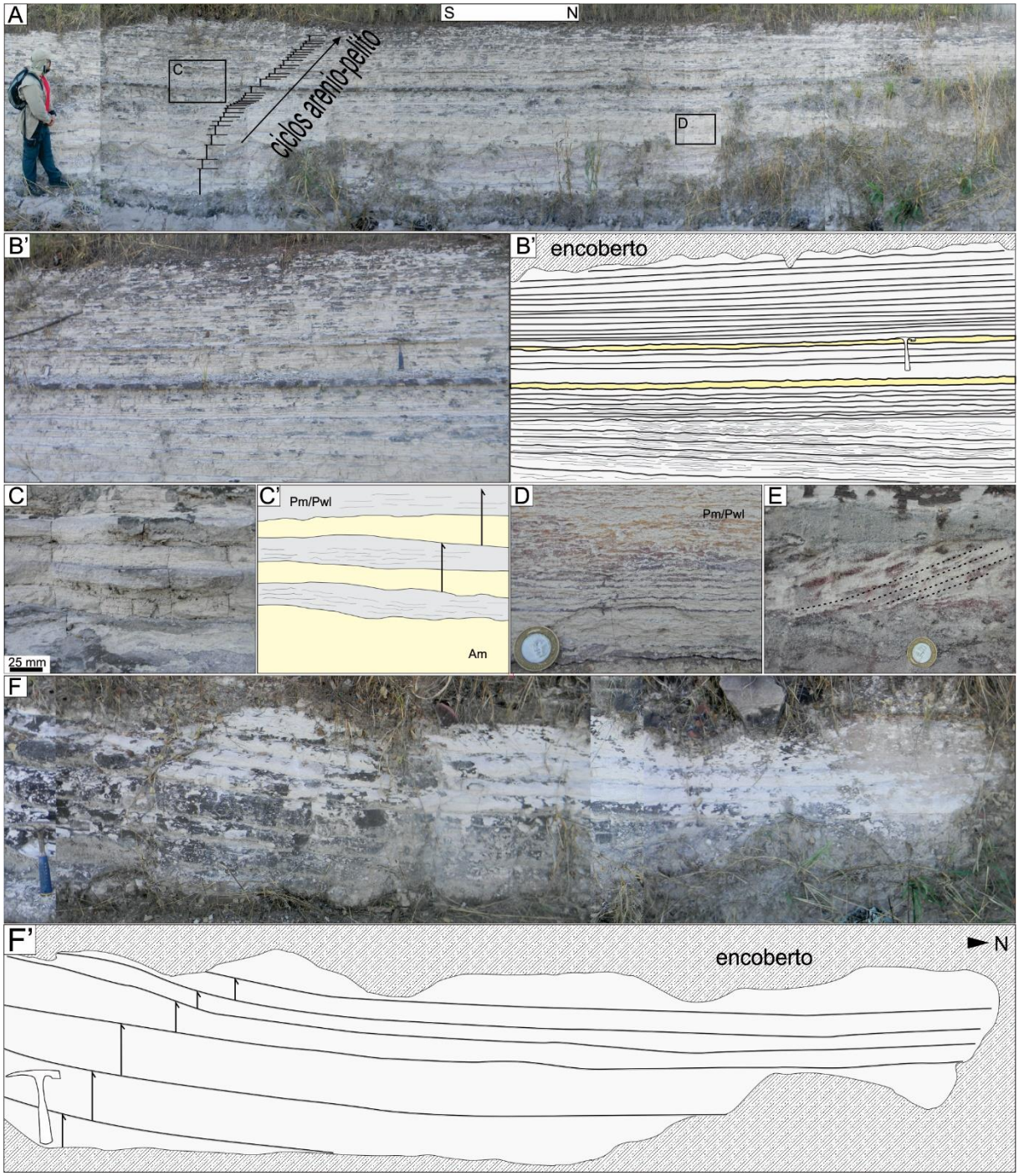

Figura 5- Característica geral da AF1 com camadas disposta em padrão *flat-lying*. **A)** Intercalação arenito muito fino (Aom)/pelito (fácies Pm/Pwl) com 32 ciclos centimétricos. **B-B')** Geometria fortemente tabular da fácies Aom. **C-C')** Detalhe dos ciclos Aom/Pm/Pwl. Notar a base plana da fácies Aom. **D)** Detalhe da fácies Pm/Pwl com acamamento *wave-linsen*. **E)** Lateralmente podem ocorrer laminações cruzadas (tracejado preto). **F-F')** Arenito com estratificação cruzada sigmoidal (As). Afloramento as margens da BR-153 em Frente a Santo Antônio, próximo a Colinas do Tocantins-TO.

A AF1 reflete deposição por suspensão em ambiente lacustre de clima árido, extenso e pouco profundo, com influxos esporádicos de correntes de turbidez (*underflow*s) e lobos em suspensão (*overflows*) sob regime de fluxos hiper e homopicnal, respectivamente, associados

a sistemas fluviais efêmeros gerados por eventos de rápida inundação (Renaut & Gierlowski-Kordesch 2010). Camadas de arenito fino de geometria tabular representam porções distais desses sistemas alimentadores não canalizados com correntes de turbidez resultantes de cheias esporádicas (Fisher et al. 2007; Tooth 1999). Eventos modernos de inundação ocorrem frequentemente em regiões áridas, com tempo de duração variando entre minutos a horas em um único pico do evento, ou se estender por dias (e.g. semanas) sendo alimentados por múltiplos picos de inundação (Lang et al. 2004; Reid & Frostick 1997; Tooth & Nanson 1995). Esses eventos deixam como registros característicos, delgadas camadas de arenito fino a grosso de geometrias tabulares, lateralmente extensas (*sandflats*) (Blair 2000; Tooth 1999).

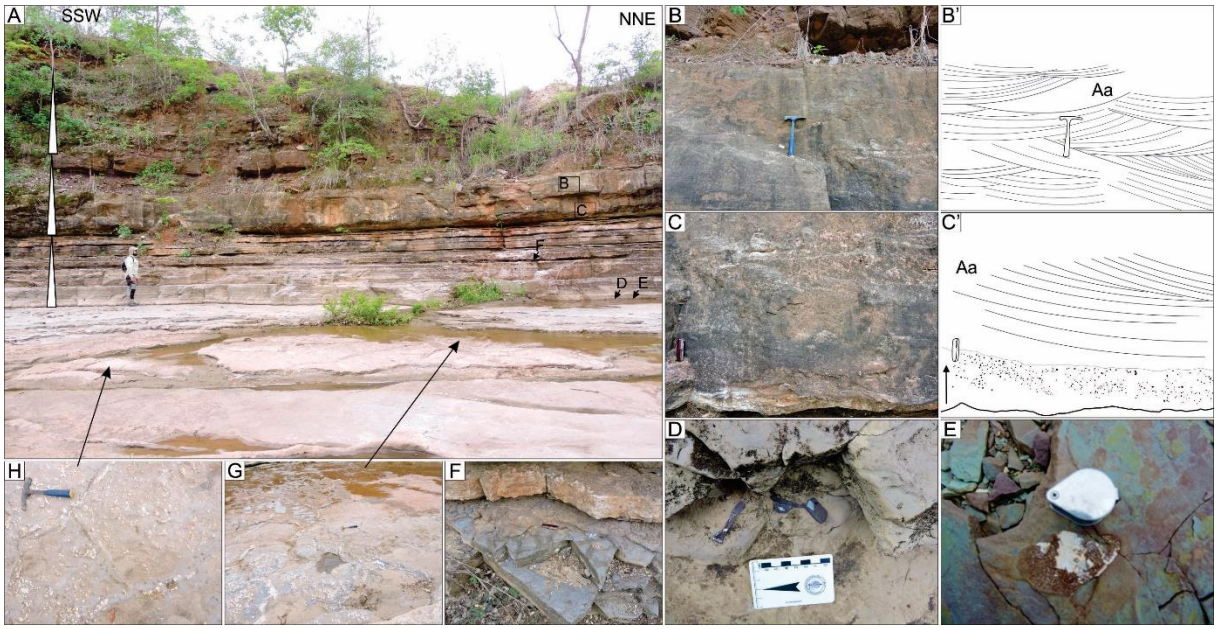

Figura 6- Característica geral da AF1. **A)** Ciclos gronodecrescentes ascendentes decimétricos (setas na porção esquerda superior da foto), formados por camadas tabulares (*flat-lying*) de arenitos fino a médio intercalados (fácies Aom e Aa) por pelitos da fácies Pm. **B-B')** Arenito fino a médio com estratificação cruzada acanalada (fácies Aa). **C-C')** Níveis de clastos de quartzo na base em padrão gronocrescente ascendente. **D-E)** Escamas fósseis de peixes desarticulados (espécie não-identificada) ocorre na base da fácies Pm. Afloramento no leito do riacho Pedra de Fogo, região de Nova Iorque-Pastos Bons-MA. **F)** Segundo nível de gretas de dissecação associada. Diferencia-se do primeiro nível pela ausência de evaporitos, e as dimensões centimétricas dos polígonos. **H, G)** Primeiro nível de gretas de dissecação com nódulos evaporíticos entre os polígonos. Observar as dimensões decimetricas dos polígonos.

Conforme Fisher et al. (2007), essa geometria em "lençol" (*sheet bodies*) pode resultar do posterior retrabalhamento por ondas e correntes lacustres a que esses depósitos ficam submetidos. De acordo com North & Davidson (2012), se o nível da água em um lago cair, a foz de um rio que anteriormente alimentou diretamente aquele lago ficará encalhada na paisagem como uma costa abandonada. Este é um fenômeno particularmente comum para lagos rasos localizados em regiões de clima quente e árido, alimentados por rios efêmeros, pois a taxa de recuo da costa desses lagos pode facilmente exceder a capacidade desses

fluviais (esporádicos) de estender seu canal através dos andares inferiores destes lagos. Satisfeita essas condições, após a retirada do lago, e no ponto em que o rio costumava encontrar a linha de costa lacustre, as águas que passam pelo canal mudam rapidamente de uma condição de confinamento lateral impostas pelas margens do canal, para uma condição onde não há nada para retê-las, permitindo assim que o fluxo se torne desconfinado ou não-confinando. A consequência é que a profundidade do fluxo diminui rapidamente pelo aumento da distância radial e a descompressão e desbaste pelo espalhamento do fluxo, o que gera deposição de sedimentos em camadas tabulares delgadas e extensas lateralmente diretamente sobre o leito plano desses lagos (Fisher et al. 2008; Lang et al. 2004). Para Renaut & Gierlowski-Kordesch (2010), dependendo da densidade do fluxo de inundação em relação à densidade do lago receptor, a carga de fundo pode ser levada por tração (*underflows*) sobre o leito lacustre até porções mais distantes das margens. Por outro lado, se a densidade do fluxo é menor que a densidade do lago, plumas em suspensão (*overflows*) com predomínio de sedimentos finos serão geradas, com predomínio de sedimentação por decantação.

Arenitos com estratificação cruzada acanalada e conglomerados maciços representam as porções proximais e ainda confinados no tronco principal desses sistemas de fluviais efêmeros alimentadores (Gibling & Rust 1984; Miall 1977; Miall 2010). A geometria sigmoidal indica rápida desaceleração do influxo sedimentar de caráter mesopicnal ao adentrar o meio lacustre de baixa energia, provavelmente com lâmina d'água pouco espessa, gerando progradação de lobos de suspensão nas partes proximais desses sistemas receptores (Nichols & Hirst 1998; Renaut & Gierlowski-Kordesch 2010).

As camadas tabulares de arenitos predominantemente finos e maciços são relacionadas tanto a fluxos potencialmente energéticos - dominados por carga de fundo, sugerido pelas eventuais ocorrências de *lags* de quartzo e sílex na base, além dos caules silicificados em posição concordante ao acamamento - assim como fluxos menos energéticos dominados por carga em suspensão, indicada pelo predomínio de arenitos com granulometria entre areia muito fina a fina (Figuras 4, 5).

A ausência de estruturas sedimentares pode ser em decorrência de inúmeras causas que imcluem: supressão das estruturas por altas concentrações de sedimentos em suspensão (Leeder 1999), deposição rápida de sedimentos fora do domínio da suspensão (Alexander et al. 2001; Tunbridge 1984), intenso retrabalhamento pós deposicional por organismos (Retallack 2001; Talbot et al. 1994;) e recristalização (Tucker 2001). Nós sugerimos que a principal causa para a ausência de estruturas sedimentares nesses arenitos são as altas concentrações de sedimentos em suspensão. Causas secundárias podem incluir rápida

deposição, e principalmente recristalização, dada as ocorrências de cimento carbonático, além da expressiva silicificação.

Durante o escoamento desses rios efêmeros, fragmentos de troncos expostos nas margens poderiam ser capturados e transportados para o interior das bacias lacustres, sendo posteriormente recobertos por pelitos. As porções periféricas desses lagos eram colonizadas por paleoflora, como é indicado pela ocorrência de troncos silicificados (Figura 9), muitos ainda em posição de vida (Figura 9 A, B).

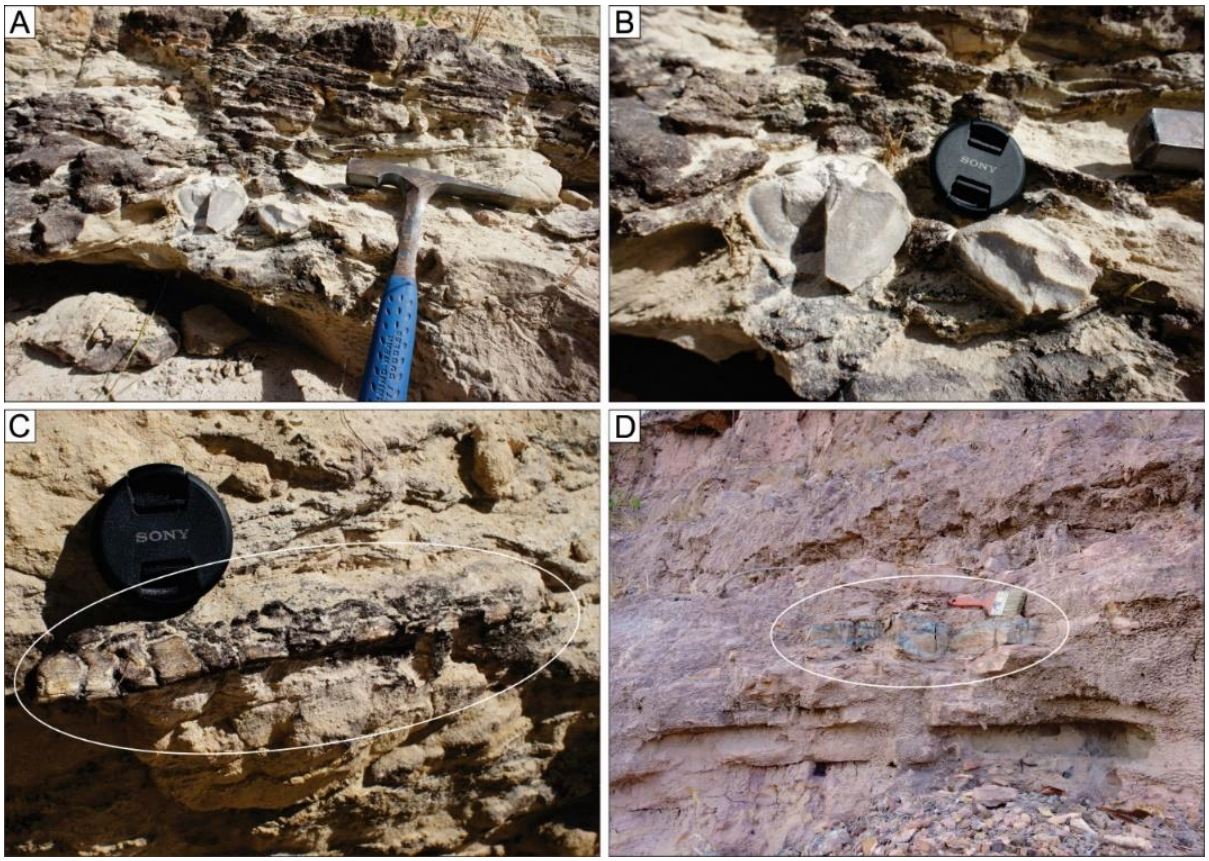

Figura 7- Característica geral da AF1. **A-B)** Fácies Cm com seixos de quartzo, eventualmente *cherts*. **C-D)** Caules de samambaia silicificados. A, B, C) Afloramento próximo a Bielândia-TO. D) Afloramento na MA-034 próximo a Duque Bacelar-MA.

.

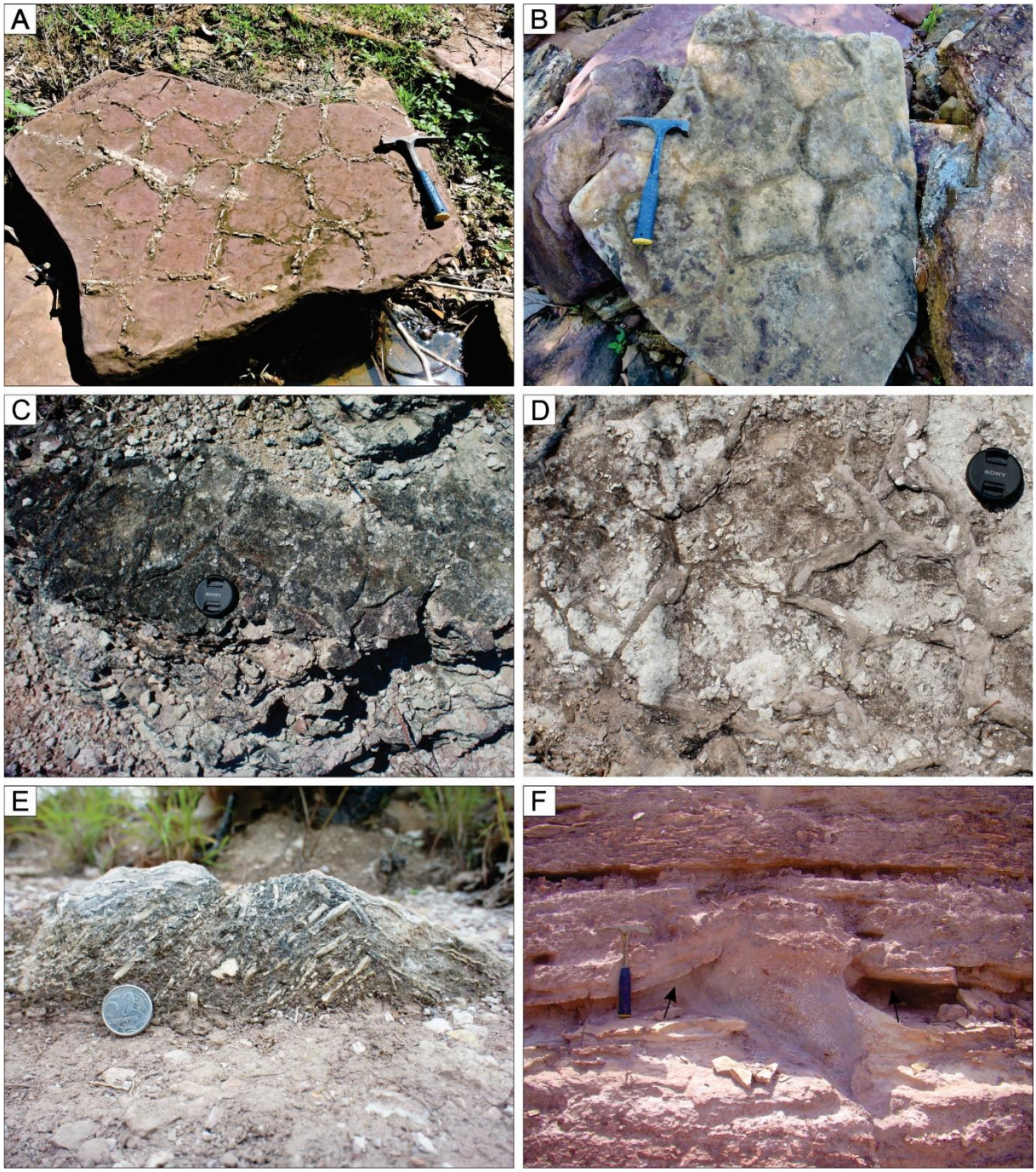

Figura 8- Gretas de dissecação e estruturas *tepees* ocorrem comumente na AF1. **A)** Gretas decimétrica associadas à fácies Pm. Nódulos evaporíticos ocorrem nos polígonos. **B)** Gretas associadas ao pelito/arenito muito fino, maciço. Os polígonos são marcados por relevos negativos. **C-D)** Gretas decimétricas com polígonos em relevo positivo. Cimento carbonático ocorre nos polígonos. **E)** Estrutura *tepees* centimétrica marcada por clastos silicificados tabulares arqueados. **F)** Estrutura *tepees* decimétrica marcada pelo arqueamento das camadas de arenito fino. Canalizações se desenvolvem associadas a estes *tepees.* A, B) Afloramento próximo a Monsenhor Gil-PI. C-E) Afloramento próximo a Bielândia-TO. F) Afloramento na rodovia estadual PI-130, próximo a Palmeirais-PI.

Figura 9-Caules silicificados de Gimnospermas e Samambaias da AF1. A-B) Caules silicificados de Gimnospermas em posição de vida (Legenda continua na próxima página).

(Continuação). **C-F)** Caules de gimnospermas rolados. **D)** Observar o alargamento em uma das extremidades do tronco adernado (setas amarelas), indicativo de sua base. **G)** Caules de gimnosperma semi-adernado (setas amarelas). **H)** Caules silicificados de Samambaias. Observar a estruturação interna preservada, núcleo e casa. A-F) Afloramentos na região de Duque Bacelar-MA. G) Afloramento no Parque Floresta Fóssil, margem direita do rio Poti, Teresina-PI.

A ocorrência de gretas de dissecação associadas a nódulos evaporíticos, além de estruturas *tepees*, são condizentes com lagos extensos e rasos, com elevada salinidade, associadas a altas taxas de evaporação, configurando balanço hídrico negativo relacionado à *sabkha* continental ou *playa* (Briere 2000; Lowenstein & Hardie 1985; Smoot & Lowenstein 1991). A sedimentação da AF1 provavelmente envolvia interações sazonais com oscilação do nível dos lagos em reposta a períodos de maior aridez climática; indicado por precipitações químicas (evaporitos), e exposições cíclicas de suas margens, evidenciada pela ocorrência de gretas de contração e *tepees*. E períodos de menor aridez; com predomínio de decantação de pelitos, e aumento do influxo de terrígenos carreados por rios efêmeros, bem como pela colonização de suas margens por vegetais, evidenciada pela massiva ocorrência de troncos fósseis.

A boa preservação das estruturas organosedimentares e principalmente dos troncos, fundamentalmente aqueles em posição de vida é sugestiva de silicificação sindeposicionais eogenética (Folk & Pittman 1971; Hesse 1989; Milliken 1979).

Nearshore lacustre dominado por ondas (AF2)

A AF2 é constituída por arenito com laminação ondulada a maciço (Aom), arenito com laminação truncada por onda (Alo) e Arenito fino com estratificação cruzada *hummocky* (Ah). Esta associação ocorre intercalada a AF1. São arenitos finos a médio, com predomínio de médios (Figura 10), com laminações onduladas, simétricas e assimétricas, laminações truncadas por ondas e arenitos com estratificação cruzada *hummocky* são frequentes na parte inferior da Formação Pedra de Fogo (Figura 11). Arenito com estratificação cruzada *hummocky* tende a ser menos frequente para a parte superior (Figuras 3 e 11). A ocorrência de laminações onduladas e laminações cruzadas truncadas por ondas são indicativas da ação de ondas produzidas pelo vento em períodos de tempo bom, induzindo uma baixa velocidade orbital em águas rasas com profundidades máximas de poucos centímetros, suficiente para a superfície da onda retrabalhar o substrato (Pochat et al. 2005). Por outro lado, a ocorrência de estratificação cruzada *hummocky* sugere períodos em que o vento atingiu energia suficiente para produzir ondas de tempestades (Dott & Bourgeois 1982; Dumas & Arnott 2006; Greenwood & Sherman 1986). Ondas de tempestades em sistemas lacustres são associadas às

porções costeiras (*nearshore*) (Allen 1981; Duke 1985; Eyles & Clark 1986; Greenwood & Sherman 1986; Li et al. 2014; Renaut & Gierlowski-Kordesch 2010; Wang et al. 2015). A ocorrência de estruturas características de ondas de tempestades (Harms et al. 1975), sugere que os lagos Pedra de Fogo eram suficientemente extensos para que o *fetch* possibilitasse que os ventos induzissem uma alta velocidade orbital gerando fluxos oscilatórios mais rápidos que 50 cm/s, e sob um período de tempo de até 10 s (Dumas & Arnott 2006).

Aspectos petrográficos e mineralógicos

A análise petrográfica foi realizada somente nos arenitos de AF2, que foram classificados como quartzo arenitos (*sensu* Folk, 1968). De forma geral, apresentam granulometria entre areia fina e areia média, com predomínio de areia média (0,25-0,4 mm). Eventualmente ocorrem grãos de granulometria areia grossa (0,8 mm). Os grãos são mal a moderadamente selecionados, muito angulosos a subarredondados (Figuras 10A-D). A esfericidade é múltipla, com predomínio da esfericidade baixa. O arcabouço é fechado, com índice de empacotamento de 67%. Os contatos são principalmente retos (84%), com menores proporções de pontuais (9%) e côncavo-convexos (7%). Apresentam como principal componente detrítico quartzo monocristalino, com proporções médias de 96,03% e, secundariamente, intraclastos (2,30%) e feldspatos (1,67%). Os grãos de quartzo são monocristalinos, esporadicamente policristalinos. Muitos grãos apresentam extinção ondulante, e bordas com múltiplas concavidades, profundamente corroídas (Figuras 10E, F). Os intraclastos são principalmente grãos detríticos de chert, arredondados e com esfericidade alta. O aspecto fibroso destes grãos indica provavelmente calcedônia (Figuras 10C). Feldspatos são raros e/ou estão alterados da caulinita (K) (Figuras 10H). Micas e minerais pesados ocorrem em proporções inferiores a 1%. Muitas micas estão recurvadas ou quebradas por efeito da compactação mecânica (Figuras 10D). A pseudomatriz ocorre como clastos dúcteis deformados e são relativamente frequentes (Figuras 10G). Caulinita ocorre como produto de alteração de feldspatos (Figuras 10I). A porosidade tem distribuição inomogênea, é fundamentalmente intergranular, com menores proporções de poros móldicos e intragranular. Muitos poros são agigantados.

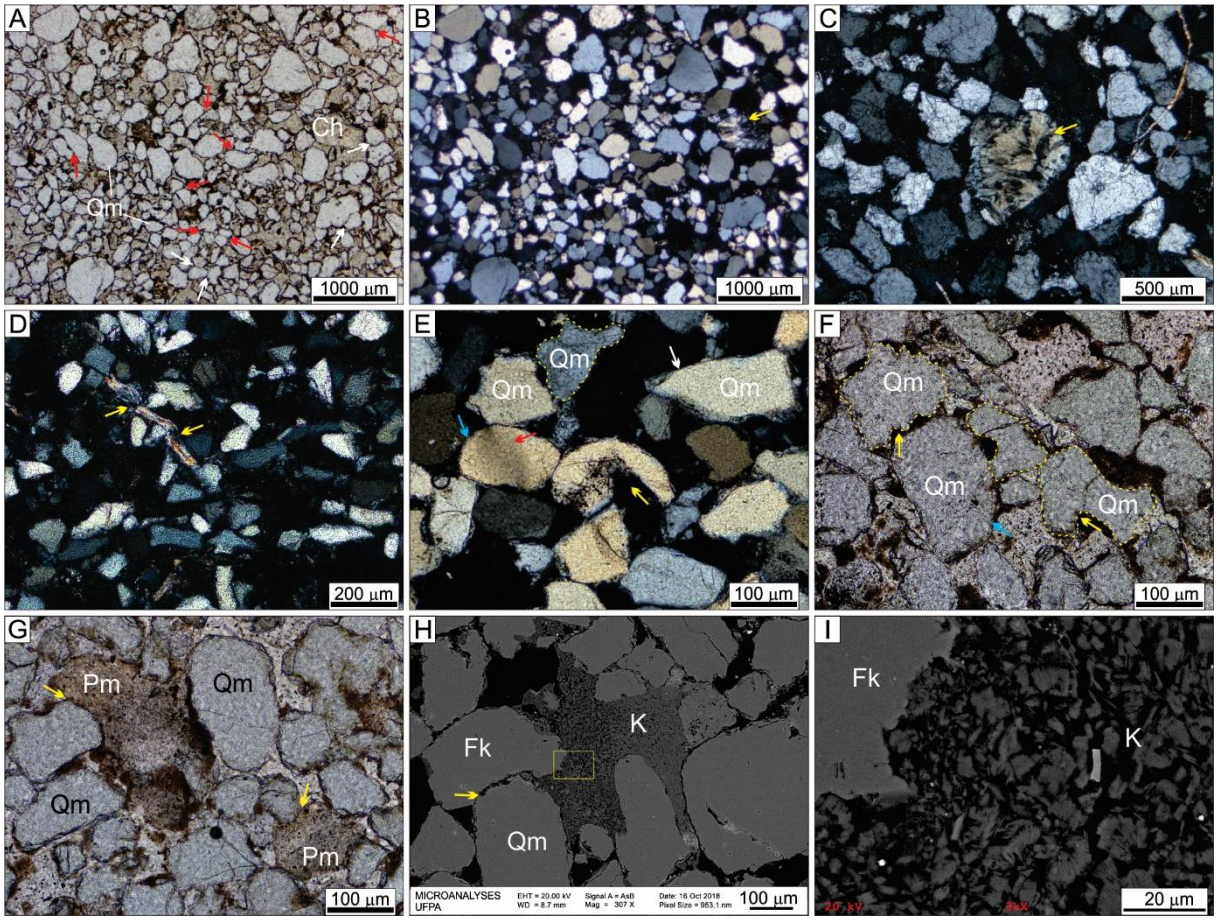

Figura 10- Fotomicrografias do quartzo arenito representativo da AF2. **A-B)** Aspecto geral do arcabouço formado predominantemente por grãos de quartzo monocristalinos (Qm) e grãos detríticos de chert (Ch-seta amarela). Grãos mal a moderadamente selecionados, muito angulosos a subarredondados, esfericidade alta. Predomínio da granulometria entre areia fina e média, esporadicamente areia grossa. Observar o predomínio de contatos restos (setas vermelhas), e secundariamente côncavo-convexos (setas brancas). **C)** Grão detrítico de chert. O aspecto fibroso (seta amarela) indica provavelmente calcedônia. **D)** Muscovita parcialmente rompida pelo efeito da compactação mecânica (setas amarelas). **E-F)** Grãos de quartzo monocristalino (Qm), com fraca extinção ondulante (seta vermelha). Observar os aspectos morfológicos dos grãos desde muito angulosos (seta branca), com formas irregulares (tracejado amarelo) e esfericidade baixa, até muito arredondados (seta azul). Comumente os grãos de quartzo apresentam bordas profundamente corroídas (setas amarelas). **G)** Pseudomatriz (Pm) na forma de grãos de argila esmagados (setas amarelas). **H)** Imagem de MEV (elétrons secundários) mostrando grão de quartzo em contato concâvo-convexo com provável grão detrítico de feldspato (Fk), alterando para caulinita (K) (retângulo amarelo). **I)** Imagem de MEV (elétrons secundários) mostrando cristais pseudohexagonais de caulinita arranjados sob forma de livretos.

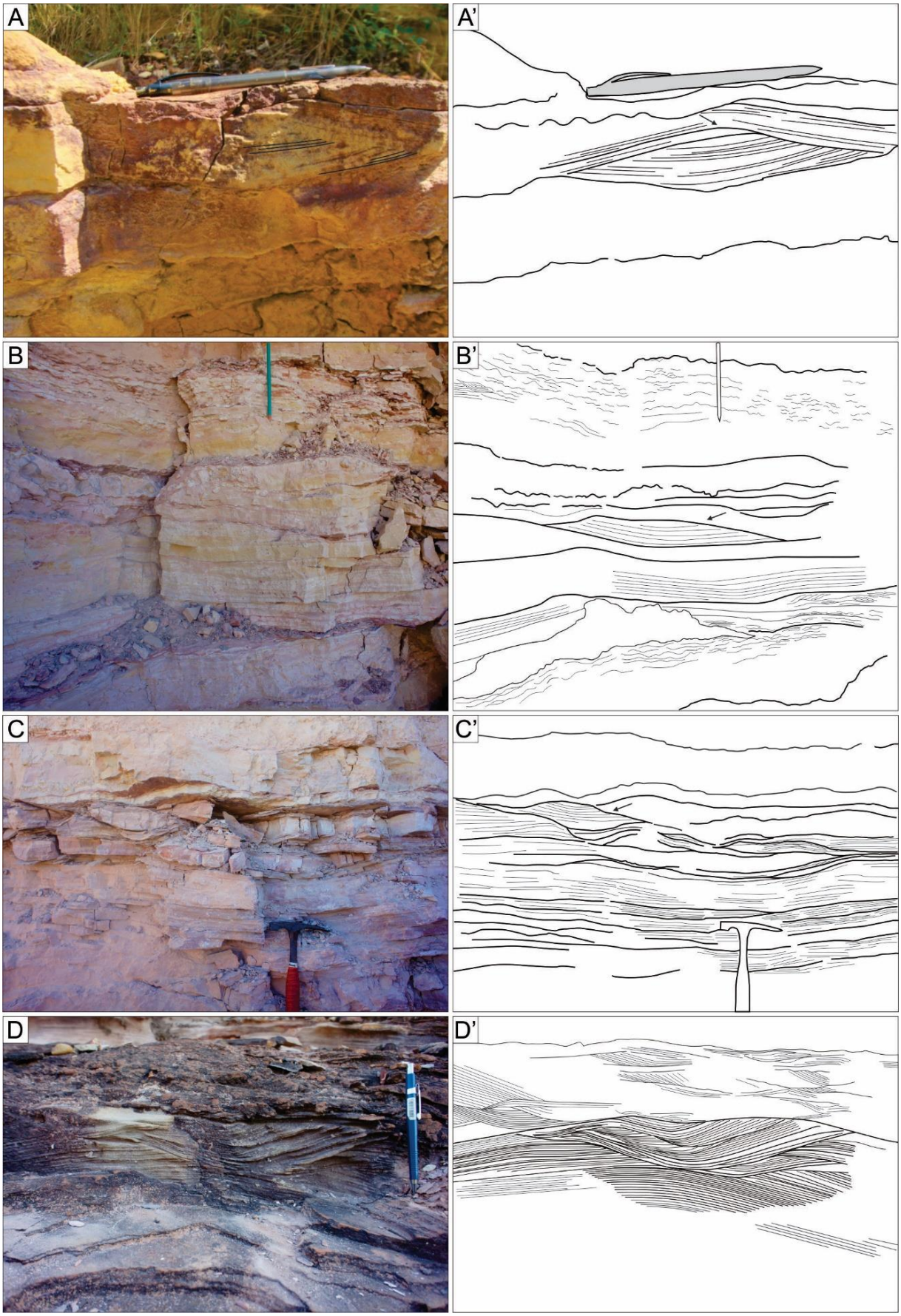

Figura 11-Depósitos representativos da AF2. A ocorrência de estratificação cruzada hummocky é relativamente comum na AF2. (Legenda continua na próxima página)

(Continuação). **A-A')** Estratificação cruzada *hummocky* anisotrópica mostrando uma nítida simetria entre a superfície basal escavada e um bem definido antiforme ou *hummock*, truncando laminações internas características dessas estruturas. **B-B')** Estratificação cruzada *hummocky* com suave superfície de escavação truncada lateralmente por superfície antiforme. **C-C')** Estratificação cruzada *hummocky* isotrópica (seta). **D-D')** Estratificação cruzada *hummocky* mostrando suavizado antiforme excepcionalmente claro (centro) truncando lateralmente pronunciada superfície de escavação

Lacustre central (AF3)

A AF3 ocorre na parte superior da sucessão estudada, diretamente sobreposta a Associação AF1, e/ou em variação lateral com esta (Figura 12). A Associação AF3 constitui uma sucessão de até 30 m de espessura, com pelitos avermelhados maciço, eventualmente laminado (fácies Plm) com até 2 m de espessura, contendo camadas tabulares centimétricas de arenito fino a síltico, com laminação ondulada a maciço, eventualmente cruzada, e por vezes com cimento carbonático (fácies Aom). Os ciclos têm tendências granodecrescente ascendente.

Esta associação foi gerada em ambiente de baixa energia, em processos de sedimentação contínua com predomínio de decantação (fácies Plm e Am). Eventuais influxos de areia provenientes de fluxos não-confinados advindos de suas margens depositavam extensas e delgadas camadas de arenito fino de geometria tabular (fácies Aom). Essas camadas sobre o substrato lacustre provavelmente eram submetidas ao retrabalhameto por ondas durante os períodos de queda do nível lacustre e redução da coluna de água. Estas características são condizentes com sedimentação nas porções mais centrais de sistemas lacustres áridos, eventualmente afetados pelas porções distais de eventos de inundação (Renaut & Gierlowski-Kordesch 2010; Talbot & Allen 1996). A espessura total desta associação de cerca de 30 m, com camadas de pelito da fácies Plm com até 18 m de espessura contínua, é atribuída a um aumento na taxa de subsidência durante a fase final de sedimentação da sucessão estudada.

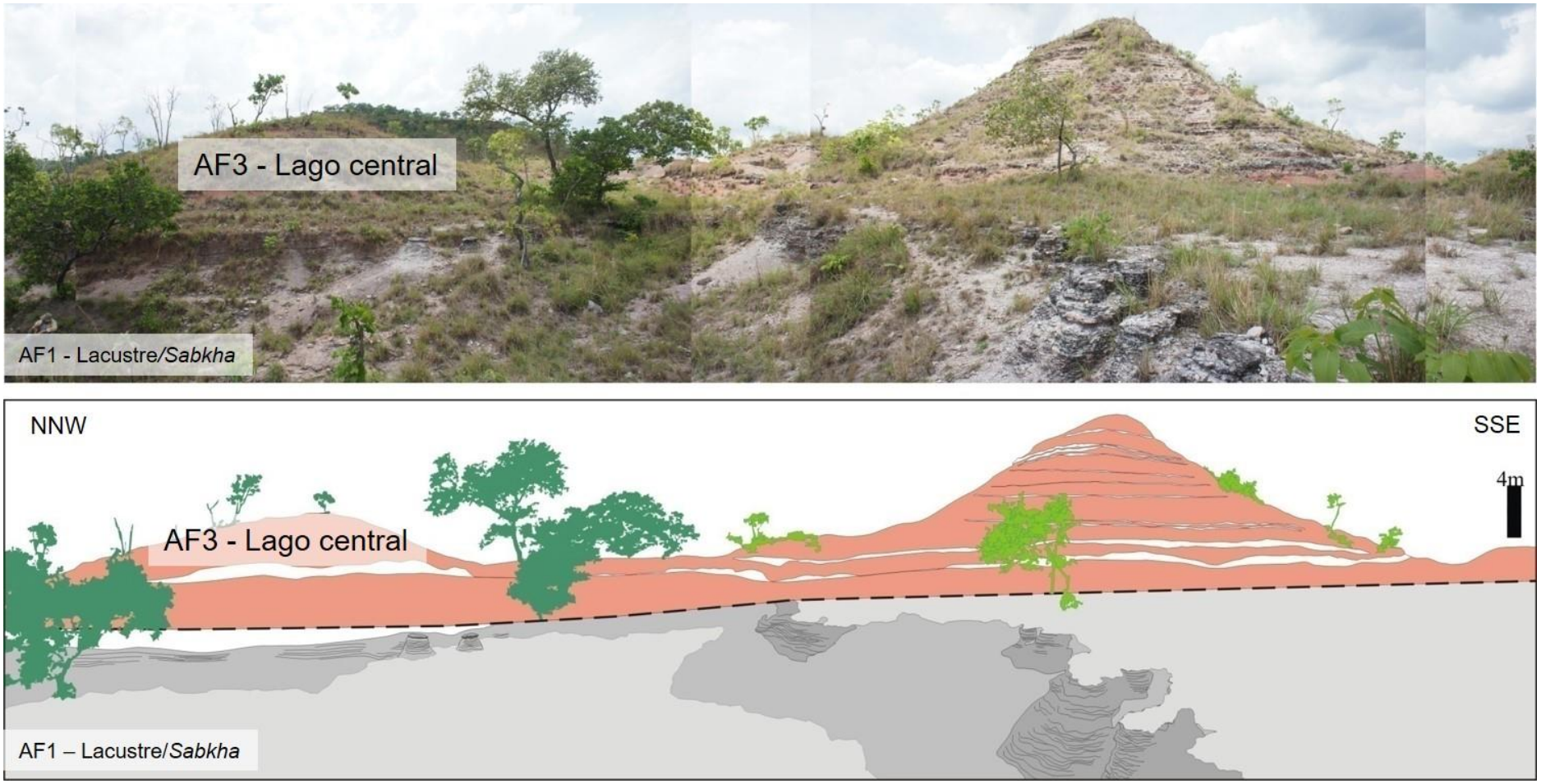

Figura 12- Seção mostrando o aspecto geral da Associação AF3 – Lacustre central recobrindo a Associação AF1. Notar as espessas camadas de pelito avermelhado e maciço, intercalados com delgadas camadas tabulares de arenito muito fino. Afloramento no km 39 da rodovia TO-222, próximo ao município de Araguaína-TO.

DISCUSSÕES

Ambientes lacustres constituem excelentes indicadores paleoclimáticos (Johnson 1984; Talbot & Allen 1996; Pochat et al. 2005). Os depósitos estudados sugerem que durante o início do Permiano, um extenso sistema lacustre raso com planícies de sabkha adjacentes se implantou discordantemente sobre os depósitos flúvio-eólicos da Formação Piauí (Figura 13). Essa configuração estratigráfica indica uma elevação no nível de base local, condicionada por subida do nível freático (Catuneanu 2011; Kocurek 1988; Shanley & McCabe 1994). A intercalação cíclica entre camadas de arenito com geometria tabular/em lençol (*sheet sandstone beds*), e pelitos relativamente mais espessos, sugere que esses lagos eram alimentados por uma rede de fluviais efêmeros com prevalência de fluxos não-confinados, diretamente depositado sobre substratos lacustres planos, rasos e lateralmente extensos. Esse padrão geométrico é comum em registros análogos antigos e recentes (Fisher et al. 2007; Fisher et al. 2008; Lang et al. 2004; Nichols & Fisher 2007; North & Davidson 2012; Tooth 1999).

As múltiplas camadas de arenito amalgamadas, concentrados principalmente na parte central-inferior da sucessão estudada, indicam alta frequência dessas correntes efêmeras alimentadoras deste sistema lacustre durante sua fase inicial de implantação. A ocorrência relativamente comum de estratificação cruzada *hummocky* na parte inferior da sucessão estudada sugere que esse sistema lacustre era comumente afetado por eventos de tempestades (Duke 1985; Marsaglia & Klein 1983). Estes regimes de tempestades eram provavelmente causados pela prevalência de um clima fortemente sazonal, condicionado por sistemas de megamonções dominantes durante o início do Permiano em toda a parte centra do Pangeia (Parrish 1990). Além disso, a frequência de estratificação cruzada *hummocky* sugere que esse sistema lacustre era grande o suficiente para possibilitar um *fetch*, que permitia que os ventos de tempestades atingissem velocidades suficientemente altas para movimentar a superfície lacustre, gerando fluxos oscilatórios rápidos, e com tempo de propagação das ondas compatíveis para a formação da estratificação cruzada *hummocky* (Dott & Bourgeois 1982; Duke 1985; Dumas & Arnott 2006; Eyles & Clark 1986).

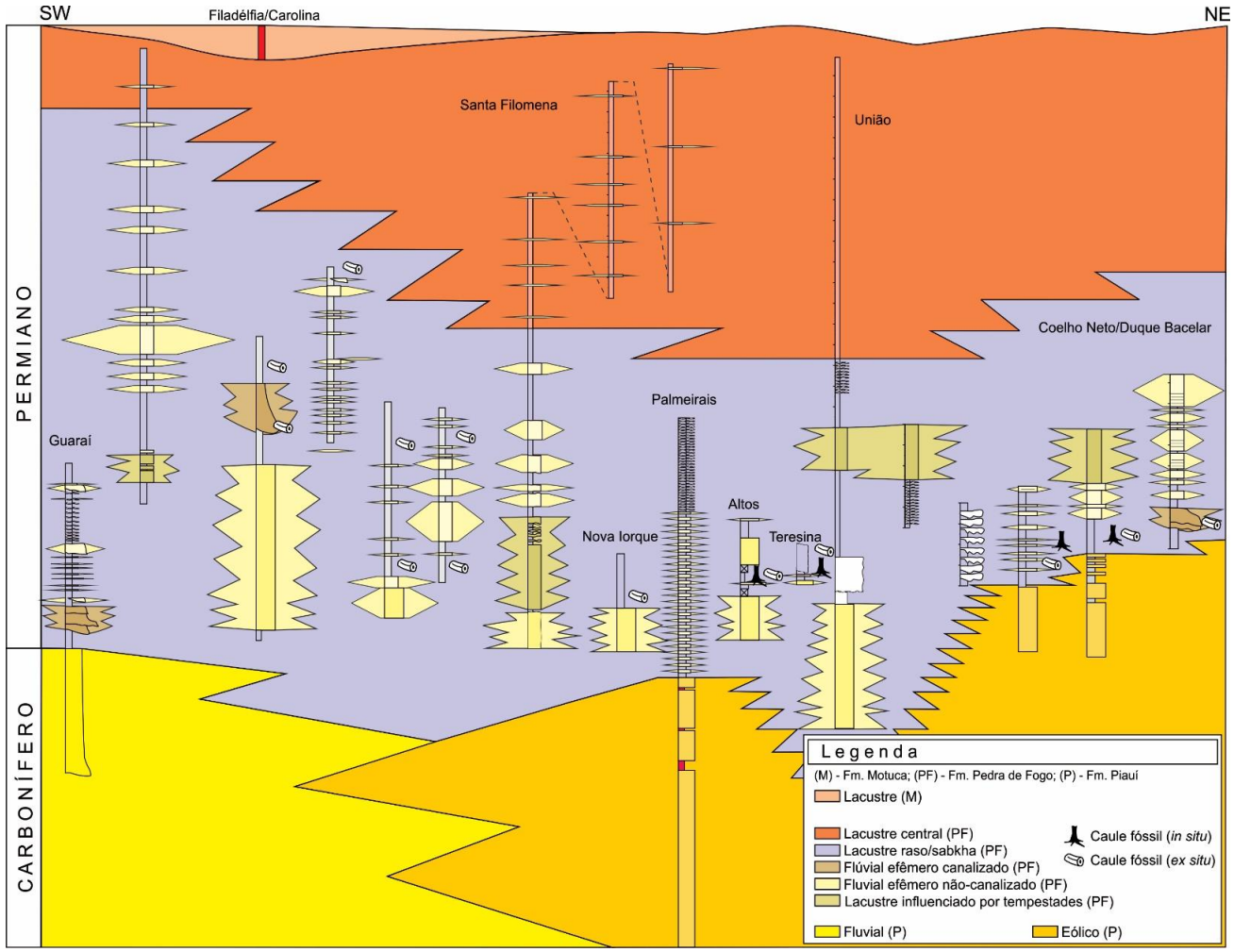

Figura 13-Seção estratigráfica simplificada da sucessão sedimentar da Formação Pedra de Fogo, que recobre discordantemente os arenitos Fúlvio-eólicos da Formação Piauí ao longo das bordas leste, sul e oeste da Bacia do Parnaíba (Legenda continua na próxima página)

(Continuação). A parte inferior da seção pertencente à Formação Pedra de Fogo é formada por sistemas lacustres rasos-sabkha, ciclicamente intercalada por múltiplos e frequentes eventos de inundações efêmeras registrados por depósitos de fluviais efêmeros predominantemente não-canalizados. Núcleos da paleoflora Pedra de Fogo ocorrem concentrados nesta porção da sucessão. Evidências de eventos de tempestades ocorrem ao longo da faixa inferior da Formação Pedra de Fogo, e é reduzida ou ausente para o topo. A parte superior é dominada por depósitos relacionados as porções centrais do sistema lacustre, com predomínio de sedimentação pelítica, e infrequentes intercalações com delgadas camadas de arenito. A sucessão Pedra de Fogo é recoberta concordantemente por depósitos predominantemente pelíticos e igualmente lacustres da Formção Motuca.

A presença massiva de caules silicificados de grandes dimensões (até 5,35 m de comprimentos e 1,15 m de diâmetro; *ver* Conceição et al. 2016), muitos em posição de vida, concentrados na porção basal da sucessão, é indicativo de períodos de maior umidade relativa nesse sistema lacustre, durante a fase inicial de implantação deste sistema (Conceição et al., 2016, DiMichele et al., 2009; Iannuzzi et al., 2018). Por outro lado, a pouca espessura dos pelitos, e o aspecto fortemente oxidado sugere lagos relativamente rasos sem estratificação da coluna d'água. A ocorrência frequente de gretas de contração, estruturas *tepees* e nódulos evaporíticos, indicam períodos de elevadas temperaturas, com contração do sistema lacustre e provável exposição da planície lacustre. Nessas regiões, condicionadas pelas altas taxas de evaporação e provável elevada salinidade do lençol freático ocorriam a precipitação de cristais evaporíticos-carbonáticos na interface da zona capilar próxima da superfície (Lowenstein 1987; Schubel & Lowenstein 1997; Warren 2000). Esses depósitos são frequentes ao longo de toda a sucessão estudada.

A porção central superior da sucessão é dominada por espessos pacotes de pelitos, eventualmente interrompidos por delgadas camadas de arenito, sugerindo aumento na taxa de subsidência e redução na frequência dos eventos de inundação fluvial (Figura 13). Estes fatores, aliado a ausência de estratificações cruzadas *hummocky*, indicam cessação dos regimes de tempestades e diminuição da periodicidade, e provavelmente da magnitude dos eventos de inundação. A sobreposição em contato concordante dos pelitos avermelhados maciços, e igualmente lacustres da Formação Motuca (Abrantes Jr. & Nogueira 2013; Plummer 1946), com presença mais expressiva de depósitos evaporitícos (Abrantes Jr. et al. 2016), é interpretado como prevalência crescente das condições climáticas áridas e aumento na taxa de subsidência. Conforme Góes et al. (1990), o Grupo Balsas marca o início da continentalização na Bacia do Parnaíba. A formação do supercontinente Pangeia durante o

final do Pernsilvaniano e início do Cisuraliano, aliada a um aumento das temperaturas globais, submeteu a parte central do Pangeia a condições de crescente aridez (Benison et al. 1998; Boucot et al. 2013 Chumakov & Zharkov 2002; Zambito & Benison 2013). Esta tendência paleoclimática global é registrada na sucessão estudada pela alta frequência de depósitos fluviais efêmeros não-canalizados, intercalados por pelitos lacustre com repetidos registros de eventos de tempestades, principalmente na base da sucessão (Fig. 13). Para o topo, esses eventos de tempestades tendem a minguar ou se extinguir. Esta sucessão é recoberta pelos pelitos da Formação Motuca. A monotonia litológica dos depósitos da Formação Motuca, provavelmente representam condições climáticas permanentemente mais áridas, com redução ou ausência das condições sazonais indicadas pela ciclicidade, e múltipla variedade litológica da Formação Pedra de Fogo. O registro desta sedimentação cíclica relacionada ao extenso sistema lacustre de clima árido descrito neste estudo, indica que durante no início do Permiano-Cisuraliano (Cisneros et al. 2015), a deposição da Formação Pedra de Fogo, se estendia ao longo das bordas leste, sul e oeste da Bacia do Parnaíba, e estava fortemente condicionada por regime de sazonalidade climática prevalescente neste período na porção oeste-central do Pangeia (Parrish 1990; Parrish 1993; Kutzbach & Gallimore 1989).

CONCLUSÃO

A elaboração de uma seção estratigráfica feita com dezoito perfis sedimentares na Formação Pedra de Fogo, ao longo das bordas leste, sul e oeste da Bacia do Parnaíba, permitiu visualizar de forma mais ampla e abrangente o conjunto de subambientes deposicionais que formam esta unidade sedimentar.

Foram definidas 10 fácies sedimentares agrupadas em três associações de fácies: *Sabkha*-Lacustre com rios efêmeros (AF1); *Nearshore* lacustre dominado por ondas (AF2), e Lacustre central (AF3).

O sistema lacustre da Formação Pedra de Fogo era constituído por lagos extensos e rasos, alimentados por múltiplos eventos de inundação com predomínio de fluxos não-confinados. Estes lagos eram constantemente afetados por eventos de tempestades registrados pela frequente ocorrência de estratificação cruzada *hummocky*, concentrada principalmente na base da sucessão. Submetidos a um padrão climático dominantemente árido, mas sob forte condicionante sazonal, esses lagos constantemente sofriam expansão e contração de suas de sua massa d'água, com migração de sua linha de costa. Durante os períodos de maior aridez relativa, a exposição da planície lacustre era sítio de precipitação evaporítica, com formação de estruturas *tepees* e desenvolvimento de gretas de dessecação. Por outro lado, nos períodos

de maior umidade relativa, sua periferia era colonizada por uma pujante tafoflora, formada fundamentalmente por samambaias e gimnospermas de médio a grande porte.

A multiplicidade e pouca espessura da intercalação cíclica pelito/arenito das associações AF1 e AF2, indicam que durante a sedimentação da porção inferior da Formação Pedra de Fogo, a taxa de subsidência manteve-se relativamente estável, enquanto o nível freático oscilou sazonalmente. O aumento significativo na espessura das camadas de pelito, e a diminuição na frequência e espessuras das camadas de arenito para o topo da sucessão (AF3) sugerem maior estabilização no nível freático, aumento na taxa de subsidência, e redução ou interrupção dos eventos de inundação e de tempestades. Todo esse conjunto de rochas, de forma heterogênea, encontra-se afetado por silicificação eo-mesodiagenética. Estes fatores provavelmente estão relacionados à tendência paleoclimática global de estabilização de condições quentes e áridas prevalecente no final do Paleozoico.

Este estudo constitui importante contribuição para o entendimento das mudanças paleoambientais, paleogeográficas e paleoclimáticas ocorridas na porção oeste-central do Pangeia durante o início do Permiano (Cisuraliano).

AGRADECIMENTOS

Agradecemos à Coordenação de Aperfeiçoamento de Pessoal de Nível Superior (CAPES, código de financiamento 001) e Conselho Nacional de Pesquisa (CNPq no.141968/2016-8) pela concessão da bolsa de doutorado. Ao Programa de Pós-Graduação em Geologia e Geoquímica da Universidade Federal do Pará (UFPA) pelo apoio institucional. Ao Laboratório de Microscopia Eletrônica da UFPALABMEV.

REFERÊNCIAS

Abrantes Jr., F.R., & Nogueira, A.C.R., 2013, Reconstituição paleoambiental das formações Motuca e Sambaíba, Permo-Triássico da Bacia do Parnaíba no sudoeste do Estado do Maranhão, Brasil: Geologia USP, Série Científica, v. 13, p. 65-82.

Abrantes Jr., F.R., Nogueira, A.C.R., & Soares, J.L., 2016, Permian paleogeography of west-central Pangea: Reconstruction using sabkha-type gypsum-bearing deposits of Parnaíba Basin, Northern Brazil: Sedimentary Geology, v. 341, p. 175-188.

Abrantes Jr., F.R., Nogueira, A.C.R., Andrade, L.S., Bandeira, J., Soares, J.L., & Medeiros, R.S.P., 2019, Register of increasing continentalization and palaeoenvironmental changes in the west-central pangaea during the Permian-Triassic, Parnaíba Basin, Northern Brazil: Journal of South American Earth Sciences, v. 93, p. 294-312.

Aguiar, G.A., 1964, Semi-detalhe da região de sudoeste de Balsas [Relatório 21BM]: PETROBRÁS, DIREX/RENOR, 40 p.

Alexander, J., Bridge, J.S., Cheel, R.J., & Leclair, S.F., 2001, Bedforms and associated sedimentary structures formed under supercritical water flows over aggrading sand beds: Sedimentology, v. 48, p. 133-152.

Allen, P.A., 1981, Wave-generated structures in the Devonian lacustrine sediments of south-east Shetland and ancient wave conditions: Sedimentology, v. 28, p. 369-379.

Andrade, L.S., Nogueira, A.C.R., & Silva Junior, J.B.C., 2014, Evolução de um sistema lacustre árido Permiano, parte superior da Formação Pedra de Fogo, borda oeste da Bacia do Parnaíba: Geologia USP, Série Científica, v. 14, p. 39-60.

Araújo, R.N., Nogueira, A.C.R., Bandeira, J., & Angélica, R.S., 2016, Shallow lacustrine system of the Permian Pedra de Fogo Formation, Western Gondwana, Parnaíba Basin, Brazil: Journal of South American Earth Sciences, v. 67, p. 57-70.

Barbosa, O., & Gomes, F. de A., 1957, Carvão mineral na Bacia do Tocantins-Araguaia: Departamento Nacional de Produção Mineral, Divisão Geologia e Mineralogia, Boletim, v. 174, p. 1-34.

Benison, K.C., Goldstein, R.H., Wopenka, B., Burruss, R.C., and Pasteris, J.D., 1998, Extremely acid Permian lakes and groundwaters in North America: Nature, v. 392, p. 911–914

Blair, T.C., 2000, Sedimentology and progressive tectonic unconformities of the sheetflood-dominated Hells Gate alluvial fan, Death Valley, California: Sedimentary Geology, v. 132, p. 233–262.

Blakey, R.C., 2008, Gondwana paleogeography from assembly to breakup - A 500 m.y. odyssey, *in* Fielding, C.R., Frank, T.D., & Isbell, J.L., eds., Resolving the late Paleozoic ice age in time and space: Geological Society of America, Special Paper, v. 441, p. 1-28.

Boucot, A.J., Chen, X., Scotese, C.R., & Morley, R.J., 2013, Phanerozoic Paleoclimate: An Atlas of Lithologic Indicators of Climate: SEPM, Concepts in Sedimentology and Paleontology, v. 11, 478 p.

Briere, P.R., 2000, Playa, playa lake, sabkha: Proposed definitions for old terms: Journal of Arid Environments, v. 45, p. 1–7.

Caldas, E.B., Mussa, D., Lima Filho, F.P., & Rosier, O., 1989, Nota sobre a ocorrência de uma floresta petrificada de idade permiana em Teresina, Piauí: Boletim do Instituto de Geociências da USP, Publicação Especial, Paleobotânica e Palinologia na América do Sul, v. 7 p. 69-87.

Catuneanu, O., 2011, Principles of Sequence Stratigraphy: Elsevier Science, 375 p.

Chumakov, N.M., & Zharkov, M.A., 2002, Climate during Permian–Triassic Biosphere Reorganizations, Article 1: Climate of the Early Permian. Stratigraphy and Geological Correlation, v. 10, p. 586–602.

Chumakov, N.M., & Zharkov, M.A., 2003, Climate during the Permian–Triassic Biosphere Reorganizations. Article 2. Climate of the Late Permian and Early Triassic: General Inferences: Stratigraphy and Geological Correlation, v. 11, p. 361–375.

Cisneros, J.C., Abdala, F., Rubidge, B.S., Dentzien-Dias, P.C., and Bueno, A.O., 2011, Dental Occlusion in a 260-Million-Year-Old Therapsid with Saber Canines from the Permian of Brazil: Science, v. 331, p. 1603-1605.

Cisneros, J.C., Marsicano, C., Angielczyk, K.D., Smith, R.M.H., Richter, M., Fröbisch, J., Kammerer, C.F., & Sadleir, R.W., 2015, New Permian fauna from tropical Gondwana: Nature Communications, v. 6, p. 8676.

Coimbra, A.M., & Mussa, D., 1984, Associação lignitatoflorística na Formação Pedra de Fogo (Arenito Cacunda), Bacia do Maranhão - Piauí, Brasil: Congresso Brasileiro de Geologia, 33, Rio de Janeiro, Anais, v. 2, p. 591-605.

Conceição, D.M., Andrade, L.S., Cisneros, J.C., Iannuzzi, R., Pereira, A.A., & Machado, F.C., 2016a, New petrified forest in Maranhão, Permian (Cisuralian) of the Parnaíba Basin, Brazil: Journal of South American Earth Sciences, v. 70, p. 308-323.

Conceição, D.M., Cisneros, J.C., & Iannuzzi, R., 2016b, Novo registro de floresta petrificada em Altos, Piauí; relevância e estratégias para geoconservação: Pesquisas em Geociências, v. 43, p. 311-324.

Courtillot, V.E., & Renne, P.R., 2003, On the ages of flood basalt events Sur l ' âge des trapps basaltiques: Comptes Rendus Geoscience, v. 335, p. 113-140.

Cunha, F.M.B., 1964, Geologia do sudeste de Balsas [Relatório 224M]: PETROBRÁS, DIREX/RENOR, 46 p.

Dalrymple, R.W., 2010, Interpreting Sedimentary Sucessions: Facies, Facies Analysis and Facies Models, *in* James, N.P., & Dalrymple, R.W., eds., Facies Models 4: St. John's Newfoundland, Geological Association of Canada, p. 3–18.

Daly, M. C., Andrade, V., Barousse, C. A., Costa, R., McDowell, K., Piggott, N., & Poole, A. J., 2014, Brasiliano crustal structure and the tectonic setting of the Parnaíba basin of NE Brazil: Results of a deep seismic reflection profile: Tectonics, v. 33, p. 2102– 2120.

Daly, M.C., Tozer, B., and Watts, A.B., 2018a, Cratonic basins and the Wilson cycle: a perspective from the Parnaíba Basin, Brazil, *in* Wilson, R.W., Houseman, G.A., McCaffrey, K.J.W., Doré, A.G., & Buiter, S.J.H., eds., Fifty Years of the Wilson Cycle Concept in Plate Tectonics: Geological Society of London, Special Publications, v. 470.

Daly, M.C, Fuck, R.A, Juliá, J., MacDonald, D.I.M., & Watts, A.B., 2018b, Cratonic basin formation: a case study of the Parnaíba Basin of Brazil, *in* Daly, M.C., Fuck, R.A., Julià, J., MacDonald, D.I.M., & Watts, A.B., eds., Cratonic Basin Formation: A Case Study of the Parnaíba Basin of Brazil: Geological Society of London, Special Publications, v. 472, p. 1-15.

De Castro, D.L., Fuck, R.A., Phillips, J.D., Vidotti, R.M., Bezerra, F.H.R., & Dantas, E.L., 2014, Crustal structure beneath the Paleozoic Parnaíba Basin revealed by airborne gravity and magnetic data, Brazil: Tectonophysics, v. 614, p. 128-145.

Dickins, J.M., 1996, Problems of a Late Palaeozoic glaciation in Australia and subsequent climate in the Permian: Palaeogeography, Palaeoclimatology, Palaeoecology, v. 125, p. 185-197.

DiMichele, W.A., Montañez, I.P., Poulsen, C.J., & Tabor, N.J., 2009, Climate and vegetational regime shifts in the late Paleozoic ice age earth: Geobiology, v. 7, p. 200-226.

Dino, R., Antonioli, L., & Braz, S.M.N., 2002, Palynological data from the Trisidela Member of Upper Pedra de Fogo Formation ("Upper Permian") of the Parnaíba Basin, northeastern Brazil: Revista Brasileira de Paleontologia, p. 24-35.

Dott, R.J., & Bourgeois, J., 1982, Hummocky stratification: Significance of its variable bedding sequences: Geological Society of America, Bulletin, v. 93, p. 663-680.

Duke, W.L., 1985, Hummocky cross-stratification, tropical hurricanes, and intense winter storms: Sedimentology, v. 32, p. 167-194.

Dumas, S., & Arnott, R.W.C., 2006, Origin of hummocky and swaley cross-stratification – The controlling influence of unidirectional current strength and aggradation rate: Geology, v. 34, p. 1073-1076.

Eugster, H.P., & Jones, B.F., 1979, Behavior of major solutes during closed-basin brine evolution: American Journal of Science, v. 279, p. 609-631.

Eugster, H.P., 1986, Lake Magadi, Kenya: a model for rift valley hydrochemistry and sedimentation?, *in* Frostick, L.E., Renaut, R.W., Reid, I., and Tiercelin, J.J., eds., Sedimentation in the African Rifts: Geological Society of London, Special Publications, v. 25, 177-189.

Eyles, N., & Clark, B.M., 1986, Significance of hummocky and swaley cross-stratification in late Pleistocene lacustrine sediments of the Ontario basin, Canada: Geology, v. 14, p. 679-682.

Eyles, C.H., Eyles, N., & Gostin, V.A., 1996, Facies and Allostratigraphy of Highlatitude Glacially Influenced Marine Strata of the Early Permian southern Sydney Basin: Sedimentology, v. 45, p. 121-161.

Faria Jr., L.E.C., 1979, Estudo sedimentológico da Formação Pedra de Fogo – Permiano – Bacia do Maranhão [Dissertação de Mestrado]: Universidade Federal do Pará, 57 p.

Faria Jr., L.E.C., & Truckenbrodt, W., 1980a, Estratigrafia e petrografia da Formação Pedra de Fogo – Permiano da Bacia do Maranhão: Congresso Brasileiro de Geologia, 31, Balneário Camboriú, Anais, v. 2, p. 740-754.

Faria Jr., L.E.C., & Truckenbrodt, W., 1980b, Estromatólitos na Formação Pedra de Fogo, Permiano, Bacia do Maranhão: Congresso Brasileiro de Geologia, 31, Balneário Camboriú, Anais, v. 5, p. 3056-3067.

Figueroa, R.T., & Gallo, V., 2017, New chondrichthyan fin spines from the Pedra de Fogo Formation, Brazil: Journal of South American Earth Sciences, v.76, p. 389-396.

Fisher, J.A., Nichols, G.J., & Waltham, D.A., 2007, Unconfined flow deposits in distal sectors of fluvial distributary systems: examples from the Miocene Luna and Huesca Systems, northern Spain: Sedimentary Geology, v. 195, p. 55-73.

Fisher, J.A., Krapf, C.B.E., Lang, S.C., Nichols, G.J., & Payenberg, T.H.D., 2008, Sedimentology and architecture of the Douglas Creek terminal splay, Lake Eyre, central Australia: Sedimentology, v. 55, p. 1915-1930.

Folk, R.L., 1968, Petrology of sedimentary rocks: Austin: Hemphill's, 182p.

Folk, R.L., & Pittman, J.S., 1971, Length-slow chalcedony; a new testament for vanished evaporites: Journal of Sedimentary Research, v. 41, p. 1045–1058.

Gibling, M.R., & Rust, B.R., 1984, Channel margins in a Pennsylvanian braided, fluvial deposit: The Morien Group near Sydney, Nova Scotia, Canada: Journal of Sedimentary Research, v. 3, p. 773-782.

Góes, A.M.O., Souza, J.M.P., & Teixeira, L.B., 1990, Estágio exploratório e perspectivas petrolíferas da Bacia do Parnaíba: Boletim de Geociências da Petrobrás, v. 4, p. 55-64.

Góes, A.M.O., & Feijó, F.J., 1994, Bacia do Parnaíba: Boletim de Geociências da Petrobrás, v. 8, p. 57-67.

Góes, A.M., 1995, A Formação Poti (Carbonífero Inferior) da Bacia do Parnaíba [Tese de Doutorado]: Universidade de São Paulo, 171 p.

Greenwood, B., & Sherman, D.J., 1986, Hummocky cross-stratification in the surf zone: flow parameters and bedding genesis: Sedimentology, v. 33, p. 33-45.

Harms, J.C., Southard, J.B., Spearing, D.R., & Walker, R.G., 1975, Depositional environments as interpreted from primary sedimentary structures and stratification sequences: Society for Sedimentary Geology (SEPM) Short Course 2, 161 p.

Hatcher Jr., D.R., 2002, Alleghanian (Appalachian) orogeny, a product of zipper tectonics: Rotational transpressive continent-continent collision and closing of ancient oceans along

irregular margins, *in* Catalán, J.R.M, Hatcher Jr., R.D., Arenas., R., & García, F.D., eds., Variscan-Appalachian dynamics, The building of the late Paleozoic basement: Geological Society of American, Special Papers, v. 364.

Hesse, R., 1989, Silica diagenesis: origin of inorganic and replacement cherts: Earth-Science Reviews, v. 26, p. 253-284.

Iannuzzi, R., Neregato, R., Cisneros, J.C., Angielczyk, K.D., Rößler, R., Rohn, R., Marsicano, C., Fröbisch, J., Fairchild, T., Smith, R.M.H., Kurzawe, F., Richter, M., Langer, M.C., Tavares, T.M.V., Kammerer, C.F., Conceição, D.M., Pardo, J.D., & Roesler, G.A., 2018, Re-evaluation of the Permian macrofossils from the Parnaíba Basin: biostratigraphic, palaeoenvironmental and palaeogeographical implications, *in* Daly, M.C., Fuck, R.A., Julià, J., MacDonald, D.I.M., & Watts, A.B., eds., Cratonic Basin Formation: A Case Study of the Parnaíba Basin of Brazil: Geological Society of London, Special Publications, v. 472, p. 223-249.

Johnson, T.C., 1984, Sedimentation in Large Lakes: Annual Review of Earth and Planetary Sciences, v. 12, p. 179-204.

Kocurek, G., 1988, First-order and super bounding surfaces in eolian sequences-Bounding surfaces revisited: Sedimentary Geology, v. 56, p. 193-206.

Kutzbach, J.E., & Gallimore, R.G., 1989, Pangaean climates: Megamonsoons of the megacontinent: Journal Geophysical Research, v. 94, p. 3341- 3357.

Lang, S.C., Payenberg, T.H.D., Reilly, M.R.W., Hicks, T., Benson, J., & Kassan, J., 2004, Modern analogues for dryland sandy fluvial-lacustrine deltas and terminal splay reservoirs: Journal of the Australian Petroleum Production & Exploration Association, v. 44, p. 329-356.

Leeder, M., 1999, Sedimentology and Sedimentary Basins: From Turbulence to Tectonics: Blackwell Science, Oxford, UK.

Li, F., Yang, Y., Li, J., Yang, C., Dai, T., Zhao, J., & Yi, H., 2014, Lacustrine tempestite and its geological significance in the Cenozoic study of the Qaidam Basin: Journal of Asian Earth Sciences, v. 92, p. 157-167.

Lima, E.A.M., & Leite, J.F., 1978, Projeto estudo global dos recursos Minerais da Bacia Sedimentar do Parnaíba: Integração geológico-metalogenética, Etapa III, Relatório Final, v. 16, 212 p.

Lowenstein, T.K., & Hardie, L.A., 1985, Criteria for the recognition of salt-pan evaporites: Sedimentology, v. 32, p. 627-644.

Lowenstein, T.K., 1987, Evaporite depositional fabrics in the deeply buried Jurassic Buckner Formation, Alabama: Journal of Sedimentary Research, v. 57, p.108–116.

Marsaglia, K.M., & Klein, G.D., 1983, The Paleogeography of Paleozoic and Mesozoic Storm Depositional Systems: The Journal of Geology, v. 91, p. 117-142.

Martins, R.A., 2000, Fósseis de vegetais da Formação Pedra de Fogo: aspectos taxonômicos, mineralogia e composição química [Dissertação de Mestrado]: Universidade Federal do Pará, 92 p.

Melo, M.T., & Prade, G.O., 1968, Geologia da região sudeste de São Raimundo das Mangabeiras-Maranhão [Relatório 297M]: PETROBRÁS, DIREX/RENOR, 37 p.

Miall, A., 1977, A Review of the Braided-River Depositional Environment: Earth-Science Reviews, v. 13, p. 1-62.

Miall, A., 2010, Alluvial deposits, *in* James, N.P., & Dalrymple, R.W., eds., Facies Models 4: St. John's Newfoundland, Geological Association of Canada, p. 105–137.

Milliken, K.L., 1979, The silicified evaporite syndrome; two aspects of silicification history of former evaporite nodules from southern Kentucky and northern Tennessee: Journal of Sedimentary Research, v. 49, p. 245–256.

Moore, B., 1964, Geological reconnaissance of the southern margin of the Maranhão Basin [Relatório 216M]: PETROBRÁS, DIREX/RENOR, 46 p.

Nichols, G.J., & Fisher, J.A., 2007, Processes, facies and architecture of fluvial distributary system deposits: Sedimentary Geology, v. 195, p. 75-90.

Nichols, G.J., & Hirst, J.P.P., 1998, Alluvial fans and fluvial distributary systems, Oligo Miocene, northern Spain: contrasting processes and products: Journal of Sedimentary Research, v. 68, p. 879– 889

North, C.P., & Davidson, S.K., 2012, Unconfined alluvial flow processes: Recognition and interpretation of their deposits, and the significance for palaeogeographic reconstruction: Earth-Science Reviews, v. 111, p. 199-223.

Ojeda, H.A., & Bembom, F.C., 1966, Mapeamento geológico de semi-detalhe do sudoeste de Riachão [Relatório 260M]: PETROBRÁS, DIREX/RENOR, 67 p.

Ojeda, H.A., & Perillo, I.A., 1967, Geologia do sudoeste de Carolina [Relatório 270M]: PETROBRÁS, DIREX/RENOR, 53 p.

Oliveira, M.A., 1961, Reconhecimento geológico no flanco oeste da Bacia do Maranhão [Relatório 171M]: PETROBRÁS, DIREX/RENOR, 77 p.

Oliveira, C.M., 1982, O padrão de distribuição dos elementos traços na Formação Pedra de Fogo, Permiano da Bacia do Maranhão e seu emprego como indicador de ambientes de sedimentação [Dissertação de Mestrado]: Universidade Federal do Pará, 94 p.

Olsen, P.E., 1990, Tectonic, Climatic, and Biotic Modulation of Lacustrine Ecosystems—Examples from Newark Supergroup of Eastern North America, *in* Katz, B.J., ed.,

Lacustrine Basin Exploration: Case Studies and Modern Analogs: American Association of Petroleum Geologists, Memoir v. 50, p. 209-224.

Parrish, J.T., 1990, Gondwanan Paleogeography and Paleoclimatology, *in* Taylor, T.N., & Taylor, E.L., eds., Antarctic Paleobiology: Springer, p. 15-26.

Parrish, J.T., 1993, Climate of the Supercontinent Pangea: The Journal of Geology, v. 101: 215-233.

Pinto, C.P., & Sad, J.H.G., 1986, Revisão da estratigrafia da Formação Pedra de Fogo, borda sudoeste da Bacia do Parnaíba: Congresso Brasileiro de Paleontologia, 34, Anais,v. 1, p. 346-356.

Plummer, F.B., 1946, Report on Maranhão and Piauí Geosyncline [Relatório 1M]: PETROBRÁS, DIREX/RENOR, 83 p.

Pochat, S., Van Den Driessche, J., Mouton, V., & Guillocheau, F., 2005, Identification of Permian palaeowind direction from wave-dominated lacustrine sediments (Lodève Basin, France): Sedimentology, v. 52, p. 809-825.

Price, L.I., 1948, Um anfibio labirintodonte da Formação Pedra de Fogo, estado do Maranhão: Departamento Nacional de Produção Mineral, Divisão Geologia e Mineralogia, Boletim, v. 124, p. 1-32.

Reid, I., & Frostick, L.E., 1997, Channel form, flows and sediments in deserts, *in* Thomas, D.S.G., ed., Arid Zone Geomorphology; Process, Form and Change in Drylands: John Wiley & Sons, Chichester p. 205– 229

Renaut, R.W., & Gierlowski-Kordesch, E.H., 2010, Lakes, *in* James, N.P., & Darlymple, R.W., eds., Facies Models 4: St. John's Newfoundland, Geological Association of Canada, p. 541-575.

Retallack, G.J., 2001, Soils of the Past: An Introduction to Paleopedology: Allen & Unwin, London, 404 p.

Röβler, R., & Galtier, J., 2002a, First Grammatopteris tree ferns from the Southern Hemisphere – new insights in the evolution of the Osmundaceae from the Permian of Brazil: Review of Palaeobotany and Palynology, v. 121, p. 205-230.

Röβler, R., & Galtier, J., 2002b, Dernbachia brasiliensis gen. nov. et sp. nov. – a new small tree fern from the Permian of NE Brazil: Review of Palaeobotany and Palynology, v. 122, p. 239-263.

Röβler, R., & Galtier, J., 2003, The first evidence of the fern Botryopteris from the Permian of the Southern Hemisphere reflecting growth form diversity: Review of Palaeobotany and Palynology, v. 127, p. 99-124.

Röβler, R., 2006, Two remarkable Permian petrified forests: correlation, comparison and significance, *in* Lucas, S.G., Cassinis, G., & Schneider, J.W., eds., Non-Marine Permian

Biostratigraphy and Biochronology: Geological Society of London, Special Publications, v. 265, p. 39-63.

Santos, M.E.C.M., & Carvalho, M.S.S., 2009, Paleontologia das Bacias do Parnaíba, São Luís e Grajaú: Reconstituições paleobiológicas, in Serviço Geológico do Brasil. DIEDIG/DEPAT, 215 p.

Santos, P.R., Rocha-Campos, A.C., & Canuto, J.R., 1996, Patterns of late Palaeozoic deglaciation in the Paraná Basin, Brazil: Palaeogeography, Palaeoclimatology, Palaeoecology, v. 125, p. 165-184.

Santos, R.S., 1994, Paleoictiofaunula da Formação Pedra do Fogo, Bacia do Parnaíba, NE do Brasil: II. Eugeneodontida – Agassizodontidae: Anais da Academia Brasileira de Ciências, v. 66, p. 413-424.

Schobbenhaus, C., Campos, D.A., Derze, G.R., & Asmus, H.E., eds., 1984, Geologia do Brasil. Texto Explicativo do Mapa Geológico do Brasil e da área oceânica adjacente incluindo depósitos minerais. Escala 1:2500.000. Brasília: DNPM, p. 9–53

Schubel, K.A., & Lowenstein, T.K., 1997, Criteria for the recognition of shallow-perennial-saline-lake halites based on recent sediments from the Qaidam Basin, western China: Journal of Sedimentary Research, v. 67, p. 74-87.

Scotese, C.R., Boucot, A.J., & McKerrow, W.S., 1999, Gondwanan palaeogeography and palaeoclimatology: Journal of African Earth Sciences, v. 28, p. 99-114.

Shanley, K.W., & McCabe, P.J., 1994, Perspectives on the sequence stratigraphy of continental strata: American Association Petroleum Geological Bulletin, v. 78, p. 544-568.

Smoot, J.P., & Lowenstein, T.K., 1991, Chapter 3 Depositional Environments of Non-Marine Evaporites: Developments in Sedimentology, v. 50, p. 189–347.

Talbot, M.R., & Allen, P.A., 1996, Lakes, *in* Reading, H.G., ed., Sedimentary Environments: Processes, Facies and Stratigraphy: Blackwell Science, Oxford, p. 83–124.

Talbot, M.R., Holm, K., & Williams, M.A.J., 1994, Sedimentation in low gradient desert margin systems; a comparison of the Late Triassic of northwest Sommerset (England) and the Late Quaternary of east-central Australia, *in* Rosen, M.R., ed., Palaeoclimate and Southern Idaho: American Association of Petroleum Geologist, Bulletin v. 83, p. 635–665.

Tooth, S., & Nanson, G.C., 1995, The geomorphology of Australia's fluvial systems: retrospect, perspect and prospect: Progress in Physical Geography, v. 19, p. 35– 60.

Tooth, S.D., 1999, Floodouts in Central Australia, in Miller, A.J. & Gupta, A., eds., Varieties of Fluvial Form: John Wiley and Sons, Chichester, p. 219–247.

Tucker, M.E., 2003, Sedimentary rocks in the field: a practical guide: Chichester, Wiley, 234 p.

Tunbridge, I.P., 1984, Facies model for a sandy ephemeral stream and clay playa complex: The Middle Devonian Trentishoe Formation of North Devon, U.K: Sedimentology, v. 31, p. 697-715.

Vaz, P.T., Resende, N.G.A.M., Wanderley Filho, J.R., & Travassos, W.A., 2007, Bacia do Parnaíba: Boletim de Geociências Petrobrás, v. 15, p. 253-263.

Visser, J.N.J., 1997, A Review of the Permo-Carboniferous Glaciation in Africa, in Martini, I.P. ed., Late Glacial and Postglacial Environmental Changes: New York: Oxford University, p.169–191.

Walker, R.G., 1992, Facies, facies models and modern stratigraphic concepts, in Walker, R.G., & James, N.P., eds., Facies models: response to sea level change: St. John's Newfoundland, Geological Association of Canada, p. 1-14.

Wang, J., Jiang, Z., & Zhang, Y., 2015, Subsurface lacustrine storm-seiche depositional model in the Eocene Lijin Sag of the Bohai Bay Basin, East China: Sedimentary Geology, v. 328, p. 55-72.

Warren, J.K., 2001, Evaporites, brines and base metals: low-temperature ore emplacement controlled by evaporite diagenesis: Australian Journal of Earth Sciences, v. 47, p.179–208.

Zambito, J.J., & Benison, K.C., 2013, Extremely high temperatures and paleoclimate trends recorded in Permian ephemeral lake halite: Geology, v. 41, p .587-590.

5 THE EVOLUTION OF CISURALIAN DEPOSITS IN THE EASTERN PARNAÍBA BASIN, BRAZIL: UNRAVELLING THE FLOURISHING OF THE EQUATORIAL FOREST IN THE WESTERN GONDWANA

Luiz Saturnino de Andrade[1,2*], Afonso César Rodrigues Nogueira[2], Domingas Maria da Conceição[4], Juan Carlos Cisneros[3], Roberto Iannuzzi[4]

[1] Programa de Pós-Graduação em Geologia e Geoquímica-PPGG, Instituto de Geociências-IG, Universidade Federal do Pará-UFPA, 66075-110, Belém, Pará, Brasil.
E-mail: geoandrade.sl@gmail.com

[2] Grupo de Análise de Bacias Sedimentares da Amazônia, Universidade Federal do Pará-UFPA.
E-mail: afonsonogueir@gmail.com

[3] Centro de Ciências da Natureza, Universidade Federal do Piauí-UFPI, Ininga, 64049-550, Teresina, PI, Brasil
E-mail: juan.cisneros@ufpi.edu.br

[4] Departamento de Paleontologia e Estratigrafia, Universidade Federal do Rio Grande do Sul-UFRGS, Avenida Bento Gonçalves 9.500, 91501-970, Porto Alegre, RS, Brasil.
E-mail: domingasmary@hotmail.com; roberto.iannuzzi@ufrgs.br

*Corresponding author

ABSTRACT

The late Paleozoic experienced the transition between glacial and non-glacial climates at multiple temporal scales, accompanied by global warming tendency. Pennsylvanian–Cisuralian transition is marked by tropical warming and drying with prevalescent seasonally climate during the Permian period. Through detailed sedimentologic and stratigraphic study in deposits of Early Permian, east border of the Parnaiba Basin, northertn Brazil. This study shows the interaction between Permian forest and the dynamic arid lacustrine environmental, in response to climate seasonality regime in western part of the Gondwana. The geographic distribution of this importante petrified fossil plants is associated of the large domain of the Pedra de Fogo Lacustrine System, and strongly indicate the terrestrial character of this deposits, suggesting an already complete continentalisation this portion of the western Gondwana during Early Permian.

Keywords: Early Permian; Parnaíba Basin; Pedra de Fogo Formation; Lacustrine system; petrified fossil

INTRODUCTION

The Permian records the transition from a glacial phase, especially in the eastern part of Gondwana, to a period of progressive rise in the global temperature, until 'Greenhouse' conditions at the Permo-Triassic limit (Scotese et al. 1999; DiMichele et al. 2001; Chumakov and Zharkov 2002; Chumakov and Zharkov 2003; DiMichele et al. 2009). This transition may have been especially rapid during the Lower Permian (Zambito and Benison 2013). Mountain belts in the interior and at the edges of Pangea, resulting from intense tectonic collisions, caused significant changes in the wind circulation regime, causing its innermost regions to be affected by an increasing and irregular rising of the global temperature and aridity, potentially under monsoon regime (Rowley et al. 1985; Kutzbach and Gallimore 1989; Parrish 1993).

Climate fluctuations during this period varied significantly from humid/sub-humid to semi-arid to arid (Oplustil 2013). According to DiMichele et al. (2010), these climate trends clearly operated at various time scales, and had a profound effect on the composition of fauna and flora. Similarly, sedimentation cycles and sedimentary environments were significantly influenced by paleogeographic variations, and mainly climatic, short-term as much as long-term, which had occurred during the late Carboniferous and throughout the Permian periods (Golonka and Ford 2000).

In Brazil, the Pedra de Fogo Formation, of Kungurian age (Cisneros et al. 2015), has one of the most significant volumes of fossil occurrences, both animal and vegetal (Price 1948; Coimbra and Mussa 1984; Caldas et al. 1989; Santos 1989a, 1989b, 1990; Cox and Hutchinson 1991; Santos 1994; Martins 2000; Röβler and Galtier 2002a, 2002b, 2003; Cisneros et al. 2015; Conceição et al. 2016; Figueroa and Gallo 2017; Iannuzzi et al. 2018). Especially the palaeoflora, historically recorded in all its extension, which constitutes one of its strongest stratigraphic characteristics. Although recent works, geographically restricted (Dias-Brito et al. 2007; Capretz and Rohn 2013; Kurzawe et al. 2013a, 2013b; Tavares et al. 2014; Neregato et al. 2015; Kauffmann et al. 2016; Neregato et al. 2017), have repositioned fossil woods in the overlying sedimentary unit (Motuca Formation), so far, the Pedra de Fogo Formation is the only sedimentary unit in the Parnaíba Basin that has woods in life position, within a wide geographical distribution (Caldas et al. 1989; Conceição et al. 2016).

In addition, the Pedra de Fogo Formation records a cyclic sedimentation composed of a variety of lithologies, from carbonates, evaporites, claystones, shales, sandstones and mainly chert (Plummer 1946; Barbosa and Gomes 1957; Melo and Prade 1968; Faria Jr. and Truckenbrodt 1980a, 1980b). This variety of lithology and fossil content reflects a

depositional dynamics, probably caused by the enhanced monsoon character of the climate with more contrast seasonal and annual alternation of arid and humid periods prevailing in the late Paleozoic (Scotese et al. 1999; Chumakov and Zharkov 2002; DiMichele et al. 2006, Montañez et al. 2007; Boucot et al. 2013).

Climate is one of the most important controlling parameters of sedimentation (Cecil 1990). Both directly and indirectly, climate controls especially the development of cyclic sedimentation, as well as the diversity of fauna and flora. It affects the chemical parameters of water (salinity, pH, temperature, turbidity, etc.) through changes in temperature and precipitation volume, which also alters cementation and/or dissolution cycles (Zharkov and Chumakov 2001; Lever 2004). Among sedimentary environments, lake systems are the ones that the best and most quickly respond to climate variations, whether autocyclic or allocyclic (Carroll and Bohacs 1999; Talbot and Allen 1996; Gierlowski-Kordesch and Kelts 2000). Especially the marginal lacustrine sedimentation, is especially sensitive to climate fluctuations, due to the responses in the lakes level fluctuation, and consequent migration of its shoreline, which quickly affects the distribution of microbialites as well as the surrounding vegetation (Casanova and Hillaire-Marcel 1992; Dearing 1997; DiMichelle et al. 2011).

This study documents the depositional dynamics of the so-called “Pedra de Fogo Lacustrine System” (SLPF), through the facies, stratigraphic and biostratigraphic analysis of the Pedra de Fogo Formation. In addition, we discuss the interrelationship between SLPF depositional geometry and the occurrence of paleoflora and microbialites, resulting from recurrent climatic fluctuations throughout the beginning and later during the Permian period.

GEOLOGICAL SETTING

In this paper we report on investigations in the Cisuralian deposits (Cisneros et al. 2015), regionally known as Pedra de Fogo Formation (Plummer 1946). This sedimentary unit is characterized by expressive silicification in all its extension, with abundant and varied cherts layers (Faria Jr. 1979) besides sheltering a vast content of silicified permian trunks (Röβler and Galtier 2002a, 2002b, 2003; Conceição et al. 2016; Iannuzzi et al. 2018).

The Pedra de Fogo Formation is inserted in the Neocarboniferous-Eotriassic sequence, recorded by the deposition of the Balsas Group, started in the Pennsylvanian with the Piauí Formation, and ended in the Eotriassic with the Sambaíba Formation (Vaz et al. 2007). According to Góes et al. (1990), the Balsas Group marks the beginning of continentalization in the Parnaíba Basin, with progressive desertification and displacement of its depocenter to its central part. According to Barbosa et al. (2016), the Neocarboniferous-Eotriassic Sequence

began with fluvio-aeolian deposits, which were later drowned by marine and coastal deposits, also were progressively replaced by lacustrine and desert systems resulting from increasingly arid to semi-arid climatic conditions.

The Balsas Group occurs mainly in the center-south portions and part of the west and east-northeast regions of the basin, and is formed from the bottom to the top by the Piauí, Pedra de Fogo, Motuca and Sambaíba formations, which record intense and significant structural and environmental changes during its deposition (Góes and Feijó 1994). Clearly, the Pedra de Fogo Formation is the unit with the greatest lithological diversification of the Parnaíba Basin (Figure 1), probably reflecting the intense climatic seasonality that occurred during its deposition at the end of the Paleozoic.

METHODS

Eleven outcrops of the Pedra de Fogo Formation that occur discontinuously along highways of Piauí and Maranhão states (Figure 2), in the riverside of Poti River (Teresina-PI) and Parnaíba River (Boa Esperança Dam – Nova Iorque-MA), as well as on the flank of small hills (Altos-PI; Coelho Neto and Duque Bacelar-MA) up to 40 m high.

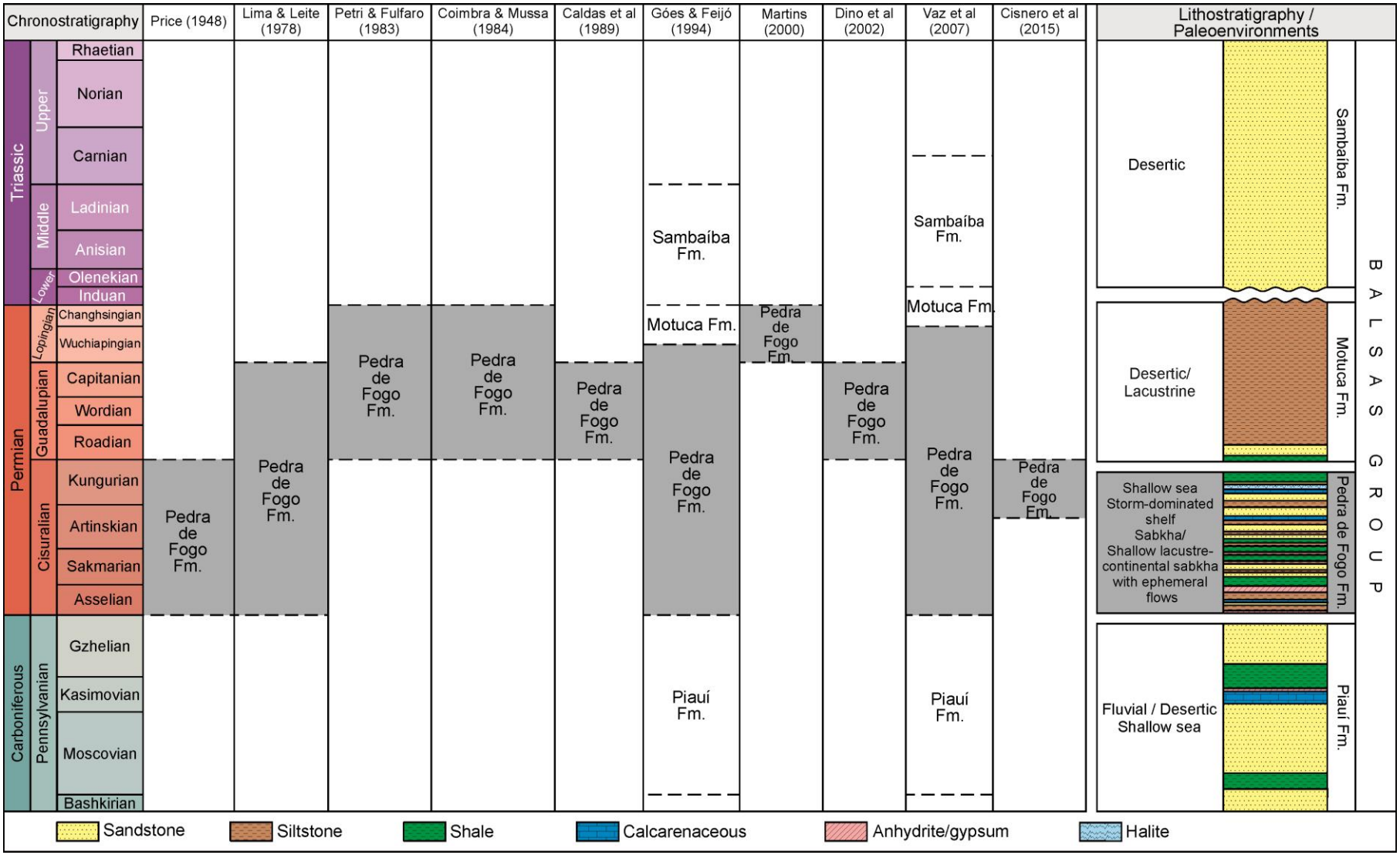

Figure 1-Lithostratigraphic chart of the Pedra de Fogo Formation, showing its comparative chronostratigraphic differences by different works. Also note the paleoenvironmental and lithological diversification of this unit. Detailed explanations are in the text.

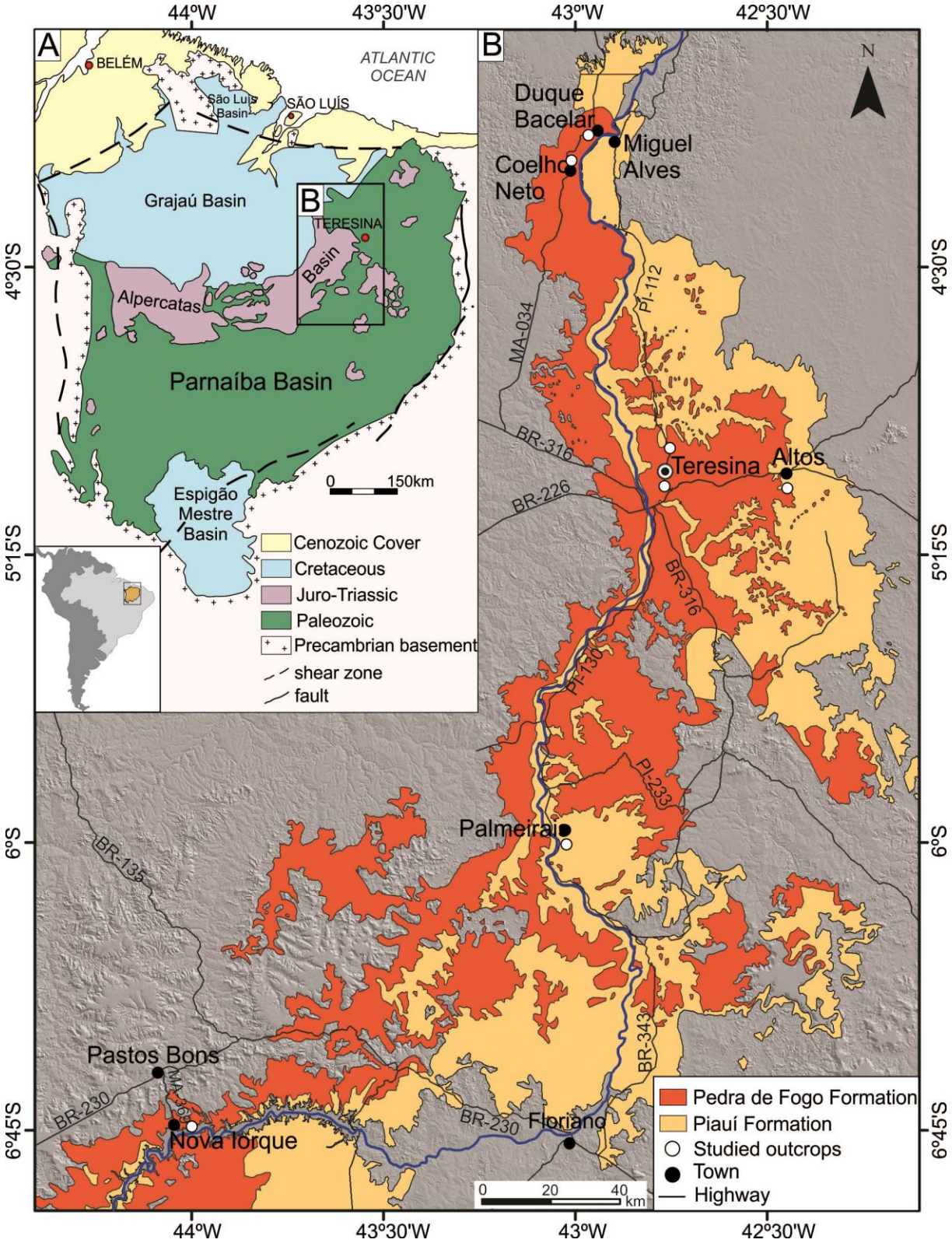

Figure 2-Simplified geologic map of the Parnaíba Basin in Northern Brazil and geographic distribution of the Permian Pedra de Fogo Formation in the eastern portion of the basin (Modified from Góes 1995).

FACIES ASSOCIATION

The facies association studied is related to the lower part of the Pedra de Fogo Formation (Faria Jr. 1979) and corresponds to predominantly mudrock deposits, colors red to orange, sometimes mottled, with a predominance of undulating lamination at the base, which grade to reddish siltstone, with asymmetrical climbing-ripple cross-lamination. These siltstone are interspersed with centimeter to decimeter tabular layers of fine sandstone with horizontal lamination to massive, eventually with erosive base, overlapped by sandstones presenting wavy cross-lamination and apparent pinch-and-swell geometry.

Silicified gymnosperm stems occur along this succession, both horizontal or in life-position. Massive, nodular and breccia cherts mark the basis of this succession, as well as, the laterally discontinuous silicified siltstones with stratiform and columnar microbialite features. Fifteen sedimentary facies were obtained by making seven columnar sections, with eleven facies grouped into three associations belonging to the Pedra de Fogo Formation: Onshore flat (FA1), Nearshore wave and storm dominated (FA2) and Terminal splays (FA3). As a way of positioning stratigraphically the studied portion of the Pedra de Fogo Formation, four facies were grouped into one facies association referring to the Piauí Formation: Distal breaded (FA4) (Figure 3; Table 1, 2).

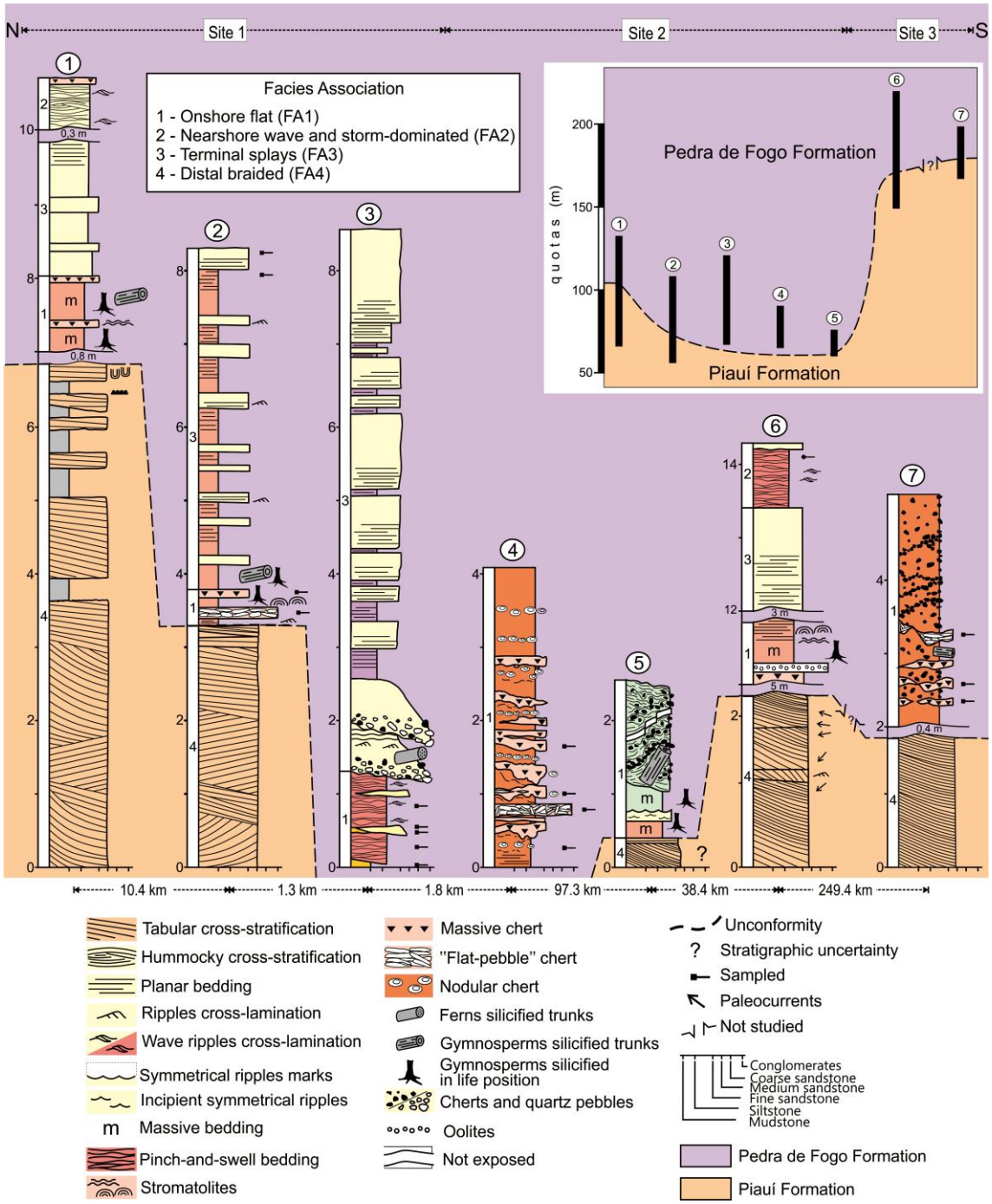

Figure 3- Lithostratigraphic section of the studied areas in the regions of Coelho Neto, Duque Bacelar and Nova Iorque in the state of Maranhão, and Teresina and Altos in the state of Piauí (see the location of this section in Figure 2). The frame in the upper right corner shows the profiles according to their current dimensions. The vertical exaggeration between the profiles, especially between 5 and 6, is due to the out-of-scale horizontal distance.

Table 1: Facies and depositional processes of the succession studied on the east-southeast edges of the Parnaíba Basin.

FACIES	DESCRIPTION	INTERPRETATION	
Massive mudrock (**Mm**)	Tabular layers (0.1-1.7 m) of light red to mottled solid mudrock with abundant chert nodules; incipient plane-parallel lamination at the base of the layer; silicified gymnosperms stems of in life position in the facies lower areas; interspersed with the Mch and Chb facies	Deposition by decantation. Syndepositional to eodiagenetics plants silicification. Eogenetic post-depositional alteration	**Onshore flat**
Massive chert (**Chm**)	Layers of massive chert (0.06-0.3 m); relatively flat top, irregular base with apparent overload; occurs interspersed with Mm facies	Silicification of coalesced nodules. Pseudo overload	
Nodular chert (**Chn**)	Relatively continuous complex of nodular chert. The nodules are between 2 and 25 cm in their longest axis; spherical shapes to oblate spheroids; occur at ordered as well as randomly dispersed levels in the Mm facies	Syndepositional to eodiagenetic silicification of carbonates-evaporites	
Chert breccia (**Chb**)	Tabular layer (~ 0.2 m), white, with tabular to prolate chert fragments, supported matrix. Intraclasts are up to 8 cm long (C axis); most are arranged sub-horizontally; top of the layer is usually flat while the base is irregular	Post-depositional silicification	
Sandstone wave-formed ripples (**Sw**)	Tabular layers, red to white (0.1-0.3), laterally continuous, with very fine sandstone to siltstone with lamination truncated by wave. Locally occurs as symmetrical straight-crested small ripples	Oscillatory flow deposition under wave action in fair-weather periods in shallow water depth	**Nearshore wave and storm dominated**
Sandstone hummocky cross-stratification (**Shs**)	Fine whitish sandstone (≤ 0.6 m), pinch-and-swell geometry, laterally continuous with hummocky cross-stratification (HCS); HCS has a height of about 18 cm, and inclination of the hummocks in their sharpest parts up to 11º	Combined flow deposition dominantly oscillatory from wave action during storm periods	
Silicified microbialites (**Ms**)	Columnar complex laminated, silicified, centimetric height	Mat formation through microbial activities in shallow and calm waters with sporadic siliciclastic inflows (?). Post-depositional silicification	
Sandstone/Siltstone horizontal lamination (**Shl**)	Tabular layers (0.2-1.1 m), very fine sandstone/siltstone, red, with horizontal parallel lamination	Unidirectional currents with bedding plane generation	

Continuation

Massive claystone (**Cm**)	Lenticular layers of massive yellowish claystone, with thicknesses between 0.2 and 0.4 m, and widths between 1.00 and 2.00 m.	Deposition by decantation in low energy environment	**Terminal splay**
Sandstone subcritically climbing ripples cross-lamination (**Sc**)	Tabular layers (≤ 0.2 m); fine sandstone to silt whitish red with subcritically climbing ripples cross-lamination.	Unidirectional current with predominance of traction over suspension.	
Massive sandstone (**Sm**)	Tabular, lenticular layers (0.2-1.4 m); very fine to medium sandstone, pink to off-white; massive bedding; eventual incipient plane stratification and lags at the base of the layers; lags formed by spherical rounded quartz grains and chert fragments; Silicified woods of ferns occur concordant to the bedding.	Very rapid deposition	
Laminated mudrock (**Ml**)	Tabular, centimetric layer of light gray mudrock with wavy lamination.	Deposition by decantation in low energy environment	**Distal braided**
Sandstone supercritically climbing ripples cross-lamination (**Scs**)	Tabular layers (≤ 0.1 m); fine sandstone with supercritically climbing ripples cross – lamination.	Unidirectional current with predominance of over suspension traction.	
Sandstone horizontal stratification (**Sh)**	Fine to medium sandstone, cream-orange, composed by quartz, with well-selected and well-rounded grains, with horizontal stratification. It always occurs at the top of the cosets.	Unidirectional current deposition under high flow regime, with intense grain movement	
Sandstone tabular cross-stratification (**St)**	Fine to medium sandstone (0.4-6 m), cream orange, composed by quartz, with well selected and well rounded grains; tabular cross stratification, sometimes with tangential basis. Sets (≤ 0.5 m); reactivation surfaces.	Deposition during migration of small to medium sized 2D bed shapes.	

Table 2- Facies association of Pedra de Fogo and Piauí Formation, Parnaíba Basin.

Litostratigraphy unit	Facies association	Facies	Depositional systems
	FA1	Mm, Chm, Chn, Chb	Onshore flat
Pedra de Fogo Formation	FA2	Mm, Sw, Shs, Ms, Shl	Nearshore wave and storm dominated
	FA3	Cm, Sc, Sm	Terminal splay
Piuaí Formation	FA4	Ml, Scs, Sh, St	Distal breaded

Onshore flat (FA1)

Description: The FA1 is composed of massive mudrock (Mm), massive chert (Chm), nodular chert (Chn), and chert breccia (Chb). Its thickness is about 6 m, predominantly formed by tabular layers of centimeter thickness, laterally continuous of massive mudrock (Mm facies), mottled, friable, locally pedogenized, interbedded with layers of massive chert (Chm), nodular chert (Chn). The chert layers are laterally continuous, with occasional centimeter interruptions. The thickness vary from millimeter to centimeter (up to 20 cm). The tops of the chert are weakly undulating with low amplitude grooves, while the base is strongly irregular with high amplitude grooves (Figures 4A-D). Small chert chips are locally scattered on the mudrock. Chert nodules also occur isolated, but relatively aligned within the "intercherts" mudrock (Figure 4E). Chert breccia levels (Chb facies) mark the basis of this succession (Figures 5A, B).

Fossil plant assemblages occur significantly, mainly in the basal portions of the studied succession. The silicified gymnosperm woods occur autochthonous or in life position over a wide area of sites 1 and 2 (Figure 3). These are large (Figures 5C, D), with a length ranging from about 0.1-5.0 m, and diameters from 0.05-1.15 m (*see* Conceição et al. 2016). Many occur along the slopes of small hills (up to 40 m in height), or in a horizontal position, scattered randomly over the pavement, resulting from the recent erosive retraction of the slopes. On the other hand, silicified tree-fern stems occur *ex situ*, restricted to sites 1 and 3 (Figure 3). They have smaller sizes with lengths between 0.1-0.5 m and diameters between 0.04-0.05 m. These stems sometimes occur immersed in the Mm facies, and sometimes associated with the Ms facies.In all occurrences, fern stems are concordant with the bedding of the respective facies. The local abundance of these fragments enables partial reconstruction of woods up to 1.3 m in length (Figure 5E). These woods keep the outer structure well preserved, while the inner parts are often completely obliterated by silicification. More detailed information about these fossil records is found in Conceição et al. (2016); Iannuzzi et al. (2018). Stratigraphically, FA1 is positioned at the base of the studied succession, usually in discordant contact with pennsylvanian sandstones of the Piauí Formation.

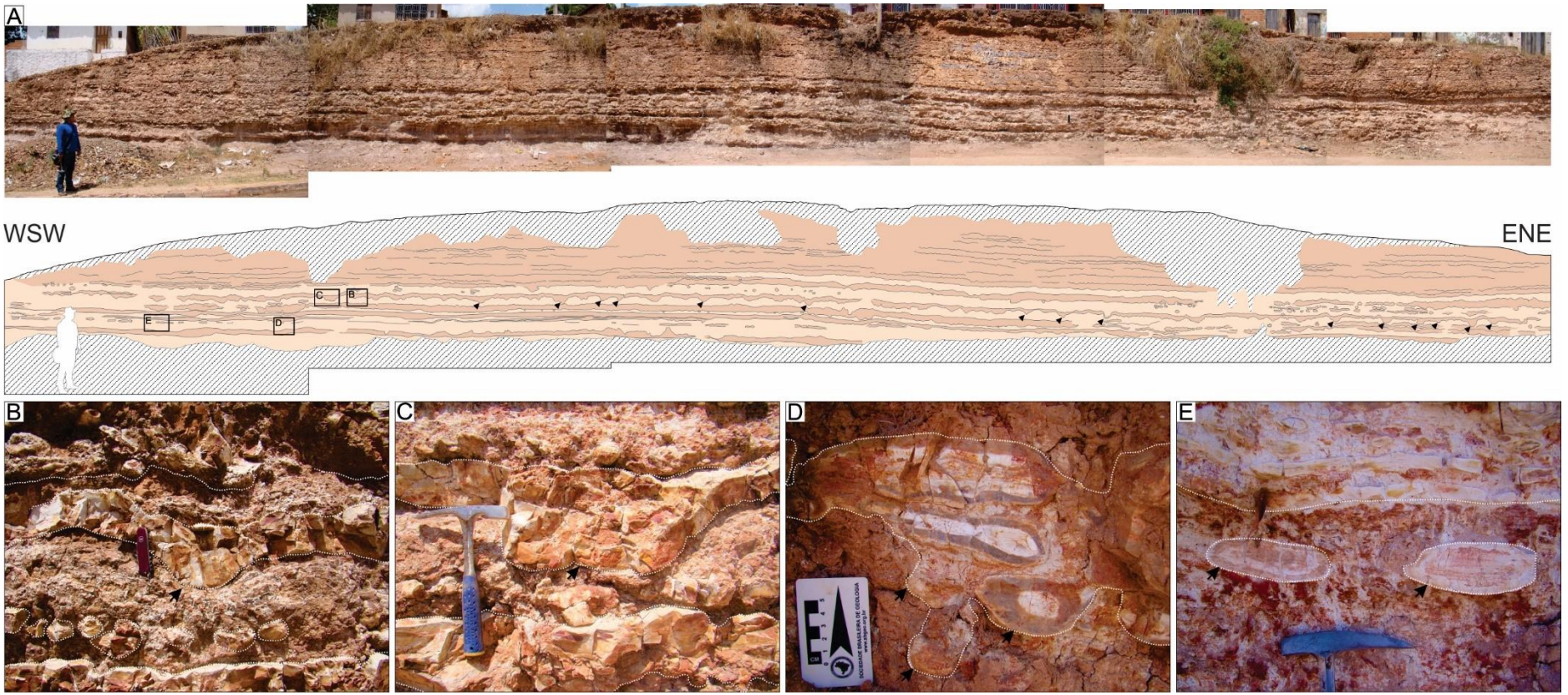

Figure 4-**A)** Overview of FA1 association in the region of Coelho Neto-MA. Note the irregularity in the basal parts of the chert layers (black arrows). **B, C)** Detail of the strong irregularity of the lower part of the chert levels. Although layers of massive chert predominate, nodular chert occurs frequently throughout the section. **D)** Coalesced nodules "sunk" in the mudrock. **E)** Chert nodules aligned (arrows), with oblate spheroid shapes with main axis consistent with the bedding. Dimension of main axis (horizontal) varies between 14 and 25 cm. Layer thickness ranges between 6-15 cm.

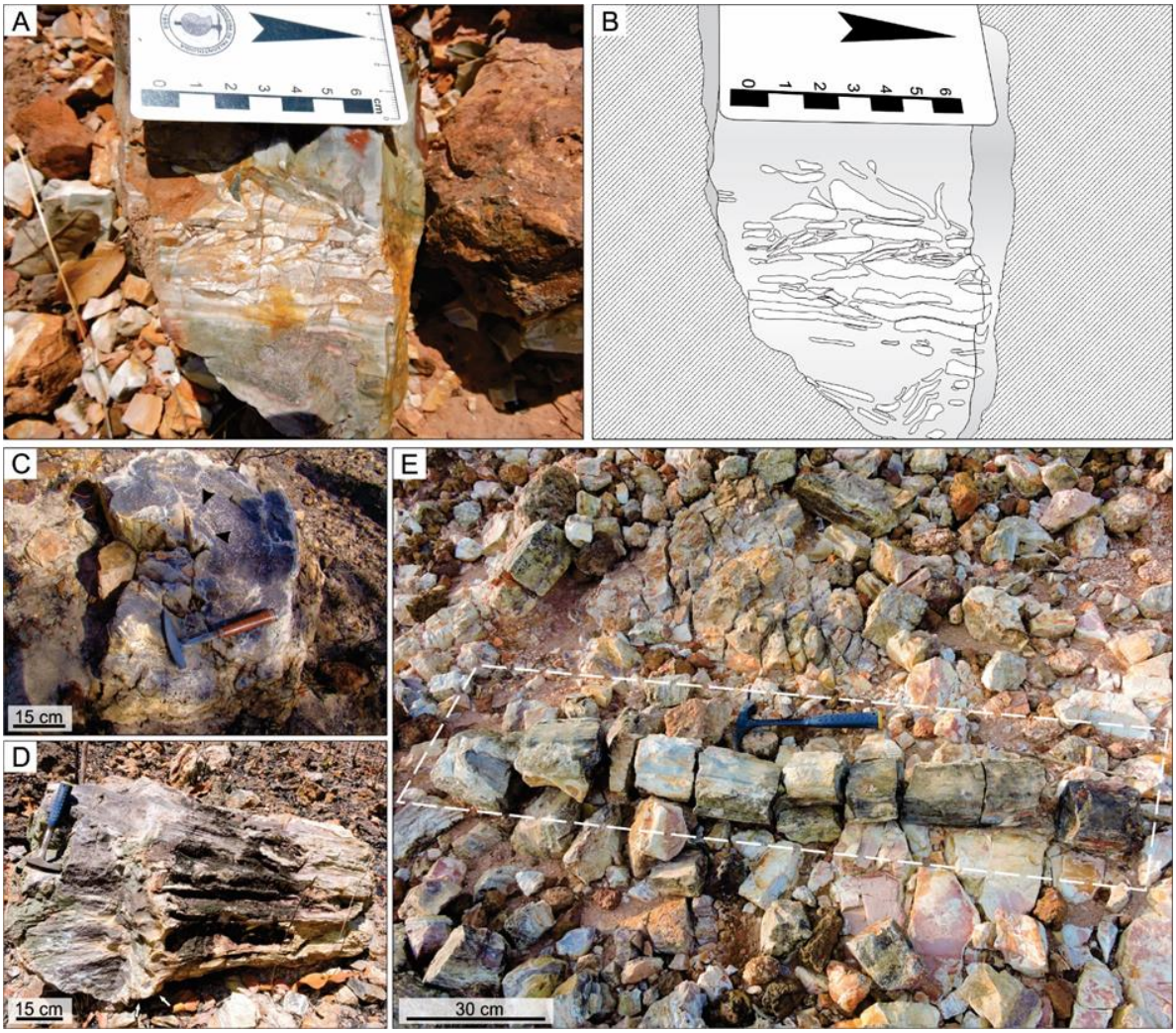

Figure 5-Registered occurrences at the basis of the studied succession. **A, B)** Intraformational Chert "Breccia" with oblate clasts up to 4 cm long on its largest axis. **C)** Silicified trunk of gymnosperm in life position. Arrows indicate circular features within the trunks associated with the growth rings. **D)** Gymnosperm rolled trunk. Although listed, these fossils are "autochthonous" because they have not been under significant transportation, only rolled from the hillsides as a result of the current erosion (Duque Bacelar / Coelho Neto-MA region). E) Partially reconstituted (dashed) fern wood (Nova Iorque-MA region).

Interpretation: The thickness of the predominantly massive mudrock (Mm) package, eventually with incipient horizontal lamination, and abundant fossil plants fragments in life position, "autochthonous" is associated with the marginal portions of a lacustrine system (Conceição et al. 2016). The alternation between Mm, and Chm, Chn, Chb facies is attributed to seasonal variations in pH values resulting from relatively wetter depositional periods interspersed with relatively drier periods. Studies of modern lacustrine environments show that the pH of alkaline lakes is controlled by the ratio of freshwater inflow *versus* evaporation (Eugster, 1967; 1969), as well as by seasonal variation in the own bioproductivity of the lakes (Peterson and Von Der Borch 1965).

The mottled massive appearance of the '*intercherts*' mudrock (Mm facies) is associated with alternations between oxidizing and reducing conditions, suggestive of groundwater fluctuations, caused by climatic seasonality between drier and wetter periods, or by pedogenetic processes, confirmed by the massive aspect, and the registration of gymnosperm trunks in their life position (Retallack 2001; Wagner and Mayoral 2007). According to amill, the occurrence of silicified wood in continental deposits is another indication of a relatively wet climate, characterized by climatic seasonality. The strong deformation of the chert layers may have been caused by two independent and non-exclusive mechanisms:

1) Soft sediment deformation - when the overlapping siltic sediments were deposited, the cherts were soft and fragile, and could be plastically deformed, and eventually detached as fragments, indicated by the chert chips inside the *interchert* mudrock. The chert was probably in the silica gel stage. This may be related to the low amplitude deformations of the top of the chert as well as the discontinuity of the layers resulting from the plastic stage rupture.

2) Nodule growth and coalescence - The strong irregularity at the base of the Nch facies (Figure 4) may result from nodule growth and coalescence (Warren 2016), highlighted during the burial by reverse density gradation. The reverse density gradient is established due to the different porosities of chert, usually less than 1% (Nagy 1970), and mudrocks, between 70% and 90%. These textural relationships produce a metastable arrangement that is also influenced by the cohesion and viscosity of the sediments, favored by the tender compacting of the mudrocks at the eodiagenetic stage (Mills 1983).

According to Knauth (1994), the occurrence of Nodules chert (Chn) with oblate spheroid shapes is typical of limestone replacement, where the long axis is indicative of the bedding plane of the pre-existing limestone host rock (Figure 4E). According to Southgate (1986), asymmetric nodules arranged in orderly horizons with a flat upper surface are expected when silicification occurs under the influence of the water table at the sediment-water interface. The absence of desiccation cracks and other features of subaerial exposure, suggests permanent water cover, and/or dense vegetation cover that prevented the formation and/or preservation of these features.

Nearshore wave and storm dominated (FA2)

Description: The facies constituting FA2 are: massive mudrock (Mm), sandstone wave lamination (Sw), sandstone hummocky (Shs), silicified microbialites (Ms), sandstone/siltstone horizontal lamination (Shl). It has a thickness up to 5 m, formed by tabular to lenticular layers, red whitish to gray, slightly friable (Mm, Sw, Shl, Shs facies), locally silicified, also

with the presence of microbialites (Ms facies; Figure 6). The Mm facies is restricted to the most basal part of FA2 and occurs interspersed with the Sw and Shl facies. The Sw facies is formed by a very fine sandstone to silt, have its wavy cross-lamination (*micro-hummocky*), with its wavelength not exceeding 5 cm, and a height up to 4 cm (Figure 7). The Sw facies is the most expressive of this association, being correlated along tens of kilometers. Locally this facies occur as symmetrical straight-crested small oscillation ripples. Symmetrical wave ripples are characterized by a mean wavelength ranging from 1 to 3 cm with amplitudes up to 0.5 cm. In cross-section, this ripples are symmetrical with rounded shapes, whilst in plan view they show numerous tuning fork bifurcations (Figures 7E, F). Two generations of symmetrical ripples has distinct crest alignment (1-E-W; 2-NE-SW). The Shl facies is formed by very fine sandstone, possibly siltstone, with horizontal lamination. Its occurrence is relatively restricted, and is associated with both Sw facies (Figures 7A-D) and Shs facies (Figure 8). The Shs facies occurs in the middle part of the studied succession. It has a thickness of about 60 cm, formed by thin to very thin, poorly selected, quartz sandstone with hummocky cross-stratification (Shs). The Shs has a height of about 18 cm, with the hummocks in its most accented parts tilting up to 11º. The hummock zone is well developed with clear convexity, while the erosion zone (swale) is less expressive internally, and more evident on the shape's *troughpoint* (Figure 8). The internal intersection between the laminations is predominantly tangential. The Ms facies is composed of a columnar-laminated microbialitic complex. This facies features sub-millimeter bimodal lamination between a thicker light colored lamination and a thinner darker lamination. The stratiform base lamination is about 2 to 3 cm thick, low synoptic relief, with moderately convex lamination with high laminar inheritance (Figure 6). In its median portion, approximately 4.5 cm, there are pseudo-columnar microbialites ranging from 2 to 7 cm wide, with vertical growth vector, have asymmetric parabolic lamination and a high degree of laminar inheritance. At the top, the columnar portion forms a branch that retains the same characteristics as the anterior portion. The FA2 has a more restricted extension than the FA1, and occurs stratigraphically in the intermediate to upper part of the studied sequence, sometimes interdigitated with the FA1 and FA3 associations.

Interpretation: The FA2 represents the shoreface portion of a lake subjected to a reworking by far-weather waves (Sw facies), and eventually storm waves (Shl and Shs facies). During quiescence, mud precipitation (Mm) was dominant. Symmetrical wave ripples are common features in lake sediments, formed in shallow portions with depths not exceeding 20 cm (Allen 1981). These microforms are generated by oscillatory flow resulting from

currents produced by wind friction on the surface of lake water in far-weather periods (Bagnold 1946; Schnurrenberger et al. 2003; Greenwood 2006). The presence of symmetrical undulations in the upper sections of sand bodies indicates wave rework after deposition (Guion et al. 1995; Marshall 2000). The presence of very thin sandstone with horizontal lamination (Shl) is interpreted as a result of high oscillatory flow intensity under probable storm conditions, with a predominance of one-way currents under higher flow regime in lacustrine sandy clay substrate. As the height of the wave accumulated under storm influences, peripheral portions of the lake substrate were subjected to orbital velocities greater than the ripple threshold velocity, from which the sedimentary particles began to move on a flat bed, with consequent generation of Shl facies (Reineck and Singh 1975; Allen 1981).

The occurrence of sandstone with HCS (Shs facies), refers to possible storm occurrences, and reinforces the presence of Sw and Shl facies. According to Dott and Bourgeois (1982), a very fine sandstone to siltstone, with wave-formed ripples and horizontal lamination (Sw and Shl facies, this work) is part of the typical succession associated with HCS, and the Sw facies developed where water depths are greatest and the sand source at the site is reduced sufficiently to form only small HCS, while the sandstone with horizontal lamination (Shl) are considered to be HCS hybrids, and represent strong oscillation in flow intensity between unidirectional and undulatory, respectively. Although HCS is commonly related to the lower shoreface of the marine coastal environment (Dott and Bourgeois 1982; Walker and Plint 1992; Cheel and Leckie 1993; Dumas and Arnott 2006), they are often described in undoubtedly lacustrine deposits (Murty and Polavartaru 1975; Allen 1981; Eyles and Clark 1986; Duke 1985; Greenwood and Sherman 1986; Liu et al. 2012; Li et al. 2014; Wang et al. 2015).

In an extensive survey of the occurrence of HCS in sedimentary records from Proterozoic to recent, Duke (1985) states that HCS in lake deposits, generated at water depths between 1-2 m, are essentially identical to the various marine occurrences, and with similar formation process. According to this author, while HCS related to shallow marine environments has its occurrence conditioned to hurricane events and intense winter storms, its lacustrine analogues are strongly associated with less energetic events of terrestrial wave cyclones.

For Duke (1985), the preservation of HCS generated at relatively shallow water depths and less violent storm events associated with lake environments does not necessarily imply that these structures, when generated in shallow marine environments and under less energetic storms, also preserve themselves. Because the constant erosive intensity of far-weather waves

and tidal currents, among others, significantly reduces the preservation potential of these structures in very shallow marine environments. On the other hand, in the lake environment, far-weather waves are usually low in energy, and tidal influence is disrupted, allowing HCS to be preserved at lower bathymetric levels than those normally accepted for its marine analogs (Duke, 1985). According to Eyles and Clark (1986), the common presence of HCS facies in late Pleistocene lake sediments in the Ontario basin is a reliable record of the shoreface portions of lake basins.

The peripheral portions of the Pedra de Fogo Lacustrine System (SLPF) were the site of development of columnar-laminated microbialite (Ms facies), especially in the driest periods, most conducive to the development of these organosedimentary structures (Link et al. 1978; Casanova and Hillaire-Marcel 1992; Vennin et al. 2019). The stratiform base shape suggests a calm paleoenvironment, which corresponds to the idea of developing a lacustrine system in peripheral portions, as stated above. The transition from stratiform to pseudo-columnar is probably related to some paleoenvironmental change, probably increased paleobatimetry of the lake system and/or greater siliciclastic input (Hofmann 1973).

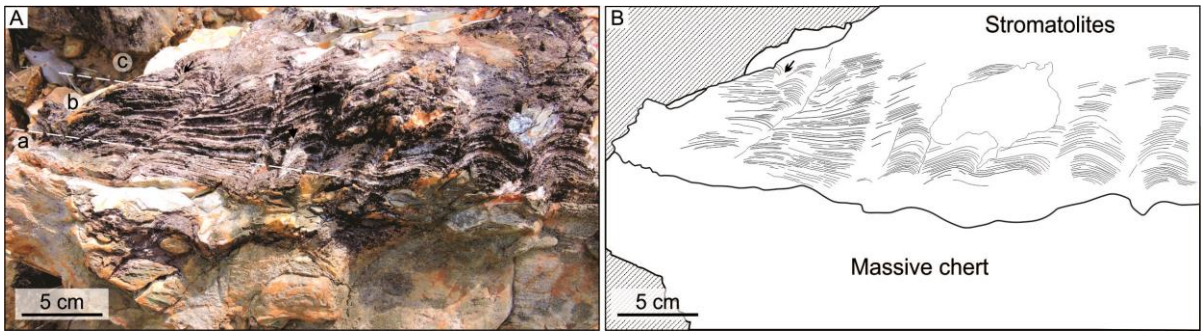

Figure 6-**A, B)** Columnar-laminated microbialitic complex with sub-millimeter bimodal lamination alternating between a thicker light colored lamination and a thinner dark lamination. The lower portion (a) has stratiform lamination, moderately convex with high laminar inheritance and dome synoptic relief. In the middle portion (b) there are cylindrical columnar microbialites with vertical growth vector, contiguous structures and asymmetric parabolic lamination with high degree of laminar inheritance. The top (c) columnar portion branches (arrows) with horizontal beta-like shape that maintain the same characteristics as the median portion.

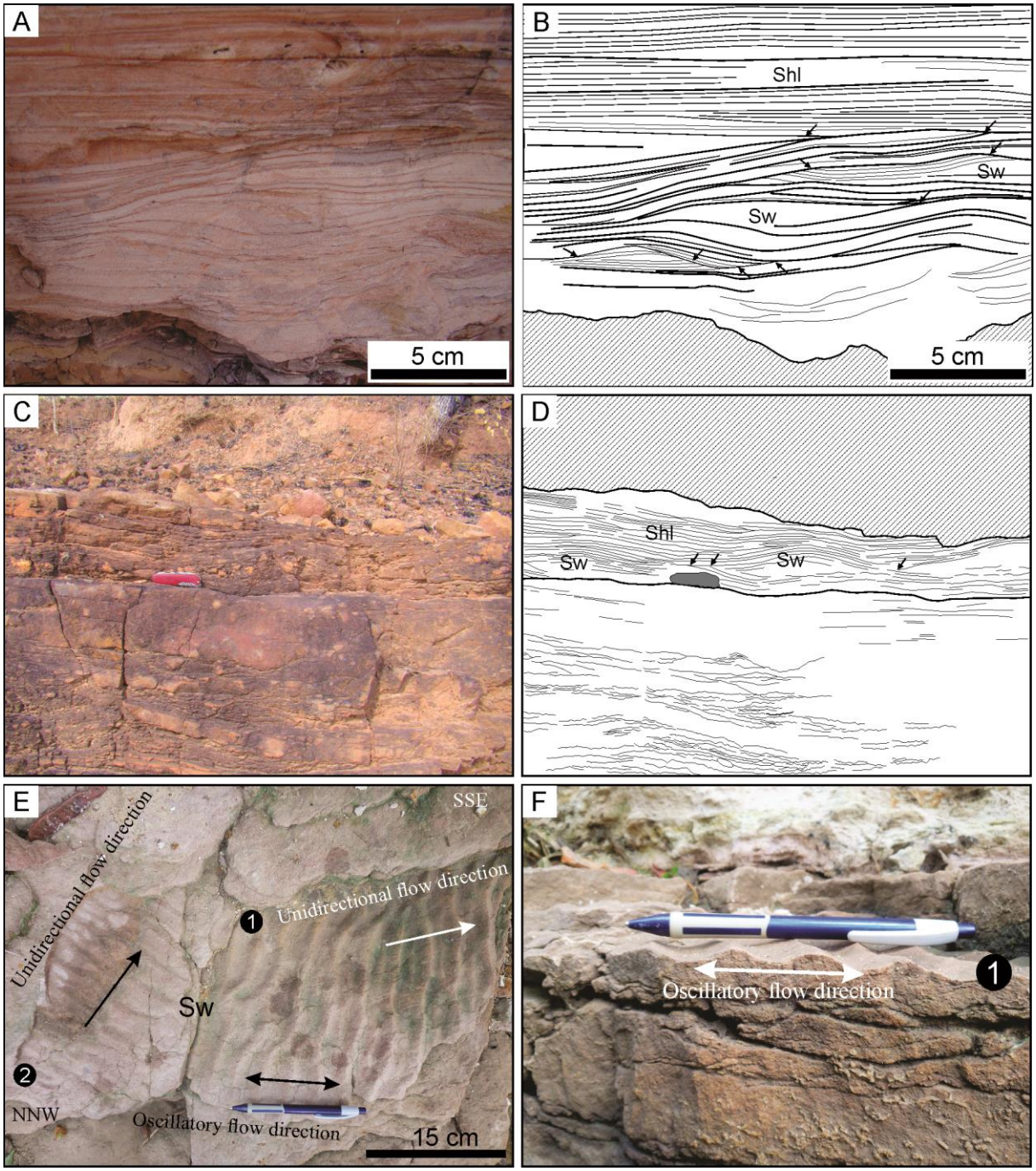

Figure 7-General aspect of the FA2 association (Nearshore wave and storm dominated). **A-D)** Very fine sandstone/siltstone with horizontal lamination (Shl) and wave-formed ripples (Sw). Arrows indicate micro-hummocky surfaces. **E)** Two generations of symmetrical wavy ripples (Sw) in plan view. 1-ripples with a rounded shape and weakly sinuous 3D crest and tuning fork bifurcations. Note that the ripple lee-side slope is directed towards SSE. Oscillatory flow direction is N010°. 2-ripples with a rounded shape. Note that the ripple lee-side slope is directed towards ESE. First generation of wavy ripple in profile view. Note the symmetric and rounded shape. C, D) pocket knife measures 9 cm. E, F) pencil measures 15 cm.

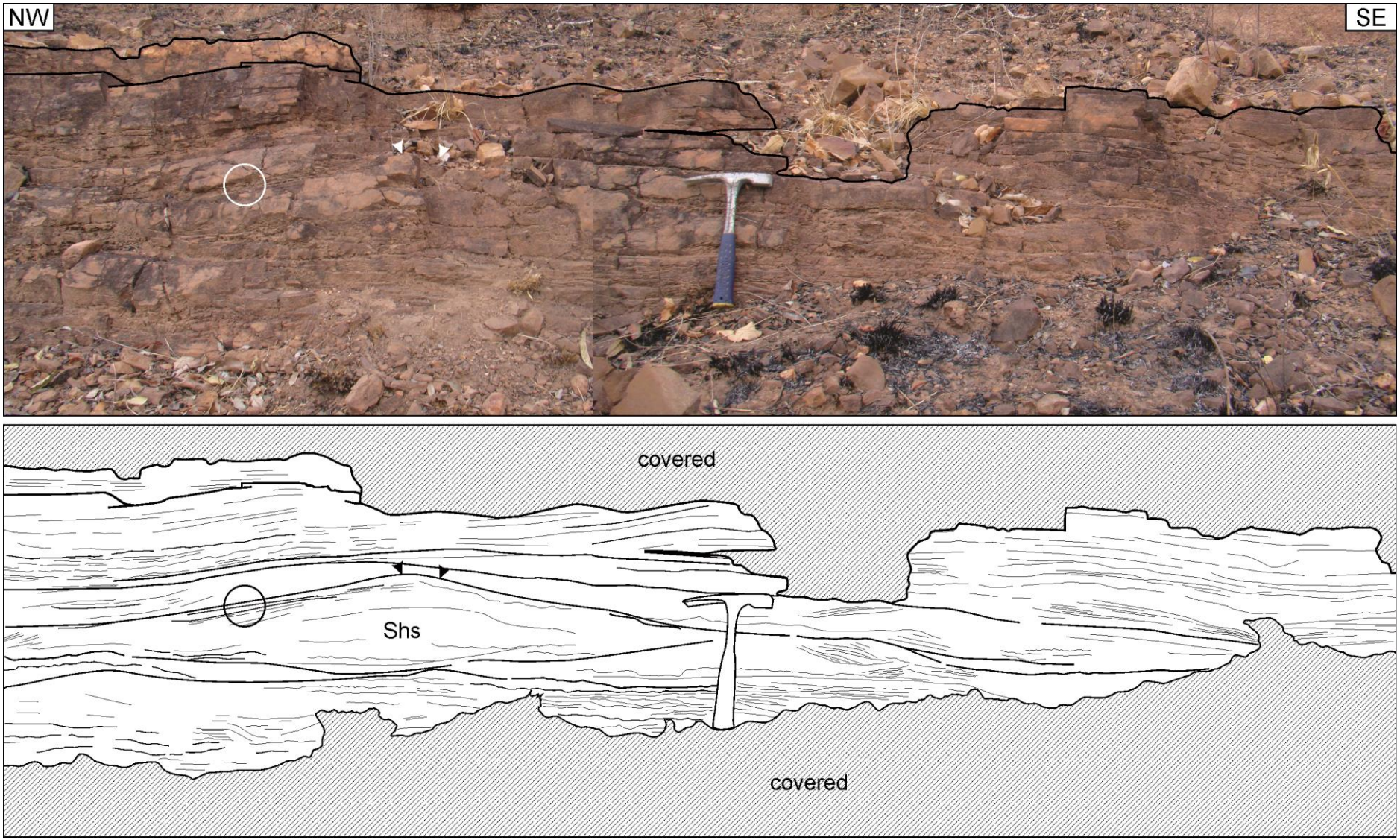

Figure 8-Fine Sandstone hummocky cross-stratification (Shs facies). The circle shows the low dip angle of the lenses (~ 11º), the arrows indicate the aggradation part of the structure or hummock.

Terminal splays (FA3)

Description: The FA3 association is made by massive claystone (Cm), sandstone subcritically climbing ripples cross-lamination (Sc) and massive sandstone (Sm). The geometry of the layers was grouped into four basic types (Figure 9), related to the degree of flow confinement (channeled and non-channeled), and the textures, sedimentary structures and contact relationships seen in the field (Fisher et al. 2007; Nichols and Fisher 2007; Fisher et al. 2008; North and Davidson 2012).

The FA3 layers are light red, with thicknesses between 0.1 and 1.4 m and widths between 2.0 and 11.0 m. They consist predominantly of fine, eventually coarse sandstone. The top of the layers are straight and regular, sometimes with an erosive base, marked by lags of rounded quartz and chert clasts of up to 5 cm in diameter with chert nodules and eventual fragments of silicified ferns, rolled in a concordant position to bedding (Figures 10 A, B). Individual lenses can be attached laterally and/or vertically, or isolated by the Shl and Sw facies of the FA2. As such, they form both amalgamated and interconnected sand bodies as well as isolated units (Figures 10 C, D). This association occurs in the lower part of the studied sequence, usually associated with FA2, and eventually with FA1.

Interpretation: The geometry of the layers, textures, facies, thicknesses and contact ratios allowed the interpretation of FA3 as ephemeral systems, partly unconfined, deposited directly on a relatively shallow lacustrine substrate. The reduced thickness of the G1 layers, their sheet geometry predominating fine grains, non-erosive base and the lack of depositional structures represent the distal part of a relatively low magnitude unconfined flow dominated by the fine grain load transport in suspension (North and Davidson 2012). The interlaying with Mm facies indicates that deposition occurred in multiple events, interrupted by periods of relative quiescence (Love and Williams 2000).

The also tabular geometry of G2, the absence of sedimentary structures and particle size contrast, as well as the interlaying with thin siltstone levels suggest deposition under a regime similar to the Kneller (1995) depletive steady flows. The low thickness of the interbedded mudrocks, compared to the greater thickness of G2, indicates that the deposition occurred in proximal regions of the splay/lacustrine system. The erosive base of the G3 beds suggests that, at least initially, the depositional flow was relatively energetic. The lack of grain size variation and apparent suppression of sedimentary structures suggest rapid flow deceleration, resulting in the deposition of sediment in suspension (Fisher et al. 2008).

The isolated (lenticular) part of G3 may be related to more distal deposits of the terminal splays that have moved further away from the main stream. Alternatively, the isolation of sand bodies may be due to a long period between the return of potential events in that particular sector of the distributive system (Fisher et al. 2007). This interpretation is reinforced by the fact that these lenses are engulfed by the Shl and Sw facies, indicative of intense wave rework (Allen 1981; Alexander et al. 2001). The erosive base, thinness, presence of quartz and chert pebbles, as well as a 60 cm long silicified fern wood fragment in a horizontal position, suggests that G4 represents the early stages of a flow that turned itself unconfined, but still retained the erosional component, indicating proximity to the splay region (Bustillo et al. 2002). Scattered quartz and chert pebbles supported by fine to coarse sandy matrix, in addition to the occurrence of wood fragment indicates that as the stream became unconfined, this fraction of proximal sediment was transported and deposited as a bed load (Tunbridge 1984; Jorgensen and Fielding 1996). It is assumed that the lack of primary structure is a result of the high concentrations of suspended sediment in this proximal zone (Alexander et al. 2001).

The presence of a transported wood fragment suggests that eventually the floods were strong enough to generate overbank flow events into trunk channels, capture and transport eventual fragments of its banks (Alexander et al. 1999). In recent analogous environments, this process of flow extravasation is relatively common but potentially less energetic (Lang et al. 2004). The registration of an ephemeral systems in the studied deposits is reinforced by the identification of sclerenchymal tissue in the spine of two gymnosperm species - *Kaokoxylon astrosclereidea sp. nov.* and *Cordaixylon sp.* - identified by Conceição et al. (2019, submitted for publication), in the same outcrops described together with this work, which its main function is the sustenance, being characteristic of plants that live in environments under constant flooding.

The variation in layer thickness, punctual presence of fern woods up to 60 cm, as well as localized occurrence of quartz lags and other fragments can be interpreted as a consequence of variations in sediment load and magnitude of terminal splays events, and/or be directly related to the preserved portion of the deposit. Whereas, according to Fisher et al. (2007), terminal splays are deposited by unconfined flows that show radial decrease in flow velocity and thickness with increasing source distance. Thus, the levels containing quartz pebbles and centimeter woods of bedload-dominated ferns should be related to the proximal portions of splays, which still preserve sufficiently high energy to carry these fragments. While the levels with very thin sandstone to siltstone, possibly suspended load-dominated, and with thinner

thickness, are related to the more distal parts of the splays, resulting from the spreading and consequent decrease in the energy of the event (Fisher et al. 2008).

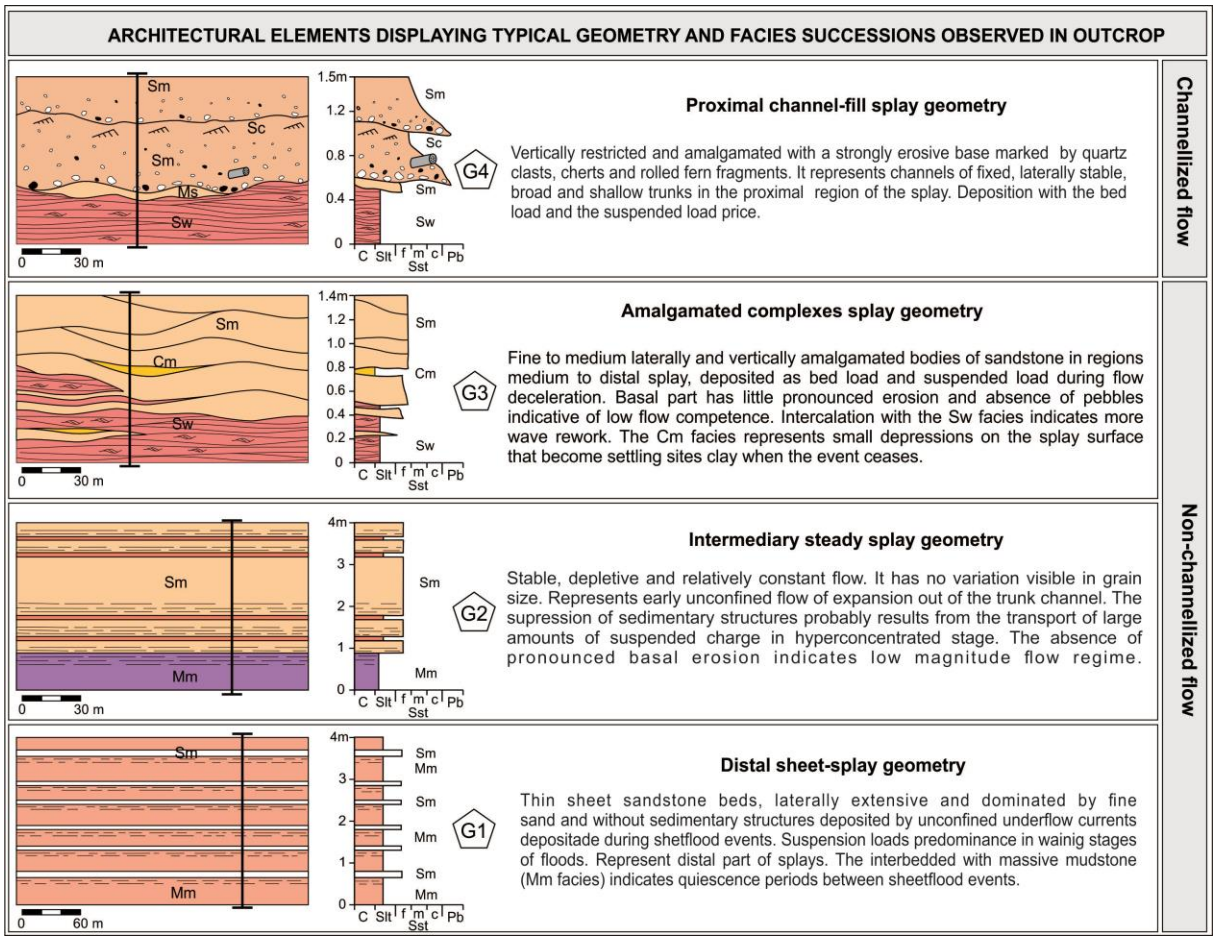

Figure 9-Architectural elements and facies observed for the Terminal Splays deposit (FA3). According to the geometry of the elements, they were grouped into four representative distinct types of; G1-distal sheet-splay geometry; G2-intermediatery steady splay-geometry; G3-Amalgamated complexes splays geometry; and G4-Proximal channel-fill splay geometry.

According to North and Davidson (2012), after the retreat of the lake, the point where the main flow used to meet the coast becomes the point of decondition of subsequent floods with rapid decrease in flow depth, and consequent deposition of the sedimentary load. This feature was reported by Lang et al. (2004) and Fisher et al. (2008) as terminal splay, and by Tooth (1999) as terminal floodout. The massive clay lenses of the Cm facies, interspersed with very fine sandstone layers (Sc), are interpreted as small depressions on the surface of the splays that become ponds and later sites of mudrock precipitation after flash flood events.

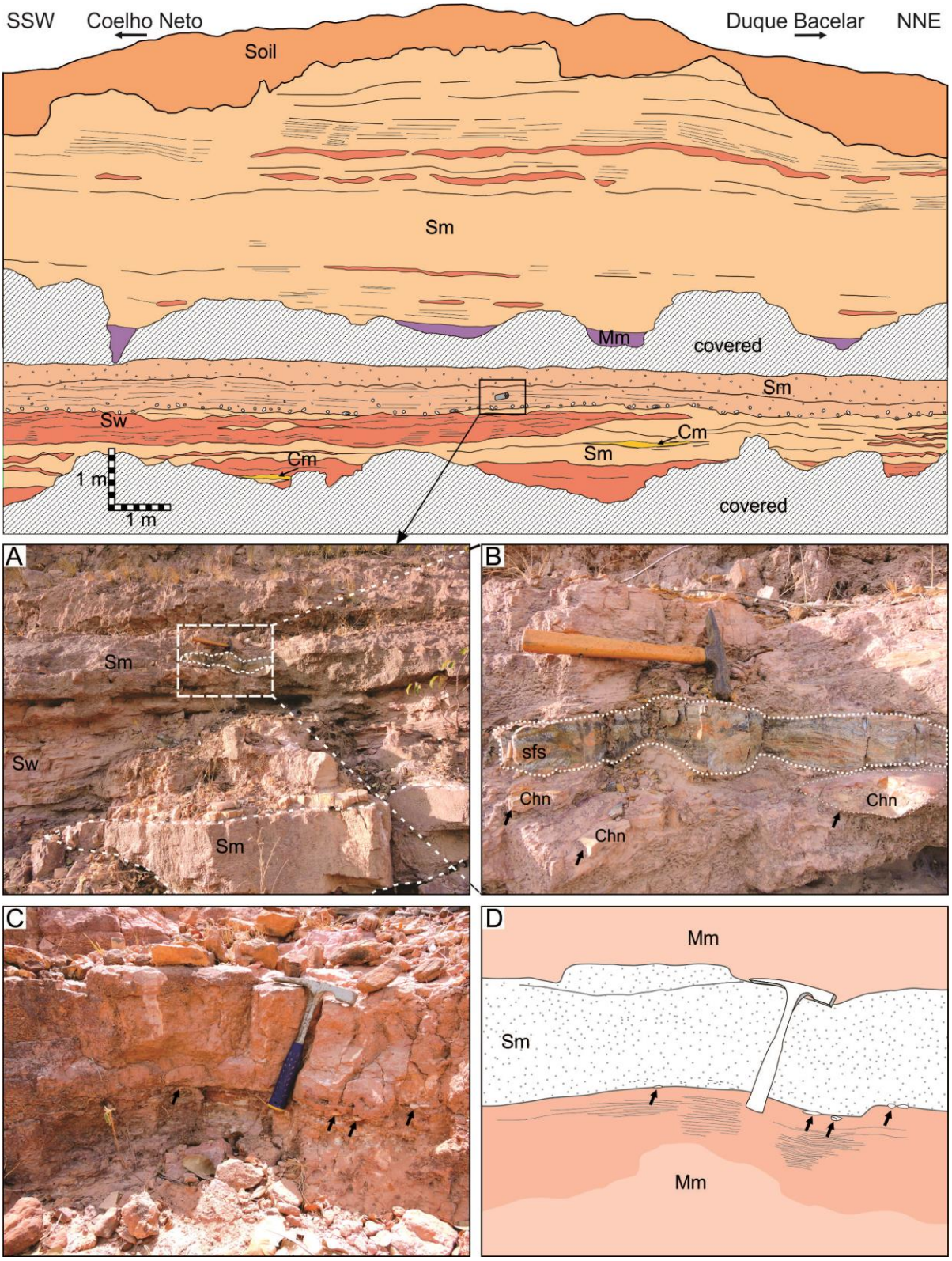

Figure 10-Overview of the FA3 association. **A)** Tabular layer of fine to coarse massive sandstone (Sm facies) with tabular geometry with silicified wood. Fine sandstone lenses (lower dotted), equally massive inside the sandstone with wave-formed ripples (Sw facies). **B)** Detail of silicified fern stem (sfs) (~ 60 cm long) strongly amalgamated because of compaction. Chert detrital nodules (Chn) (arrows). **C, D)** Thin, massive sandstone layer about 30 cm thick, flat top and bottom, with no apparent variation in grain size. Chert fragments about 5 cm in diameter occur at the contact between the Sm and Mm facies (black arrows).

Distal braided (FA4)

Description: The FA4 association consists of laminated mudrock (Ml), sandstone supercritically climbing ripples cross-lamination (Scs), sandstone horizontal stratification (Sh), sandstone tabular cross-stratification (St). This association is formed by metric tabular layers laterally continuous, cream/orange, composed of fine to medium, subordinately coarse sandstones, mainly composed by quartz, with well-selected and well-rounded grains, forming horizontal cross-stratification sets, sometimes with tangential basis (St facies) of small to medium size, in addition to horizontal stratification (Sh facies) and sandstone supercritically climbing ripples cross-lamination (Scs).

The sets have thinning-upward with generally flat topsets. The base of the cosets has thicker sets (~ 40 cm), and is characterized by the occurrence of St facies. To the top, the sets thin and are about 10 cm thick, with a predominance of Sh and Scs facies (Figure 11). The paleocurrent direction varies between SW/NW, with predominance of the SW vector. Eventually, thin layers of light to reddish gray mudrock with massive wavy bedding (Ml facies) intersect with the top of the St facies. This association is restricted to the base of hills up to 200 m high that constitute the predominant relief in the vicinity of the municipalities of Coelho Neto and Duque Bacelar-MA, and Altos-PI. In the Nova Iorque-MA, and Teresina-PI section, the FA4 association is restricted to the Boa Esperança Dam and Poti River beds, respectively.

Interpretation: The laterally continuous tabular geometry and organization in fining upward cycles of the St, Sh, Scs and Ml facies sandstones suggest braided fluvial deposition (Miall 1977; Gibling and Rust 1984). St facies sandstones indicate the migration of straight ridged bed shapes (2D), related to the unidirectional flow actuation for SW/NW in pipelines under lower flow regime. Reactivation surfaces in St facies indicate periods of stopping and reactivation of bedform sedimentation associated with changes in sedimentary energy/flow in these facies (Lindholm 1987; Tucker 2003).

The occurrence of Sh facies suggests periods of increase in flow velocity with bedding plane sandy traction load deposition under higher flow conditions (Reineck and Singh 1975). In addition, the presence of sandstone supercritically climbing ripples cross-lamination (Scs facies) at thin levels between the St facies sets, is interpreted as the bottomset of adjacent bed shapes in the channel migration dynamics, and suggests deceleration in the flow regime with suspension predominance, and consequent increase in sedimentation. Possible restricted and sheltered marginal portions of the more energetic flow of the channel were the mudrock settling site evidenced by the Ml facies. The FA4 association is compatible with braided

fluvial deposits that migrated preferentially to SW. The geographical positioning, stratigraphic, paleocurrent pattern, sedimentological and depositional characteristics were preponderant to relate it to Piauí Formation (Ribeiro 2000).

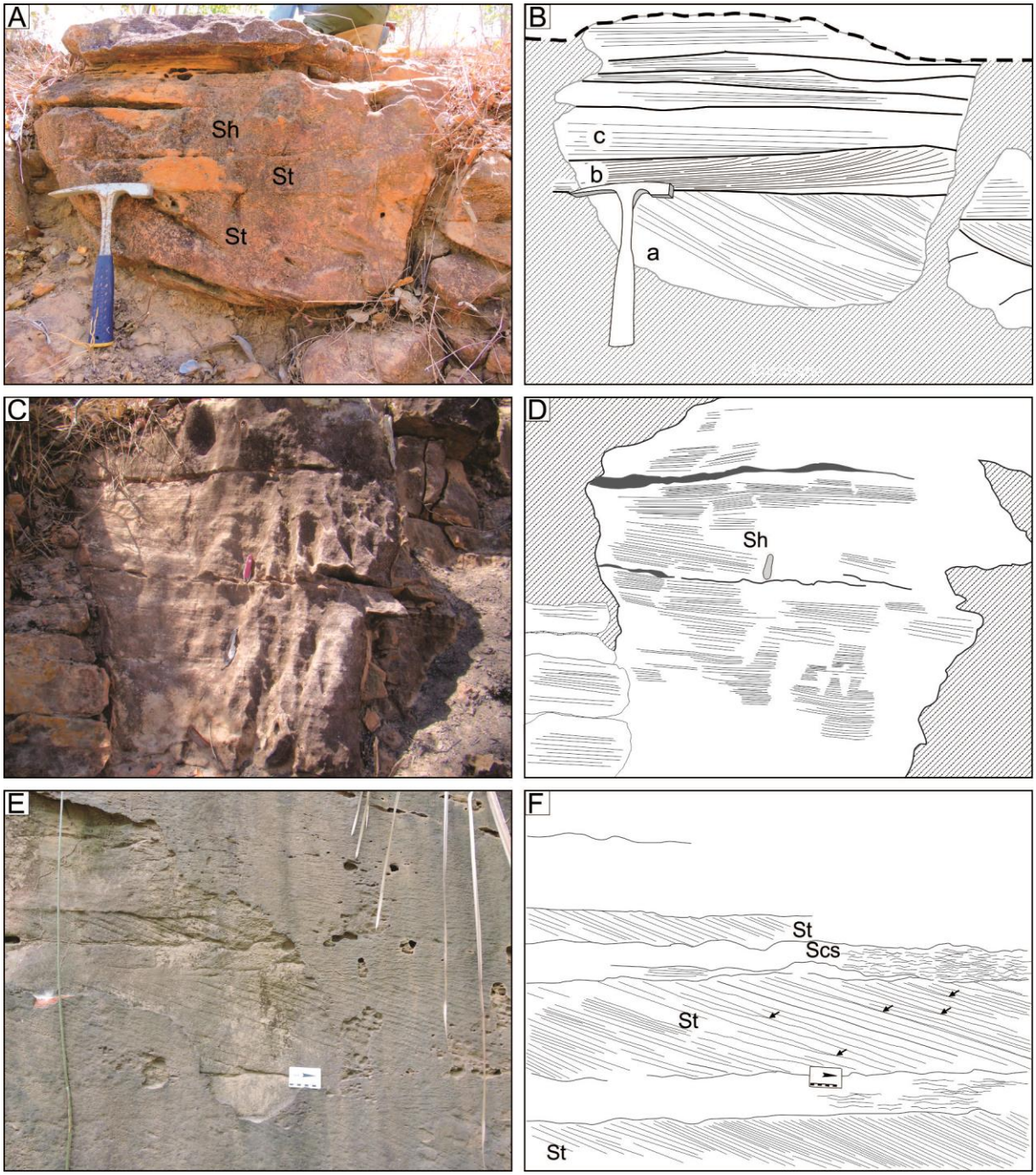

Figure 11- Overview of the FA4 Association. **A, B)** Tabular cross-stratified sandstone with tangential base (St) and thinning-upward of the sets, containing horizontal stratification (Sh). **C, D)** Fine to medium sandstone with horizontal stratification (Sh). **E, F)** Tabular cross-stratification sets (St), sectioned by levels with sandstone supercritically climbing ripples cross-lamination (Scs). Arrows indicate reactivation surfaces

DISCUSSION

PALEOCLIMATE INFLUENCE IN THE SEDIMENTATION SYSTEM

Outcrops on the east-southeast edges of the Parnaíba Basin, north-northeast region of Brazil, expose part of the Pedra de Fogo Formation sedimentary succession. The predominance of fine-grained siliciclastic sedimentation, interspersed with thin tabular to lenticular layers of fine to medium sandstone, with associated microbialites and fossil plants, many in their living position, is consistent with an endorheic lacustrine system, periodically subjected to episodic storm and flood events.

The depositional environment of the Pedra de Fogo Formation has historically been described as having a marine influence, ranging from fluvio-deltaic to shallow marine (Aguiar 1964; Moore 1964; Lima and Leite 1978; Faria Jr. 1979; Faria Jr. and Truckenbrodt 1980a, 1980b; Coimbra and Mussa 1984; Caldas et al. 1989; Dino et al. 2002), to sabkha plains under occasional storm influences (Góes and Feijó 1994). Only recently, works of bio and lithostratigraphic matter have suggested restrictive continental environments (fluvio-lacustrine), under episodic flooding with climatic seasonality (Andrade et al. 2014; Araújo et al. 2016).

This apparent divergence regarding the paleoenvironment is due to the varied lithological set, formed by sedimentation cycles of sandstones, siltstones, shales, limestone, gypsum and mainly chert (Plummer 1946; Barbosa and Gomes 1957; Melo and Prade 1968; Faria Jr. and Truckenbrodt 1980a, 1980b). Along with a diverse fossil record, from fish remains and labyrinthodont amphibian (Price 1948; Santos 1989a, 1989b, 1990; Cox and Hutchinson 1991; Santos 1994), and more recently, new *genus* and species such as: *Timonya anneae*, *Procuhy nazariensis*, *Rhinesuchidae indet.*, *Captorhinus aguti* (Cisneros et al. 2015), *Sphenacanthus ignis sp. nov.*, *Bythiacanthus lopesi sp. nov.* and *Rubencanthus diplotuberculatus gen. et sp. nov.* (Figueroa and Gallo 2017). In addition to this vast faunal content, the deposits of Pedra de Fogo Formation have a characteristic floristic content: *Calamitáceas* (*Arthropitys cacundensis*), *Cordaitales* (*Carolinapitys maranhensis*), *Amielon bieloi* (Coimbra and Mussa 1984), *Pteridospermophyta*, *Teresinoxylon* e *Eusebioi* (Caldas et al. 1989), *Tietea singularis* e *Psaronius brasiliensis* (Martins 2000), *Grammatopteris freitasii* nov. sp. (Röβler and Galtier 2002a), *Dernbachia brasiliensis gen. nov. et sp. nov.* (Röβler & Galtier 2002b), *Botryopteris nollii sp. nov.* (Röβler and Galtier 2003). More recently Conceição et al. (2016) and Iannuzzi et al. (2018) have described a variety of *Psaroniaceae* e *Gymnospermaceae*, many of which are in a life position.

Although the global paleoclimatic trend, after the end of carboniferous glaciation had been the general temperature increase (Retallack 1999; Scotese et al. 1999; Gibbs et al. 2002; Winguth et al. 2002; Chumakov and Zharkov 2002, 2003; Kiehl and Shields 2005; Wagner 2003; Roscher et al. 2011; Boucot et al. 2013; Zambito and Benison 2013), the prevailing weather pattern during the permian is described as climate seasonality, strongly influenced by a regime of monsoon (Kutzbach and Gallimore 1989; Gibbs et al. 2002).

The geographical/temporal positioning of the "Pedra de Fogo Lacustrine System" (SLPF) strongly suggests that it was subject to these seasonal climate fluctuations, similar to what occurred in other parts of Pangea (Crowley et al. 1989; Hmich et al. 2006; Wagner and Mayoral 2007; Lojka et al. 2009). Moreover, the multiplicity of environments and the vast fossil content reflect the intense paleoclimatic and paleogeographic changes that occurred in the Early Permian (DiMichele et al. 2001; Scheffler et al. 2006; Blakey 2008; Boucot et al. 2013), indicating that these changes significantly influenced the depositional framework of the Pedra de Fogo Formation in this portion of Pangea (Torsvik and Cocks 2004).

EVIDENCES FOR FLUCTUATIONS IN LAKE LEVEL

Microbialites are important indicators of lacustrine palaeoshorelines (Casanova and Hillaire-Marcel 1992). According to Vennin et al. (2019), microbial deposits are powerful environmental proxies that can provide valuable information on local physicochemical conditions such as: accommodation space, hydrodynamics and water chemistry. Moreover, when temporally analyzed, they may record shoreline migration and consequent elevation evolution, surface area, volume and chemical composition of lakes. Although there are no climate restrictions for microbialite development, since microbial deposits occur in a wide variety of physicochemical conditions, from low to high temperatures (Krumbein et al. 1977; Sumner et al. 2015), from low to high pH (Van der Meer et al. 2005; Beam et al. 2016), and from freshwater to hypersaline (Freytet and Verrecchia 1998; Arp et al. 2010; Arenas and Jones 2017; Lindsay et al. 2017). These structures are generally abundant in restricted, often hypersaline, marine and continental environments (eg, hypersaline and freshwater lakes, and carbonate sources), and are most developed in more arid periods or climates (Casanova and Hillaire-Marcel 1992).

The occurrence of microbialites (Ms facies) stratigraphically associated with woods in the life position (Figure 5C), sometimes underlaying (section 2), sometimes overlapping (section 6), or between levels with woods (sections 1 and 5; Figures 3), are interpreted as resulting from dynamic expansion and contraction movements of the SLPF, with migration of

its palaeoshoreline, in response to the prevailing Early Permian climate seasonality regime (Lojka et al. 2009; Horton et al. 2012; Laya et al. 2013). This alternation of woods in life position and microbialites is indicative that these plants inhabited peripheral regions of these lakes, where the moisture level remained higher (DiMichele et al. 2001; Hmich et al. 2006; Montañez et al. 2007; DiMichele et al. 2009, 2010).

Studies on recent and current endorheic lake systems under arid to semi-arid climate show that climate fluctuations are the main controlling parameter in fluctuating lake levels (Richardson and Richardson 1972; Haberyan and Hecky 1987; Halfman and Johnson 1988; Casanova and Hillaire-Marcel 1992; Lall and Mann 1995; Godsey et al. 2005; Bouton et al. 2016; Vennin et al. 2019). In addition to climate, tectonic activity also influences the variation of the lake base level (Shanley and McCabe 1994; Catuneanu 2011). However for Bouton et al. (2016) this should only be considered as an additional factor in the distribution of microbial deposits when there is a peculiar straight distribution of these deposits along an acute topographic fall, and in tectonically active regions such as occurs on Antelope Island on the Great Salt Lake, northwest of Utah (USA).

Our results suggest that spatial/stratigraphic variations between microbial and woods position records, together with the found facies associations (FA2 and FA3), are associated with bathymetric fluctuations of SLPF, which was effectively controlled by factors, since no faults or other structures indicating significant tectonic activity were recorded. Moreover, the Parnaíba Basin genetically does not present effective tectonism (Figueiredo and Raja Gabaglia 1986).

PALEOENVIRONMENTAL OF LACUSTRINE SYSTEM PEDRA DE FOGO

The volume, dimensions and geographic distribution of the fossil plants registered here and in other studies (Caldas et al. 1989; Röβler and Galtier 2002a, 2002b, 2003; Iannuzzi and Langer 2014; Conceição et al. 2016), shows that this taphoflora proliferated near the SLPF, which is a current area of the Parnaíba Basin, located in the central part of Pangea during the Cisuralian (Figure 12).

According to Carroll and Bohacs (1999), lake basins are subjected to rapid water surface oscillations, with a relative balance between the potential accommodation rate (fundamentally tectonic) and the water and sediment filling (fundamentally climatic), what makes the lacustrine system an excellent indicator of climatic and tectonic variations both in hand specimen and outcrop scales (Kutzbach 1980; Talbot and Allen 1996; Gierlowski-Kordesch and Kelts 2000; Golonka and Ford 2000).

The volume, dimensions and geographical distribution of woods recorded in this and other studies (Caldas et al. 1989; Röβler and Galtier 2002a, 2002b, 2003; Iannuzzi and Langer 2014; Conceição et al. 2016), show that taphoflora spread near the SLPF, which covered a large area of the current Parnaíba Basin, located in the south-central portion of Pangea during the Cisuralian (Figure 12).

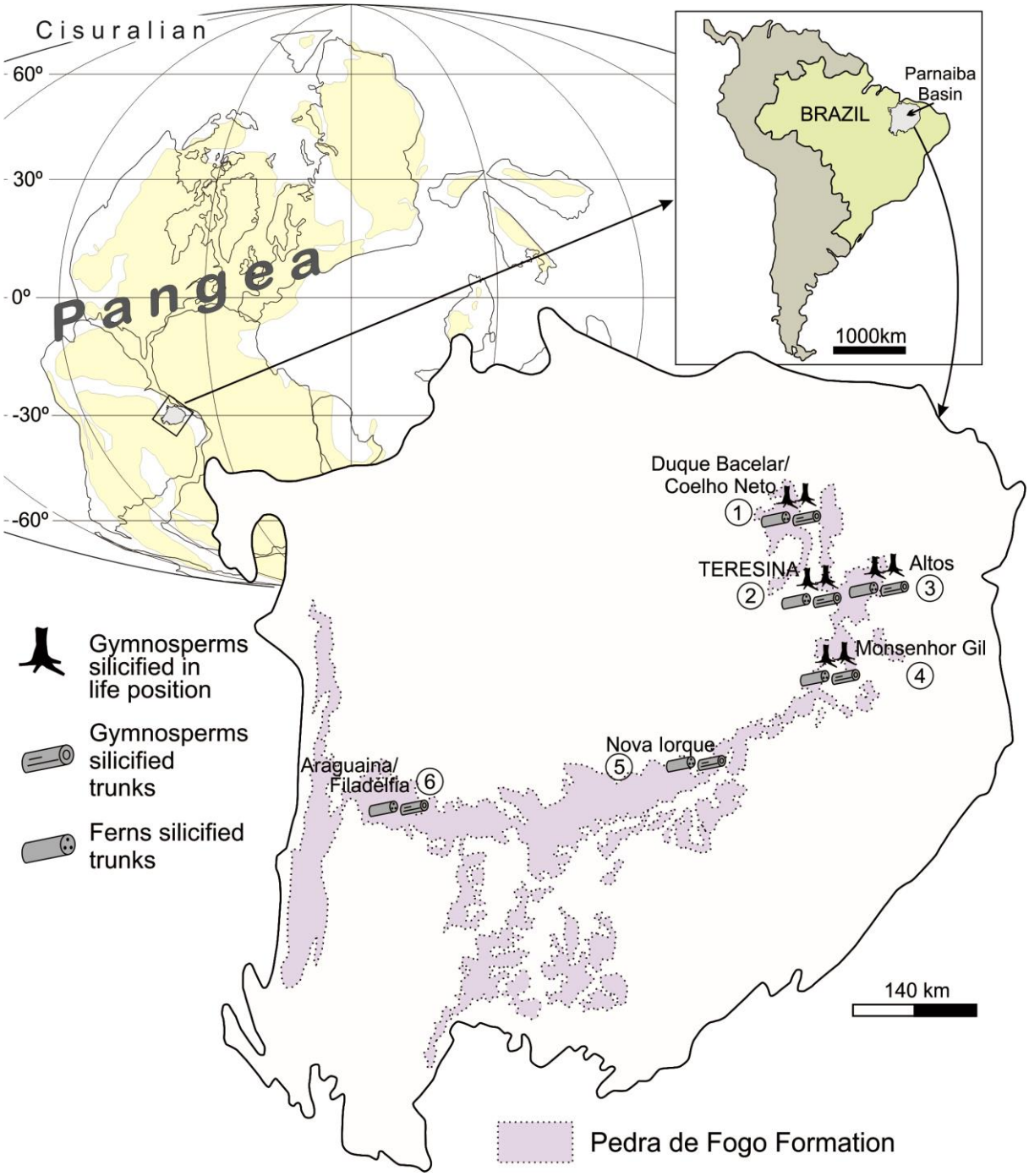

Figure 12-Occurrences distribution of fossil woods in the Pedra de Fogo Formation. 1, 2, 3, 4, 5) In this study; 1) Conceição et al. (2016); 2) Caldas et al. (1989); 5) Iannuzzi and Langer (2014); 6) Röβler and Galtier (2002a, 2002b, 2003).

Conceição et al. (2019, submitted for publication), show that gymnosperm species that occur in the study area do not have true growth rings, only small and poor growth interruptions. This indicates that these trees developed under an environment that allowed for continued year-round exchange activity under conditions favorable to growth. These elements suggest that the moisture content was high enough (at least seasonally) to keep the water table high for the growth and scattering of this riparian flora, developed on the SLPF lakeshore plains. These data are consistent with recent paleontological records in the studied region (Cisneros et al. 2015; Conceição et al. 2016; Iannuzzi et al. 2018). In addition, Conceição et al. (2019, submitted for publication) identified anatomical structures in some of the analyzed taxa, such as: gaps, septations, and canals in the medullary tissue - interpreted as a xeromorphic resource to facilitate aeration or water storage into its tissues during dry-phase, that are facilitators of aeration or water storage indicating a xeromorphic resource to facilitate water retention in periods of low water oxygenation or prolonged drought.

According to Rees et al. (1999), temperature, precipitation and seasonality are critical factors in the control and pattern of vegetation. This suggests a less arid “microclimate” in contrast to the globally registered (Gastaldo et al. 1996; Scotese et al. 1999; Rees et al. 1999; Chumakov and Zharkov 2002, 2003; Tabor et al. 2008; Boucot et al. 2013; Zambito and Benison 2013). This flora, given the size of the fossilized woods (Figure 5E), was able to grow and proliferate over a period of time (hundreds to a few thousand years). However, the absence of extensive layers of coal indicates that although there was sufficient moisture for the proliferation and vertical and horizontal expansion of this taphoflora (Figure 12), the *sensu lato* climate remained under semi-arid conditions sufficiently to not allow formation and/or coal preservation (Cecil et al. 1985; Ziegler et al. 1987).

The massive occurrence of cherts layers and nodules replacing cabonatic/evaporitic molds, microbialites and large woods, many in life position, are strong indications that during the deposition of Pedra de Fogo Formation the climate was semi-arid to seasonal (Cecil 2015). Under these conditions, rainfall was probably reduced during a long dry (semiarid) season, which reduces the amount of erosion and clastic sedimentary transport (Figure 13). According to Cecil (1990), maintaining these conditions, the erosion and transport of clasts will occur mainly by underwater currents from catastrophic flood events. At the same time these conditions contributed to the carbonate/evaporite precipitation.

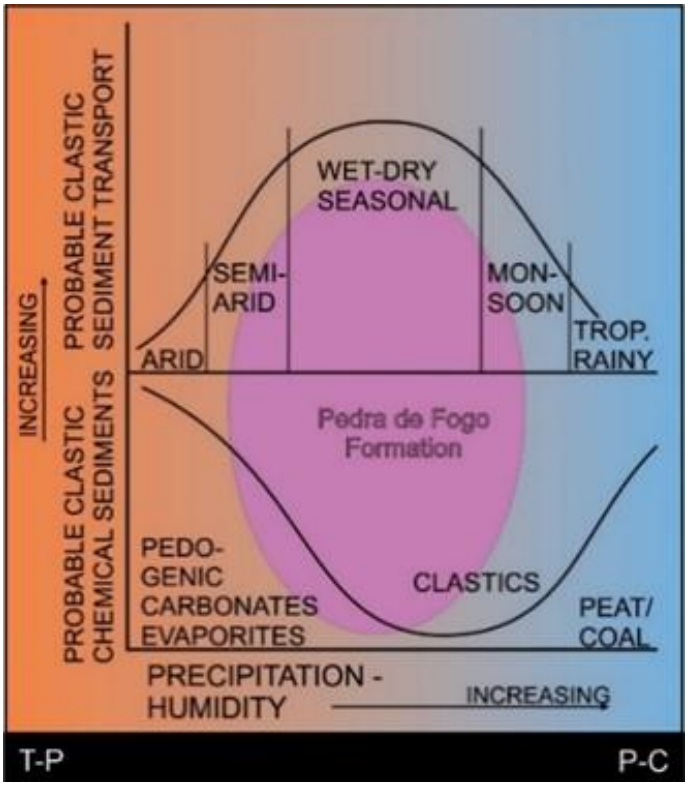

Figure 13- Suggested climate regime for the Pedra de Fogo Formation based on the found facies associations, modified from Cecil (1990).

The sedimentary facies show that SLPF was subjected to seasonal weather conditions, often affected by storm regimes (Marsaglia and Klein 1983; Duke 1985) and/or monsoon (Vos and Hobday 1977; Kutzbach and Gallimore 1989; Parrish 1993; Kutzbach et al. 2008; Wang et al. 2014). These climatic events triggered high density torrential flows that caused rapid burial with consequent fossilization of woods in life position. In their terminal portions, these currents spread, losing energy and depositing tabular and sheet layers under plain and shallow lacustrine substrate. In periods of quiescence between one event and another, these deposits were subject to intense rework by waves of far-weather, and eventually storms (Figure 14).

The humidity at the edges of SLPF was high enough to meet the water needs of a mesophilic taphoflora, that spread in the surrounding peripheral portions of these lakes, and along morphological features periodically flooded by ephemeral currents, from occasional flash floods, resulting from episodic precipitations, keeping these lake basins at least seasonally under a probable monsoon and/or climatic seasonality regime, initiated in the Late Carboniferous, and prevalent throughout the Permian period (Crowley et al. 1989; Wang et al. 2014).

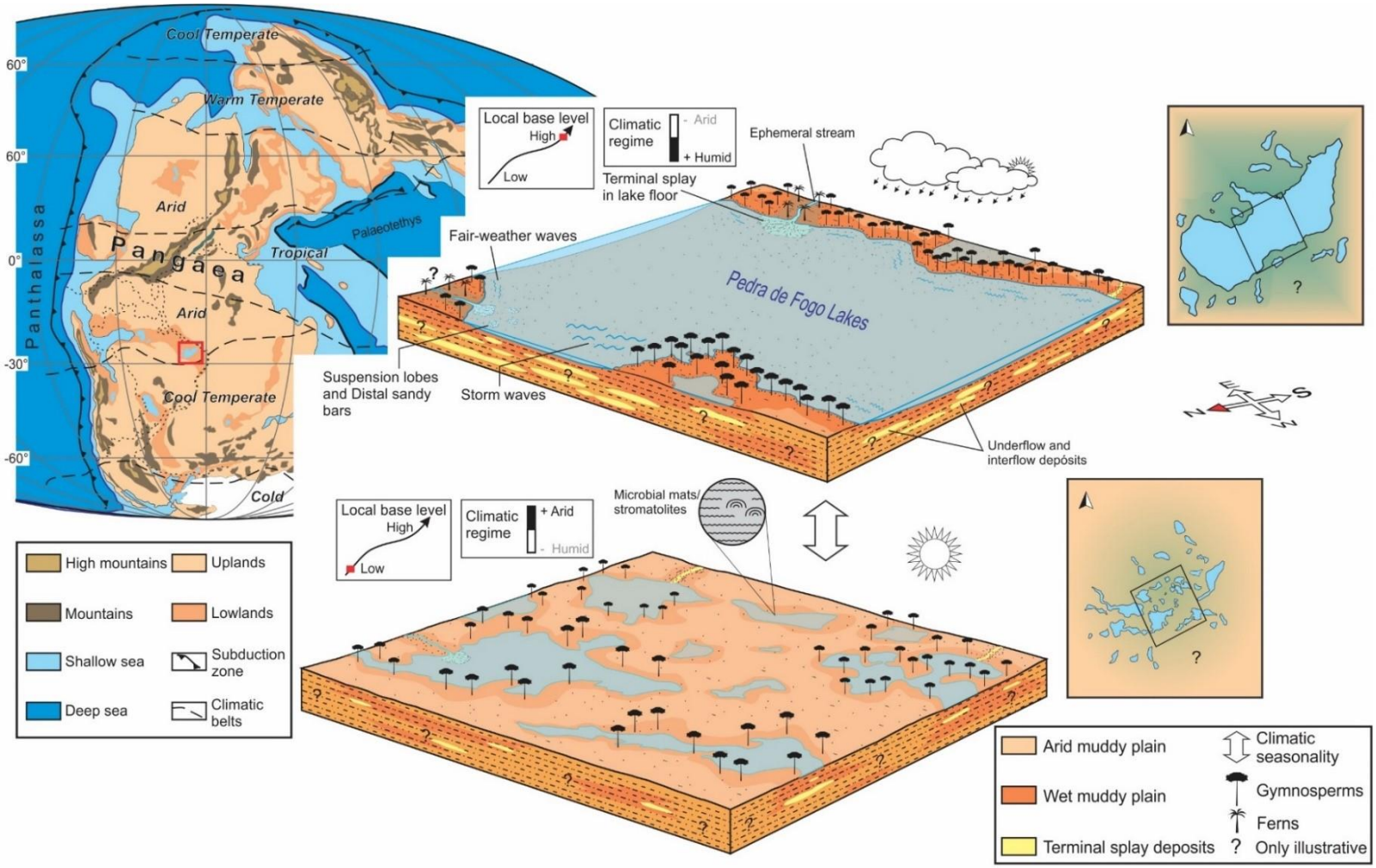

Figure 14-Paleoenvironmental model for the studied succession. Under a climate seasonality regime, the "Pedra de Fogo Lacustrine System" (SLPF) had periodic fluctuations in its level, with consequent expansion and contraction of its margins, in response to climatic conditions: wetter (A) and more arid (B), respectively. Similarly, taphoflora was suppressed in the driest periods (B), and proliferated in the wettest periods (A), where the greater frequency and intensity of flash flood events reactivated ephemeral fluvial systems that supplied these lake basins. In the upper right corner, the red square places the SLPF in the paleogeographic and paleoclimatic context of the Early Permian. Paleogeographic map modified from Warren (2017).

CONCLUSIONS

The facies analysis of Cisuralian deposits in the eastern border of the Parnaíba Basin allowed to differentiate three facies associations related to the Pedra de Fogo Formation, and one related to the Piauí Formation. The FA1-Onshore flat, FA2-Nearshore wave and storm dominated, and FA3-Terminal splay associations were associated with Pedra de Fogo Formation. The FA4-Distal Braided Association was related to Piauí Formation.

The facies association of the Pedra de Fogo Formation reveals an extensive arid climate lacustrine system, constantly affected by unconfined flows. The thin thickness of the sandstone layers with tabular/sheet (sheet bodies) geometry indicate that unconfined flows were deposited directly over a large flat lacustrine floor under a shallow water depth. This entire system was reworked by good weather and eventually storm waves. The occurrence of hummocky cross stratification reveals that this lacustrine system was potentially extensive to allow the formation of storm waves with sufficient energy and time for the reworking of the lacustrine substrate and the generation of tempestites.

The predominance of fine-grained and potentially massive sandstones, with flat-based or relatively minor erosive scours, suggests the predominance of unconfined, predominantly suspended-flowing streams deposited far from channelized trunks. The constant and cyclic occurrence of these tabular sandstone layers interspersed with pelitic levels suggests a high frequency of sheetflood events separated by relative quiescence. The multiple levels of massive and nodular chert are associated with fluctuations in the pH levels of these lakes, conditioned by climatic seasonality. The presence of silicified woods, many in life position, together with the occurrence of stratiform microbialites (stromatolites) suggests syn-eodiagenetic silicification.

The variation in stratigraphic positioning between microbialites and fossil plants in life position is related to lake shoreline migrations, conditioned by climatic seasonality.

The large presence of taphoflora consisting of large silicified woods indicates that the Pedra de Fogo Lacustrine System, although subjected to a hot and increasingly arid climate in the west-central part of Pangea during the early Permian, had potentially high humidity to maintain this paleoflora that proliferated along its edges. The wide paleogeographic distribution of these silicified fossil plants in the studied deposits reveals that the Parnaíba Basin was an “oasis” capable of generating a sustainable microclimate among the increasingly arid desert conditions that prevailed in the interior of Pangea throughout the Permian Period.

ACKNOWLEDGMENTS

This work is part of the Ph.D. dissertation of the first author with technical support of the PPGG (Programa de Pós-Graduação em Geologia e Geoquímica) of the University Federal of Pará (UFPA). We are grateful to the CNPq (National Council for Scientific and Technological Development - CNPq no.141968/2016-8) and the CAPES (Coordination for the Improvement of Higher Education Personnel; financial code 001) as the funding agency of Brazil to the concession of fellowship research to the first author. The fieldwork was supported by CNPq no.456608/2014-1 e 305688/2016-2.

REFERENCES

Aguiar, G.A., 1964, Semi-detalhe da região de sudoeste de Balsas [Relatório 21BM]: PETROBRÁS, DIREX/RENOR, 40 p.

Alexander, J., Fielding, C.R., and Pocock, G.D., 1999, Flood behaviour of the Burdekin River, tropical north Queensland, Australia, in Marriott, S.B., and Alexander, J., eds., Floodplains: Interdisciplinary Approaches: Geological Society of London, Special Publications, v. 163 p. 27-40.

Alexander, J., Bridge, J.S., Cheel, R.J., and Leclair, S.F., 2001, Bedforms and associated sedimentary structures formed under supercritical water flows over aggrading sand beds: Sedimentology, v. 48, p. 133-152.

Allen, P.A., 1981, Wave-generated structures in the Devonian lacustrine sediments of south-east Shetland and ancient wave conditions: Sedimentology, v. 28 p. 369-379.

Andrade, L.S., Nogueira, A.C.R., and Silva Junior, J.B.C., 2014, Evolução de um sistema lacustre árido Permiano, parte superior da Formação Pedra de Fogo, borda oeste da Bacia do Parnaíba: Geologia USP, Série Científica, v. 14, p. 39-60.

Araújo, R.N., Nogueira, A.C.R., Bandeira, J., and Angélica, R.S., 2016, Shallow lacustrine system of the Permian Pedra de Fogo Formation, Western Gondwana, Parnaíba Basin, Brazil: Journal of South American Earth Sciences, v. 67, p. 57-70.

Arenas, C., and Jones, B., 2017, Temporal and environmental significance of microbial lamination: Insights from Recent fluvial stromatolites in the River Piedra, Spain: Sedimentology, v. 64, p. 1597-1629.

Arp, G., Bissett, A., Brinkmann, N., Cousin, S., De Beer, D., Friedl, T., Mohr, K.I., Neu, T., Reimer, A., Shiraishi, F., Stackebrandt, E., and Zippel, B., 2010, Tufa-forming biofilms of German karstwater streams: microorganisms, exopolymers, hydrochemistry and calcification, in Rogerson, M., and Pedley, H.M., eds., Tufas and Speleothems: Unravelling the Microbial and Physical Controls: Geological Society of London, Special Publications, v. 336, p. 83-118.

Bagnold, R.A., 1946, Motion of waves in shallow water, interaction between waves and sand bottoms: Royal Society of London, Proceedings, Serie A, Mathematical, Physical and Engineering Sciences, v. 187, p. 1-18.

Barbosa, E.N., Córdoba, V.C., and Souza, D.C., 2016, Evolução Estratigráfica da Sequência Neocarbonífera-Eotriássica da Bacia do Parnaíba, Brasil: Brazilian Journal of Geology, v. 46, p. 181-198.

Barbosa, O., and Gomes, F. de A., 1957, Carvão mineral na Bacia do Tocantins-Araguaia: Departamento Nacional de Produção Mineral, Divisão Geologia e Mineralogia, Boletim, v. 174, p. 1-34.

Beam, J.P., Bernstein, H.C., Jay, Z.J., Kozubal, M.A., Jennings, R.D., Tringe, S.G., and Inskeep, W.P., 2016, Assembly and succession of iron oxide microbial Mat communities in acidic geothermal springs: Frontiers Microbiology, v. 7, p. 1-15.

Blakey, R.C., 2008, Gondwana paleogeography from assembly to breakup - A 500 m.y. odyssey, *in* Fielding, C.R., Frank, T.D., and Isbell, J.L., eds., Resolving the late Paleozoic ice age in time and space: Geological Society of America, Special Paper, v. 441, p. 1-28.

Boucot, A.J., Chen, X., Scotese, C.R., and Morley, R.J., 2013, Phanerozoic Paleoclimate: An Atlas of Lithologic Indicators of Climate: SEPM, Concepts in Sedimentology and Paleontology, 11, 478 p.

Bouton, A., Vennin, E., Boulle, J., Pace, A., Bourillot, R., Thomazo, C., Brayard, A., Déesaubliaux, G., Goslar, T., Yokoyama, Y., Dupraz, C., and Visscher, P.T., 2016, Linking the distribution of microbial deposits from the Great Salt Lake (Utah, USA) to tectonic and climatic processes: Biogeosciences, v.13, p. 5511–5526.

Bustillo, M.A., Arribas, M.E., and Bustillo, M.A., 2002, Dolomitization and silicification in low-energy lacustrine carbonates (Paleogene, Madrid Basin, Spain): Sedimentary Geology, v. 151, p. 107-126.

Caldas, E.B., Mussa, D., Lima Filho, F.P., and Rosier, O., 1989, Nota sobre a ocorrência de uma floresta petrificada de idade permiana em Teresina, Piauí: Boletim do Instituto de Geociências da USP, Publicação Especial, Paleobotânica e Palinologia na América do Sul, v. 7 p. 69-87.

Capretz, R.L., and Rohn, R., 2013, Lower Permian stems as fluvial paleocurrent indicators of the Parnaíba Basin, northern Brazil: Journal of South American Earth Sciences, v. 45, p. 69-82.

Carroll, A.R., and Bohacs, K.M., 1999, Stratigraphic classification of ancient lakes; balancing tectonic and climatic controls: Geology, v. 27, p. 99-102.

Casanova, J., and Hillaire-Marcel, C., 1992, Late holocene hydrological history of Lake Tanganyika, East Africa, from isotopic data on fossil stromatolites: Palaeogeography, Palaeoclimatology, Palaeoecology, v. 91, p. 35-48.

Catuneanu, O., 2011, Principles of Sequence Stratigraphy: Elsevier Science, 375 p.

Cecil, C.B., 1990, Paleoclimate controls on stratigraphic repetition of chemical and siliciclastic rocks: Geology, v. 18, p. 533-536.

Cecil, C.B., Stanton, R.W., Neuzil, S.G., Dulong, F.T., Ruppert, L.F., and Pierce, B.S., 1985, Paleoclimate controls on late Paleozoic sedimentation and peat formation in the central Appalachian basin (U.S.A.): International Journal of Coal Geology, v. 5, p. 195-230.

Cecil, C.B., 2015, Paleoclimate and the Origin of Paleozoic Chert: Time to Re-Examine the Origins of Chert in the Rock Record: The Sedimentary Record, v. 13, p. 4-10.

Cheel, R.J., and Leckie, D.A., 1993, Hummocky cross-stratification, in Wright, V.P., ed., Sedimentology Review/1: Blackwell Scientific Publications, Oxford, UK. p. 103–122.

Chumakov, N.M., and Zharkov, M.A., 2002, Climate during Permian–Triassic Biosphere Reorganizations, Article 1: Climate of the Early Permian. Stratigraphy and Geological Correlation, v. 10, p. 586–602.

Chumakov, N.M., and Zharkov, M.A., 2003, Climate during the Permian–Triassic Biosphere Reorganizations. Article 2. Climate of the Late Permian and Early Triassic: General Inferences: Stratigraphy and Geological Correlation, v. 11, p. 361–375.

Cisneros, J.C., Marsicano, C., Angielczyk, K.D., Smith, R.M.H., Richter, M., Fröbisch, J., Kammerer, C.F., and Sadleir, R.W., 2015, New Permian fauna from tropical Gondwana: Nature Communications, v. 6, p. 8676.

Coimbra, A.M., and Mussa, D., 1984, Associação lignitatoflorística na Formação Pedra de Fogo (Arenito Cacunda), Bacia do Maranhão - Piauí, Brasil: Congresso Brasileiro de Geologia, 33, Rio de Janeiro, Anais, v. 2, p. 591-605.

Conceição, D.M., Andrade, L.S., Cisneros, J.C., Iannuzzi, R., Pereira, A.A., and Machado, F.C., 2016, New petrified forest in Maranhão, Permian (Cisuralian) of the Parnaíba Basin, Brazil: Journal of South American Earth Sciences, v. 70, p. 308-323.

Conceição, D.M., Crisafulli, A., Neregato, R., Iannuzzi, R., Cisneros, J., and Andrade, L.S., 2019, Permian gymnosperm woods from the Pedra de Fogo Formation in the Parnaíba Basin, northeastern Brazil. Part I: submitted for publication.

Cox, C., and Hutchinson, P., 1991, Fishes and amphibians from the Late Permian Pedra de Fogo Formation of northern Brazil: Palaeontology, v. 34, p. 561–573.

Crowley, T.J, Hyde, W.T., and Short, D.A., 1989, Seasonal cycle variations on the supercontinent of Pangaea: Geology, v. 17, p. 457-460.

Dearing, J.A., 1997, Sedimentary indicators of lake-level changes in the humid temperate zone: a critical review: Journal of Paleolimnology, v. 18, p. 1–14.

Dias-Brito, D., Rohn, R., Castro, J.C., Dias, R.R., and Röβler, R., 2007, Floresta Petrificada do Tocantins Setentrional - O mais exuberante e importante registro florístico tropical-subtropical permiano no Hemisfério Sul, in Winge, M., Schobbenhaus, C., Berbet-Born, M., Queiroz, E.T., Campos, D.A., Souza, C.R.G., and Fernanes, A.C.S., eds., Sítios Geológicos e Paleontológicos do Brasil, p.1-16.

DiMichelle, W.A., Pfefferkorn, H.W., and Gastaldo, R.A., 2001, Response of Late Carboniferous and Permian Early Permian Plant Communities to Climate Change: Annual Review of Earth and Planetary Sciences, v. 29, p. 461-487.

DiMichele, W.A., Tabor, N.J., Chaney, D.S., and Nelson, W.J., 2006, From wetlands to wet spots: Environmental tracking and the fate of Carboniferous elements in Early Permian tropical floras, *in* Greb, S.F., DiMichele, W.A., eds., Wetlands through Time: Geological Society of America, Special Papers, v. 399, p. 223-248.

DiMichele, W.A., Montañez, I.P., Poulsen, C.J., and Tabor, N.J., 2009, Climate and vegetational regime shifts in the late Paleozoic ice age earth: Geobiology, v. 7, p. 200-226.

DiMichele, W.A., Cecil, C.B., Montañez, I.P., and Falcon-Lang, H.J., 2010, Cyclic changes in Pennsylvanian paleoclimate and effects on floristic dynamics in tropical Pangaea: International Journal of Coal Geology, v. 83, p. 329-344.

DiMichele, W.A., Cecil, C., Chaney, D.S., Elrick, S.D., Lucas, S.G., Lupia, R., Nelson, W.J., and Tabor, N.J., 2011, Pennsylvanian-Permian vegetational changes in tropical Euramerica, in Harper, J.A., ed., Geology of the Pennsylvanian-Permian in the Dunkard Basin: Guidebook for the 76th Annual Field Conference of Pennsylvania Geologists, p. 60–102.

Dino, R., Antonioli, L., and Braz, S.M.N., 2002, Palynological data from the Trisidela Member of Upper Pedra de Fogo Formation ("Upper Permian") of the Parnaíba Basin, northeastern Brazil: Revista Brasileira de Paleontologia, p. 24-35.

Dott, R.J., and Bourgeois, J., 1982, Hummocky stratification: Significance of its variable bedding sequences: Geological Society of America, Bulletin, v. 93, p. 663-680.

Duke, W.L., 1985, Hummocky cross-stratification, tropical hurricanes, and intense winter storms. Sedimentology, v. 32, p. 167-194.

Dumas, S., and Arnott, R.W.C., 2006, Origin of hummocky and swaley cross-stratification – The controlling influence of unidirectional current strength and aggradation rate: Geology, v. 34, p. 1073-1076.

Eugster, H.P., 1967, Hydrous sodium silicates from Lake Magadi, Kenya: Precursors of bedded chert: Science, v. 15, p. 1177-1180.

Eugster, H.P., 1969, Inorganic bedded cherts from the Magadi area, Kenya: Contributions to Mineralogy and Petrology, v. 22, p.1-31.

Eyles, N., and Clark, B.M., 1986, Significance of hummocky and swaley cross-stratification in late Pleistocene lacustrine sediments of the Ontario basin, Canada: Geology, v. 14, p. 679-682.

Faria Jr., L.E.C., 1979, Estudo sedimentológico da Formação Pedra de Fogo – Permiano – Bacia do Maranhão [Dissertação de Mestrado]: Universidade Federal do Pará, 57 p.

Faria Jr., L.E.C., and Truckenbrodt, W., 1980a, Estratigrafia e petrografia da Formação Pedra de Fogo – Permiano da Bacia do Maranhão: Congresso Brasileiro de Geologia, 31, Balneário Camboriú, Anais, v. 2, p. 740-754.

Faria Jr., L.E.C., and Truckenbrodt, W., 1980b, Estromatólitos na Formação Pedra de Fogo, Permiano, Bacia do Maranhão: Congresso Brasileiro de Geologia, 31, Balneário Camboriú, Anais, v. 5, p. 3056-3067.

Figueiredo, A.M.F., and Raja Gabaglia, G.P., 1986, Sistema Classificatório Aplicado às Bacias Sedimentares Brasileiras: Revista Brasileira de Geociências, v. 16, p. 350-369.

Figueroa, R.T., and Gallo, V., 2017, New chondrichthyan fin spines from the Pedra de Fogo Formation, Brazil: Journal of South American Earth Sciences, v.76, p. 389-396.

Fisher, J.A., Nichols, G.J., and Waltham, D.A., 2007, Unconfined flow deposits in distal sectors of fluvial distributary systems: examples from the Miocene Luna and Huesca Systems, northern Spain: Sedimentary Geology, v. 195, p. 55-73.

Fisher, J.A., Krapf, C.B.E., Lang, S.C., Nichols, G.J., and Payenberg, T.H.D., 2008, Sedimentology and architecture of the Douglas Creek terminal splay, Lake Eyre, central Australia: Sedimentology, v. 55, p. 1915-1930.

Freytet, P., and Verrecchia, E.P., 1998, Freshwater organisms that build stromatolites: a synopsis of biocrystallization by prokaryotic and eukaryotic algae: Sedimentology, v. 45, p. 535–563.

Gastaldo, R.A., DiMichele, W.A., and Pfefferkorn, H.W., 1996, Out of the Icehouse into the Greenhouse: A Late Paleozoic Analog for Modern Global Vegetational Change: Geological Society American Today, v. 6, p. 1-7.

Gibbs, M.T., Rees, P.M., Kutzbach, J.E., Ziegler, A.M., Behling, P.J., and Rowley, D.B., 2002, Simulations of Permian Climate and Comparisons with Climate-Sensitive Sediments: The Journal of Geology, v. 110, p. 33-55.

Gibling, M.R., and Rust, B.R., 1984, Channel margins in a Pennsylvanian braided, fluvial deposit: The Morien Group near Sydney, Nova Scotia, Canada: Journal of Sedimentary Research, v. 54, p. 773-782.

Gierlowski-Kordesch, E.H., and Kelts, K.R., 2000, Lake Basins Through Space and Time: American Association of Petroleum Geologists Studies in Geology, 46, 638 p.

Godsey, H.S., Currey, D.R., and Chan, M.A., 2005, New evidence for an extended occupation of the Provo shoreline and implications for regional climate change, Pleistocene Lake Bonneville, Utah, USA: Quaternary Research, v. 63, p. 212-223.

Góes, A.M.O., Souza, J.M.P., and Teixeira, L.B., 1990, Estágio exploratório e perspectivas petrolíferas da Bacia do Parnaíba: Boletim de Geociências da Petrobrás, v. 4, p. 55-64.

Góes, A.M.O., and Feijó, F.J., 1994, Bacia do Parnaíba: Boletim de Geociências da Petrobrás, v. 8, p. 57-67.

Golonka, J., and Ford, D., 2000, Pangean (Late Carboniferous–Middle Jurassic) paleoenvironment and lithofacies: Palaeogeography, Palaeoclimatology, Palaeoecology, v. 161, p. 1-34.

Greenwood, B., and Sherman, D.J., 1986, Hummocky cross-stratification in the surf zone: flow parameters and bedding genesis: Sedimentology, v. 33, p. 33-45.

Greenwood, B., 2006, Bimodal Cross-Lamination in Wave-Ripple Form Sets: A Possible Origin: Journal of Coastal Research, v. 22, p. 1220-1229.

Guion, P.D., Banks, N.L., and Rippon, J.H., 1995, The Silkstone Rock (Westphalian A) from the east Pennines, England: implications for sand body genesis: Journal of the Geological Society, London, v. 152, p. 819–832.

Haberyan, K.A., and Hecky, R.E., 1987, The late Pleistocene and Holocene stratigraphy and paleolimnology of Lakes Kivu and Tanganyika: Palaeogeography, Palaeoclimatology, Palaeoecology, v. 61, p. 169-197.

Halfman, J.D., and Johnson, T.C., 1988, High-resolution record of cyclic climatic change during the past 4 ka from Lake Turkana, Kenya: Geology, v. 16, p. 496-500.

Hmich, D., Schneider, J.W., Saber, H., Voigt, S., and Wartiti, M.E., 2006, New continental Carboniferous and Permian faunas of Morocco: implications for biostratigraphy, palaeobiogeography and palaeoclimate, *in* Lucas, S.G., Cassinis, G., and Schneider, J.W., eds., Non-Marine Permian Biostratigraphy and Biochronology: Geological Society of London, Special Publications, v. 265, p. 297-324.

Hofmann, H.J., 1973, Stromatolites: Characteristics and utility: Earth-Science Reviews, v. 9, p. 339-373.

Horton, D.E., Poulsen, C.J., Montanez, I.P., and DiMichele, W.A., 2012, Eccentricity-paced late Paleozoic climate change: Palaeogeography, Palaeoclimatology, Palaeoecology, v. 331-332, p. 150-161.

Iannuzzi, R., and Langer, M.C., 2014, The presence of callipterids in the Permian of north-eastern Brazil: stratigraphic and phytogeographical implications, *in* Rocha, R., Pais J.,

Kullberg J.C., and Finney, S., eds., 1st International Congress on Stratigraphy, Springer, Cham, Switzerland, p. 403–406.

Iannuzzi, R., Neregato, R., Cisneros, J.C., Angielczyk, K.D., Rößler, R., Rohn, R., Marsicano, C., Fröbisch, J., Fairchild, T., Smith, R.M.H., Kurzawe, F., Richter, M., Langer, M.C., Tavares, T.M.V., Kammerer, C.F., Conceição, D.M., Pardo, J.D., and Roesler, G.A., 2018, Re-evaluation of the Permian macrofossils from the Parnaíba Basin: biostratigraphic, palaeoenvironmental and palaeogeographical implications, *in* Daly, M.C., Fuck, R.A., Julià, J., Macdonald, D.I.M., and Watts, A.B., eds., Cratonic Basin Formation: A Case Study of the Parnaíba Basin of Brazil: Geological Society of London, Special Publications, v. 472, p. 223-249.

Jorgensen, P.J., and Fielding, C.R., 1996, Facies architecture of alluvial floodbasin deposits: three-dimensional data from the Upper Triassic Callide Coal Measures of east central Queens-land, Australia: Sedimentology, v. 43, p. 479-495.

Kauffmann, M., Jasper, A., Uhl, D., Meneghini J., Osterkamp, I.C., Zvirtes, G., and Pires, E.F., 2016, Evidence for palaeo-wildfire in the Late Permian palaeotropics - Charcoal from the Motuca Formation in the Parnaíba Basin, Brazil; Palaeogeography, Palaeoclimatology, Palaeoecology, v. 450, p. 122-128.

Kiehl, J.T., and Shields, C.A., 2005, Climate simulation of the latest Permian: Implications for mass extinction: Geology, v. 33, p. 757–760.

Knauth, L.P., 1994, Petrogenesis of chert, *in* Heaney, P.J., Prewitt, C.T., and Gibbs, G.V., eds., Silica: physical behavior, geochemistry and materials applications: Reviews in Mineralogy Geochemistry, v. 29, p. 233-258.

Kneller, B., 1995, Beyond the turbidite paradigm: physical models for deposition of turbidites and their implications for reservoir prediction, *in* Hartley, A.J., and Prosser, D.J., eds., Char-acterization of Deep Marine Clastic Systems: Geological Society, London, Special Publications, v. 94, p. 31-49.

Krumbein, W.E., Cohen, Y., and Shilo, M., 1977, Solar Lake (Sinai). 4. Stromatolitic cyanobacterial mats: Limnology and Oceanograph, v. 22, p. 635-656.

Kurzawe, F., Iannuzzi, R., Merlotti, S., Röβler, R., and Noll, R., 2013a, New gymnospermous woods from the Permian of the Parnaíba Basin, Northeastern Brazil, Part I: Ductoabietoxylon, Scleroabietoxylon and Parnaiboxylon: Review of Palaeobotany and Palynology, v. 195, p. 37-49.

Kurzawe, F., Iannuzzi, R., Merlotti, S., and Röβler, R., 2013b, New gymnospermous woods from the Permian of the Parnaíba Basin, Northeastern Brazil, Part II: Damudoxylon, Kaokoxylon and Taeniopitys: Review of Palaeobotany and Palynology, v. 195, p. 50-64.

Kutzbach, J.E., 1980, Estimates of past climate at Paleolake Chad, North Africa, based on a hydrological and energy-balance model, Quaternary Research (United States), v. 14, p. 210-223.

Kutzbach, J.E., and Gallimore, R.G., 1989, Pangaean climates: Megamonsoons of the megacontinent: Journal Geophysical Research, v. 94, p. 3341- 3357.

Kutzbach, J.E., Liu, X., Liu, Z., and Chen, G., 2008. Simulation of the evolutionary response of global summer monsoons to orbital forcing over the past 280,000 years: Climate Dynamics, v. 30, p. 567-579.

Lall, U., and Mann, M., 1995, The Great Salt Lake: A Barometer of Low-Frequency Climatic Variability: Water Resources Research, v. 31, p. 2503-2515.

Lang, S.C., Payenberg, T.H.D., Reilly, M.R.W., Hicks, T., Benson, J., and Kassan, J., 2004, Modern analogues for dryland sandy fluvial-lacustrine deltas and terminal splay reservoirs: Journal of the Australian Petroleum Production & Exploration Association, v. 44, p. 329-356.

Laya, J.C., Tucker, M.E., and Perez-Huerta, A., 2013, Metre-scale cyclicity in Permian ramp carbonates of equatorial Pangea (Venezuelan Andes): Implications for sedimentation under tropical Pangea conditions: Sedimentary Geology, v. 292, p. 15-35.

Lefranc, J.P., and Guiraud, R., 1990, The continental intercalaire of northwestern Sahara and its equivalents in the neighbouring regions: Journal of African Earth Sciences, v. 10, p. 27-77.

Lever, H., 2004, Climate Changes and Cyclic Sedimentation in the Mid-Late Permian: Kennedy Group, Carnarvon Basin, Western Australia: Gondwana Research, v. 7, p. 135-142.

Li, F., Yang, Y., Li, J., Yang, C., Dai, T., Zhao, J., and Yi, H., 2014, Lacustrine tempestite and its geological significance in the Cenozoic study of the Qaidam Basin: Journal of Asian Earth Sciences, v. 92, p. 157-167.

Lima, E.A.M., and Leite, J.F., 1978, Projeto estudo global dos recursos Minerais da Bacia Sedimentar do Parnaíba: Integração geológico-metalogenética, Etapa III, Relatório Final, v. 16, 212 p.

Lindholm, R.C., 1987, A practical approach to sedimentology: London, Allen & Unwin, 276 p.

Lindsay, M.R., Anderson, C., Fox, N., Scofield, G., Allen, J., Anderson, E., Bueter, L., Poudel, S., Sutherland, K., Munson-McGee, J.H., Van Nostrand, J.D., Zhou, J., Spear, J.R., Baxter, B.K., Lageson, D.R., and Boyd, E.S., 2017, Microbialite response to an anthropogenic salinity gradient in Great Salt Lake, Utah: Geobiology, v. 15, p. 131-145.

Link, M.H., Osborne, R.H., and Awramik, S.M., 1978, Lacustrine stromatolites and associated sediments of the Pliocene Ridge Route Formation, Ridge Basin, California: Journal of Sedimentary Research, v. 48, p. 143-157.

Liu, X., Zhong, J., Grapes, R., Bian, S., and Liang, C., 2012, Late Cretaceous tempestite in northern Songliao Basin, China: Journal of Asian Earth Sciences, v. 56, p. 33-41.

Lojka, R., Drabkova, J., Zajic, J., Sykorova, I., Francu, J., Blahova, A., and Grygar, T., 2009, Climate variability in the Stephanian B based on environmental record of the Mšec Lake de-posits (Kladno-Rakovník Basin, Czech Republic): Palaeogeography, Palaeoclimatology, Palaeoecology, v. 280, p. 78-93.

Love, S.E., and Williams, B.P.J., 2000, Sedimentology, cyclicity and floodplain architecture in the Lower Old Red Sandstone of SW Wales, *in* Friend, P.F., and Williams, B.P.J., eds., New Perspectives on the Old Red Sandstone: Geological Society of London, Special Publications, v. 180, p. 371-388.

Marsaglia, K.M., and Klein, G.D., 1983, The Paleogeography of Paleozoic and Mesozoic Storm Depositional Systems: The Journal of Geology, v. 91 p. 117-142.

Marshall, J.D., 2000, Sedimentology of a Devonian fault-bounded braid plain and lacustrine fill in the lower part of the Skrinkle Sandstones, Dyfed, Wales: Sedimentology, 47, 325–342.

Martins, R.A., 2000, Fósseis de vegetais da Formação Pedra de Fogo: aspectos taxonômicos, mineralogia e composição química [Dissertação de Mestrado]: Universidade Federal do Pará, 92 p.

Melo, M.T., and Prade, G.O., 1968, Geologia da região sudeste de São Raimundo das Mangabeiras-Maranhão [Relatório 297M]: PETROBRÁS, DIREX/RENOR, 37 p.

Miall, A., 1977, A Review of the Braided-River Depositional Environment: Earth-Science Reviews, v. 13, p. 1-62.

Mills, P.C., 1983, Genesis and diagnostic value of soft-sediment deformation structures- A review: Sedimentary Geology, v. 35, p. 83-104.

Montañez, I.P., Tabor, N.J., Niemeier, D., DiMichele, W.A., Frank, T.D., Fielding C.R., Isbell, J.L., Birgenheier, L.P., and Michael, C.R., 2007, CO_2-Forced Climate and Vegetation Instability During Late Paleozoic Deglaciation: Science, v. 315, p. 87-91.

Moore, B., 1964, Geological reconnaissance of the southern margin of the Maranhão Basin [Relatório 216M]: PETROBRÁS, DIREX/RENOR, 46 p.

Murty, T.S., and Polarvaparu, R.J., 1975, Reconstruction of some of the early storm surge; on the Great Lakes: Journal of Great Lakes Research, v. 1, p. 116-129.

Nagy, B., 1970, Porosity and permeability of the Early Precambrian Onverwacht chert: Origin of the hydrocarbon content: Geochimica et Cosmochimica Acta, v. 34, p. 525-527.

Neregato, R., Röβler, R., Iannuzzi, R., Noll, R., and Rohn, R., 2017, New petrified calamitaleans from the Permian of the Parnaíba Basin, central-north Brazil, part II, and phytogeographic implications for late Paleozoic floras: Review of Palaeobotany and Palynology, v. 237, p. 37-61.

Neregato, R., Röβler, R., Rohn, R., and Noll, R., 2015, New petrified calamitaleans from the Permian of the Parnaíba Basin, central-north Brazil. Part I: Review of Palaeobotany and Palynology, v. 215, p. 23-45.

Nichols, G.J., and Fisher, J.A., 2007, Processes, facies and architecture of fluvial distributary system deposits: Sedimentary Geology, v. 195, p. 75-90.

North, C.P., and Davidson, S.K., 2012, Unconfined alluvial flow processes: Recognition and interpretation of their deposits, and the significance for palaeogeographic reconstruction: Earth-Science Reviews, v. 111, p. 199-223.

Opluštil, S., 2013, Flora from the Líně Formation (Czech Republic) as an example of floristic dynamics around thé Carboniferous/Permian boundary, *in* Lucas, S.G., DiMichele, W.A., Barrick, J.E., Schneider, J.W., and Spielmann, J.A., eds., The Carboniferous–Permian Transition: New Mexico Museum of Natural History and Science, Bulletin, v. 60, p. 314–321.

Parrish, J.T., 1993, Climate of the Supercontinent Pangea: The Journal of Geology, v. 101, p. 215-233.

Peterson, M.N.A., and Von Der Borch, C.C., 1965, Chert: modern inorganic deposition in a carbonate-precipitating locality: Science, v. 149, p. 1501-1503.

Petri, S., and Fúlfaro, V.J., 1983, Geologia do Brasil: Fanerozóico: Biblioteca de Ciências Naturais, Editora da USP, 631 p.

Plummer, F.B., 1946, Report on Maranhão and Piauí Geosyncline [Relatório 1M]: PETROBRÁS, DIREX/RENOR, 83 p.

Price, L.I, 1948, Um anfibio labirintodonte da Formação Pedra de Fogo, estado do Maranhão: Departamento Nacional de Produção Mineral, Divisão Geologia e Mineralogia, Boletim, v. 124, p. 1-32.

Rees, P.M., Gibbs, M.T., Ziegler, A.M., Kutzbach, J.E., and Behling, P.J., 1999, Permian climates; evaluating model predictions using global paleobotanical data: Geology, v. 27, p. 891-894.

Reineck, H.E., and Singh, I.B., 1973, Depositional Sedimentary Environments: Springer-Verlag, 439 p.

Retallack, G.J., 1999, Postapocalyptic greenhouse paleoclimate revealed by earliest Triassic Paleosols in the Sydney Basin, Australia: Geological Society of America, Bulletin, v. 111, p. 52-70.

Retallack, G.J., 2001, Soils of the Past: An Introduction to Paleopedology, Allen & Unwin, London, 404 p.

Ribeiro, C.M.M., 2000, Análise faciológica das formações Poti e Piauí (Carbonífero da Bacia do Parnaíba) na região de Floriano-PI [Dissertação de Mestrado]: Universidade Federal do Pará, 57 p.

Richardson, J.L., and Richardson, A.E., 1972, History of an African Rift Lake and Its Climatic Implications: Ecological Monographs, v. 42, p. 499-534.

Roscher, M., Stordal, F., and Svensen, H., 2011, The effect of global warming and global cooling on the distribution of the latest Permian climate zones: Palaeogeography, Palaeoclimatology, Palaeoecology, v. 309, p. 186-200.

Rowley, D.B., Raymond, A., Parrish, J.T., Lottes, A.L., Scotese, C.R., and Ziegler, A.M., 1985, Carboniferous paleogeographic, phytogeographic, and paleoclimatic reconstructions: International Journal of Coal Geology, v. 5, p. 7-42.

Röβler, R., and Galtier, J., 2002a, First Grammatopteris tree ferns from the Southern Hemisphere – new insights in the evolution of the Osmundaceae from the Permian of Brazil: Re-view of Palaeobotany and Palynology, v. 121, p. 205-230.

Röβler, R., and Galtier, J., 2002b, Dernbachia brasiliensis gen. nov. et sp. nov. – a new small tree fern from the Permian of NE Brazil: Review of Palaeobotany and Palynology, v. 122, p. 239-263.

Röβler, R., and Galtier, J., 2003, The first evidence of the fern Botryopteris from the Permian of the Southern Hemisphere reflecting growth form diversity: Review of Palaeobotany and Palynology, v. 127, p. 99-124.

Santos, R.S., 1989a, A ictiofáunula da Formação Pedra do Fogo, Bacia do Parnaíba, NE do Brasil: Holocephali – Edestida: Congresso Brasileiro de Paleontologia, 11, Curitiba, Resumos, p. 32-33.

Santos, R.S., 1989b, A ictiofáunula da Formação Pedra do Fogo, bacia do Parnaíba, NE do Brasil: Sarcopterygii- Actinista e Dipnoi: Congresso Brasileiro de Paleontologia, 11, Curitiba, Resumos, p. 33-34.

Santos, R.S., 1990, Paleoictiofáunula da Formação Pedra do Fogo, bacia do Parnaíba, Nordeste do Brasil: Holocephali- Petalodontidae: Anais da Academia Brasileira de Ciências, v. 62, p. 347-355.

Santos, R.S., 1994, Paleoictiofáunula da Formação Pedra do Fogo, Bacia do Parnaíba, NE do Brasil: II. Eugeneodontida – Agassizodontidae: Anais da Academia Brasileira de Ciências, v. 66, p. 413-424.

Scheffler, K., Buehmann, D., and Schwarkc, L., 2006, Analysis of late Palaeozoic glacial to postglacial sedimentary successions in South Africa by geochemical proxies – Response

to climate evolution and sedimentary environment: Palaeogeography, Palaeoclimatology, Palaeoecology, v. 240, p. 184-203.

Schnurrenberger, D., Russell, J., and Kelts, K., 2003, Classification of lacustrine sediments based on sedimentary components: Journal of Paleolimnology, v. 29, p. 141–154.

Scotese, C.R., Boucot, A.J., and McKerrow, W.S., 1999, Gondwanan palaeogeography and palaeoclimatology: Journal of African Earth Sciences, v. 28, p. 99-114.

Shanley, K.W., and McCabe, P.J., 1994, Perspectives on the sequence stratigraphy of continental strata: American Association Petroleum Geological Bulletin, v. 78, p. 544-568.

Southgate, P.N., 1986, Depositional environment and mechanism of preservation of microfossils, upper Proterozoic Bitter Springs Formation, Australia: Geology, v. 14, p. 683-686.

Sumner, D.Y., Hawes, I., Mackey, T.J., Jungblut, A.D., and Doran, P.T., 2015, Antarctic microbial mats: A modern analog for Archean lacustrine oxygen oases: Geology, v. 43, p. 887-890.

Tabor, N.J., Montañez, I.P., Scotese, C.R., Poulsen, C.J. and Mack, G.H., 2008, Paleosol archives of environmental and climatic history in paleotropical western Pangea during the latest Pennsylvanian through Early Permian, *in* Fielding, C.R., Frank, T.D., and Isbell, J.L., eds., Resolving the late Paleozoic ice age in time and space: Geological Society of America, Special Paper, v. 41, p. 291–303.

Talbot, M.R., and Allen, P.A., 1996, Lakes, in Reading, H.G., ed., Sedimentary Environments: Processes, Facies and Stratigraphy: Blackwell Science, Oxford, p. 83–124.

Tavares, T.M.V., Rohn, R., Röβler, R., and Noll, R., 2014, Petrified Marattiales pinnae from the Lower Permian of North-Western Gondwana (Parnaíba Basin, Brazil): Review of Palaeobotany and Palynology, v. 201, p. 12-28.

Tooth, S.D., 1999, Floodouts in Central Australia, *in* Miller, A.J. and Gupta, A., eds., Varieties of Fluvial Form: John Wiley and Sons, Chichester, p. 219–247.

Torsvik, T.H., and Cocks, L.R.M., 2004, Earth geography from 400 to 250 Ma: a palaeomagnetic, faunal and facies review: Geological Society of London, v. 161, p. 555-572.

Tucker, M.E., 2003, Sedimentary rocks in the field: a practical guide: Chichester, Wiley, 234 p.

Tunbridge, I.P., 1984, Facies model for a sandy ephemeral stream and clay playa complex: The Middle Devonian Trentishoe Formation of North Devon, U.K: Sedimentology, v. 31, p. 697-715.

Van der Meer, M.T.J., Schouten, S., Bateson, M.M., Nübel, U., Wieland, A., Küuhl, M., de Leeuw, J.W., Sinninghe Damsté, J.S., and Ward, D.M., 2005, Diel Variations in Carbon Metabolism by Green Nonsulfur-Like Bacteria in Alkaline Siliceous Hot Spring Microbial Mats from Yellowstone National Park: Applied and Environmental Microbiology, v. 71, p. 3978-3986.

Vaz, P.T., Resende, N.G.A.M., Wanderley Filho, J.R., and Travassos, W.A., 2007, Bacia do Parnaíba: Boletim de Geociências Petrobrás, v. 15, p. 253-263.

Vennin, E., Bouton, A., Bourillot, R., Pace, A., Roche, A., Brayard, A., Thomazo, C., Virgone, A., Eric, C.G., Desaubliaux, G., and Pieter, T.V., 2019, The lacustrine microbial carbonate factory of the successive Lake Bonneville and Great Salt Lake, Utah, USA: Sedimentology, v. 66, p. 165-204.

Vos, R.G., and Hobday, D.K., 1977, Storm beach deposits in the late Palaeozoic Ecca Group of South Africa: Sedimentary Geology, v. 19, p. 217-232.

Wagner, R.H., 2003, Climatic changes as mirrored by Carboniferous and Permian floral distribution: Monografías del Jardín Botánico de Córdoba, v. 11, p. 29-39.

Wagner, R.H., and Mayoral, E.J., 2007, The Early Permian of Valdeviar in Sevilla province, SW Spain: basin history and climatic/palaeogeographic implications: Journal of Iberian Geology, v. 33, p. 93-124

Walker, R.G., and Plint, A.G., 1992, Wave-and storm-dominated shallow marine systems, *in* Walker, R.G., and James, N.P. eds., Facies models: response to sea level change: St. John's Newfoundland, Geological Association of Canada, p. 219-238.

Walker, R.G., 1992, Facies, facies models and modern stratigraphic concepts, *in* Walker, R.G., and James, N.P., eds., Facies models: response to sea level change: St. John's Newfoundland, Geological Association of Canada, pp. 1-14.

Wang, J., Jiang, Z., and Zhang, Y., 2015, Subsurface lacustrine storm-seiche depositional model in the Eocene Lijin Sag of the Bohai Bay Basin, East China: Sedimentary Geology, v. 328, p. 55-72.

Wang, P.X., Wang, B., Cheng, H., Fasullo, J., Guo, Z.T., Kiefer, T., and Liu, Z.Y., 2014, The global monsoon across timescales: coherent variability of regional monsoons: Climate of the Past, v. 10, p. 2007-2052.

Warren, J., 2016, Silica mobility and replaced evaporites: 1 - Alkaline lakes: Salty Matters, Newslleter, p. 1-12.

Warren, J.K., 2017, Evaporites: Sediments, Resources and Hydrocarbons: Springer-Verlag Berlin Heidelberg, 1041 p.

Winguth, A.M.E., Heinze, C., Kutzbach, J.E., Maier-Reimer, E., Mikolajewicz, U., Rowley, D., Rees, A., and Ziegler, A.M., 2002, Simulated warm polar currents during the middle Permian: Paleoceanography and Paleoclimatology, v. 17, p. 9-1-9-18.

Zambito, J.J., and Benison, K.C., 2013, Extremely high temperatures and paleoclimate trends recorded in Permian ephemeral lake halite: Geology, v. 41, p .587-590.

Zharkov, M.A., and Chumakov, N.M., 2001, Paleogeography and Sedimentation Settings during Permian-Triassic Reorganizations in Biosphere: Stratigraphy and Geological Correlation, v. 9, p. 340–363.

Ziegler, A.M., Raymond, A.L., Gierlowski, T.C., Horrell, M.A., Rowley, D.B., and Lottes, A.L., 1987, Coal, climate and terrestrial productivity: the present and early Cretaceous com-pared, in Scott, A.C., ed., Coal and coal-bearing strata: Recent advances: Geological Society, London, Special Publications, v. 32, p. 25-49.

6 THE PERMIAN CONTINENTAL CHERTS FROM THE PARNAIBA BASIN: ORIGIN AND GLOBAL CORRELATION THROUGOUT THE WEST GONDWANA

Luiz Saturnino de Andrade[1,2]* & Afonso César Rodrigues Nogueira[2]

[1] Programa de Pós-Graduação em Geologia e Geoquímica-PPGG, Instituto de Geociências-IG, Universidade Federal do Pará-UFPA, 66075-110, Belém, Pará, Brasil.

E-mail: geoandrade.sl@gmail.com

[2] Grupo de Análise de Bacias Sedimentares da Amazônia, Universidade Federal do Pará-UFPA.

E-mail: afonsonogueir@gmail.com

***Corresponding author**

ABSTRACT

Using a combination of detailed outcrop study and petrographic analyses, this paper describes, for the first time, the microtexturall aspects from pervasive silicification that developed during the Early Permian deposits of the Parnaiba Basin, northertn Brazil. This significant Permian chert is associated of the Cisuralian Pedra de Fogo Formation, depositaded in the shallow lacustrine-sabkha influenced by expansion and contraction stages under climatic seasonality regime prevailing in the west-central part of Neo-Gondwana (Pangaea) during yours deposition. The silicified succession is an assemblage of characteristics shared by evaporite-replacement and includes both mineralogical and textural aspects. The sequence of textures includes the groundmass representaded by largely of a mosaic from microquartz with different sizes and optic axes randomly oriented and/or showing a gridwork pattern. Filling phases includes chalcedonic overlays, zebraic chalcedony, microflamboyant quartz and mainly spherulites of length-slow quartzine and mosaic megaquartz. This study is an important contribution to the understanding of the inorganic silicification process.

Keywords: Permian chert; Parnaíba Basin; Pedra de Fogo Formation; Lacustrine-sabkha; Silicification process

INTRODUCTION

Silicification events in the Paleozoic basins worldwide has been related as exclusively of marine settings linked to the accumulation of biogenic silica basically after degradation of siliceous skeletal from sponges, radiolarians and diatomaceous denominated of Permian Chert Event (Harper and Knoll 1975; Pisciotto 1981; Banahan and Goering 1986; Hesse 1988; Maliva et al. 1989; Gao and Land 1991; Murchey and Jones 1992; Beauchamp and Baud 2002; Volpi et al. 2003; Gates et al. 2004; Feng et al. 2005; Takiguchi et al. 2006; Neuweiler et al. 2014). In contrast, an abiogenic origin of chert cannot be discarded. Even where siliceous microfossils are present in chert, this does not mean that the source is exclusively biogenic (see discussion in Pettijohn 1975, p. 402-407). Abiogenic silica forming chert-bearing sedimentary units can be originated by burial diagenesis and/or hydrothermal events related to the igneous intrusions triggered release silica to the environment (White et al.1964; Walter 1976). In addition, abiogenic cherts are found in saline, alkaline and carbonate lakes and playas, as well as, paleosoils or silcretes (Eugster 1967, 1969, 1980; Hay 1968, 1970; Surdam et al. 1972; Summerfield 1983a, 1983b; Sheppard and Gude 1986; Parnell 1988; Schubel and Simonson 1990; Krainer and Spotl 1998; Bustillo 2001). Generally, the rich-silica sedimentary system is strongly conditioned by warm and arid climatic variants under seasonality (Cecil 1990).

Precambrian and Phanerozoic cherts deposits have been recorded worldwide, related to different sedimentary environments, since lacustrine, carbonate and siliciclastic shelves until deep ocean basins (Eugster 1967; Chowns and Elkins 1974; Robertson 1977; Rubin and Friedman 1981; Yamamoto 1987; Bustillo et al. 1998; Krainer and Spötl 1998; Gates et al. 2004; Chen et al. 2006; Bustillo and Alonso-Zarza 2007; Moore Jr. 2008, Qui and Wang 2011; Beauchamp and Grasby 2012). Finally, the silica has several sources formed in different settings and precipitation phases not completely explained, which difficult the complete understanding of its genesis. The precipitation and solubility phases of silica are controlled mainly by pH, temperature, presence of CO_2, and water turbidity (Laschet 1984). Therefore, other allogenic parameters such as climate and tectonics have been influenced directly or indirectly the continental weathering rates, topography, vegetation, size and surface area, adsorption of impurities and reduction conditions (Laschet 1984).

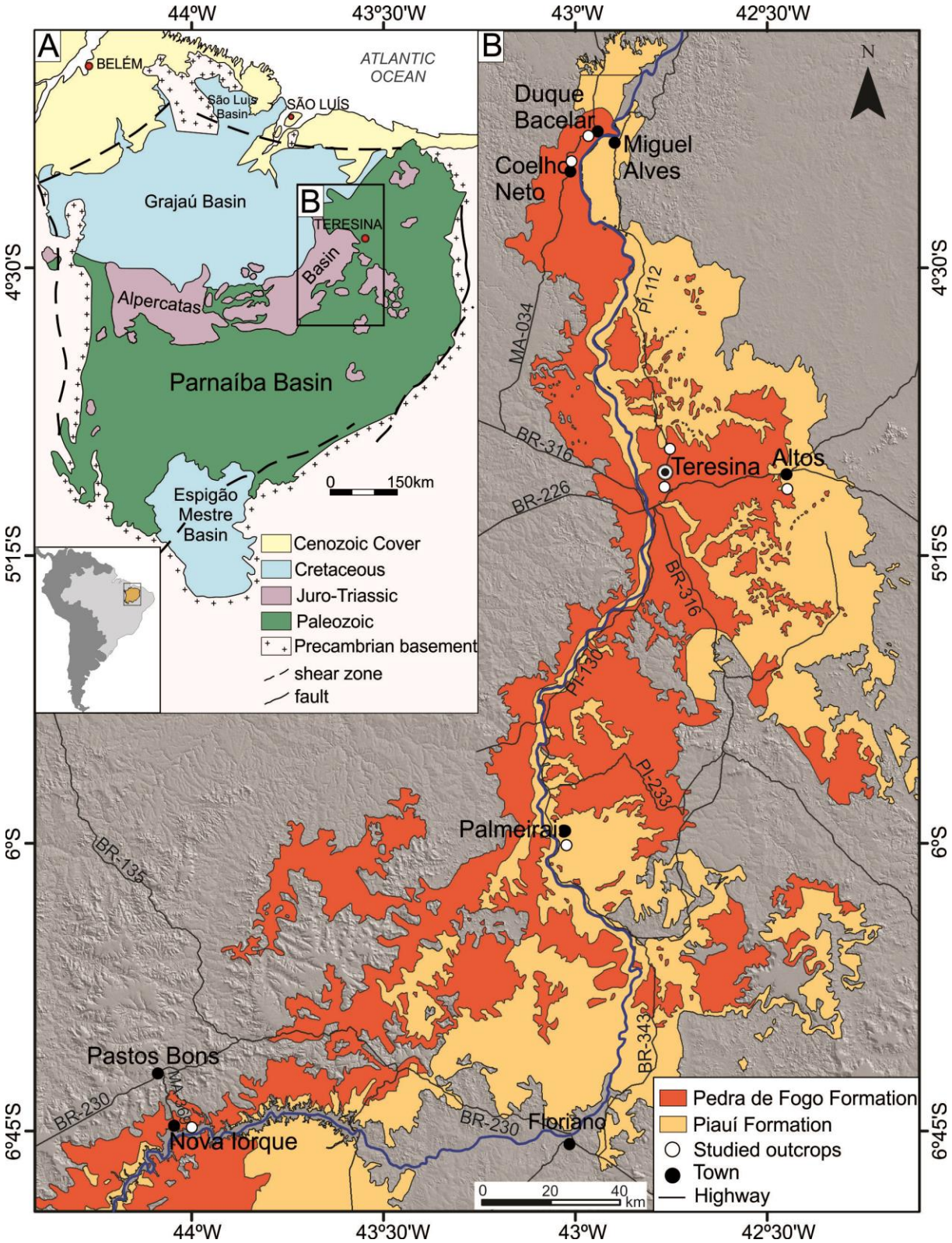

Figure 1-Simplified map of the Parnaíba Basin in Northern Brazil and geographic distribution of the Permian Pedra de Fogo Formation in the eastern portion of the basin (Modified from Góes 1995).

Expressive record of Permian chert is exposed to the Parnaíba Basin, northern Brazil, hosted in siliciclastic deposits of the Cisuralian Pedra de Fogo Formation (Fig. 1). In comparison with other examples worldwide, the previous paleoenvironmental interpretation for the Pedra de Fogo chert (PF-Chert) (Plummer 1946; Faria Jr. 1979; Cisneros et al. 2015) considers an origin exclusively continental. In this work, facies, stratigraphic and petrographic studies carried out on drill cores and outcrops of the lower Pedra de Fogo Formation confirmed the previous continental interpretation for this unit and provided new geological data to discuss the origin of the abundant silica horizons in this unit. Furthermore, we discuss the PF-Chert precipitation in the continental settings under dry climate comparing its petrographic characteristics with other examples worldwide. A priori, this work strongly refutes a marine origin to the PF-chert providing geological evidence to propose a new Permian Chert Event, exclusively continental, that occurred in this part of West Gondwana.

GEOLOGICAL SETTING

The Parnaíba Basin is an intracratonic basin located in north-eastern Brazil, covering an area of approximately 600,000 km2 and filled with approximately 3.5 km of predominantly siliciclastic rocks in its depocenter (Góes and Feijó 1994; Vaz et al. 2007). Vaz et al. (2007). The lithostratigraphic units were grouped in five depositional sequences: 1) Silurian, 2) Mesodevonian-Eocarboniferous, 3) Neocarboniferous-Eotriassic, 4) Jurassic and 5) Cretaceous, separated by important unconformities correlated throughout the basin (Fig. 1). The chert-bearing Permian deposits of the Pedra de Fogo Formation are inserted in the Balsas Group of the Neocarboniferous-Eotriassic sequence (Vaz et al. 2007). The Pedra de Fogo Formation conformably overlies the Carboniferous Piauí Formation, is conformably overlaid by the Permian Motuca Formation and, laterally to the west of the basin, is in unconformity with Eotriassic Sambaíba Formation (Vaz et al. 2007). The Carboniferous Piauí Formation consists in fine- to coarse-grained sandstone and conglomerates with large-scale cross-stratification, trough cross-stratification, and reddish siltstone, as well as, limestones lenses representative of fluvial and aeolian systems with brief marine incursions under warm and semi-arid climate (Lima and Leite 1978, Souza et al. 2010). The Sambaíba sandstone is a record of a desert system and represents the climax of the continentalization of the Parnaíba Basin. According to Góes et al. (1990), the Late Carboniferous to Permian Balsas Group marks the beginning of the continentalization in the Parnaíba Basin, with desertification climax represented by the fine- to medium-grained aeolian sandstone of the Triassic

Sambaiba Formation, accompanied by the progressive displacement of the depocenter to the northwestern of the basin.

The Permian chert-bearing deposits of the Pedra de Fogo Formation (PF-chert) is interbedded with other lithologies, such as carbonate, evaporite, argillite, shale and sandstone organized in a cyclic sedimentation and with abundant and diversified fossil content (Plummer 1946; Barbosa and Gomes 1957; Melo and Prade 1968; Faria Jr. and Truckenbrodt, 1980a, 1980b). The fossils are represented by tetrapods (Cisneros et al. 2011; 2015), fishes, amphibians (Santos 1994; Figueroa and Gallo 2017), stromatolites and a variety of silicified woods (Faria Jr. and Truckenbrodt 1980b; Coimbra and Mussa 1984; Martins 2000; Rößler and Galtier, 2002a, 2002b and 2003; Rößler 2006; Santos and Carvalho 2009; Conceição et al. 2016a, b; Iannuzzi et al. 2018). The PF-chert was deposited in shallow marine- to coastal-system with deltaic and tidal flat settings (Faria Jr. and Truckenbrodt 1980a; Góes and Feijó 1994), as well as, in an extensive lacustrine system with inland sabkha and aeolian dunes (Andrade et al. 2014). The tetrapod-based on biostratigraphy indicates a Cisuralian age for the upper Pedra de Fogo Formation (Cisneros et al. 2015).

METHODS

The paleoenvironmental reconstitution of Permian deposits was performed based on facies analysis following the suggestions of Walker (1992, pg. 1-14) and Dalrymple (2010, pg. 3-18), i.e., the individualization and description of sedimentary facies, the comprehension of depositional processes and the association of cogenetic and contemporaneous facies indicative of paleoenvironment. The description of the PF-chert is integrated with the facies association, as well as, the systematic sampling for petrographic study. Fifteen thin sections were examined with standard optical transmitted light microscopy. Additional methods include X-ray diffraction (XRD) to identify the precise mineralogy and silica phase and Scanning Electron Microscope (SEM) with EDS systems integrated to characterize better the textural and superficial features. SEM-EDS observations were obtained from the Microanalysis Laboratory of the Institute of Geosciences (IG) of the Federal University of Pará (UFPA). The SEM equipment used was a Zeiss SEM SIGMAVP model belonging to the Vale Technological Institute (ITV) installed in the UFPA. The operating conditions were: the electron beam current = 80 μA and the constant acceleration voltage = 10 kV with working distance = 8.5 mm. The samples were mechanically separated from the bulk specimens, then

assembled in a slide glass using a graphite-based adhesive and simultaneously coated with gold.

RESULTS

THE STRATIGRAPHIC RELATIONSHIP AND FACIES ASSOCIATIONS

The Late Carboniferous-Permian siliciclastic deposits that include the top of Piauí Formation and the base of the Pedra de Fogo Formation, are exposed in road cuts and small hills reaching up to 40 m-thick, being laterally continuous for hundreds of meters (Fig. 1 and 2). The outcrops extend discontinuously for about 160-km from northeast to south-southwest following the east and south border of the Parnaíba Basin (Fig. 1). Three facies associations (FA) were detailed in the two main sections and consist in (Fig. 2): FA1) dune field deposits, FA2) nearshore lacustrine/sabkha and FA3) central shallow lakes. The FA1 belong to the Carboniferous Piaui Formation and consists predominantly of fine- to medium-grained sandstone with planar and medium-scale tangential cross-bedding, locally bioturbated by sub-vertical and horizontal trace fossils (Fig. 2). The contact with the Permian Pedra de Fogo deposits is a flat bounding surface, considered here as an important unconformity marked by tabular beds of aeolian sandstone overlain by abundant wavy bedding mudstone interbedded with centimetric layers of chert related to the FA2 (Fig. 2). The chert is found as different forms (elongated, oblate, spheric, enterolithic) are recurrent in the studied succession and generally is interpreted as the replacement of evaporite molds (Fig. 3). These facies associations are organized in centimetric-scale asymmetrical cycles forming a flat-lying geometry (Fig. 2 and 3). The chert-bearing deposits are more frequently found in contact with aeolian facies than with the fluvial deposits of Piauí Formation (Fig. 3).

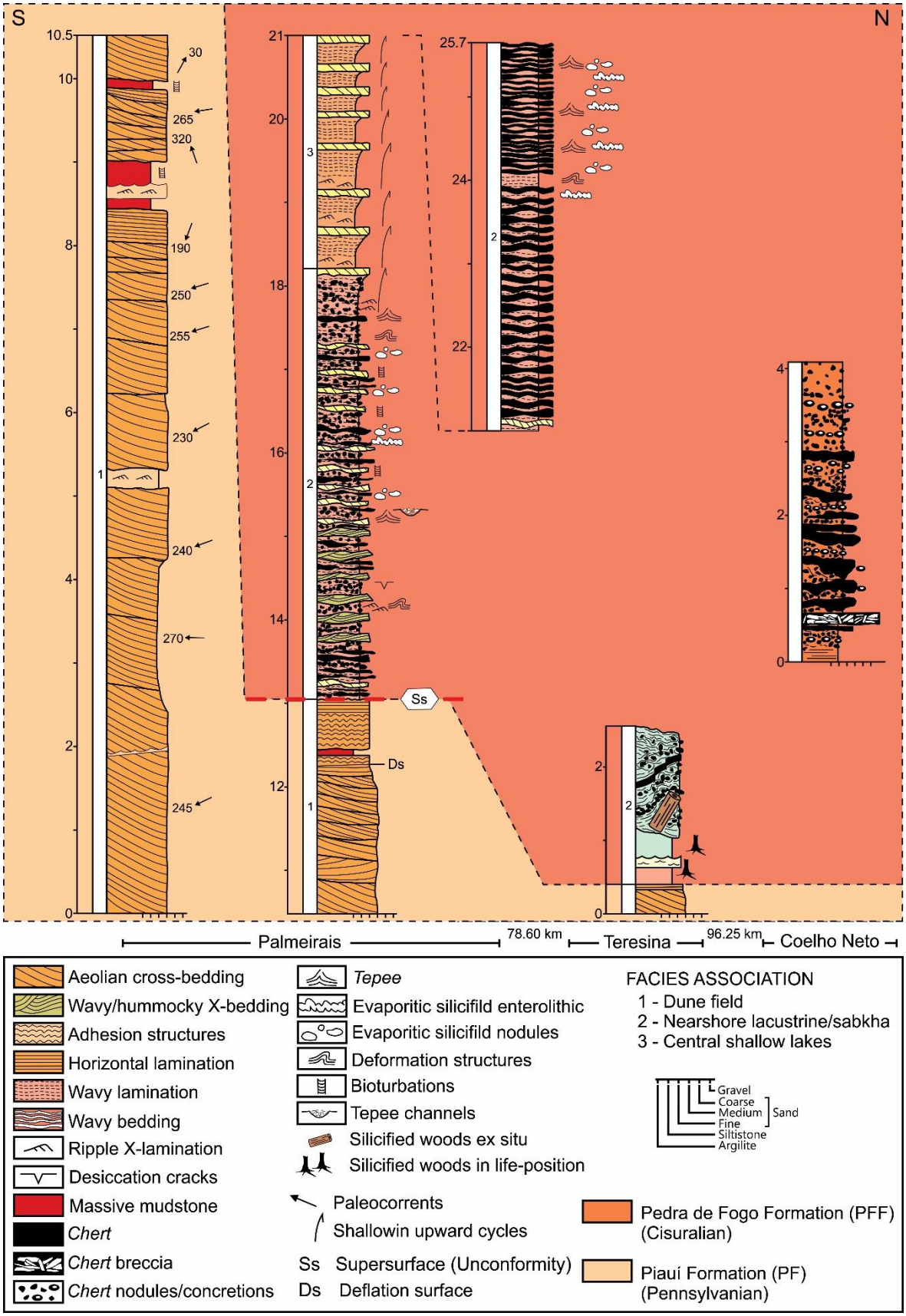

Figure 2-Stratigraphic logs representative of the Permian chert-bearing succession of the Parnaíba Basin. The contact between FA1 and FA2 is interpreted as a regional unconformity (Supersuface-Ss). See local sites in figure 1.

Dune field deposits (FA1)

Description The FA1 occurs as 13m-thick, composed of light orange well-sorted and well-rounded, fine-to medium-grained sandstone with even parallel stratification and predominantly medium-scale trough and tangential cross-stratification (Fig. 2 and 3A, B). The sandstone with tangential cross-bedding is organized into 0.5-2.7 m-thick sets. Asymptotic foresets displaying a dip ranging from 030° to 320°, with preferential paleowind directions point to SW (Fig. 2). The most bounding surfaces between sets are smooth and corrugated (~ 0.2 m), with fine-to medium-grained sandstone with warts adhesion lamination type warst (Fig. 3C). Locally sets are compound, and reactivation surfaces are relatively common (Fig. 3D, E). Cross strata in plan view show a "zig-zag" pattern indicating an apparent reversion but the dip of foresets does not reach 180º indicating small variations of dip apparently in the same quadrant (Fig. 3F). The internal part of cross-strata sets is dominated by wind ripple laminae, secondarily grainflow (Fig. 3G). The sets showing a thinning upward tendency with even parallel stratified sandstone arranged in sets with 0.2 to 0.5 m-thick (Fig. 3H, H'). Interdune deposit (damp surface) is composed of light reddish thin levels of massive and bioturbated mudstone with up to 0.30 m-thick laterally continuous between cross-bedding sets (Fig. 3I, J). The vertical and horizontal tubes were attributed to *Scoyenia* trace fossil. The top of the AF1 is interrupted by a deflation horizon (~ 0.6 m) dominated by adhesion warts and evaporitic-adhesion structures. This horizon showing a typical smooth aspect, with thin irregularities and grain roughness (Fig. 3K, L).

Interpretation: The predominance of fine- to medium-grained sandstone with well-rounded and highly spherical grains, organized in medium- to large-scale cross-bedding interbedded with wind ripple laminae suggests aeolian dune deposits (Hunter 1977; Kocurek 1991, 1996; Lancaster 1996). The occurrence of even parallel beds between cross-bedded sandstone was interpreted as interdune area reworked by small bedforms climbing on the lower planar surface generating subcritically translatent strata (Brookfield 1977). The bidirectionality observed in the cross-strata, as well as the presence of reactivation surfaces, indicate not unimodal wind regime albeit that preferential net dune transport preferentially to the south-west (see Fig. 2). The change in orientation (by ca. 20º) is interpreted as a response to the wind direction variation and the readjustment of a convex nose of the dune. Although each interval of climbing sets originates upon a planar and deflationary surface, no interval shows a basal portion representing dune-field initiation, in which small sets occur and evolve to meter-scale sets upsection (Kocurek and Day 2018). The corrugated surfaces between sets suggest

that these dune fields were at least partially wet systems (Kocurek 1981). The intensity of bioturbation upward probably indicates the increase of humidity that allowed the biological activity.

The relatively thick, massive and bioturbed mudstone indicates the alternance of wet and dry cycles (Brookfield and Silvestro 2010, pg. 159-164). Moreover, massive mudstone suggests elevated regional water-table level, flooding interdunes and generating development isolated wet interdune ponds, enclosed depressions in dune-field centers (Fig. 3I). The bioturbations (Fig. 3J) indicate biological activity commonly associated with colonization by local fauna (Kocurek 1981; Al-Masrahy 2017). The planar surface overlapping the deflation horizon with adhesion warts and evaporitic-adhesion structures that interrupt the desert system dominated by aeolian dune field and are associated with supersurfaces caused by a climatic shift under exceptional humid conditions (Kocurek 1988). Probably, the genesis of these supersurface has been related to the interruption of the dune field accumulation, related to the continuous bypass and deflation of aeolian sediments which created an extensive flat surface (Kocurek 1981). As Talbot (1985) noted, the relief on the supersurfaces may become quasi-planar as interdune areas may continue to fill with aeolian or lacustrine deposits and slowly bury relict dunes. The occurrence of evaporitic-adhesion structures confirms this interpretação (Kocurek and Fielder 1982). According to Kocurek (1988), traces of evaporites, horizons of preferential cementation, and polygonal fractures associated with salt cement are evidence that supersurface has been deflated to the water table. The absence of features commonly associated with subaerial exposition like plant roots (rootlets, rhizoliths, root-mottled horizons) and soil development, is suggestive of the waters with high salinity permeating this surface. As Loope (1985) noted, the relative stability of a surface deflated by the water table favors the colonization by vegetation, except if the groundwater is anomalously saline. The occurrence of deflation horizon dominated by adhesion warts and evaporitic-adhesion structures overlying the desert system with shallow lacustrine-sabkha setting is another factor that points to the high salt content of groundwater.

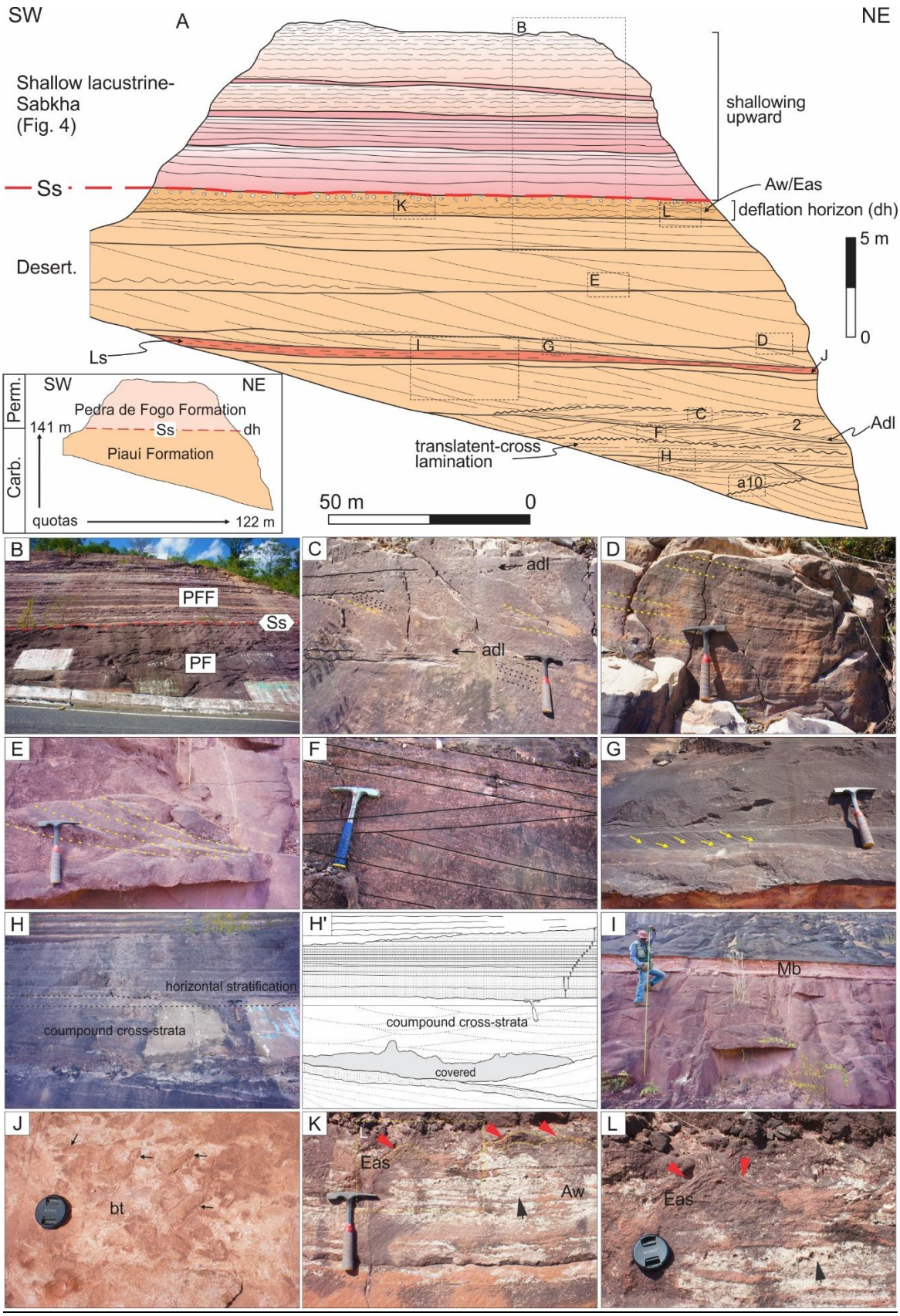

Figure 3-Faciological aspects of PF-chert succession in the Parnaiba Basin. A) Panoramic section of outcrop near of Amarantes region, showing in the base the aeolian dune field deposits of Piauí Formation (AF1) overlaid by centimetric- to decimetric-scale cycles of mudstone interbedded with sandstone of the Pedra de Fogo Formation (AF2) forming a flat-lying geometry. B) Aspects of the flat contact (Ss) between AF1 and AF2. C) Tangential cross-stratification sets separated by layers with

adhesion ripple lamination (adl); yellow dashed lines indicate reactivation surfaces, and black dashed indicate foresets. D) and E) Foresets with asymptotic base and frequent reactivation surfaces (yellow dashed). F) Cross-strata in plan-view exhibiting 'zigzag' pattern. G) Grainflow laminae in cross-lamination (arrows). H) and H') Compound cross-strata overlain by even parallel stratified sandstone with thinning upward tendency. I) General aspect of massive/bioturbated mudstone (facies Mb) layer inside in the interdune deposits. J) Plan view of bioturbation (bt-black arrows) of the facies Mb attributable to the Scoyenia *ichnofacies*. K, L) Evaporitic adhesion (Eas) and adhesion warts (Aw) features (black arrows). Note the typical dome-shaped (red arrows) microtopography, characteristic from evaporitic-adhesion structures.

Nearshore lacustrine/sabkha (FA2)

Description: The 8 m-thick FA2 directly overlies the FA1 and consists of mudstone interbedded with laminated or wave-ripple cross-laminated very fine- to fine-grained sandstone exhibiting evaporitic silicified nodules (Fig. 2). The sedimentary architecture displays regular alternations between mudstone and sandstone beds forming a sheet-like geometry (Fig. 4A, B) laterally continuous for many hundreds of meters showing only minor changes in thickness. The sandstone is whitish to yellowish-brown, brownish-gray and predominantly whitish-pink arranged in flat-lying layers between 10 to 30 cm-thick (see Fig. 3B; 4A, B). The sandstone is generally very fine- to medium-grained, moderately sorted, and have commonly wave-ripples cross-lamination, incipient cross-lamination, and subcritically to supercritically climbing-ripple cross-lamination (Fig. 4C, D, E). Hummocky cross-laminated sandstone is relatively frequent in the base of Pf-Chert succession (Fig. 4F, G). In the same way, the tepee structure is frequently observed in this association, and eventually, the broken apex of the top of this structure is coincident with a small-channelized morphology filled by chert pebble sandstone (Fig. 4H). The mudstone is reddish-yellow to pinkish-gray and sometimes drape the wavy lamination on sandstone beds. Silicified evaporite nodules with 5–10 cm in diameter exhibit irregularly shapes and are more concentrated at the uppermost part of the cycles (Fig. 4I). Centimeter-scale enterolithic folds and desiccation cracks occur typically on the base of the studied succession, and rare load structures are found on the top (Fig. 4J, K, L). Desiccation cracks and reworked centimetric rip-up mud clasts occur on the base of succession (Fig. 4L, M).

Interpretation: The composition, texture, bedding style, sedimentary structures and contact relationship allowed to interpret the FA2 as a nearshore lacustrine-sabkha setting frequently reworked by fairweather waves, and eventually by storms. The small-scale cycles formed by the regular alternance between mudstones and fine-grained sandstones suggest siliciclastic inflows provided of unconfined ephemeral flow deposited directly on a relatively shallow lacustrine substrate. Sheet flood events are generally shallow, with recorded depths

between 20 to 30 cm (McGee 1897). Tooth (1999) suggests depths of less than 30 cm and Blair (2000) indicates depths of 15–80 cm. The tabular geometry of sandstone beds observed in the studied succession is consistent with deposition from a single or amalgamated, unconfined sheet flood events (Parkash et al. 1983). The very fine-grained sandstone with incipient cross-lamination and predominance of supercritically climbing-ripples cross-lamination on the top of cycles marks the waning of the flood event (Lindholm 1987, pg. 20). The flow velocity decreases with increasing radial distance from the source reducing the sand supply and increase the flow spreading as it becomes unconfined (Beer and Jordan 1989; Tooth 1999; Lang et al. 2004). Sheet sandy bodies are also deposited in shallow lacustrine settings where river channels feed the lake with sand and suspension mud (Fisher et al. 2008). As a sediment-laden flow enters in the standing water body, the flow velocity decreases and the sediment in suspension spreads out like a plume in the lake (Collinson and Thompson 1982). The bedload and suspension sediments may be reworked by waves and currents in the lake causing a detrital redistribution along sediment spreading sheet plume (Fisher et al. 2007). The frequent occurrence of ripples marks and isolated hummocky cross-bedding indicate frequent oscillatory flows and sporadically storm waves revolving unconsolidated sediments in the lake bottom (Duke 1985; Eyles and Clark 1986; Li et al. 2007; Li et al. 2014). Hummocky cross-bedding form in very fine sand under dominantly oscillatory combined flow and a weak unidirectional component associated with sediment aggradation rates that preserve the convex-up part (hummock) of this storm bedform (Dumas and Arnott 2006). According to Eyles and Clark (1986), hummocky cross-stratification is widely preserved within the nearshore zone of the Pleistocene lacustrine deposits.

The uppermost part of the cycles contains disseminated and massive chert beds covering sandstone beds, interpreted as silicified evaporitic molds (Fig. 4). These facies indicate contraction phases of the nearshore lacustrine/sabkha that enlarged the dry mudflats (Kendall 2010, pg. 512-514). The low waters during the dry season, associated with a high evaporation rate caused the lake contraction (sabkha phases) allowing the ions saturation and precipitation of evaporites and limestones on the mudflat (stage II from Lowenstein and Hardie1985). Evaporite minerals were precipitated over grains and at the surface of this lacustrine peripheric zone and efflorescent salt crusts precipitated on the capillary zone brine above the saline groundwater level (Rosen 1994; Schubel and Lowenstein 1997; Benison et al. 2007; Kendall 2010, pg. 512-513). Nodular ‘pop-corn’ evaporites were precipitated by the same process as well as the evaporites with "chicken-wire” texture (see Fig. 12 in petrographic topic). Desiccation cracks and tepee features were formed during subaerial

exposure (Fig. 4K). The short time of exposure of the mudflat was not enough for palaeosols development and the periodical flooding also contributed to hinders the pedogenesis (Hinds et al. 2004). Likewise, the high salinity of groundwater prevented the plants' colonization. This interpretation is reinforced by the occurrence of desiccation cracks, rip-up clasts, small-scale shallow channels on the collapsed tepee. The complete exposition of the saline lake floor typically generates large polygons (Lowenstein and Hardie 1985; Schubel and Lowenstein 1997). In contrast, the small size of the desiccation cracks polygons suggests a substrate supplied by perennial water restricted to the margin of the lake. Deformed post-depositional features indicate soft-sediment deformation of water-saturated unconsolidated to semi-consolidated deposits (Rossetti 1999). The rapid deposition was accompanied by liquefaction and vertical displacement of sediments (Tunbridge 1984; Owen et al. 2011).

The well-preserved evaporitic features suggest syndepositional or early diagenetic silicification with high silica content in solution (see discussion in petrographic topic). This facies association is very similar to describe by Andrade et al. (2014) and Abrantes Jr. et al. (2019) in the western Parnaíba Basin.

The good preservation of the evaporitic features suggests syndepositional or early diagenetic silicification processes and, consecutively, a high silica content in solution (see discussion in petrographic topic). This facies association is very similar to describe by Andrade et al. (2014) and Abrantes Jr. et al. (2019) in on the western bord of the Parnaíba Basin.

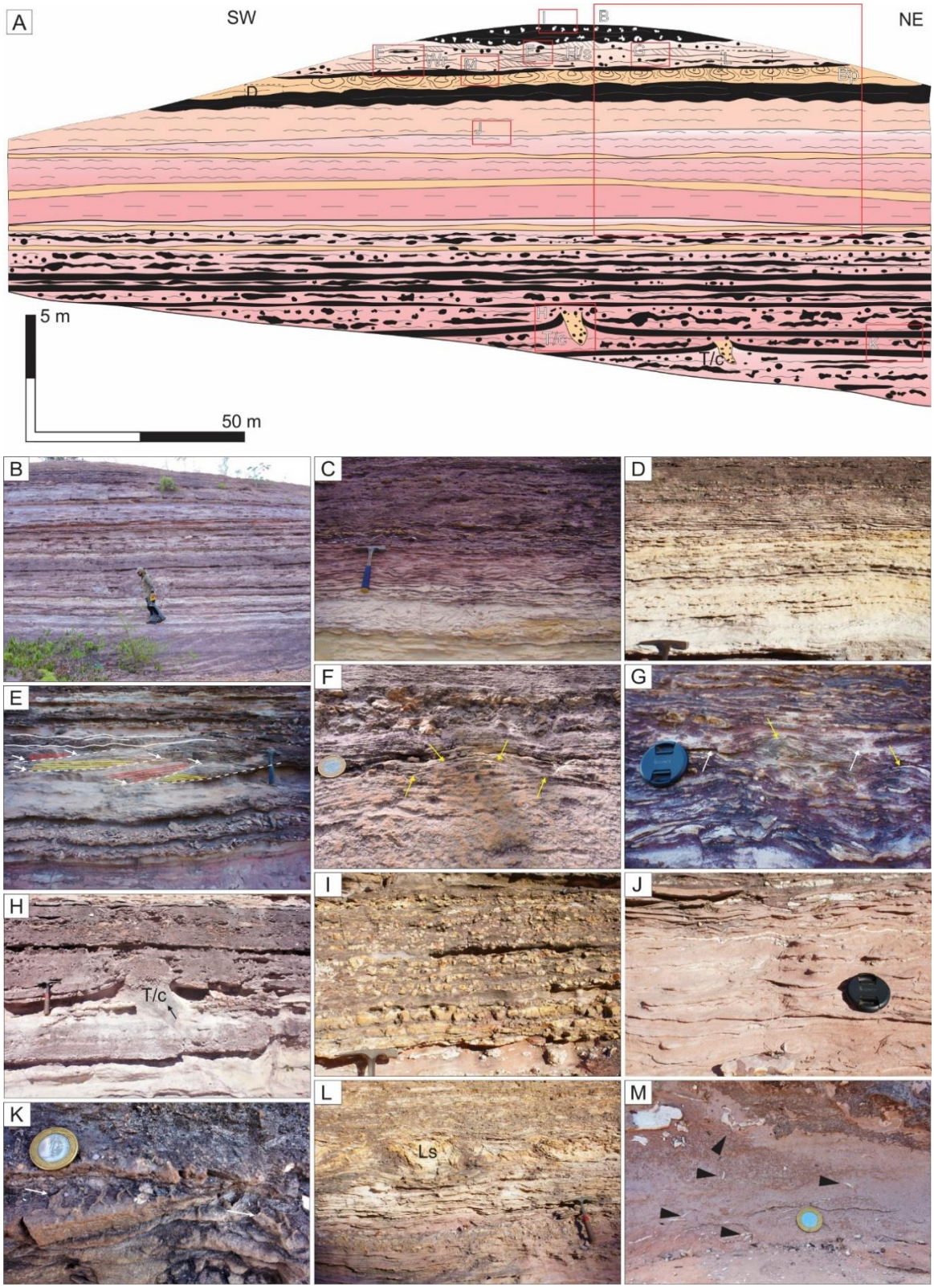

Figure 4-The shallow lacustrine-sabkha deposits exposed in the upper portion of the outcrop near of Amarantes region, the eastern Parnaiba Basin. A) An interpretative drawing showing the general arrangement in flat-lying beds constituted by centimeter-scale cycles of mudstone and sandstone with chert nodules and layers (black color) concentrated in the base and top of the outcrop marked also by convolute bedding. B) General view of the sheet-like cycle geometry. C, D) Very fine-grained sandstone with wavy bedding. E) Subcritical and supercritical climbing-ripple cross lamination; white arrows and dashed lines indicate the crest line; red and yellow lines mark respectively, the stoss-side

and lee-side laminae; the continuous and undulated white lines in the uppermost part mark predominance of supercritically climbing ripples. F) Hummocky cross-lamination (yellow arrows). G) Truncated lamination of hummock (yellow arrows) and swale (white arrows) morphology. H) Small-scale shallow channels on the collapsed tepee (T/c). I) irregular silicified evaporitic nodules interbedded with chert beds. J) Wavy bedding with small-scale folds and flame structures in sandstone and chert beds considered as an evaporitic pseudomorph. K) Centimetric desiccation cracks (white arrows). L) Convolute lamination. M) Rip-up mud clasts (black arrows). The location of figures B-M is indicated in the section shown in A.

Central shallow lake (FA3)

Description: The 3m-thick FA3 is constituted by light gray to brown and light pink mudstone (beds with up to 0.6 m-thick) interbedded with light yellow fine-grained sandstone (beds with up to 0.3 m-thick). Mudstone and fine sandstone are organized in centimetric shallowing-upward cycles and overlie sharply the FA2 (Fig. 2, 3 and 4). Upsection occurs a thinning upward of mudstone in the cycles. The FA3 is like the FA2 and similarly is characterized by mudstone interbedded with very fine- to fine-grained sandstone. The beds of FA3 are laterally continuous for hundreds of meters with few variations in facies and thickness (Fig. 2, 3 and 4). The mudstones are light orange to whitish red with incipient horizontal and some massive portions and slightly wavy bedding. However, different from FA2, the mudstone layers are relatively thicker (0.2-0.5 m-thick) and predominate even parallel lamination and some wave ripples. The whitish-pink, very fine to fine-grained, moderately sorted sandstone form tabular beds. Other structures observed in the sandstone were supercritically climbing-ripples cross-lamination and eventually massive bedding. Silicified evaporite nodules are sparse.

Interpretation: The FA3 represents the most distal deposits of the Permian PF-chert succession in the Parnaiba Basin. The predominance of the reddish color of mudstone without organic matter, sulfide, and devoid of wave reworking indicates a reduced lake stratification with an inactive thermocline and a very thick oxic zone. The fine sediments were deposited mainly by suspension related to a waning and low-velocity flow (Collinson and Thompson 1982; Jorgensen and Fielding 1996). The lack of sandy lobes and erosional surfaces suggest predominant hypopycnal flow and very low frequency of homopycnal flow. When the density of the inflow is less than that of the lake water, suspended silt- and clay-sized particles are transported as buoyant plumes far into the lake. This characteristic constitutes indirect evidence of saline lakes (Renaut and Gierlowski-Kordesch 2010, pg. 551). The sparse and incipient wavy bedding implies that apparently the FA3 was deposited without the influence of intense wave action, below the wave base (Fisher et al. 2007). The FA3 deposits were

horizontally dispersed and expanded on the lake bottom by settling out of suspension. The occurrence of supercritically climbing-ripples cross-lamination marks the waning of this flooding process (cf. Ashley et al. 1982). The lateral continuity of sheet geometry of sandstone, thin thickness, and predominance of supercritically climbing-ripple strata and eventually massive bedding, suggest a flood event performed directly over the flat lacustrine floor (Fisher et al. 2007). These sedimentary characteristics already described for sheet sandstone indicate intermediary to distal unconfined flow on the distal zone of the lake. This ephemeral flow was of relatively low magnitude and dominated by suspended load transport of fine-grained material (Alexander et al. 2001; Fisher et al. 2007; North & Davidson 2012). The sheet sandstone interbedded with centimetric beds of mudstone indicates episodic deposition from multiple ephemeral stream events, interrupted by periods of relative quiescence, but not long enough to generate thick mudstones beds, neither the allow the development of pedogenetic horizon (Tunbridge 1984; Love and Williams 2000; Bridge 2003). The relatively thin mudstones beds, it is not only related to the pulses of high-frequency flooding, but it must also be related to the small accommodation space that characterizes these dry lacustrine systems, as they typically have a shallow depth of the water column (Lowenstein and Hardie 1985). The recurrence of ephemeral streams activity on the lake may suggest a degree of "seasonality" within the system (Fisher et al. 2007). Subaerial exposure features such as mud cracks and tepee structures were not observed on FA3 indicating permanent water cover, compatible with the central part of shallow perennial saline lakes. The general tendency of shallowing-upward cycles may be indicative of arid climate conditions.

THE FIELD OBSERVATIONS OF PF-CHERTS

The PF-cherts show variable shapes, and locally is associated with massive, mottled and light-red mudstones (Fig. 5A and 6A) and its occurrence has been considered as a mineralogical constituent diagnostic of the Pedra de Fogo Formation, serving during decades as a guide for the Permian stratigraphy of the Parnaíba Basin (Plummer 1946; Faria Jr. 1979, Andrade et al. 2014; Araújo et al. 2016; Abrantes Jr. et al. 2019). This succession displays a lateral continuity for dozens of kilometers with local interruptions along of the studied area (Fig. 2). Locally, PF-chert is found as nodular, massive and intraformational "chert breccia" forming tabular to lenticular beds with up to 20 with cm-thick (Fig. 5B-H). Chert layers are commonly *deformed* into folds and boudinage with much larger *amplitudes forming synforms with 15 cm-wide and* up to 12 cm-deep (Fig. 5B). The tops are weakly undulated with low

amplitude, probably caused by early compaction. Possibly, when the sediments were deposited over the chert layer it was soft and fragile, and could be deformed plastically and boudinated isolating fragments (Fig. 5A, 6B). In this phase, the chert was a silica gel. Some fragments presenting the fitting aspect, i.e., *fragments fit* together with adjacent *fragments* like pieces of a puzzle meaning in situ fragmentation (Fig. 6C, D). The chert nodules coalesced laterally aligned with the bedding plane (Fig. 5C). The nodular cherts occur as spherical and mainly spheroids shapes, with the long axis with up to 15 cm-wide lying the bedding plane of host mudstones ("cucumbers" shapes) (Fig. 5D, E). Contorted chert was probably caused by growth and coalescence of nodules while smaller nodules grew and coalesced as a larger structure exercising vertical displacing forces in the lowest mudstone bed generating a mechanism of reverse density gradation. Chert breccia has oblate clasts ranging up to 4 cm in size following its longest axis (Fig. 5F, G, 6C, D). Microscopically the fragments are composed of microquartz and cemented also by microquartz (Fig. 5H). Sometimes, chert laminae are conformable with laminated and deformed siltstone (Fig. 6E, F).

Microbial mats occur locally, and silicified woods are abundant in almost all occurrences of Pedra de Fogo Formation (Fig. 7 and 8). The microbialites occur predominantly in the lower Pedra de Fogo Formation and are recorded mainly in the northern and southern portions of the study area (Fig. 7A-D). The fossilized microbial mats range submilimetric up to 1 cm-thick, of semi-continuous silicified laminae in sets of up to 10 cm-thick (Fig. 7A, B). These layers are typically conformable to the bedding and reflect the morphology of primary bioconstructions. Petrographically, the microbial filaments constitute bacterial colony and individual cells, totally replaced by silica with a predominance of microquartz arranged on the bedding (Fig. 7C and D). In some portions occur carbonates and little amorphous organic matter can be observed. Delicate organic walls, which may be parenchyma (plant tissue) or putative cyanobacteria. The microbial mats layers are always associated with the occurrence of silicified woods in life position, and sometimes overlies the fossilized wood beds or are overlain by them.

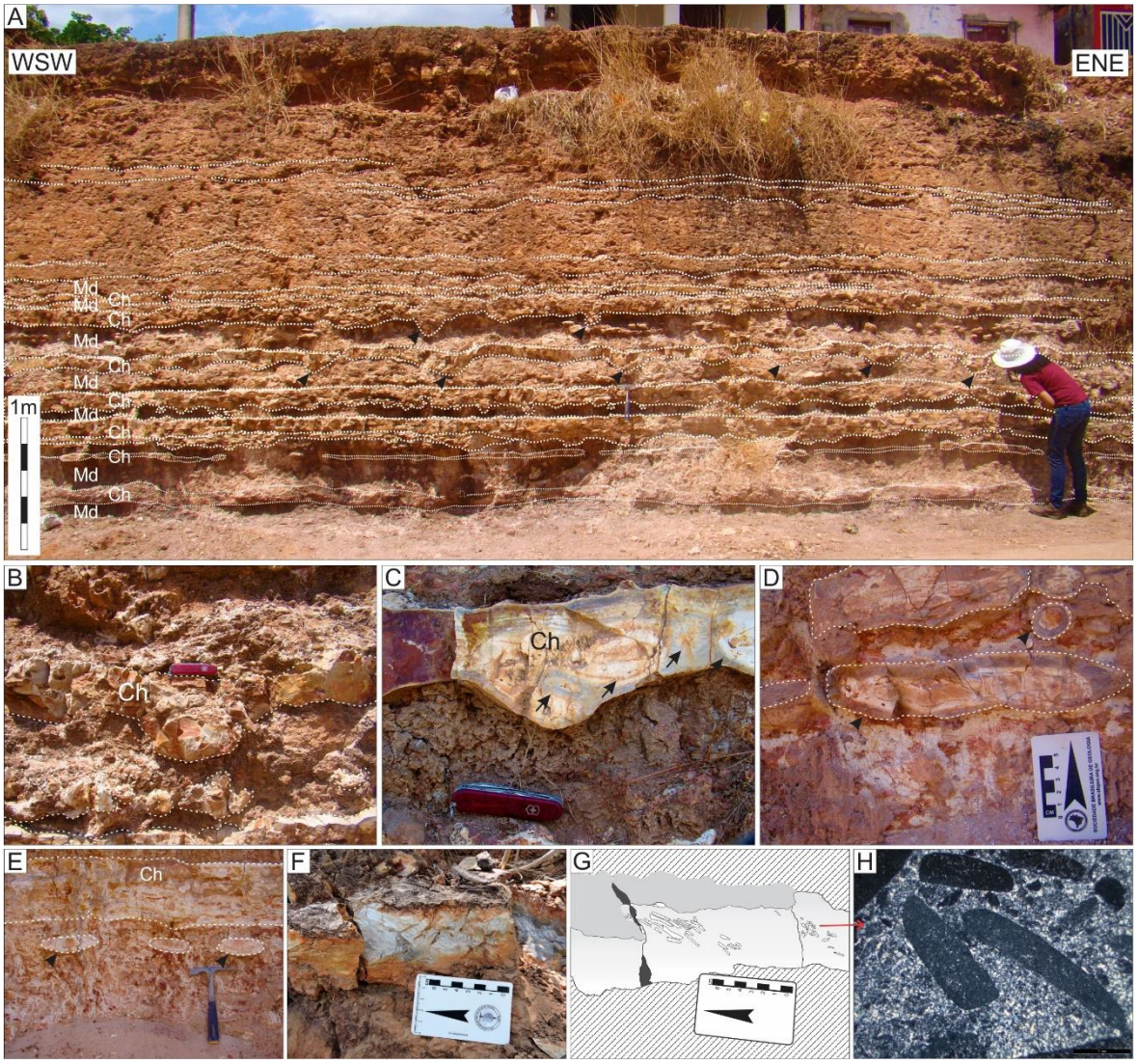

Figure 5- General view showing the stratiform PF-cherts in outcrops near to Coelho Netro and Duque Bacelar towns, the eastern Parnaiba Basin. A) Cherts layers (Ch) forming massive bodies and nodules interbedded in massive mudstone (Md). B) Contorted bed of chert. C) Nodular internal features in chert (black arrows). D) Chert oblate spheroid with its major axis lying on the bedding plane ("cucumber" shape). Nodular chert in high relief on the outcrop, due its resistance to the weathering in comparision with the host mudstone. D) and E) Isolated nodule ranging up to 25 cm in size. G) Chert layer showing breccia-like texture. H) Tabular chert fragments under microscope constituted of microquartz and are cemented also by microquartz.

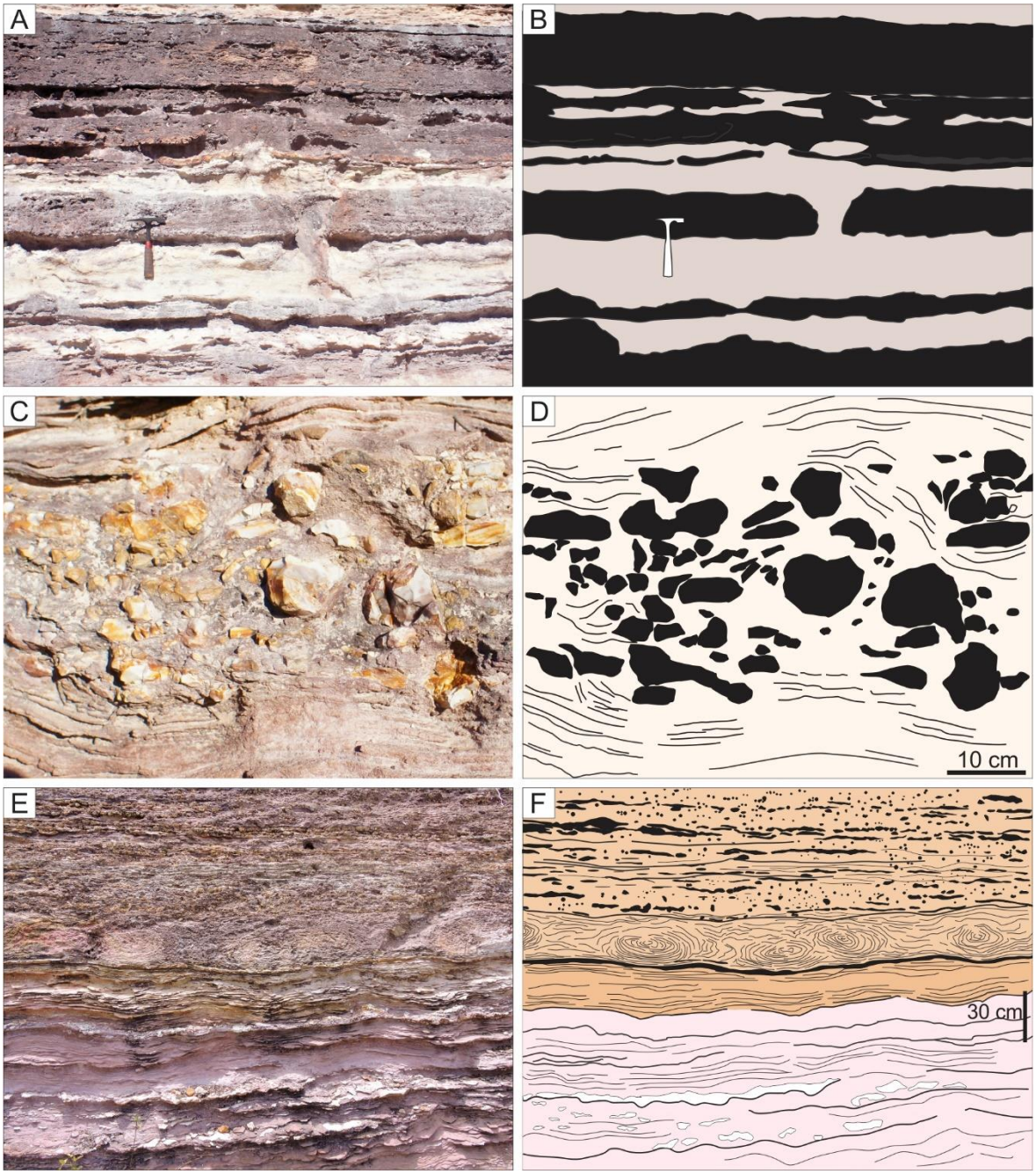

Figure 6- Geometry, textural aspects and features in PF-chert. A) and B) The laterally continuous chert layers locally interrupted and with irregular and undulated (deformed) bed limits. C) and D) Breccia with chert fragments with a fitting aspect inserted in a siliciclastic matrix displaying deformed lamination. E) and F) Thin chert laminae interbedded with siltstone with undulated lamination and ball-and pillow structure.

Silicified woods are abundant and widely distributed by all study area. However, the largest trunks (up to 2.3 m long and 1.15 m in diameter, *see* Conceição et al. 2016a), dominated by gymnosperm stems, are mostly found in life position (autochthonous specimens, Fig. 8A, B), are more restricted to the northern and central portions of the studied area (see fig. 1, parts 1 and 2). Secondarily, tree-fern stems occur in a horizontal position (allochthonous/parautochthonous specimens) scattered randomly over the current surface. The silicified woods are generally well preserved, especially the gymnosperm stems, being possible to recognize certain anatomical features, such as growth ring-like structures (Figs. 8B, C). Some gymnosperm woods show of flattened to elliptical form axes in cross-section (Fig. 8C), indicative of compression by burial (Rex and Chaloner 1983). Impressed remains fern silicified pinnules (Fig. 8D, E) and ferns stems with well preserved internal structures (Fig. 8F). This assemblage of permineralized woods occurs at the top and flanks of the hills, in areas of higher weathering, frequently in horizontal position. Petrified fossil stems in life-position are commonly found associated with mudstone layers, of both massive chert and chert breccia mark the base of Pedra de Fogo Formation, and occasionally, indicated lowlands, partially covered by soil. Horizontal stems are generally within sandstone beds bearing quartz lags and sílex nodules.Though the microbialites and silicified woods are important for the genesis of silicification, they are outside the main scope of this paper. More information is found in Caldas et al. (1989); Faria and Truckenbrodt (1980a, 1980b); Iannuzzi et al. (2018), Conceição et al. (2016a, 2016b) and Conceição et al (2019; submitted for publication).

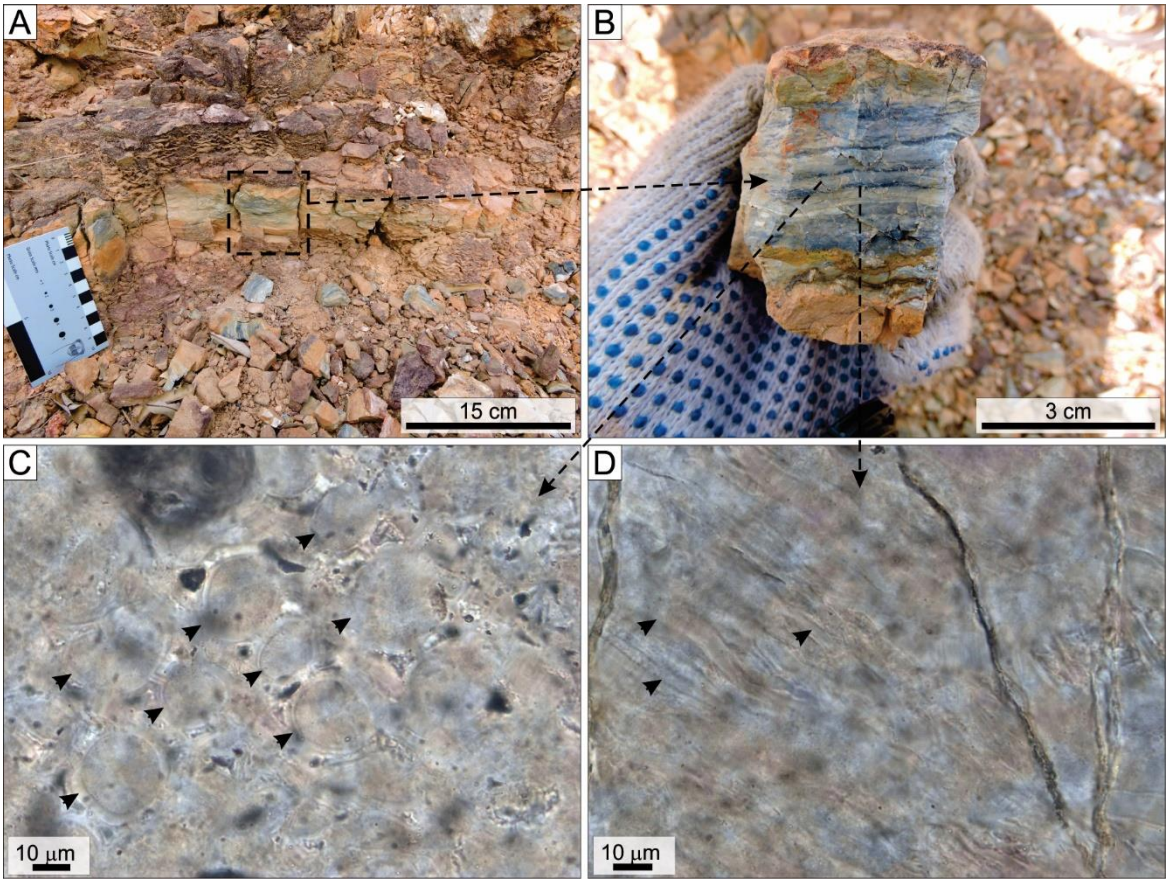

Figure 7- Microbial mats from the Pedra de Fogo Formation. A, B) Centimetre-thick beds of chert with microbial laminites. C, D) Photomicrographs showing putative morphology colony of unicellular and filamentous of microbial communities (arrows).

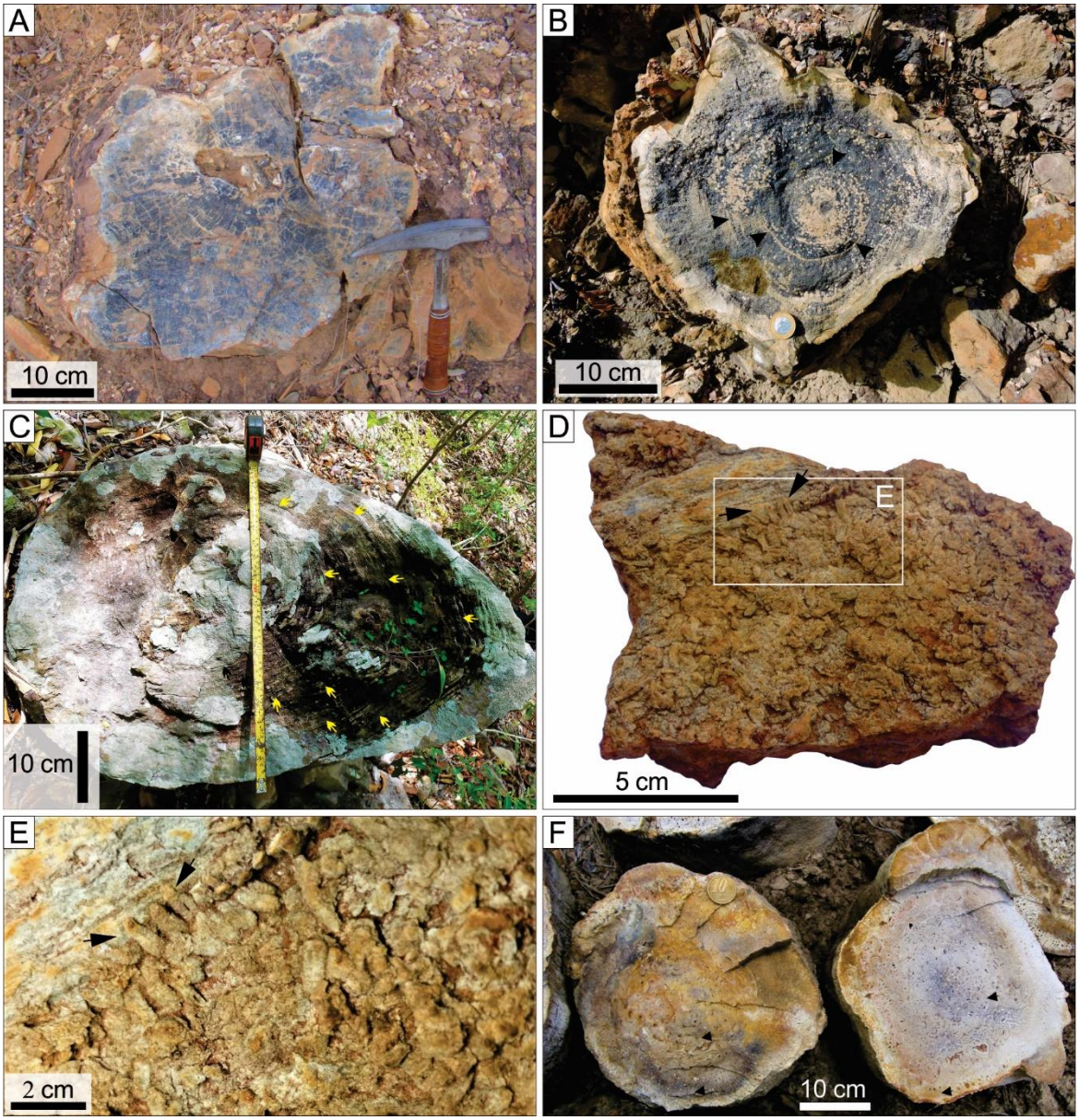

Figure 8- Petrified fossil plants from the Pedra de Fogo Formation. A, B) Gymnosperm silicified woods in life-position. B) Black arrows indicate growth ring-like structures. C) Gymnosperm silicified trunks showing flattened to elliptical form axes indicative of compaction by burial. D) Fern silicified pinnules *Buritiranopteris costata*; E) Detail from silicified pinnules partially cover trunk fragment (black arrows), indicate a very fast sin-depositional/early diagenetic silicification process. F) Detail of two ferns silicified fóssil from family *Psaroniaceae*, with well preserved internal structures (*Psaronius sp.* on the left and *Tietea singularis sp.* on the right).

PETROGRAPHY OF THE PF-CHERT

The PF-cherts fabrics are complex and heterogeneous in textures and structures. A large number of silica fabrics and quartz types recognized in thin sections follow a consistent sequence historically described by Wilson (1966), Folk and Pittman (1971) and Milliken (1979). Petrographic quartz types can be distinguished, which are generally characterized by non-uniform crystal size distribution. The PF-cherts are composed of microcrystalline quartz ("microquartz" of Folk and Pittman 1971), spherulites of length-slow (LS) quartzine, irregular-shaped mosaic megaquartz, and microflamboyant quartz. Secondarily occur chalcedonic overlays and zebraic chalcedony. The boundaries between these silica fabrics are generally gradational. Voids are usually rimmed by chalcedony overlay, and occluded by spherulites of LS-quartzine and megaquartz. The latter typically increase in crystal size into central spaces .of remnant porosity.

X-ray diffraction and EDS analysis show that all the PF-cherts consist mainly of quartz (Fig. 9).The crystallinity index (CI) (Murata and Norman 1976) ranges widely from 10.0 to values as low as 2.0, even within closely spaced samples. We checked for the presence of moganite, but we did not find traces. Moganite is a silica polymorph structurally resembles quartz and commonly associated with length-slow chalcedony (Flörke et al. 1976, Chateau et al. 1999; Schmidt et al. 2013). The diffraction pattern for quartz and moganite is similar. The distinction is made by; (1) splitting of the dominant {101} peak; (2) presence of two peaks (d = 4.45 A and 4.38 A) adjacent to the {100} quartz peak at d = 4.26 A; and (3) presence of additional moganite reflections at d = 3.11 A and 2.88 (Heaney 1995). The X-ray powder diffractogram of PF-cherts shows the quartz peaks have high intensity and absence of the extra peaks broad and very weak associated with moganite (Bustillo 2001; Graetsch and Grünberg 2011).

Groundmass

The groundmass all the PF-chert samples examined consists largely of a mosaic from microquartz with different sizes (most less than 30 μm). This is better described in terms of two end members, in which the optic axes are randomly oriented and those with a rectilinear or gridwork pattern between crossed polarizers with the gypsum plate inserted. The smallest part of the groundmass has the optic axes randomly oriented (Fig. 10A) with "pinpoint" extinction (Folk and Weaver 1952). In this domain, the microforms of quartz have a smaller size than 10 μm. In some domains, the groundmass displays gridwork extinction patterns formed by the interlocking minute quartzine spherules (Fig. 10C). The extinction zones of

gridwork patterns display a range size between 10 and 30 µm in diameter. The main feature that distinguishes the gridwork texture from the random fabric is the marked tendency for quartz crystals to go to extinction in one of two mutually perpendicular directions (Fig. 10B). The gridwork extinction pattern is particularly evident when observed with the gypsum plate inserted in an optical microscope. Under such conditions, the mosaic of minute length-slow (quartzine) spherules describe a regular grid pattern, with two elongated arranged in sub-perpendicular directions (i.e., the blue and yellow in Fig. 10B. By rotating the plate of the microscope of 45º the iso-oriented the fibers of length-slow quartzine, in which the elongation of the fibers is perpendicular to the crystallographic c-axis (Michel-Lévy and Munier-Chalmas 1892 *apud* Heaney 1995), switch alternatively from extinction position blue (first and third quadrant) to light positions yellow (second and fourth quadrant) of the minute spherulites. Pores are invariably absent in a groundmass, similar to other occurrences (Schubel and Simonson 1990; Hattori et al. 1996; Krainer and Spötl 1998). All potential pores are occluded by pervasive types of silica diagenetic fabrics.

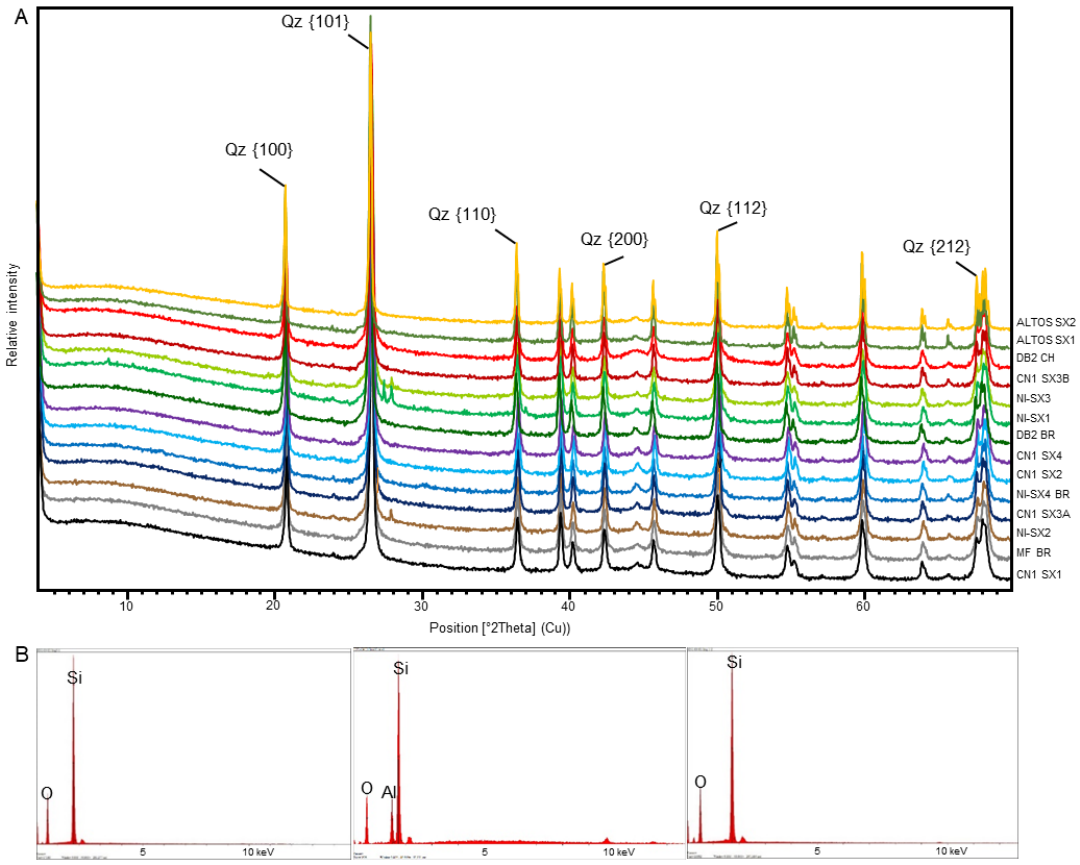

Figure 9-Composition of PF-chert. A) X-ray diffractograms from PF-cherts showing the high intensity of quartz peaks, indicative from well-crystallized quartz. B) EDS spectra demonstrating the Si-rich composition typical of PF-chert.

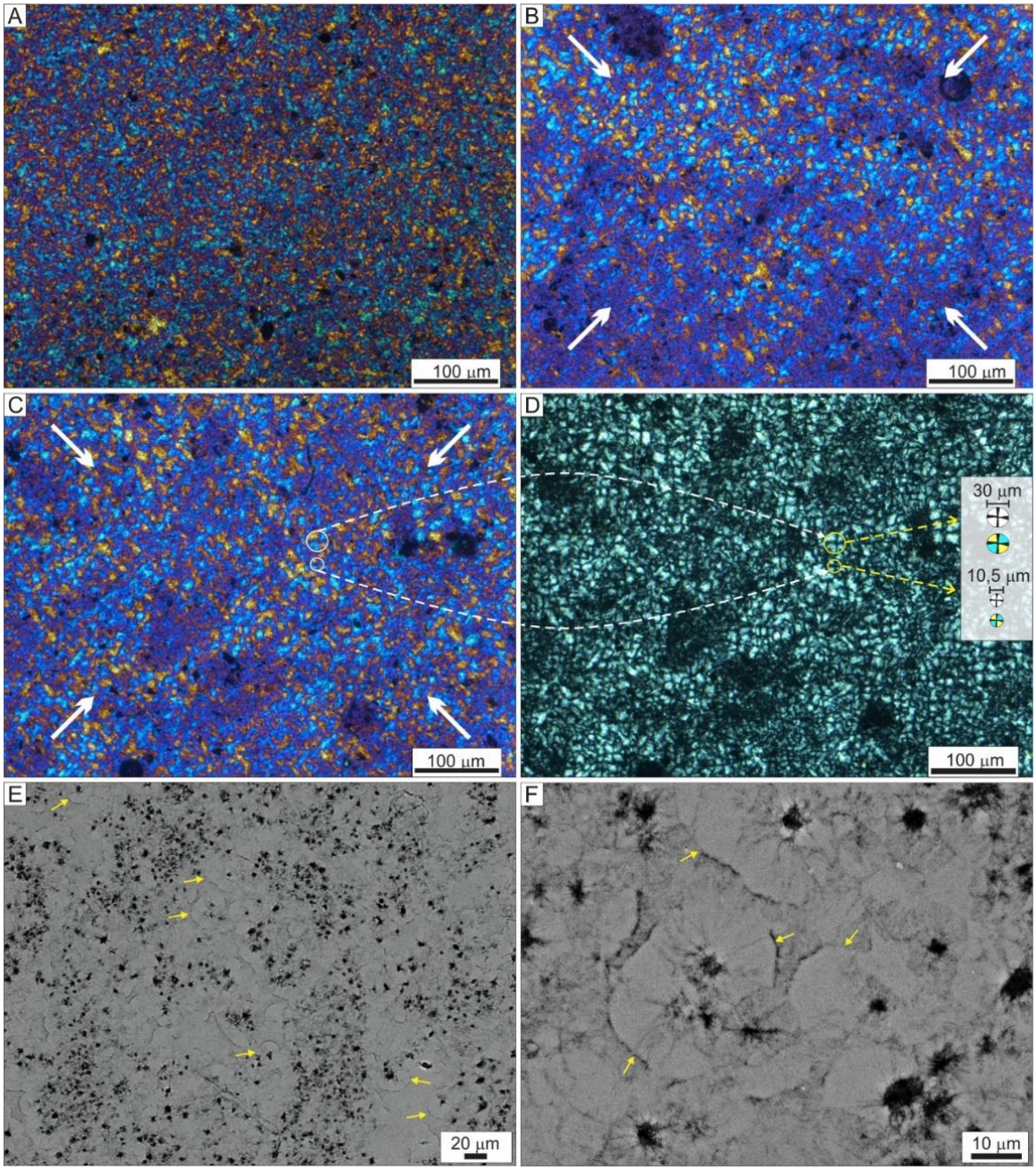

Figure 10-Photomicrographs comparing two groundmass textures in chert between crossed polarizers with gypsum plate inserted. A) Groundmass chert with randomly oriented quartz crystals with "pinpoint" extinction. B) Groundmass chert displaying a reticular or gridwork extinction pattern. Note the alignment of blue and yellow stringers parallel to diagonal white arrows. C-D) Groundmass displays gridwork extinction formed by the aggregation of minute quartzine spherules. Note the schematic drawing of spherulites (right corner), with a range size up to 30 µm. E, F) Scanning electron photomicrographs of the groundmass showing interlocking of minute quartzine spherules. All photomicrographs are a cross-polarized light. A, B and C are with gypsum plate inserted.

Besides the gridwork texture, some portions of groundmass, especially in the nodular domains, show a chicken-wire mosaic texture (Fig. 11). The "chicken-wire" or cloud-like mosaic texture (see Folk and Pittman 1971) is historically documented as typical infill or replace from evaporates nodules by chert (specially quartzine fabrics). This petrographic texture preserve a characteristic shapes of the antecedent mosaic of irregular nodules of the chicken-wire anhydrite structures (Folk and Pittman 1971; Chowns and Elkins 1974; Young 1979; Maliva 1987; Hesse 1989; Nagy et al. 2005; Warren 2016a, 2016b; Marandi et al. 2017).

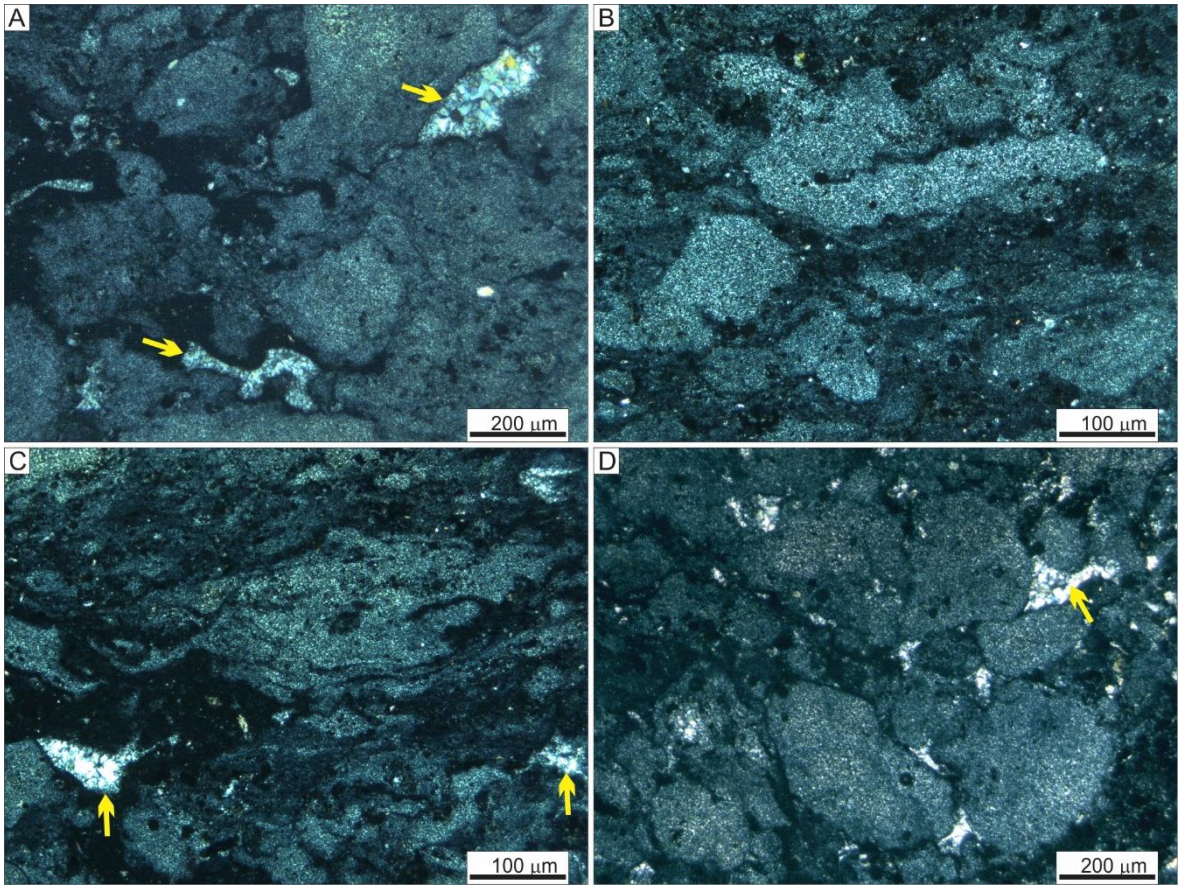

Figure 11-Photomicrographs of chicken-wire chert texture. A-D) Microcrystalline quartz groundmass mimics the chicken-wire appearance of anhydrite nodules. Note some remaining cavities occluded by mosaic quartz (yellow arrows). All photomicrographs are a cross-polarized light.

The chicken-wire chert texture consists of irregular masses of microquartz, generally less than a 1 mm in diameter. Show spherical, oval to lenticular and shapeless (amorphous) forms, which are separated by thin stringers of dark undifferentiated mass (maybe clay?). The edges of each form are well defined and conform roughly to irregularities of adjacent microquartz forms. Most microquartz masses are flattened and oriented with their long axes

lying in a horizontal plane but locally they may be inclined or randomly oriented. Mosaic megaquartz fill eventually remaining cavities (Fig. 11A, C and D).

Chicken-wire anhydrite nodules indicate sabkha and very shallow water settings (Shearman 1963; Chowns and Elkins 1974; Warren and Kendall 1985; Hussain and Warren 1989; Tucker 2001, p. 170-179; Henchiri and Slim-S'Himi 2006; Aleali et al. 2013; among others). Anhydrite (gypsum-anhydrite) nodules characteristically occur in mudflat margins both from coastal or continental sabkhas (Tucker 2001, p. 170-179; Warren 2006, p.176-285). These nodules grew during the very early diagenetic stage (syndepositional) and were partly or completely anhydrite under post-sedimentary conditions that replacively and displasively in the capillary and phreatic zones beneath the sabkha surface (Riley and Byrne 1961; Lowenstein 1987; El Tabakh *et al*. 1999; Warren 2006, p. 135; Aleali *et al*, 2013). In mudflat margins from sabkhas sub-environments, anhydrite nodules occur as smaller nodules (mm to few cm diameters). As the nodules grow, they tend to coalesce and mutually interfere, forming the characteristic "chicken-wire" structure and enterolithic folds (Chowns & Elkins, 1974; Warren, 2016b).

Filling Phases

Different types of cavities occur in isolate zones of groundmass. These voids have variable shapes (rectilinear, irregular, branched) and are filled by different quartz textures, depending on the type of fissure (Fig. 12). Mosaic megaquartz and spherulites of LS-quartzine are common, and usually occurs in fractures (or “feeders”, see Banks 1970) and cavities with aggregates and/or mosaic morphologies (Fig. 12A-G). Chalcedonic overlays (Fig. 12C-E) and microflamboyant quartz (Fig. 12A, K) and zebraic chalcedony with intersection of spherulitic sectors (Fig. 12L) however, are found only locally and in minor amounts. Spherulites of LS-quartzine are the most abundant type of filling (Fig. 12H). Large cavities typically have multiple generations of void-filling chalcedony, whereas smaller voids typically contain only one generation (Fig. 12M, N). Most of the void filling chalcedony is radial-fibrous and consists of multitude interlocking quartzine spherules that subtend angles of 360° (Fig. 12A). Under crossed polarizers fibrous extinction is seen, the orientation of the "fibers" being such that a pseudo-uniaxial extinction cross is produced (Fig. 12A, C, L). The bars of the cross are only sharply defined when the plane of section passes through the center of the spherulite. Large interlocking quartzine spherules usually contain individual "fiber" aggregates showing a polygonal outline, but in many cases, especially when growth was obstructed, complete extinction crosses are not developed (Fig. 12M).

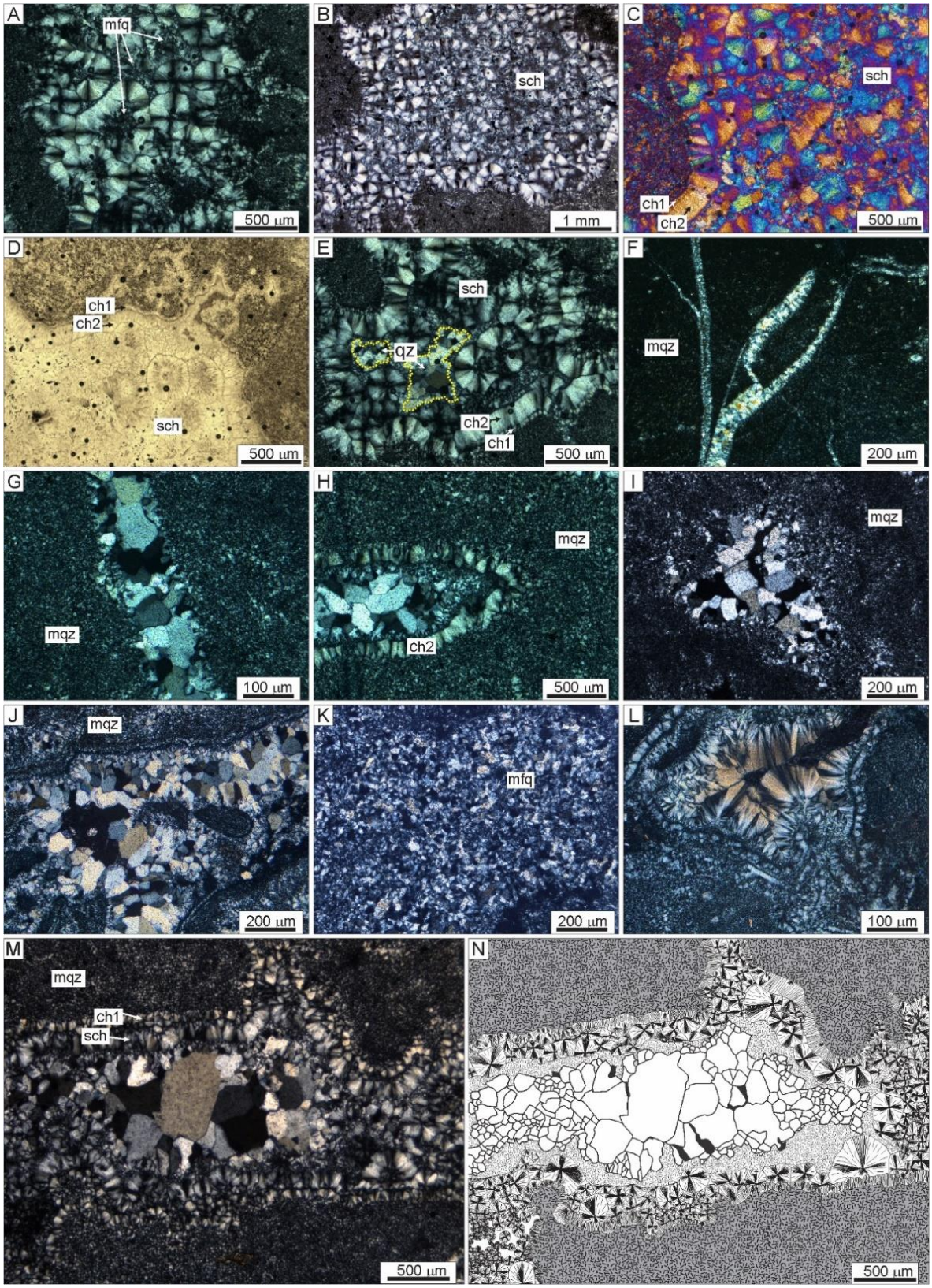

Figure 12-Photomicrographs of length-slow chalcedony and megaquartz growing into internal voids. A) Aggregates of spherulitic chalcedony (sch) that subtend angles of 90° or more; some of the aggregates in center of void subtend a full 360°. Note development of microflamboyant quartz (mfq) inside and between spherulites. B) Cavity filled by spherulitic chalcedony (sch), are lined with a chalcedonic overlay (ch1; ch2). C) Spherulites of length-slow quartzine (sch) rimmed by chalcedonic overlays (ch1; ch2). Note the positive optical sign, in consequence of the elongation of the fibers, is parallel to the crystallographic c-axis. D) Cathodoluminescence image showing the aggregate of

spherulitic chalcedony (sch) lined with chalcedonic overlays (ch1; ch2). E) Interlocking spherulitic chalcedony (sch) with the remaining void being filled by mosaic megaquartz, and grading outward into chalcedonic overlays (ch1; ch2). F-J) Branched, straight fractures/joints (“feeders”) and cavity filled inward into mosaic megaquartz. Megaquartz typically increases in crystal size from margin to center. Cavity rimmed by chalcedonic overlay (ch2) and mosaic megaquartz. K) microflamboyant quartz (mfq) occluded the cavity. L) Intersection of two pherulitic sectors in an cavity. The twisted Iibers in the two sectors are at different angles to the plane of the section. M, N) Groundmass microcrystalline quartz (mqz) envelop cavity lined with two distinct chalcedonic overlays (ch1) which merges laterally into the spherulitic chalcedony (sch) that grades inward mosaic megaquartz the center of pore. All photomicrographs are a cross-polarized light.

The spherulites of LS-quartzine measure up to 500 µm in diameter with an average of 370 µm, between those that occur in the cavities and 10 µm in the groundmass. The spherulites of LS-quartzine grades laterally into mosaic megaquartz toward a center of the voids. Although rare, two other types of chalcedony are also present. One type chalcedonic overlays or parallel-fibrous chalcedony which commonly forms rims around cavities or may line primary or secondary voids of successive layers of chalcedonic overlays (Fig. 12C, D). The thickness of the overlays may vary from 50 to 200 µm. Under crossed polarizers, the chalcedonic overlays appear fibrous, each "fiber" having an extinction position approximately normal to the lateral extent of the overlay. This fabric commonly merging inwards to spherulitic chalcedony and sometimes for mosaic megaquartz (Fig.12M, N). The other type of chalcedony is isolated and restricted to the centers of a few voids (Fig. 12L). The extinction properties result from the twisting of the fibers about the axis of fiber elongation (Frondel 1978). Some of the mosaic quartz is so undulose that crystal boundaries are very difficult to define; this is the microflamboyant quartz. Microflamboyant quartz occur partially filling cavities between spherulitic chalcedony and mosaic megaquartz (Fig. 12M, N). According to Milliken (1979) microflamboyant quartz has a variety intermediate between mosaic megaquartz and quartzine. Mosaic megaquartz strictly fills the center of the cavities, straight, irregular, branched fractures (Fig. 12F-J). The size individual crystals vary from 20 to 700 µm, with a typical increase in crystal size into pore spaces (Fig. 12M, N).

In restrict domains, coarse mosaic calcspar and bladed-prismatic calcite also occur fill voids in the PF-cherts. The crystals are subhedral to anhedral and range from 100 µm to 2.1 mm across (Fig. 13A). Bladed-prismatic calcite consists of tabular scalenohedral crystals between 100 to 500 µm long. They show the most common characteristic; grow directly towards the on coarse mosaic calcspar in the center of pore. The coarse mosaic calcspar consists of plane-sided, equant crystals with up to 2.1 mm across, occluded entire space remaining in the center of the voids. The bladed-prismatic calcite association is younger than the bladed calcite (Choquette and James 1987). CL image show typical zonation Fig. 13B).

Microscopically, fragments of PF-chert breccia (Kolodny et al. 2005) or pseudoconglomerates (Chen et al. 2009) contain flat-pebble rounded and regular-shaped with up to 4 cm along their largest axis (Fig. 5F, G and 13C, D). The clasts float in the groundmass (Fig. 5H and 13D). Microquartz groundmass fills the inner part of the clasts. Some clasts are broken and this fracture has filled by mosaic quartz (Fig. 13C, D). Transitions from the clasts to the groundmass are thin and gradational. Flow structures (Fig. 12E, F) and redeposited chert clasts were observed in some domains. Detritic quartz grains between the chert clasts is indicative of rework of cherts (Fig. 13G, H).

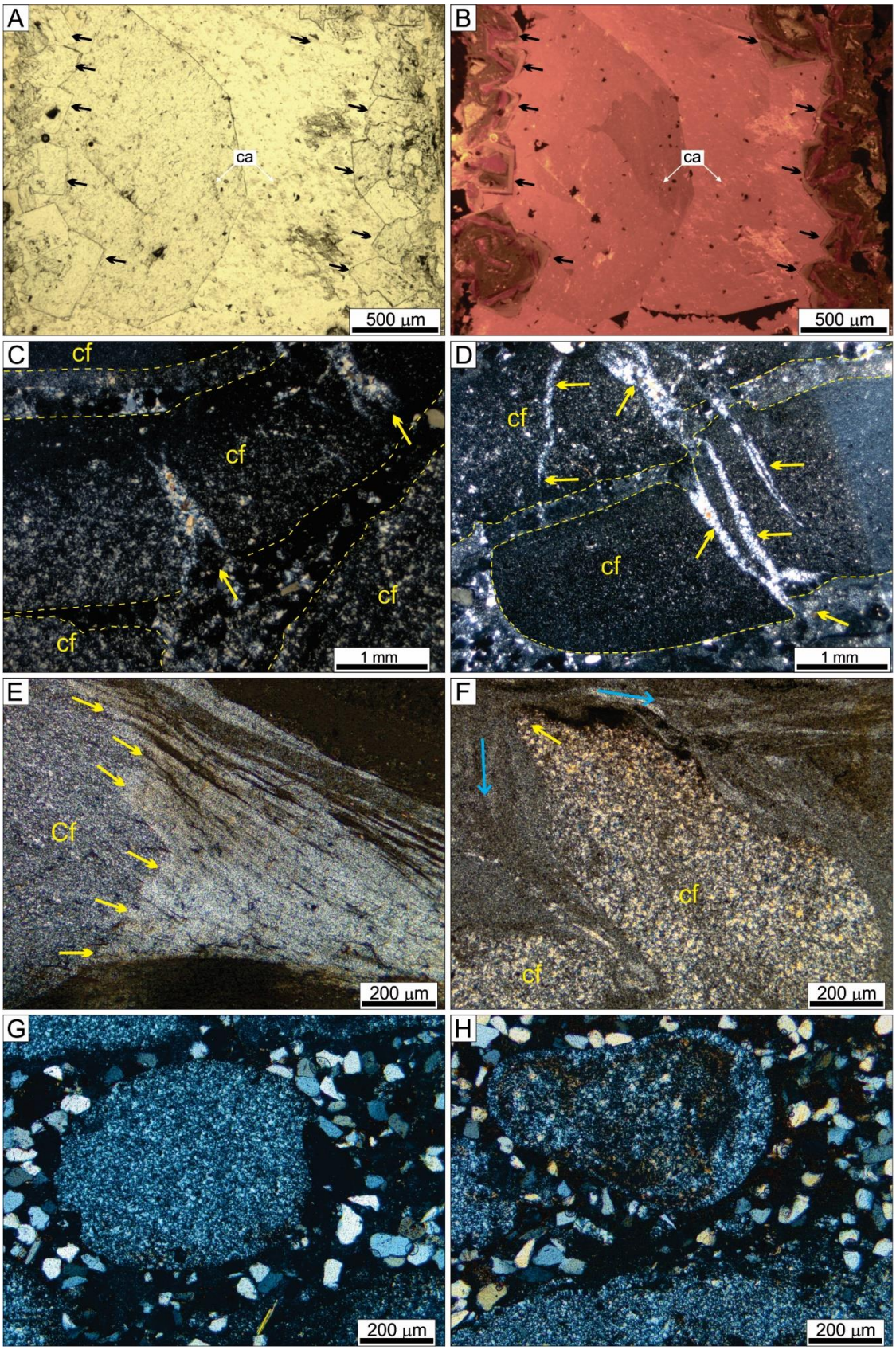

Figure 13-Photomicrographs of filling phases of calcite spar, “chert breccia” and flow structures; crossed polarizers. A) Coarse mosaic calcspar felling cavity. Note a characteristic increasing crystal size away from the substrate towards the cavity center. B) Same field of view under cathodoluminescence image showing growth zones of bladed-prismatic calcite (black arrows). C-D) Rounded large fragments (chert fragments-cf) gently distinguished from surrounding groundmass.

Note the cracks completely fill a silica cement (yellow arrows), indicative of more than one event of silicification. All photomicrographs are a cross-polarized light. E-F) Flow structures. Note the "mass scape" (blue arrows) due to compression of chert fragments (cf) in the probable initial stage of silica gel-like during very early diagenesis. G-H) Redeposited chert clasts. Note detritic quartz grains between chert clasts.

DISCUSSION

PALEOGEOGRAPHY AND DEPOSITIONAL PALEOENVIRONMENTAL OF THE PF-CHERT

The end of the Carboniferous (Pennsylvanian) and the beginning of Permian (Cisuralian) record the end of the suture between Gondwana and Laurussia, with the consequent formation of supercontinent Pangea (Zharkov and Chumakov 2001; Ford and Golonka 2003; Berra and Angiolini 2014). This tectonic event was combined with the displacement of this large continental mass northward, concentrating its largest territorial portion over a wide equatorial zone (see discussions in Zharkov and Chumakov 2001; Scotese et al. 1999; Courtillot and Renne 2003; Chumakov and Zharkov 2003). This configuration triggered rising temperatures and increasing global aridity concomitant with the retreat of the epicontinental seas and the development of dry climate sedimentary systems (Zharkov and Chumakov 2001). In this scenario, the central-western part of Gondwana was dominated by a desert system regionally attributed to the Piauí Formation (Pennsylvanian) recorded mainly in the Eastern Parnaíba Basin (Fig. 14, stage 1). The FA1 indicates that these aeolian dunes were medium-scale and migrated preferentially to SW-W, with eventual deflections to NW-NE. The occurrence of continuous layers of mudstones, some densely bioturbated, together with the frequent occurrences of adhesion laminations limiting the sets, suggests that the starved water table become more periodic, and / or relatively high enough to generate the development of interdune ponds rapidly colonized by organisms. (Fig. 14, stage 2). The thinning up tendency of the wind dune sets with an increase in the frequency of mudstone levels, and the predominance of surfaces with adhesion lamination, indicate elevation in the local base level. This level was controlled by rising groundwater with development of deflation horizon, culminating in the interruption of the aeolian deposition replaced by implementation of an arid lake system (Fig. 14, stage 3). This flat bounding surface is assumed here as a supersurface type 1, from Kocurek (1988), caused by a climatic change extremely arid to more humid conditions strongly influenced by the groundwater and (local) base level (cf. Talbot 1985). This expressive unconformity marks regionally the end of the carboniferous desert system of the Piauí Formation, and the beginning of the Permian Pedra

de Fogo Formation (Fig.14, stage 3). The passage between these units is marked by the massive occurrence of chert-bearing deposits that typify the Pedra de Fogo Formation.

The arid lacustrine system attributed to the Pedra de Fogo Formation (Cisuralian) shows sedimentary characteristics typical of endorheic basins such as thin water column, arid plains with evaporites precipitation, and multiple and small-scale cycles of mudstone and sandstone forming sheet flow geometry commonly associated with unconfined flows previously described in ancient and recent arid lake systems (Fig.14, stage 4). The occurrence of desiccation structures, together with the large occurrence of evaporitic nodules, suggests that the aridity was high enough to provide contraction of these lakes and exposure of peripheric zone rich in saline crusts. On the other hand, the predominance of rippled bedding in FA1 suggests intense and frequent rework by fairweather waves and eventually storm waves.

The occurrence of storm waves suggests a large area or fetch affected by strong winds to keep the height, speed and duration time of wave system to rework the bottom of the nearshore lake and generate hummocky cross-stratification. Exposure features were not observed in the FA3, as well as, rare wave structures, thick mudstone layers interbedded to the fine-grained sandstone with geometry similar to the FA2, indicate permanently submersed sub-storm wave base protected zones of the lake. On the other hand, the predominance of light colors in the mudstone and absence of sulfides and organic matter in these deposits indicate an elevated degree of oxidation or the absence of thermocline. The multiple sandstone-mudstone cycles with thinning up of mudstone combined with occurrence of fairweather and storm waves, together with the numerous occurrence of evaporitic nodules and concretions, suggest climatic seasonality with a strong tendency to increasing aridity. This trend is recorded in other successions of the West Gondwana and reflects the climax of the continentalisation in these basins also marked by the increase of the temperature that led to the great Permo-Triassic extinction.

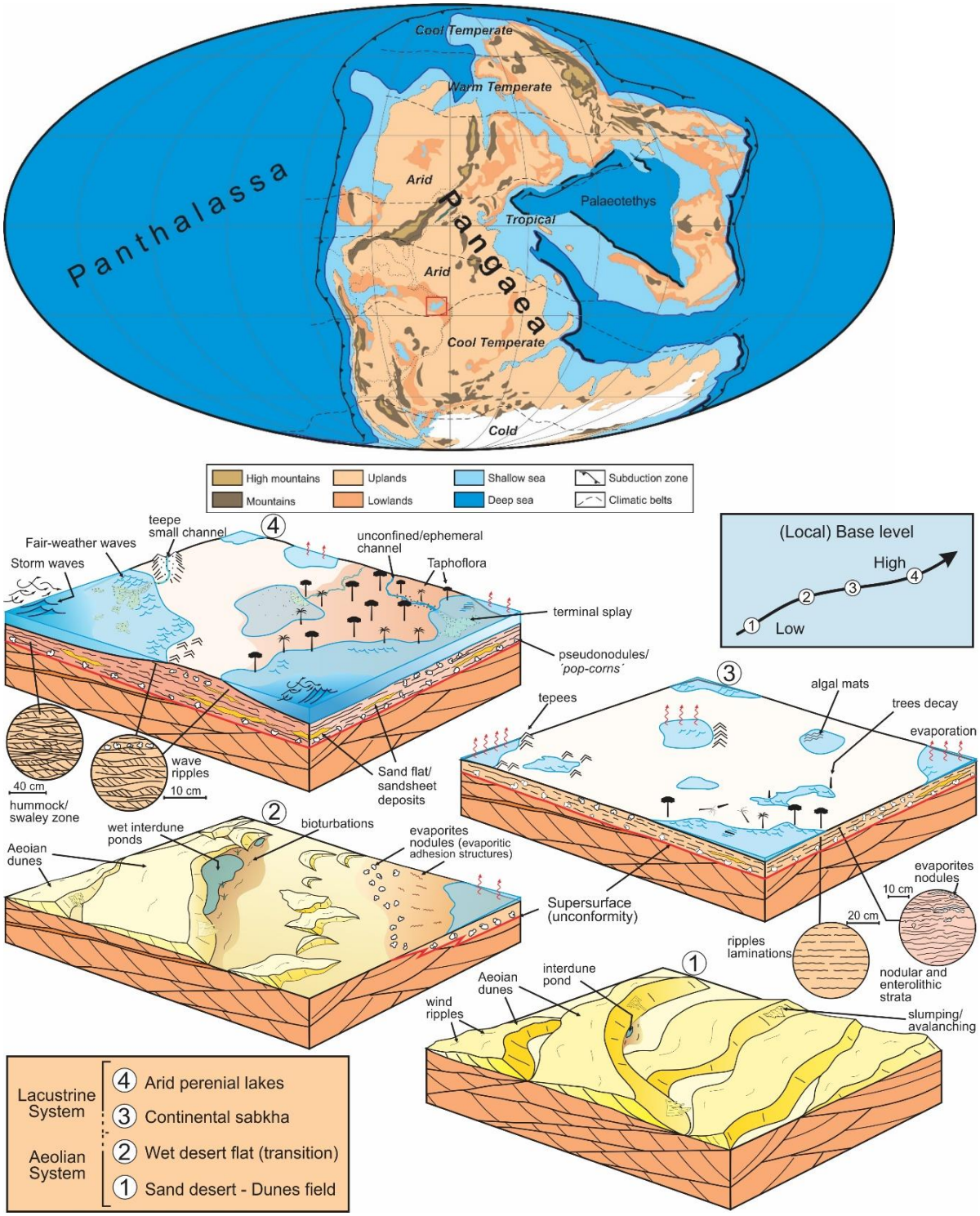

Figure 14- Paleoenvironmental and Paleoclimate Evolution of the Late Carboniferous to Permian deposits in the Parnaiba Basin, Western Gondwana. A) Stage 1- the Pennsylvanian desert system dominated by dune fields (Piauí Formation) was a dry setting bordering a narrow epicontinental sea in the center-western Gondwana. B) Stage 2 – the increase of the humidity conditions in this desert allowed a relative water saturation of the water table generating the development of interdune ponds rapidly colonized by organisms. C) Stage 3 - the elevation of e local base level controlled by rising groundwater led the development of deflation horizon or supersurface, culminating in the interruption of the aeolian deposition marking the end of the carboniferous desert (Piauí Formation), and the beginning of the Permian Pedra de Fogo Formation. D) Stage 4. The expressive evaporites precipitation and siliciclastic inflow characterize the definitive implantation of an arid lacustrine and sabkha system of the Permian Pedra de Fogo Formation.

TIMING OF DIAGENESIS AND SILICIFICATION PROCESS

Eodiagenetic regime

Factors of interest in evaluating silica precipitation during diagenesis include the timing of cementation, mechanisms for precipitating silica, and sources of silica (Hesse 1989; Boggs Jr. 2009, p. 286). Field and petrographic relations indicate that silicification occurred in multiple events. The occurrence of microquartz intraformational chert breccias, some broken and fracture-filled by mosaic megaquartz show that silicification occurred before and after effective compaction (Folk and Weaver 1952; Knoll 1985). Most silica cementation occurred during eodiagenesis and, secondarily early mesodiagenesis. During the eodiagenetic regime, characterized by intense microcrystalline quartz or microquartz zone and little physical compaction (fracturing) (Fig. 13C, D).

The occasional occurrence of redeposited chert clasts (Fig. 13G, H) is the best supportive evidence for early lithification of these cherts, and also suggests that silicification occurred while sediments were near enough to the surface to be reworked during the erosional event, perhaps sheet flood and/or storms, relatively common in the Pedra de Fogo Formation (Andrade et al. 2014; Conceição et al. 2016; Abrantes Jr. et al. 2019). Additional petrographic analysis corroborates these observations (Meyers and James 1978; Knoll 1984; Olivier et al. 2012).

The silicification process, as based on Chowns and Elkins (1974) and Warren (2016b), probably occurred following:

Syndepositional / eodiagenetic regime – the silicification began with volume for volume replacement of precursor (most anhydrite nodules -see discussion below) by silica. The quartz is microcrystalline, clouded with inclusions, and occurs in random ragged xenotopic mosaics of spherules of fibrous quartzine-lutecite aggregates (Fig. 9A, B). Quartzine is presumed by its oblique extinction (Fig. 10C, D). Microcrystalline mimic chicken wire and enterolithic anhydrite structures (Fig. 11).

Silicified woods

Syndepositional/eodiagenetic silicification is suggested by occurrence of silicified woods reported in this study (Fig. 8), and by previous works in the Pedra de Fogo Formation (Caldas et al. 1989; Martins et al. 2010; Iannuzzi and Langer 2014; Conceição et al. 2016a, 2016b; Iannuzzi et al. 2018). Many of the silicified woods are in life position (8A, B), and seem to support this view. In addition, the occurrence of fragile plant parts strengthens this idea (Fig. 8E). Furuno et al. (1986) and Fengel (1991) proposed that silica dissolved in alkali

solution penetrates wood tissue and precipitates under an acidic condition. Weibel (1996) studied petrified wood formed in Miocene fluvial sediment without traces of volcanic events and concluded that the silica was liberated by weathering and/or soil formation and that it was permeated and precipitated as opal-A or directly as quartz. In the succession of the Pedra de Fogo lacking traces of volcanic events (obvious sources of silica), the dissolved silica from siliciclastic rocks in groundwater may be enough to silicify plants, albeit on longer time scales (Knoll 1985). In general, silica availability is not the limiting factor that controls silicification in terrestrial environments (Knoll 1985; Hesse 1989; Locatelli 2014). According to Leo and Barghoorn (1976) low rate of decomposition of the plant may catalyze the process of silicification by creating an abundance of sites for hydrogen bonding. However, if too much decay of the organic matter occurs, the template on which silicification occurs is also lost. The little amorphous organic matter, ubiquitous and exceptional morphological preservation of microbial mats and silicified woods requires the rapid cessation of heterotrophic activity, and indicates the rate of silicification would have been rapid, on the scale of days, weeks, or years, depending on the tissues and environment (Knoll 1985; Channing and Edwards 2003). The silicification of fossils begins with the initial deposition of silica, in the form of monomeric silicic acid H_4SiO_4, on and within cell walls of plants. Further silicification occurs through the polymerization of silicic acid and loss of water (Hesse 1989). Polymerization leads to the formation of opal-A, which then undergoes a maturation sequence to opal-CT, and finally to quartz given the right conditions and sufficient time (Buurman 1972; Leo and Barghoorn 1976; Hesse 1989).

Microbial silicified

Ubiquitous microfossil preservation, as delicate (putative) morphology of unicellular colony and filaments of microbial communities converge for the eodiagenetic silicification regime. (Fig. 7C, D). According to Bartley (1996), decomposition of cyanobacteria occurs on the time-scale of days to weeks, exceptional morphological preservation requires the rapid cessation of heterotrophic activity and indicates that silicification occurred penecontemporaneously with deposition and before the neomorphic recrystallization of mineral phases that can physically destroy organic structures. Experimental work supports the impact of early silicification on the preservation morphologies of microorganisms (Toporski et al. 2002; Kremer et al. 2012; Orange et al. 2013; among others). The entombment within silica limits the molecular degradation of microorganisms (Alleon et al. 2016). Generally, the limited evidence for the structural decomposition of cyanobacterial sheaths, suggests that the

process of silicification may play a role in the preservation of filamentous communities, specifically, environmental associated with the polymerization of silica during early diagenesis (Manning-Berg & Kah 2017; Manning-Berg et al. 2019).

Mechanical changes in the eodiagenetic regime, with the increase of compactional stress, potentially develop intricate fractures and cemented breccias in the chert (Figs. 13C, D and 15). PF-chert breccias, which are common in lower part of the Pedra de Fogo, develop during nearly all stages in the burial history of the sediments. These fractures permeability may be important as a conduit for dissolved silica (Behl and Garrison 1994). The precipitation of enough cement to fill pore spaces further requires that large volumes of water circulate through the sediments (Boggs Jr. 2009, p. 284).

Early mesodiagenetic regime

in time and burial the volume for volume exchange of silica molecules for (putative) evaporite breaks down and, it is removed in advance of replacement so that a secondary porosity develops (Fig. 15). The fill of porosity by growing silica fabrics begins by outward from the pore walls. The rim of a single layer of chalcedonic overlays partially fills cavities wall (Fig. 15). Following the burial, second and thicker rim layer of chalcedonic overlays rimmed the pore. Spherulitic chalcedony (quartzine) aggregates and mosaic quartz gradually occluded remaining pores during the time (Chowns and Elkins 1974). Enlargement and cementation of fractures by mosaic of megaquartz also occur at this stage (Warren 2016b). The massive occurrence of spherulites of LS-quartzine shows that the thermal evolution of PF-chert probably occurred under temperatures no higher than 150º C (Schmidt *et al.* 2013). It is common to find that quartz crystals formed at this stage are zoned with anhydrite inclusions, inner zones bearing more relicts than outer (Folk and Pittman 1971; Chowns and Elkins 1974; Maliva 1987; Hesse 1989; Warren 2016b). The lack of anhydrite inclusion or relicts may be attributed the pervasive and polycyclic silicification.

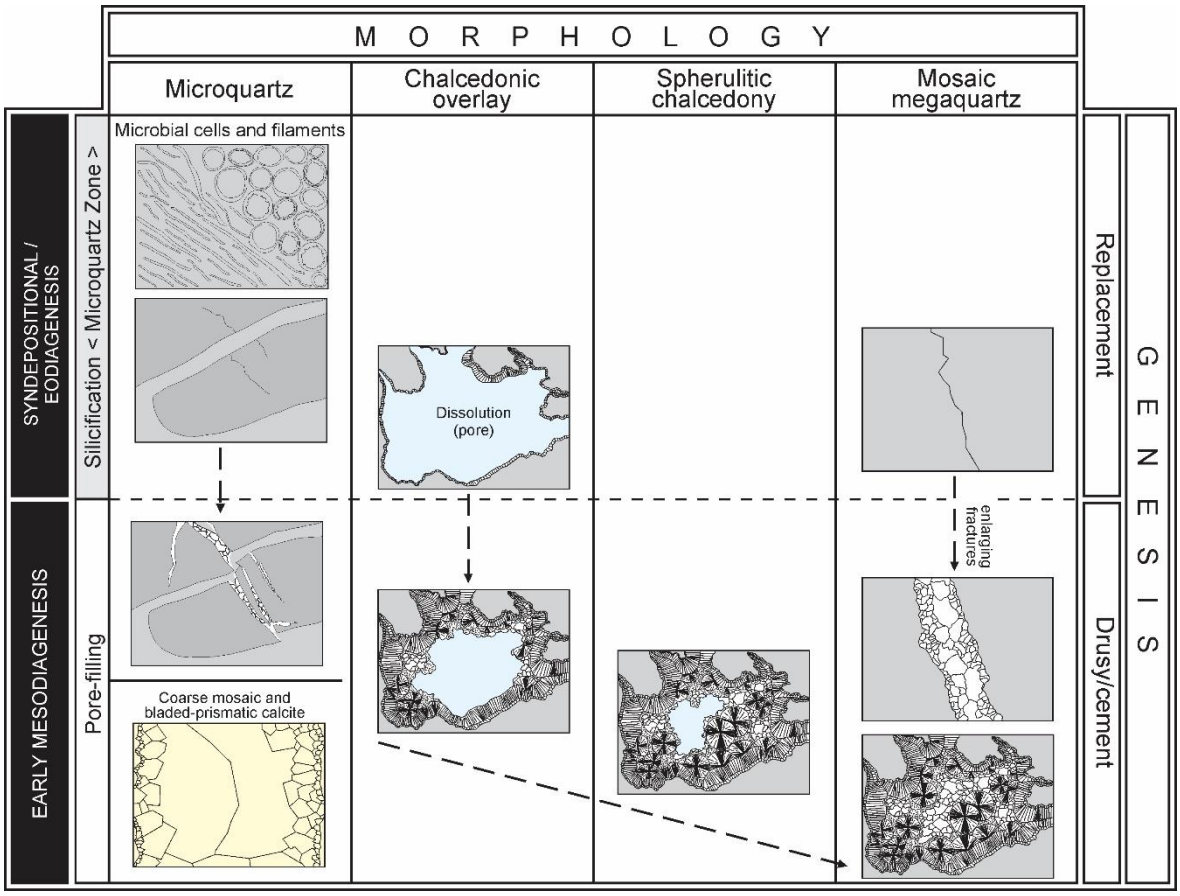

Figure 15-Morphology, genesis and diagenetic stages of silica fabrics of PF-chert. Each category is explained more fully in the text. Modified from Wilson (1966).

Chalcedonic overlays, spherulites of LS-quartzine and mosaic quartz are cement or drusy fabrics only and occur frequently associated. The occurrence of microquartz chert breccias broken, and the fracture fill by silica cement (Figs. 13C, D), is indicative that silicification event of the Pedra de Fogo occurred in more than one cycle, and in a time interval large enough for fragments of lithified microquartz chert to be fractured, and the fracture-filled by silica cement. The occlusion of fractures and large cavities (> 1mm) by cement and drusy silica fabrics is evidence of intense circulation flow supersaturated with silica into the pores (Figs. 12F,G and 13C, D). The excess silica in the pore water of a single pore can precipitate only a minute amount of silica (Simonson 1985). Once precipitation has occurred, no further cementation can take place until the flow in the pore is replaced by new water supersaturated with silica. Thus, the process of filling a pore with cement demands that silica-supersaturated water circulates through the pore many times, a process that takes a very long period of time (Sugitani et al. 1998; Boggs Jr. 2009, p. 284). The cementation by coarse mosaic calcspar with crystals of millimetric size completely filling secondary pores (Fig. 15) is indicative of the subsequent circulation of carbonate flow (Cook 1970; Boggs Jr. 2009, p. 438).

The observation of large aggregates spherulites of LS-quartzine may indicate to form in waters that, besides silica, were also enriched in sulphate and magnesium (Folk and Pittman 1971; Jacka 1974; Keene 1983). The existence of silica-rich groundwaters is confirmed in other occurrences of the Pedra de Fogo Formation, in which dolostone and gypsum were replaced (pseudomorphs) by silica (Faria Jr. 1979; Faria Jr. and Truckenbrodt, 1980). The spherulitic structure is also most likely formed by diagenetic or crystallization of silica (Williams et al. 1985; Williams and Crerar 1985; Sugitani et al. 1998). The possibility of biogenic origin is excluded by the size distributions of the spherulites (up to 500 μm), which are mostly larger than bacterial cells and are similar to those of inorganically synthesized quartz microsphere (Oehler 1976). Oehler (1976) showed experimentally that silica gel crystallizes in the form of chalcedonic spherules under hydrothermal conditions (3kb, 100-300ºC, 25-5200 hrs) and concluded that the spherulitic structure in Precambrian cherts is not biogenic in origin. The presence of cement fabrics such as interlocking spherulitic chalcedony and mosaic quartz indicates that silica was an important component of the primary sediments and that the ambient water mass was possibly supersaturated with silica (Sugitani et al. 1998). These two types of microstructure possibly reflect fluctuations of physicochemical conditions controlling diagenesis and crystallization of silica.

Post-depositional silica enrichment of the chert layers is deduced from the presence of spherulitic extinction of the groundmass (mosaic of microquartz) (Fig. 10). As summarized by Simonson (1985), the spherulitic extinction of silica can form in several ways such as competitive growth during void-filling by precipitation of fibrous crystals (Roedder 1968), replacement of other materials (Milliken 1979), and neomorphism of amorphous or opaline silica (White and Corwin, 1961). In the PF-chert, most at the extinction, if not all, were formed by rapid void-filling precipitation of fibrous quartz crystals. A replacement origin for the extinction figures is not possible, because the portions showing spherulitic extinction do not contain relict rhombic grains and other impurities that abundantly occur in the replacement of silica fabric (Simonson 1985). Their regular mutual boundaries and extinction behavior (Fig. 10B, C) also suggest that they were not formed by replacement of other materials (Simonson 1985). Some spherulites of LS-quartzine might have been formed by neomorphism of opaline or amorphous silica, but the inward growth of spherulites with megaquartz-filled centers in voids implies their growth into open spaces (Fig. 12). According to Sugitani et al. (1998), reliable evidence for silica precipitation in cavities is the internal development of mosaic megaquartz, typically represents growth into free spaces such as microcavities and fracture openings (Fig. 12E-G, H, M, N). Spaces among mosaic megaquartz

crystals filled by microcrystalline quartz indicate that the mosaic megaquartz is not recrystallized microcrystalline quartz (Knauth 1994).

The two different styles of postdepositional silica precipitation in cavities described above (i.e. fibrous crystals and euhedral-megaquartz) may be related to different silica concentrations in solutions from which the two silica phases were precipitated. The fibrous crystals suggest a rapid growth of quartz from interstitial waters highly supersaturated with quartz (Simonson 1985). In contrast, the mosaic megaquartz shows slow and intermittent growth of quartz from solutions whose silica concentration was not high enough to allow rapid growth of fibrous crystals (Sugitani et al. 1998).

PETROGRAPHIC EVIDENCE OF CHERT-FABRICS REPLACED EVAPORITES

Since Folk and Pittman (1971) has shown evidence of silica fabric replacing evaporites, based upon petrographic features, such as: 1) inclusions of anhydrite, gypsum, and/or barite; 2) silica pseudomorphs after sulfate precursors; and 3) typical cauliflower or "chicken-wire" textures after anhydrite, and associated the presence of length-slow chalcedony (quartzine or lutecite) as evidence for “vanished evaporites”. Beyond these characteristics, other mineralogical and textural features of silica fabrics have been well-documented by important studies in chert successions replacing evaporites (Siedlecka 1972, 1976; Chowns and Elkins 1974; Tucker 1976a, 1976b; Milliken 1979; Maliva 1987; Warren 2016b). However, this prevailing view was challenged firstly by Jacka (1974) and Meyers (1977), who founded length-slow chalcedony in non-evaporitic rocks, and later by Keene (1983), also described the occurrence of length-slow chalcedony in deep-water pelagic sediments, showed this not restricted to evaporitic environments. Milliken (1979), studying chert nodules from Mississippian rocks of southern Kentucky and northern Tennessee, summarised the typical petrographic sequence of quartz fabrics (the edge to centre of nodules) indicative of silicified evaporite nodules. This authoress emphasizes that one or more of the fabrics are usually missing, especially from the base and at the top of the succession. We find most of the features described by Milliken (1979): 1) isolated spherules of quartzine in randomly fibrous microcrystalline quartz (Fig. 12B). 2) Interlocking spherules of quartzine, lutecite, or microflamboyant quartz (Fig. 12A, E, K). 3) Spherules of quartzine, lutecite, or microflamboyant quartz grading into megaquartz (Fig. 12H). 4) Mosaic of megaquartz and undulose megaquartz (Fig. 12M, N). 5) Spherules of quartzine, microflamboyant quartz, or megaquartz isolated in secondary cavity filling (Fig. 12I). 6) Breccia of evaporite-replacement quartz types in secondary cavity filling (Fig. 13C, D).

The preserved characteristic of the chicken-wire structure of the antecedent anhydrite/gypsum nodule (Fig. 11), is another strong indication of replaced evaporites succession (Folk and Pittman 1971; Chowns and Elkins 1974; Tucker 1976a; Maliva 1987; Hesse 1989; Warren 2016a, 2016b). Ancient silicified sabkha anhydrite nodules have a similar morphology and distribution as modern unsilicified deposits (e.g., Young 1979; Tucker 2001, p. 169; Warren 2006, p. 174; Aleali et al. 2013; Marandi et al. 2017).

The inexistence of silicified nodules still retaining the knobbly cauliflower surface, morphology typically associated with precursor anhydrite (Folk and Pittman 1971; Chowns and Elkins 1974; Milliken 1979; Warren 2016a), and in other hand, the predominance of "cucumbers" shapes (Fig. 5D, E) its attributed of the pervasive and polycyclic silicification during burial diagenesis. According to Warren (2016a), early silica replacement in the zone of active phreatic flow is indicated by a lack of compressional flattening of the nodule, by the preservation of delicate surface ornamentation and the preservation of compactional drapes around replaced nodules. If replacement of an anhydrite nodule occurs later in the burial cycle, the anhydrite nodule has by then become flattened or sluggy and no longer retain a rugose surface, the result can be a series of "cucumbers" rather than "cauliflowers ornamentation.

ORIGIN AND GLOBAL CORRELATION OF THE PF-CHERT

There are several possible origins of PFchert. The most important factor in respect to the origin of cherts are the silica sources leading to the formation of primary and secondary cherts (Laschet 1984). Chertification of carbonates and carbonate-bearing sandstones, silicification of fossil wood and replacement of evaporites are examples of partial and minor silicification and its extent ranges from minor to pervasive (Hesse 1989). In all three examples, the source of the silica is predominantly biogenic. Abiogenic silica formation is both uncommon in the geologic past and today, where the Lake Magadi has been a type of occurrences more widely known. (Eugster 1967; Hay 1968). Analogs of this continental inorganic silicification have been reported in the USA (Mac Atee et al. 1968; Rooney et al. 1969; Surdam et al. 1972), England (Parnell 1986; 1988), Italy (Krainer and Spötl 1998), Japan (Hattori 1989) and Africa itself (Sebag et al. 2001). Magadi-type cherts, formed from sodium silicate precursors may inherit folding, lobate protrusions and extrusion forms (caused by soft-sediment deformation of the magadiite stage) and also surface reticulation cracks and polygonal ridges caused by the large change in volume associated with the conversion of magadiite to chert (Surdam et al. 1972).

According to Schubel and Simonson (1990), three textural and petrographic features are related to the Magadi-type cherts: (1) rectilinear or gridwork orientation of quartz crystals, resulting from retention of preferred crystallographic orientation of the spherulitic aggregates of plate-like crystals of magadiite, (2) inward-directed shrinkage and fenestral cracks formed by volume reduction when magadiite is converted into quartz, through expulsion of sodium and water, and (3) large crystal molds created by dissolution of associated saline minerals. Among these three petrographic features, the gridwork extinction pattern results from the retention of the preferred crystallographic orientation of the precursor mineral magadiite, is the most distinctive texture of Magadi-type cherts, however, according to the authors themselves, it is not enough to define it alone (Schubel and Simonson 1990; Hattori et al. 1996).

A peculiar gridwork texture of microcrystalline (microquartz) sedimentary quartz has been observed in investigation of pervasively silicified horizons found in diverse sedimentary successions from different geotectonic settings (Schubel and Simonson 1990; Hattori et al. 1996; Krainer and Spötl 1998; Bustillo 2001; Brigo et al. 2001; Camana et al. 2002; Chateigner et al. 2002; Dunham et al. 2017; among others). The gridwork patterns, according to Schubel and Simonson (1990), result of a volume-for-volume replacement of magadiite by quartz with retention of the crystallographic orientation of the former by the latter. Therefore, for these authors, the rectilinear or gridwork texture was inherited from the precursor magadiite, which displays a similar extinction pattern due to the presence of 10-20 μm spherical aggregates of plate-like crystals. Following the last work, based on gridwork extinction patterns and other features like - shrinkage cracks, small-scale soft-sediment deformation, besides on environmental and volcanoclastic context -, Hattori et al. (1996) and Krainer and Spötl (1998), has been interpreted the Miocene and Permian silicifications layers in central part of Japan and northern Italy, respectively, as similar to the Magadi-type cherts. On the other hand, Bustillo (2001), Brigo et al. (2001), Camana et al. (2002), Chateigner et al. (2002) and Dunham et al. (2017) has not associated the occurrence of gridwork extinction to the Magadi chert.

Camana et al. (2002) and Chateigner et al. (2002) considered the mechanism of formation of the gridwork texture a rather fast nucleation of quartz on the pre-existing morphological faces of other developed quartz crystal in angles approximately 75º and 35º, such as the prism {001}, the positive and negative rhombohedra {101} and {011}. According to Bustillo (2001), the microquartz groundmass with a gridwork structure can be explained by the influence of the shape of the plate-like crystals of the magnesian smectites that were

silicified, and the influence of the shape of moganite. This silica polymorph is directly affiliated with the evaporitic basins with extensive deposits of alkaline carbonates and hydroxides like to the Gran Canaria and Lake Magadi, both extremely arid environments (Heaney and Post 1992). Although Mg-smectite has not been detected by this study, the occurrence of this clay mineral in the Pedra de Fogo Formation is commonly known (Faria Jr. 1979; Faria Jr. and Truckenbrodt 1980). The complete absence of moganite may be due to the fact of this mineral is commonly absent in deposits older than the Cretaceous, because that with time moganite diagenetically alters to quartzine and quartz (Heaney 1995). The XRD patterns showing that all PF-cherts consist almost exclusively of quartz (Fig. 9).

Based on petrographic observations and field association, we tentatively interpret the gridwork extinction pattern of microquartz groundmass in some PF-cherts to be the result of a volume-for-volume replacement of precursor mineral by quartz with retention of the crystallographic orientation of the former by the latter. Similar to Schubel and Simonson (1990). The precursor mineral may have been moganite (cf. Bustillo 2001). Moganite may appear petrographically as microcrystalline that occur as radially fibrous spherulites with refractive index slightly lower than that of quartz, and more significantly, moganite has a length-slow optical character (Heaney 1995)

Differences in spherulites size populations within gridwork correspond to the presence of precursor mineral and suggest that nucleation of gridwork may be affected by the presence of precursor materials. Where best preserved, gridwork texture appears to be composed of a series of minute spherulitic chalcedony size between 10-30 μm in diameter that, when observed under the gypsum plate consists predominantly of length-slow (quartzine) (Fig. 10B-D and 16A). The gridwork extinction of microquartz in some PF-cherts consist of the myriad in the aggregates of small quartzine spherules. If these spherules have approximately uniform size form together hexagonal arrays, where two elongated arranged in sub-perpendicular directions, in blue and yellow direction form the gridwork pattern observed (Fig. 16B). Variation in angles of the gridwork appears to reflect the size and packing of these microspherules. Alternatively, the gridwork texture may represent crystallization from a primary gel phase that permeated microbial and porous carbonate substrates. Near-complete crystallization limited water-rock interaction and later diagenetic recrystallization, and aided in the exquisite preservation of microbial features, similar to that described by Dunham et al. (2017).

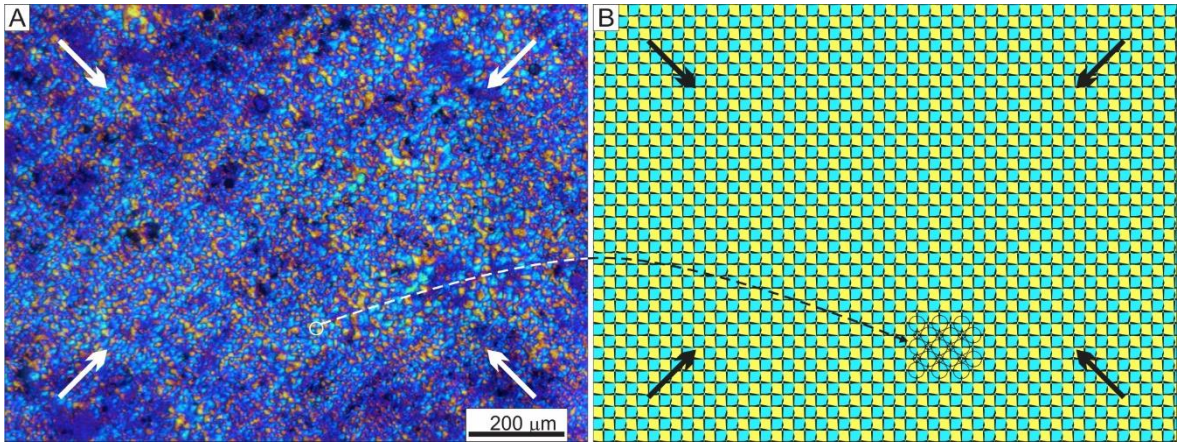

Figure 16-Photomicrographs of groundmass with a gridwork extinction. Cross-polarized light and gypsum plate inserted. A) Groundmass chertdisplaing a mosaic of minute spherulites of length-slow quartzine describe a regular gridwork pattern (white arrows).

CONSIDERATIONS ON SILICA SOURCES, CLIMATE, AND ENVIRONMENTAL CONDITIONS

Although there are similarities between the PF-cherts and those at Magadi type cherts; *I) pervasive silicification, II) climate and environmental conditions (evaporitic basin with deposits of alkaline carbonates), III) silica fabrics*. There are also significant differences between the two precursors lacustrine systems of these cherts. The environmental of Magadi-type cherts consists of alkaline brines rich in dissolved sodium carbonate-bicarbonate (Eugster 1967; Hay 1968). The environmental of PF-cherts was probably were like similar as shown in this study (Fig. 14 and 18), and others in the same sedimentary unit (Faria andTruckenbrodt 1980a, 1980b; Andrade et al. 2014; Araújo et al. 2016; Abrantes Jr. et al. 2019). However, different from the deposit at Lake Magadi, which is lie in volcanic and igneous terrane, that is the most obvious source for enriched in silica on the alkaline brines (Eugster 1967; Eugster 1969), the PF-chert deposits, to date, there are no records of hydrothermal or igneous events are known to have occurred in or near the northeast of Brazil region from Late Pennsylvanian through Early Triassic time (Marzoli et al. 1999; Merle et al. 2011). The complete lack of zeolites is another aspect between the differences in the PF-chert and Magadi-type chert. Zeolites generally form by reaction of volcanic glass with saline solutions, and phillipsite, erionite, clinoptilolite, and others are common constituents of Quaternary Magadi-type chert formations (e.g. Surdam and Eugster 1976; Renaut and Tiercelin 1994). This absence of zeolites we indicate as a strong indication that the source of silica for the PF-chert is not the volcanic origin, as is the case with chert Magadi (Eugster 1986), and other more recent units of the Parnaíba basin (Rabelo et al. 2019).

Thus, the presence of mosaic micro- and megaquartz, spherulites of LS-quartzine, chalcedonic overlays, microflamboyant quartz reflects the climate, palaeoenvironments and diagenetic history of the deposits, in particular the varying composition of the interstitial solutions with time (Wilson 1966; Folk and Pittman 1971; Milliken 1979; Laschet 1984; Hesse 1989; Boggs Jr. 2009).

Precipitation of quartzine seems to indicate pore fluids rich in sulphate and magnesium as well as being saturated with respect to quartz. This observation is supported by laboratory experiments in which quartzine was synthesized (Kastner 1980). Although the formation of quartzine reflects the interstitial chemical environment and, by itself, should not be used as an indicator of any particular environment of deposition (Keene 1983). The occurrence of quartzine, together the known palaeoenvironmental of the Pedra de Fogo Formation (Andrade et al. 2014; Cisneros et al. 2015; Araújo et al. 2016; Conceição et al. 2016a), has been used as evidence for an evaporitic lacustrine environment (Folk and Pittman 1971; Siedlecka 1972, 1976; Milliken 1979). According to Folk and Pittman (1971) quartzine forms in an environment with alkaline solutions with a high initial pH or in a sulphatic environment with free-floating ionized SiO_2-units at a high SiO_2-concentration. After Folk and Pittman (1971) postulated an evaporitic influence for the quartzine, Kastner (1980) pointed out that conditions with high pH and Mg- and/or sulphate-ion concentration are sufficient to explain the environment of quartzine formation. Quartzine can mainly be found replacing evaporites (anhydrite, gypsum), as well as fossils (Chowns and Elkins 1974; Folk and Pittman 1971; Siedlecka 1976; Tucker, 1976; Warren 2016a, 2016b). In Sabkha-like environments or sediments with alkaline or sulphate-rich pore fluids (containing Mg-, Ba-, St-, $SO^{-}_{4,}$ and Na-ions) ideal conditions are available or the formation of quartzine (McBride and Folk 1977).

Therefore the presence of just a rectilinear or gridwork orientation it is not enough to define a Magadi-type cherts origin. The occur of quartzine has been found in deep-water pelagic sediments (Kastner 1980; Keene 1983). The depositional context of the cherts studied do not show evidence of a deep marine environment, in addition, previous work has been reported as of arid lacustrine environment (Andrade et al. 2014; Araújo et al. 2016; Cisneros et al. 2015; Conceição et al. 2016a, 2016b; Abrantes Jr. et al. 2019).

Paleoclimate

The gondwanan climate was cool-temperate to periglacial as well as monsoonal over long time intervals throughout the Late Carboniferous and Early Permian (Parrish 1990). The studied Cisuralian deposits, although located in the interior of the Pangaea, were probably

affected by the prevailing monsoon regime (Crowley *et al.* 1989; Hmich *et al.* 2006; Wagner and Mayoral 2007; Lojka *et al.* 2009). These deposits were on the borderline between the cool temperate and arid belts (*see* Boucot et al. 2013). These climatic characteristics are recorded both by the common occurrence of fossil stems up to 2.3 m long and 1.15 m in diameter (*see* Conceição et al. 2016a), and by arid indicative features recorded in this paper (evaporitic nodules, enterolithic and chicken-wire texture), and others (Faria andTruckenbrodt, 1980a, 1980b; Andrade et al. 2014; Araújo et al. 2016; Abrantes Jr. et al. 2019). In addition, the occurrence of hummock cross-stratification (Fig. 4F) is indicative that the lacustrine system has been severely affected by winter storms regimes (Marsaglia and Klein, 1983).

Paleozoic chert is microcrystalline quartz and chalcedony; Mesozoic chert is opaline, chalcedonic, and microcrystalline quartz; and Tertiary chert is opaline (Cressman 1962). This suggests that cherts are precipitated as amorphous or opaline silica but recrystallize to microcrystalline quartz upon aging. However, silica in nonthermal natural waters rarely is saturated with amorphous silica. Instead, nonthermal natural waters, excepting alkaline water in ultramafic rock or alkaline connate water

It is unlikely that the PF-chert has been precipitated from either type of alkaline water associated with the ultramafic source because as described above, there are no known large ultramafic or vulcanic events in the Permian terrane of the area. Like this, we assume that water chemistry and hence precipitation were primarily climate controlled. According to Banks (1970), the simplest way to obtain supersaturation of amorphous silica is evaporative concentration. Similar to described by Banks (1970) for Leadville Formation in west-central Colorado, the conditions existed during the deposition of the Pedra de Fogo Formation, in west-central Gowndana, were favorable to evaporative concentration of silica (Fig. 14 and 17).

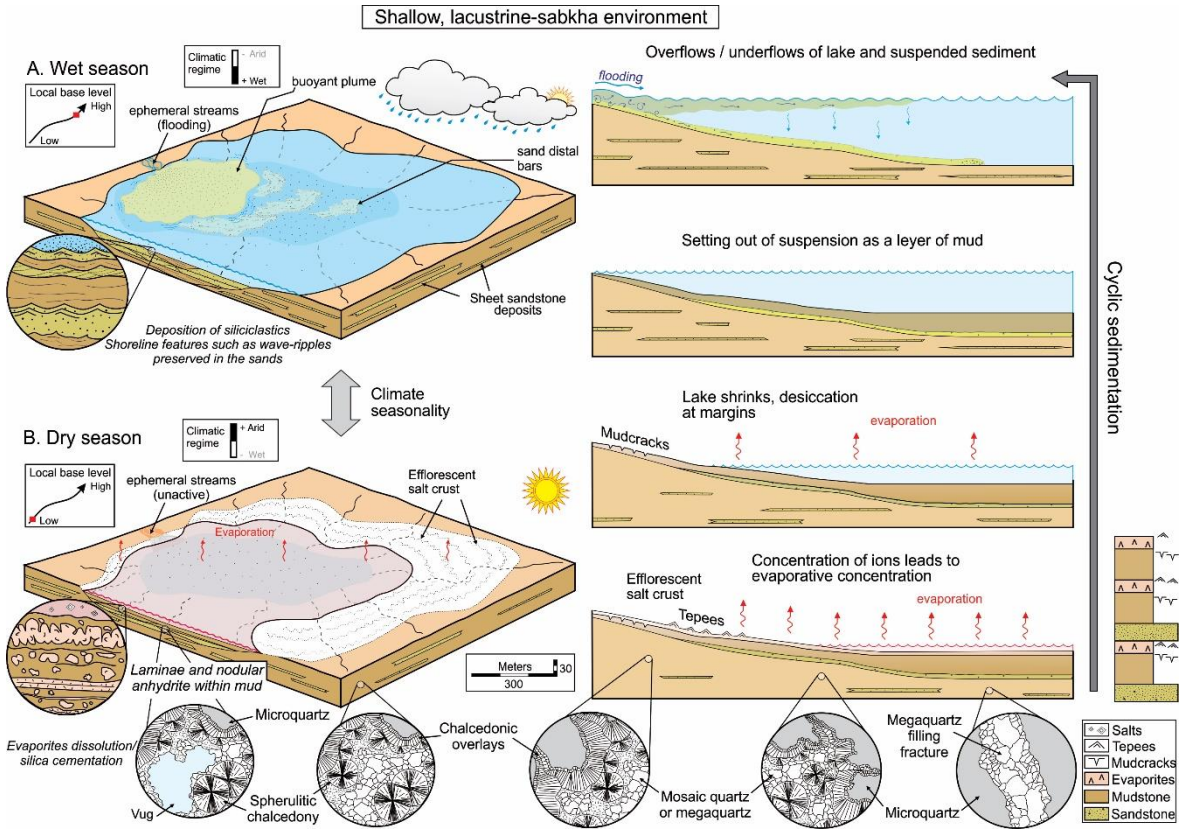

Figure 17-The paleoenvironmental and paleoclimate evolution of the cyclic sedimentation of the shallow lacustrine-sabkha influenced by expansion and contraction stages, conditioned by climatic seasonality regime during the Early Permian in the Parnaiba Basin, Western Gondwana. A) Under wet climate stage. High local base level rise controlled by groundwater elevation. The high volume of precipitation triggered frequents inundations of the lake by ephemeral streams with development of buoyant plumes. Predominance of physical sedimentary process with waves reworking and siliciclastic preferential deposition. B) Under arid climate stage. Low local base level controlled by groundwater fall. The high evaporation rate leads contraction of lake and increasing salinity. The shrinking of lake expor the lacustrine plain where salts crystallize at the surface as efflorescent crusts. The predominance of chemical process leads to synsedimentary formation of the nodular and anhydrite laminae (perhaps after gypsum?) within mud in a very shallow lacustrine. Still on synsedimentary stage the silica cementation with began with replacement and void filling. The process commences about the margins of a nodule with a volume for volume replacement of anhydrite by microcrystalline quartz. The void filling began with chalcedonic overlays rimmed the vug pororosity, and then continue with the growth of spherulitic chalcedonic. It generally ends with the growth of euhedral drusy megaquartz crystals into a central vug. Eventually fractures are equally occlude by drusy megaquartz. This edge inward evolution of the or nodule fill is typified by a variety of textural styles. This edge inward evolution of the or nodule fill is typified by a variety of silica textural styles as showing in this paper.

During dry seasons evaporation was high, resulting in an increase in lake water salinity and pH (Fig. 17B). Change toward more wet conditions, pH and salinity dropped because of increased dilution by runoff. The petrographic textures and palaeoenvironmental associations indicate that the most probable source of the PF-cherts is dissolved silica, resulting from continental chemical weathering (Fig. 18). Silica may have been released during weathering of silicate minerals. Dissolved silica from continental chemical weathering, is the main

contributing silica source initiating chert formation (Laschet 1984). According to Okamoto et al. (1957) and Krauskopf (1959), weathering of feldspars releases both silica and alumina and other cations. AI3+ and possibly other trivalent ions reduce the solubility ratio of silica and colloidal silica precipitate near even traces of aluminum. Feldspar and other aluminum-silicates are important sources of silica because during the weathering both release silica and promote its precipitation by adding Al^{3+} to the solution (Weibel 1996). The increase of solubility of silica and silicates on continents is especially initiated under conditions of chemical weathering (allitic-ferralitic) (Laschet 1984). The solubility is little affected by pH between values of 1 and 9 but rises rapidly at pH 's over 9 (Alexander et al. 1954; Krauskopf 1956). Changes in pH have the opposite effect on the solubilities of calcium carbonate and silica, explaining why one replaces the other, with or without the creation of visible porosity (e.g. Walker 1962; Eley and Jull 1982; Geeslin and Chafetz 1982). Fluctuations in pH could have been controlled by the amount of dissolved CO_2 derived from the oxidation of organic matter (perhaps catalyzed by microorganism activity and partial stem dissolution), imply cyclic precipitation, possibly caused by seasonally changing pH values during the Pedra de Fogo Formation (Parrish 1993). The pH of modern saline and alkaline lacustrine environments chert-forming is controlled either by the ratio of freshwater input versus evaporation (Eugster 1967, 1969) or by seasonal variations in bioproductivity in the lake itself (Peterson and von der Borch, 1965). Supersaturation of the lake water with respect to amorphous silica is due to reduced bioproductivity and/or high runoff from the hinterland (Krainer and Spötl, 1998).

According to Siever (1957), before dissolution and precipitation of silica during diagenesis, its availability and precipitation in the sedimentary environment must be evaluated. Thereby the models proposed for the sequence of events in which silica is available and precipitated in the sedimentary environment following the Siever (1962) and Oehler and Schopf (1971). In the restricted environments as the lacustrine arid of the Pedra de Fogo (Andrade et al. 2014; Araújo et al. 2016; Abrantes Jr. et al. 2019), the weathering of silicate rocks produces dissolved silica which is transported to a relatively restricted basin (Fig. 17). In the absence of silica-depleting organisms the water becomes saturated with respect to silicic acid and a silica colloid is formed. The colloid tends to accumulate on the bottom of the basin where it permeates microorganisms living near the sediment-water interface. Through evaporation of water from the basin, perhaps aided by pH changes associated with possible microbial activity (Fig. 14, Stages 3, 4 and 17B) or by the addition of electrolytes, the colloid becomes increasingly concentrated and is converted from the sol to the gel state, then

supersaturation and precipitation to take place non-biogenically. With continued water loss through syneresis and compaction, the gel is transformed into an amorphous opaline state; subsequent crystallization produces an interlocking mosaic of microquartz grains and subsequent silica fabrics on bedded cherts (Hesse 1989).

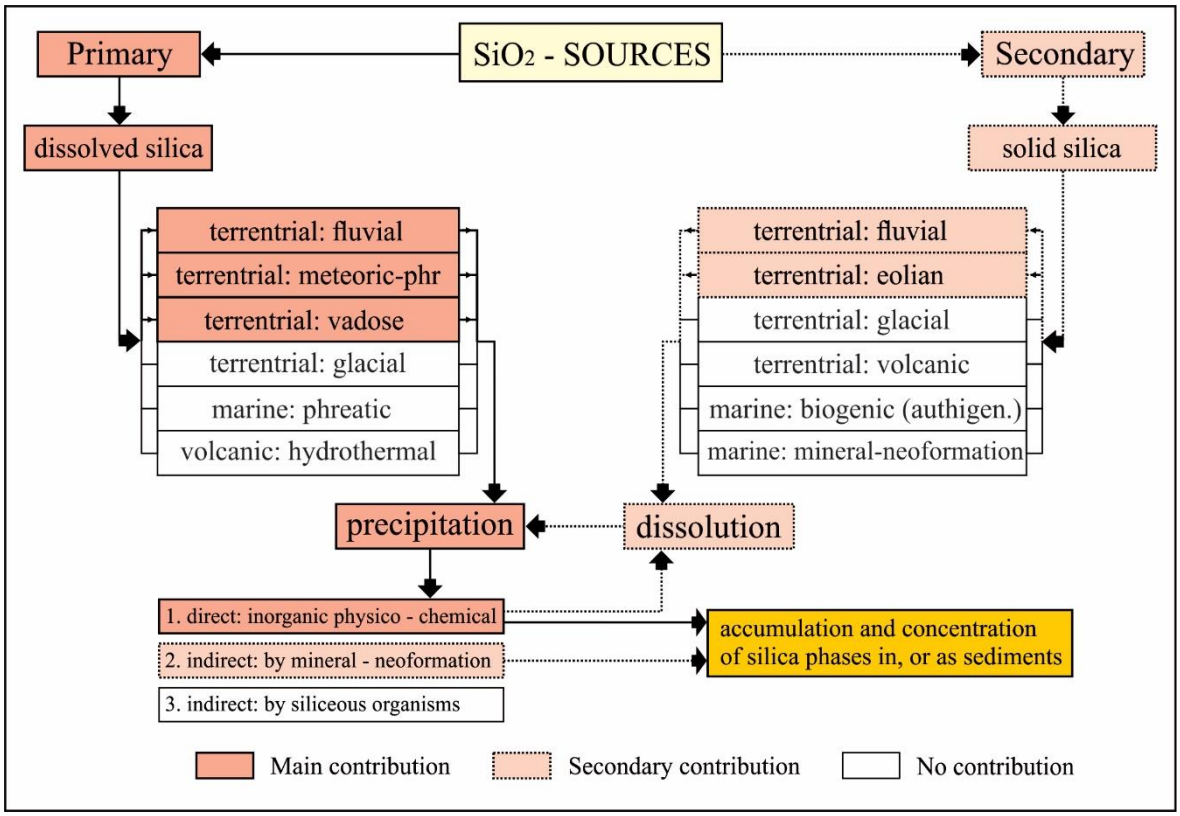

Figure 18-Circulation of dissolved and solid silica phases in the water systems (Modified from Laschet 1984).

Weathered feldspar grains have been found in the sediments at the Pedra de Fogo and may have supplied part of the silica for the chertification (Faria and Truckenbrodt, 1980a, 1980b). According to Truckenbrodt (2019, p. 94) dry continental environments (arid to semi-arid), which evaporation often exceeds the meteoric water inflow, usually have low levels of organic matter, deep groundwater levels, and heavily oxidized sediments. Under these conditions of the interstitial waters are more concentrated and tend to be dominated by Na^{+}, Ca^{2+}, $Mg^{2+,}$ and HCO_3^{-}, causing the formation of smectite, smectite/illite and clay minerals rich in Mg. In this way, the silica residuum may also have been caused by leaching of Mg from the clay or new silica was introduced from the groundwater, a transformation from Mg-clays to quartz does exist. The petrographic and field characteristics of PF-chert, shows that your genesis, primary and/or secondary, certainly have had a very close genetic relationship (Fig. 18), and the silica source may have had remained active over long periods and, whose

influence extended under broad regions of Parnaíba Basin during deposition of the Pedra de Fogo Formation (Fig. 18).

CONCLUSIONS

The studied succession in the northeast of Brazil (Parnaíba Basin) may be subdivided into three different facies associations: dune field-FA1; lacustrine nearshore/sabkha-FA2 and lacustrine central-FA3. The FA1 represents the top of the Pennsylvanian Piauí Formation and the FA2 and FA3 is included the Permian Pedra de Fogo Formation. These two sedimentary units is separated by a regional unconformity. The dune field deposits occur with medium sets of aeolian dune cross-stratification frequently limited with adhesion lamination surface and interbedded uppermost part wet interdune with centimeter-scale layers of damp interdune suggests high fluctuations of the water table resulting of alternating wet and dry cycles. The frequency adhesion lamination surface and continuo mudstone layers of damp interdune suggest wet aeolian systems. The rise of the capillary fringe associated with the wet uppermost tendency of succession interrupts the aeolian system overlaid by implantation of the shallow perennial saline sabkha lakes above the deflation horizon, representative of the regional unconformity. This endorheic lacustrine-sabkha is characterized by intense reworking by fairweather waves, and eventually storm waves. Multiples centimetric shallowing upward cycles mudstone/sandstone are representative that the árid system was powered by periódic pulses of ephemeral stream. The peripheric parts of this lacustrine system were the site of salts precipitation, suggestive of high evaporation with seasonal shrinking lake volume, increasing salinity, and marginal efflorescent salt crust. All evaporític fragments, beyond majory of succession are pervasively silicified.

The petrographic investigation of this pervasive silicification in this, and other outcrops of the Pedra de Fogo Formation, show a variety of textures from silica fabrics that have been recognized in chert-replaced carbonates and evaporites including equigranular (microcrystalline quartz or microquartz and megaquartz) and fibrous types (chalcedony, quartzine or length-slow chalcedony and microflamboyant quartz). The most distinctive texture of the groundmass is a gridwork pattern. This has been associated with the precursor of Magadi type-chert. The petrographic and SEM analysis showed that the gridwork or rectilinear extinction pattern resulting from the occurrence of aggregates minute quartzine spherules (10-30 μm diameter) in hexagonal arrays. If these spherules have approximately uniform size form, where two elongated arranged in sub-perpendicular directions, in blue and

yellow direction form the gridwork pattern observed. Variation in angles of the gridwork appears to reflect the size and packing of these microspherules.

The PF-cherts also contains a number of wholly filled by microflamboyant quartz, chalcedony overlay, and main spherulites of LS-quartzine and mosaic megaquartz. This last with typical increases crystals size into pore spaces. Silicification is a process which apparently has continued over a long period since the formation of the original precursor (evaporate/carbonates). The low amount of amorphous organic matter, the absence of pyrite, the scarcity or absence of pollen grains and spores and the possible presence of plant tissue indicate that the depositional site should be oxidizing. Preservation of delicate microbial cells and filaments, suggests that the silicification was precocious (eodiagenetic) because decomposition of cyanobacteria occurs on the time-scale of days to weeks. Exceptional morphological preservation requires the rapid cessation of heterotrophic activity and indicates that silicification occurred penecontemporaneously with deposition and prior to the neomorphic recrystallization of mineral phases that can physically destroy organic structures.

The concentric lining of overlays and mosaic megaquartz in the cavity spaces and the complete lack of replacement criteria indicate that fabrics of this type must be of cementation origin. Silica diagenesis was a multi-stage process as indicated by the variety of textures and crystal sizes of silica fabric. Void-lining and filling forms of silica precipitated subsequently to, and probably also overlapping, syndepositional precipitation of hydrous silicates.

During the Early Permian shallow perennial saline lacustrine-sabkha from the Pedra de Fogo Formation developed in a western-central part of Pangea, occupied the limits of middle latitudes in West Gondwana, and it can be inferred that the temporal alternation of wet and dry arid sedimentary systems was most likely due to climatic oscillations, probably monsoonal, and induced by orbital cycles, that influenced the rate of expansion and contraction os this arid lacustrine system.

ACKNOWLEDGMENTS

This work is part of the Ph.D. dissertation of the first author with technical support of the PPGG (Programa de Pós-Graduação em Geologia e Geoquímica) of the University Federal of Para (UFPA). We are grateful to the CNPq (National Council for Scientific and Technological Development - CNPq no.141968/2016-8) and the CAPES (Coordination for the Improvement of Higher Education Personnel; financial code 001) as the funding agency of Brazil to the concession of fellowship research to the first author. We greatly appreciate Dr. Juan Carlos Cisneros (CNPq no.456608/2014-1 e 305688/2016-2) and PhD student Domingas

Maria da Conceição for the help in the fieldwork. We thank Hudson Santos for help in the cathodoluminescence analysis performed at the Laboratory of CL of the PPGG.

REFERENCES

Abrantes Jr, F.R., Nogueira, A.C.R., Andrade, L.S., Bandeira, J., Soares, J.L., and Medeiros, R.S.P., 2019, Register of increasing continentalization and palaeoenvironmental changes in the west-central pangaea during the Permian-Triassic, Parnaíba Basin, Northern Brazil: Journal of South American Earth Sciences, v. 93, p. 294-312.

Al-Masrahy, M.A., 2017, Modelling Temporal and Spatial Sedimentary Architectural Complexity in Mixed Aeolian-Fluvial Reservoir Successions: Conference Society of Petroleum Engineers.

Aleali, M., Rahimpour-Bonab, H., Moussavi-Harami, R., and Jahani, D., 2013, Environmental and sequence stratigraphic implications of anhydrite textures: A case from the Lower Triassic of the Central Persian Gulf: Journal of Asian Earth Sciences, v. 75, p. 110-125.

Alexander, G.B., Heston, W.M., and Iler, R.K., 1954, The Solubility of Amorphous Silica in Water: The Journal of Physical Chemistry A, v. 58, p. 453-455.

Alexander, J., Bridge, J.S., Cheel, R.J., and Leclair, S.F., 2001, Bedforms and associated sedimentary structures formed under supercritical water flows over aggrading sand beds: Sedimentology, v. 48, p. 133-152.

Alleon, J., Bernard, S., Le Guillou, C., Daval, D., Skouri-Panet, F., Pont S., Delbes, L., and Robert, F., 2016, Early entombment within silica minimizes the molecular degradation of microorganisms during advanced diagenesis: Chemical Geology, v. 437, p. 98-108.

Andrade, L.S., Nogueira, A.C.R., and Silva Junior, J.B.C., 2014, Evolução de um sistema lacustre árido Permiano, parte superior da Formação Pedra de Fogo, borda oeste da Bacia do Parnaíba: Geologia USP, Série Científica, v. 14, p. 39-60.

Araújo, R.N., Nogueira, A.C.R., Bandeira, J., and Angélica, R.S., 2016, Shallow lacustrine system of the Permian Pedra de Fogo Formation, Western Gondwana, Parnaíba Basin, Brazil: Journal of South American Earth Sciences, v. 67, p. 57-70.

Ashley, G.M., Southard, J.B., and Boothroyd, J.C., 1982, Deposition of climbing-ripple beds: a flume simulation: Sedimentology, v. 29, p. 67-79.

Banahan, S., and Goering, J.J., 1986, The production of biogenic silica and its accumulation on the southeastern Bering Sea shelf: Continental Shelf Research, v. 5, p. 199-213.

Banks, N., 1970, Nature and Origin of Early and Late Cherts in the Leadville Limestone, Colorado: Geological Society of America, Bulletin, v. 81, p. 3033-3048.

Barbosa, O., and Gomes, F. de A., 1957, Carvão mineral na Bacia do Tocantins-Araguaia: Departamento Nacional de Produção Mineral, Divisão Geologia e Mineralogia, Boletim, v. 174, p. 1-34.

Bartley, J.K., 1996, Actualistic taphonomy of cyanobacteria; implications for the Precambrian fossil record: Palaios, v. 11, p. 571-586.

Beauchamp, B., and Baud, A., 2002, Growth and demise of Permian biogenic chert along northwest Pangea: evidence for end-Permian collapse of thermohaline circulation: Palaeogeography, Palaeoclimatology, Palaeoecology, v. 184, p. 37-63.

Beauchamp, B., and Grasby, S.E., 2012, Permian lysocline shoaling and ocean acidification along NW Pangea led to carbonate eradication and chert expansion: Palaeogeography, Palaeoclimatology, Palaeoecology, v. 350, p. 352:73-90.

Beer, J.A., and Jordan, T.E., 1989, The effects of Neogene thrusting on deposition in the Bermejo Basin, Argentina: Journal of Sedimentary Research, v. 59, p. 330–345.

Behl, R., and Garrison, R.E., 1994, The origin of chert in the Monterey Formation of California (USA), in Iijima, A., Abed, A.M., and Garrison, R.E., eds., Siliceous, phosphatic and glauconitic sediments of the Tertiary and Mesozoic: Proceedings of the 29th International Geological Congress, Part C, p. 101-132.

Benison, K.C., Bowen, B.B., Oboh-Ikuenobe, F.E., Jagniecki, E.A., Laclair, D.A., Story, S.L., Mormile, M.R., and Hong, B.Y., 2007, Sedimentology of acid saline lakes in southern Western Australia: newly described processes and products of an extreme environment: Journal of Sedimentary Research, v. 77, p. 366–388.

Berra, F., and Angiolini, L., 2014, The Evolution of the Tethys Region throughout the Phanerozoic: A Brief Tectonic Reconstruction, in Marlow, L., Kendall, C.C.G., and Yose, L.A., eds., Petroleum Systems of the Tethyan Region: American Association of Petroleum Geologists, v. 106, p. 1-27.

Blair, T.C., 2000, Sedimentology and progressive tectonic unconformities of the sheetflood-dominated Hell's Gate alluvial fan, Death Valley, California: Sedimentary Geology, v. 132, p. 233-262.

Boggs Jr., S., 2009, Petrology of Sedimentary Rock: Cambridge University Press, 600 p.

Boucot, A.J., Chen, X., Scotese, C.R., and Morley, R.J., 2013, Phanerozoic Paleoclimate: An Atlas of Lithologic Indicators of Climate: SEPM, Concepts in Sedimentology and Paleontology, v. 11, 478 p.

Bridge, J., 2003, Rivers and Floodplains - Forms, Processes and Sedimentary: Wiley-Blackwell, 504 p.

Brigo, L., Camana, G., Rodeghiero, F., and Potenza, R., 2001, Carbonate-hosted siliceous crust type mineralization of Carnic Alps (Italy-Austria): Ore Geology Reviews, v. 17, p. 199-214.

Brookfield, M.E., 1977, The origin of bounding surfaces in ancient aeolian sandstones. Sedimentology, v. 24, p. 303-332.

Brookfield, M.E., and Silvestro, S., 2010, Eolian systems, in James, N.P., and Darlymple, R.W., eds., Facies Models 4: St. John’s Newfoundland, Geological Association of Canada, p. 139-166.

Buurman, P., 1972, Mineralization of fossil wood: Scripta Geologica, v. 12, p. 1-43.

Bustillo, M.A., and Alonso-Zarza, A.M., 2007, Overlapping of pedogenesis and meteoric diagenesis in distal alluvial and shallow lacustrine deposits in the Madrid Miocene Basin, Spain: Sedimentary Geology, v. 198, p. 255-271.

Bustillo, M.A., Delgado, A., Rey, J., and Ruiz-Ortiz, P.A., 1998, Meteoric water participation in the genesis of Jurassic cherts in the Subbetic of southern Spain — a significant indicator of penecontemporaneous emergence: Sedimentary Geology, v. 119, p. 85-102.

Bustillo, M.A. 2001, Cherts with Moganite in Continental Mg-Clay Deposits: An Example of "False" Magadi-Type Cherts, Madrid Basin, Spain: Journal of Sedimentary Research, v. 71, p. 436-443.

Caldas, E.B., Mussa, D., Lima Filho, F.P., and Rosier, O., 1989, Nota sobre a ocorrência de uma floresta petrificada de idade permiana em Teresina, Piauí: Boletim do Instituto de Geociências da USP, Publicação Especial, Paleobotânica e Palinologia na América do Sul, v. 7, p. 69-87.

Camana, G., Chateigner, D., Zucali, M., and Artioli. G., 2002, The grid-work texture of authigenic microcrystalline quartz in siliceous crust-type (SCT) mineralized horizons: American Mineralogist, v. 87, p. 1128–1138.

Cecil, C.B., 1990, Paleoclimate controls on stratigraphic repetition of chemical and siliciclastic rocks: Geology, v. 18, p. 533-536.

Channing, A., and Edwards, D., 2003, Experimental taphonomy: silicification of plants in Yellowstone hot-spring environments: Royal Society of Edinburgh, Transactions, Earth Sciences, v. 94, p. 503-521.

Chateau, C., Haines, J., Léger, J.M., LeSauze, A., and Marchand, R., 1999, A moganite-type phase in the silica analog phosphorus oxynitride: American Mineralogist, v. 84 p. 207-210.

Chateigner, D., Camana, G., and Trimby, P.W., 2002, Textural Analysis of a Microcrystalline Quartz using X-Ray and Electron Backscatter Diffraction (EBSD) Techniques: Materials Science Forum, v. 408-412, p. 1675-1680.

Chen, D., Qing, H., Yan, X., and Li, H., 2006, Hydrothermal venting and basin evolution (Devonian, South China): Constraints from rare earth element geochemistry of chert: Sedimentary Geology, v. 183, p. 203-216.

Chen J., Chough, S. K., Chun, S.S., and Han, Z., 2009, Limestone pseudoconglomerates in the Late Cambrian Gushan and Chaomidian Formations (Shandong Province, China): soft-sediment deformation induced by storm-wave loading: Sedimentology, v. 56, p. 1174-1195.

Choquette, P.W., and James, N.P., 1987, Diagenesis in Limestones - 3. The Deep Burial Environment: Geoscience Canada, v. 14, p. 3-35.

Chowns, T.M., and Elkins, J.E., 1974, The origin of quartz geodes and cauliflower cherts through the silicification of anhydrite nodules: Journal of Sedimentary Research, v. 44, p. 885–903.

Chumakov, N.M., and Zharkov, M.A., 2003, Climate during the Permian–Triassic Biosphere Reorganizations. Article 2. Climate of the Late Permian and Early Triassic: General Inferences: Stratigraphy and Geological Correlation, v. 11, p. 361–375.

Cisneros, J.C., Abdala, F., Rubidge, B.S., Dentzien-Dias, P.C., and Bueno, A.O., 2011, Dental Occlusion in a 260-Million-Year-Old Therapsid with Saber Canines from the Permian of Brazil: Science, v. 331, p. 1603-1605.

Cisneros, J.C., Marsicano, C., Angielczyk, K.D., Smith, R.M.H., Richter, M., Fröbisch, J., Kammerer, C.F., and Sadleir, R.W., 2015, New Permian fauna from tropical Gondwana: Nature Communications, v. 6, p. 8676.

Coimbra, A.M., and Mussa, D., 1984, Associação lignitatoflorística na Formação Pedra de Fogo (Arenito Cacunda), Bacia do Maranhão - Piauí, Brasil: Congresso Brasileiro de Geologia, 33, Rio de Janeiro, Anais, v. 2, p. 591-605.

Collinson, J.D., and Thompson, D.B., 1982, Sedimentary Structures: Allen and Unwin, London, 194 p.

Cook, P.J., 1970, Repeated Diagenetic Calcitization, Phosphatization, and Silicification in the Phosphoria Formation: Geological Society of American, Bulletin, v. 81, p. 2107-2116.

Conceição, D.M., Andrade, L.S., Cisneros, J.C., Iannuzzi, R., Pereira, A.A., and Machado, F.C., 2016a, New petrified forest in Maranhão, Permian (Cisuralian) of the Parnaíba Basin, Brazil: Journal of South American Earth Sciences, v. 70, p. 308-323.

Conceição, D.M., Cisneros, J.C., and Iannuzzi, R., 2016b, Novo registro de floresta petrificada em Altos, Piauí; relevância e estratégias para geoconservação: Pesquisas em Geociências, v. 43, p. 311-324.

Conceição, D.M., Crisafulli, A., Neregato, R., Iannuzzi, R., Cisneros, J., and Andrade, L.S., 2019, Permian gymnosperm woods from the Pedra de Fogo Formation in the Parnaíba Basin, northeastern Brazil. Part I: submitted for publication.

Courtillot, V.E., and Renne, P.R., 2003, On the ages of flood basalt events Sur l ' âge des trapps basaltiques: Comptes Rendus Geoscience, v. 335, p. 113-140.

Cressman, E.R., 1962, Nondetrital siliceous sediments: Geological Survey Professional Paper, p. T1-T23.

Crowley, T.J, Hyde, W.T., and Short, D.A., 1989, Seasonal cycle variations on the supercontinent of Pangaea: Geology, v. 17, p. 457-460.

Dalrymple, R.W., 2010, Interpreting Sedimentary Sucessions: Facies, Facies Analysis and Facies Models, in James, N.P., & Dalrymple, R.W., eds., Facies Models 4: St. John's Newfoundland, Geological Association of Canada, p. 3–18.

Duke, W.L., 1985, Hummocky cross-stratification, tropical hurricanes, and intense winter storms: Sedimentology, v. 32, p. 167-194.

Dumas, S., and Arnott, R.W.C., 2006, Origin of hummocky and swaley cross-stratification – The controlling influence of unidirectional current strength and aggradation rate: Geology, v. 34, p. 1073-1076.

Dunham, J.I., 2017, Understanding 'gridwork' textures within Proterozoic Early diagenetic chert: Geological Society of American, Annual Meeting, Abstracts with Programs, v. 49, p. 6.

El Tabakh, M., Grey, K., Pirajno, F., B., and Schreiber, C., 1999, Pseudomorphs after evaporitic minerals interbedded with 2.2 Ga stromatolites of the Yerrida basin, Western Australia: Origin and significance: Geology, v. 27, p. 871-874.

Eugster, H.P., 1967, Hydrous sodium silicates from Lake Magadi, Kenya: Precursors of bedded chert: Science, v. 15, p. 1177-1180.

Eugster, H.P., 1969, Inorganic bedded cherts from the Magadi area, Kenya: Contributions to Mineralogy and Petrology, v. 22, p.1-31.

Eugster, H.P., 1980, Lake Magadi, Kenya, and its precursors, in Nissembaum, A., ed., Hypersaline brines and evaporitic environments: Developments in Sedimentology, v. 28, p. 195–232,

Eugster, H.P., 1986, Lake Magadi, Kenya: a model for rift valley hydrochemistry and sedimentation?, in Frostick, L.E., Renaut, R.W., Reid, I., and Tiercelin, J.J., eds., Sedimentation in the African Rifts: Geological Society of London, Special Publications, v. 25, 177-189.

Eyles, N., and Clark, B.M., 1986, Significance of hummocky and swaley cross-stratification in late Pleistocene lacustrine sediments of the Ontario basin, Canada: Geology, v. 14, p.

679-682.

Faria Jr., L.E.C., 1979, Estudo sedimentológico da Formação Pedra de Fogo – Permiano – Bacia do Maranhão [Dissertação de Mestrado]: Universidade Federal do Pará, 57 p.

Faria Jr., L.E.C., and Truckenbrodt, W., 1980a, Estratigrafia e petrografia da Formação Pedra de Fogo – Permiano da Bacia do Maranhão: Congresso Brasileiro de Geologia, 31, Balneário Camboriú, Anais, v. 2, p. 740-754.

Faria Jr., L.E.C., and Truckenbrodt, W., 1980b, Estromatólitos na Formação Pedra de Fogo, Permiano, Bacia do Maranhão: Congresso Brasileiro de Geologia, 31, Balneário Camboriú, Anais, v. 5, p. 3056-3067.

Fengel, D., 1991, Aging and fossilization of wood and its components: Wood Science and Technology, v. 25, p. 153–177.

Feng, Q., Malila, K., Wonganan, N., Chonglakmani, C., Helmcke, D., Ingavat-Helmcke, R., and Caridroite, M., 2005, Permian and Triassic Radiolaria from Northwest Thailand: paleogeographical implications: Revue de Micropaléontologie, v. 48, p. 237-255.

Figueroa, R.T., and Gallo, V., 2017, New chondrichthyan fin spines from the Pedra de Fogo Formation, Brazil: Journal of South American Earth Sciences, v.76, p. 389-396.

Fisher, J.A., Nichols, G.J., and Waltham, D.A., 2007, Unconfined flow deposits in distal sectors of fluvial distributary systems: examples from the Miocene Luna and Huesca Systems, northern Spain: Sedimentary Geology, v. 195, p. 55-73.

Fisher, J.A., Krapf, C.B.E., Lang, S.C., Nichols, G.J., and Payenberg, T.H.D., 2008, Sedimentology and architecture of the Douglas Creek terminal splay, Lake Eyre, central Australia: Sedimentology, v. 55, p. 1915-1930.

Flörke, O.W., Hollmann, R., von Rad, U., and Rösch, H., 1976, Intergrowth and twinning in opal-CT lepispheres: Contributions to Mineralogy and Petrology, v. 58, p.235-242.

Folk, R.L., and Pittman, J.S., 1971, Length-slow chalcedony; a new testament for vanished evaporites: Journal of Sedimentary Research, v. 41, p. 1045–1058.

Folk, R.L., and Weaver, C.E., 1952, A study of the texture and composition of chert: American Journal of Science, v. 250, p. 498-510.

Ford, D., and Golonka, J., 2003, Phanerozoic paleogeography, paleoenvironment and lithofacies maps of the circum-Atlantic margins: Marine and Petroleum Geology, v. 20, p. 249–285.

Frondel, C., 1978, Characters of quartz fibers: American Mineralogist, v. 63, p. 17-27.

Furuno, T., Watanabe, T., Suzuki, N., Goto, T., and Yokoyama, K., 1986, Microstructure and silica mineralization in the formation of silicified woods, 2: Distribution of organic carbon and the formation of quartz in the structure of silicified wood: Mokuzai Gakkaishi, v. 32, p. 575– 583.

Gao, G., and Land, L.S., 1991, Nodular chert from the Arbuckle Group, Slick Hills, SW Oklahoma: a combined field, petrographic and isotopic study: Sedimentology, v. 38, p. 857-870.

Gates, L., James, N.P., and Beauchamp, B., 2004, A glass ramp: shallow-water Permian spiculitic chert sedimentation, Sverdrup Basin, Arctic Canada: Sedimentary Geology, v. 168, p. 125-147.

Geeslin, J.H., and Chafetz, H.S., 1982, Ordovician Aleman Ribbon Cherts: An Example of Silicification Prior to Carbonate Lithification: Journal of Sedimentary Research, v. 52, p.

1283-1293.

Góes, A.M.O., Souza, J.M.P., and Teixeira, L.B., 1990, Estágio exploratório e perspectivas petrolíferas da Bacia do Parnaíba: Boletim de Geociências da Petrobrás, v. 4, p. 55-64.

Góes, A.M.O., and Feijó, F.J., 1994, Bacia do Parnaíba: Boletim de Geociências da Petrobrás, v. 8, p. 57-67.

Góes, A.M., 1995, A Formação Poti (Carbonífero Inferior) da Bacia do Parnaíba [Tese de Doutorado]: Universidade de São Paulo, 171 p.

Graetsch, H.A., and Grünberg, J.M., 2011, Microstructure of flint and other chert raw materials: Archaeometry, v. 54, p. 18-36.

Harper, H.E., and Knoll, A.H, 1975, Silica, diatoms, and Cenozoic radiolarian evolution: Geology, v. 3, p. 175-177.

Hattori, I., 1989, Length-Slow Chalcedony in Sedimentary Rocks of the Mesozoic Allochthonous Terrane in Central Japan and Its Use for Tectonic Synthesis, in Hein, J.R., and Obradović, J., eds., Siliceous Deposits of the Tethys and Pacific Regions, p. 201-215.

Hattori, I., Umeda, M., Nakagawea, T., and Yamamoto, H, 1996, From chalcedonic chert to quartz chert: diagenesis of chert hosted in a Miocene volcanic-sedimentary succession, central Japan: Journal of Sedimentary Research, v. 66, p. 163-174.

Hay, R.L., 1968, Chert and its sodium-silicate precursors in sodium-carbonate lakes of East Africa: Contributions to Mineralogy and Petrology, v. 17, p. 255-274.

Hay, R.L., 1970, Silicate reactions in three lithofacies of a semi-arid basin, Olduvai Gorge, Tanzania: Mineralogical Society of American, Special Papers, v. 3, p. 237-255.

Heaney, P.J., 1995, Moganite as an indicator for vanished evaporites; a testament reborn?: Journal of Sedimentary Research, v. 65, p. 633-638.

Heaney, P.J., and Post, J.E., 1992, The Widespread Distribution of a Novel Silica Polymorph in Microcrystalline Quartz Varieties: Science, v. 255, p. 441-443.

Henchiri, M., and Slim-S'Himi, N., 2006, Silicification of sulphate evaporites and their carbonate replacements in Eocene marine sediments, Tunisia: two diagenetic trends: Sedimentology, v. 53, p. 1135-1159.

Hesse, R., 1988, Origin of chert: Diagenesis of biogenic siliceous sediments: Geoscience Canada, v. 15, p. 171-192.

Hesse, R., 1989, Silica diagenesis: origin of inorganic and replacement cherts: Earth-Science Reviews, v. 26, p. 253-284.

Hinds, D.J., Aliyeva, E., Allen, M.B., Davies, C.E., Kroonenberg, S.B., Simmons, M.D., and Vincent, S.J., 2004, Sedimentation in a discharge dominated fluvial-lacustrine system: the Neogene Productive Series of the South Caspian Basin, Azerbaijan: Marine and Petroleum Geology, v. 21, p. 613-638.

Hmich, D., Schneider, J.W., Saber, H., Voigt, S., and Wartiti, M.E., 2006, New continental Carboniferous and Permian faunas of Morocco: implications for biostratigraphy, palaeobiogeography and palaeoclimate, in Lucas, S.G., Cassinis, G., and Schneider, J.W., eds., Non-Marine Permian Biostratigraphy and Biochronology: Geological Society of London, Special Publications, v. 265, p. 297-324

Hunter, R.E., 1977, Basic types of stratification in small eolian dunes: Sedimentology, v. 24, p. 361-387.

Hussain, M., and Warren, J.K., 1989, Nodular and enterolithic gypsum: the “sabkha-tization” of Salt Flat playa, west Texas: Sedimentary Geology, v. 64, p. 13-24.

Iannuzzi, R., Neregato, R., Cisneros, J.C., Angielczyk, K.D., Rößler, R., Rohn, R., Marsicano, C., Fröbisch, J., Fairchild, T., Smith, R.M.H., Kurzawe, F., Richter, M., Langer, M.C., Tavares, T.M.V., Kammerer, C.F., Conceição, D.M., Pardo, J.D., and Roesler, G.A., 2018, Re-evaluation of the Permian macrofossils from the Parnaíba Basin: biostratigraphic, palaeoenvironmental and palaeogeographical implications, in Daly, M.C., Fuck, R.A., Julià, J., MacDonald, D.I.M., and Watts, A.B., eds., Cratonic Basin Formation: A Case Study of the Parnaíba Basin of Brazil: Geological Society of London, Special Publications, v. 472, p. 223-249.

Iannuzzi, R., and Langer, M.C., 2014, The presence of callipterids in the Permian of northeastern Brazil: stratigraphic and phytogeographical implications, in Rocha, R., Pais J., Kullberg J.C., and Finney, S., eds., 1st International Congress on Stratigraphy, Springer, Cham, Switzerland, p. 403–406.

Jacka, A.D., 1974, Replacement of fossils by length-slow chalcedony and associated dolomitization: Journal of Sedimentary Research, v. 44, p. 421–427.

Jorgensen, P.J., and Fielding, C.R., 1996, Facies architecture of alluvial floodbasin deposits: three-dimensional data from the Upper Triassic Callide Coal Measures of east-central Queensland, Australia: Sedimentology, v. 43, p. 479-495.

Kastner, M., 1980, Length-slow chalcedony: The end of the new testament (abstract): EOS, v. 61, p. 399.

Keene, J.B., 1983, Chalcedonic quartz and occurrence of quartzine (length-slow chalcedony) in pelagic sediments: Sedimentology, v. 30, p. 449-454.

Kendall, A.C., 2010, Marine Evaporites, in James, N.P., and Darlymple, R.W., eds., Facies Models 4: St. John’s Newfoundland, Geological Association of Canada, p. 505-539.

Knauth, L.P., 1994, Petrogenesis of chert, in Heaney, P.J., Prewitt, C.T., and Gibbs, G.V., eds., Silica: physical behavior, geochemistry and materials applications: Reviews in Mineralogy Geochemistry, v. 29, p. 233-258.

Knoll, A.H., 1985, Exceptional preservation of photosynthetic organisms in silicified carbonates and silicified peats: Royal Society of London, Philosophical Transactions, Series B, Biological Science, v. 311, p. 111-122.

Knoll, A.H, 1984, Microbiotas of the Late Precambrian Hunnberg Formation, Nordaustlandet, Svalbard: Journal of Paleontology, v. 58, p. 131-162.

Kocurek, G., 1981, Significance of interdune deposits and bounding surfaces in aeolian dune sands: Sedimentology, v. 28, p. 753–780.

Kocurek, G., 1988, First-order and super bounding surfaces in eolian sequences-Bounding surfaces revisited: Sedimentary Geology, v. 56, p. 193-206.

Kocurek, G., 1991, Interpretation of ancient eolian sand dunes: Annual Review of Earth and Planetary Sciences, v. 19, p. 43–75.

Kocurek, G., and Fielder, G., 1982, Adhesion structures: Journal of Sedimentary Research, v. 52, p. 1229–1241.

Kocurek, G., 1996, Desert aeolian systems, in Reading, H.G., ed., Sedimentary Environments and Facies: Blackwell Science, Oxford, p. 125–153.

Kocurek, G., and Day, M., 2018, What is preserved in the aeolian rock record? A Jurassic

Entrada Sandstone case study at the Utah–Arizona border: Sedimentology, v. 65, p. 1301-1321.

Kolodny, Y., Chaussidon, M., and Katz, A., 2005, Geochemistry of a chert breccia: Geochimica et Cosmochimica Acta, v. 69,p. 427-439.

Krainer, K., and Spötl, C., 1998, Abiogenic silica layers within a fluvio-lacustrine succession, Bolzano Volcanic Complex, northern Italy: a Permian analogue for Magadi-type cherts?: Sedimentology, v. 45, p. 489-505.

Krauskopf, K.B., 1956, Dissolution and precipitation of silica at low temperatures: Geochimica et Cosmochimica Acta, v. 10, p. 1-26.

Kremer, B., Kazmierczak, J., Łukomska-Kowalczyk, M., and Kempe, S., 2012, Calcification and Silicification: Fossilization Potential of Cyanobacteria from Stromatolites of Niuafo‘ou's Caldera Lakes (Tonga) and Implications for the Early Fossil Record: Astrobiology, v. 12, p. 535-548.

Lancaster, N., 1996, Field studies of sand patch initiation processes on the northern margin of the Namib sand sea: Earth Surface Processes and Landforms, v. 21, p. 947-954.

Lang, S.C., Payenberg, T.H.D., Reilly, M.R.W., Hicks, T., Benson, J., and Kassan, J., 2004, Modern analogues for dryland sandy fluvial-lacustrine deltas and terminal splay reservoirs: Journal of the Australian Petroleum Production & Exploration Association, v. 44, p. 329-356.

Laschet, C., 1984, On the origin of cherts: Facies, v. 10, p. 257–289.

Leo, R.F., and Barghoorn, E.S., 1976, Silicification of wood: Botanical Museum Leaflets, v. 25, p. 1-47.

Li, Y., Sha, J., Wang, Q., and Chen, S., 2007, Lacustrine tempestite litho- and biofacies in the Lower Cretaceous Yixian Formation, Beipiao, western Liaoning, northeast China: Cretaceous Research, v. 28, p. 194-198.

Li, F., Yang, Y., Li, J., Yang, C., Dai, T., Zhao, J., and Yi, H., 2014, Lacustrine tempestite and its geological significance in the Cenozoic study of the Qaidam Basin: Journal of Asian Earth Sciences, v. 92, p. 157-167.

Lima, E.A.M., and Leite, J.F., 1978, Projeto estudo global dos recursos Minerais da Bacia Sedimentar do Parnaíba: Integração geológico-metalogenética, Etapa III, Relatório Final, v. 16, 212 p.

Lindholm, R.C., 1987, A practical approach to sedimentology: London, Allen & Unwin, 276 p.

Locatelli, E., 2014., The Exceptional Preservation of Plant Fossils: A Review of Taphonomic Pathways and Biases in the Fossil Record: The Paleontological Society Papers, v. 20, p. 237-258.

Lojka, R., Drabkova, J., Zajic, J., Sykorova, I., Francu, J., Blahova, A., and Grygar, T., 2009, Climate variability in the Stephanian B based on environmental record of the Mšec Lake deposits (Kladno-Rakovník Basin, Czech Republic): Palaeogeography, Palaeoclimatology, Palaeoecology, v. 280, p. 78-93.

Loope, D.B., 1985, Episodic deposition and preservation of eolian sands: A late Paleozoic example from southeastern Utah: Geology, v. 13, p. 73-76.

Love, S. E., and Williams, B.P.J., 2000, Sedimentology, cyclicity and floodplain architecture in the Lower Old Red Sandstone of SW Wales, in Friend, P.F., and Williams, B.P.J.,

eds., New Perspectives on the Old Red Sandstone: Geological Society of London, Special Publications, v. 180, p. 371-388.

Lowenstein, T.K., 1987, Evaporite depositional fabrics in the deeply buried Jurassic Buckner Formation, Alabama: Journal of Sedimentary Research, v. 57, p.108–116.

Lowenstein, T.K., and Hardie, L.A., 1985, Criteria for the recognition of salt-pan evaporites: Sedimentology, v. 32, p. 627-644.

McAtee, J.L., House, R., and Eugster, H.P., 1968, Magadiite from Trinity County, California: American Mineralogist, v. 53, p. 2061–2069.

Maliva, R.G., 1987, Quartz geodes; early diagenetic silicified anhydrite nodules related to dolomitization: Journal of Sedimentary Research, v. 57, p. 1054–1059.

Maliva, R.G., Knoll, A. H., and Siever, R., 1989, Secular change in chert distribution; a reflection of evolving biological participation in the silica cycle: Palaios, v. 4, p. 519–532.

Manning-Berg, A.R., and Kah, L.C., 2017, Proterozoic microbial mats and their constraints on environments of silicification: Geobiology, v. 15, p. 469-483.

Manning-Berg, A.R., Wood, R.S., Williford, K.H., Czaja, A.D., and Kah, L.C., 2019, The Taphonomy of Proterozoic Microbial Mats and Implications for Early Diagenetic Silicification: Geosciences, v. 9, p. 1-31.

Marandi, M., Jahani, D., Uromeihy, A., and Reihan, M.K., 2017, Analysis of Structure and Textures of Anhydrite Mineral in Gachsaran Formation in Gotvand Area, Iran: Open Journal of Geology, v. 7, p. 1478-1493.

Marsaglia, K.M., and Klein, G.D., 1983, The Paleogeography of Paleozoic and Mesozoic Storm Depositional Systems: The Journal of Geology, v. 91, p. 117-142.

Martins, R.A., 2000, Fósseis de vegetais da Formação Pedra de Fogo: aspectos taxonômicos, mineralogia e composição química [Dissertação de Mestrado]: Universidade Federal do Pará, 92 p.

Martins, R.A., Costa, M.L., and Moraes, M.S., 2010, Floresta fossilizada do Tocantins: uma flora preservada por milhões de anos: Editora IFRN, 120 p.

Marzoli, A., Renne, P.R., Piccirillo, E.M., Ernesto, M., Bellieni, G., and De Min, A., 1999, Extensive 200-Million-Year-Old Continental Flood Basalts of the Central Atlantic Magmatic Province: Science, v. 284, p. 616-618.

McBride, E.F., and Folk, R.L., 1977, The Caballos Novaculite revisited; Part II, Chert and shale members and synthesis: Journal of Sedimentary Research, v. 47 p. 1261–1286.

McGee, W.J., 1897, Sheetflood erosion: Geological Society of American, Bulletin, v. 8, p. 87–112.

Merle, R., Marzoli, A., Bertrand, H., Reisberg, L., Verati, C., Zimmermann, C., Chiaradia, M., Bellieni, G., and Ernesto, M., 2011, 40Ar/39Ar ages and Sr–Nd–Pb–Os geochemistry of CAMP tholeiites from Western Maranhão basin (NE Brazil): Lithos: v. 122, p. 137–151.

Melo, M.T., and Prade, G.O., 1968, Geologia da região sudeste de São Raimundo das Mangabeiras-Maranhão [Relatório 297M]: PETROBRÁS, DIREX/RENOR, 37 p.

Meyers, W.J., 1977, Chertification in the Mississippian Lake Valley Formation, Sacramento Mountains, New Mexico: Sedimentology, v.24, p. 75-105.

Meyers, W.J., and James, A.T., 1978, Stable isotopes of cherts and carbonate cements in the

Lake Valley Formation (Mississippian), Sacramento Mts, New Mexico: Sedimentology, v. 25, p. 105-124.

Michel-Lévy, A., and Munier-Chalmas, C.P.E., 1892, Memoires sur diverses formes affectees par le reseaux elementaire du quartz: Bulletin, v. 15, p. 159-190.

Milliken, K.L., 1979, The silicified evaporite syndrome; two aspects of silicification history of former evaporite nodules from southern Kentucky and northern Tennessee: Journal of Sedimentary Research, v. 49, p. 245–256.

Moore Jr, T.C., 2008, Chert in the Pacific: Biogenic silica and hydrothermal circulation: Palaeogeography, Palaeoclimatology, Palaeoecology, v. 261, p. 87-99.

Murata, K.J., and Norman, M.B., 1976, An index of crystallinity for quartz: American Journal of Science, v. 276, p.1120-1130.

Murchey, B.L., and Jones, D.L., 1992, A mid-Permian chert event: widespread deposition of biogenic siliceous sediments in coastal, island arc and oceanic basins: Palaeogeography, Palaeoclimatology, Palaeoecology, v. 96, p. 161-174.

Nagy, Z.R., Somerville, I.D., Gregg, J.M., Becker, S.P., and Shelton, K.L., 2005, Lower Carboniferous peritidal carbonates and associated evaporites adjacent to the Leinster Massif, southeast Irish Midlands: Geological Journal, v. 40, p. 173-192.

Neuweiler, F., Larmagnat, S., Molson, J., and Fortin-Morin, F., 2014, Sponge Spicules, Silicification, and Sequence Stratigraphy: Journal of Sedimentary Research, v. 84, p. 1107–1119.

North, C.P., and Davidson, S.K., 2012, Unconfined alluvial flow processes: Recognition and interpretation of their deposits, and the significance for palaeogeographic reconstruction: Earth-Science Reviews, v. 111, p. 199-223.

Oehler, J.H., 1976, Hydrothermal crystallization of silica gel: Geological Society of American, Bulletin, v. 87, p. 1143-1152.

Oehler, J.H., and Schopf, J.W., 1971, Artificial Microfossils: Experimental Studies of Permineralization of Blue-Green Algae in Silica: Science, v. 174, p. 1229-1231.

Okamoto, G., Okura, T., and Goto, K., 1957, Properties of silica in water: Geochimica et Cosmochimica Acta, v. 12, p. 123-132.

Olivier, N., Dromart, G., Coltice, N., Flament, N., Rey, P., and Sauvestre, R., 2012, A deep subaqueous fan depositional model for the Palaeoarchaean (3.46 Ga) Marble Bar Cherts, Warrawoona Group, Western Australia: Geological Magazine, v. 149, p. 743-749.

Orange, F., Lalonde, S.V., and Konhauser, K.O., 2013, The Formation and Preservation of Synechococcus elongatus Cell Molds in Simulated Silica Sinter: Implications for the Identification of Microfossils: Journal Geomicrobiology Journal, v. 30, p. 327-336.

Owen, G., Moretti, M., and Alfaro, P., 2011, Recognising triggers for soft-sediment deformation: Current understanding and future directions: Sedimentary Geology, v. 235, p.133-140.

Parkash, B., Awasthi, A.K., and Gohain, K., 1983, Lithofacies of the Markanda terminal fan, Kurukshetra district, Haryana, India, in Collinson, J.D., and Lewin, J., eds., Modern and Ancient Fluvial Systems: Blackwell Scientific Publications, Oxford, v. 6, p. 337–344.

Parnell, J., 1986, Devonian Magadi-type cherts in the Orcadian Basin, Scotland: Journal of Sedimentary Research, v. 56, p. 495-500.

Parnell, J., 1988, Significance of lacustrine cherts for the environment of source-rock

deposition in the Orcadian Basin, Scotland, in Fleet, A.J., Kelts, K., and Talbot, M.R., eds., Lacustrine Petroleum Source Rocks: Geological Society of London, Special Publications, v. 40, p. 205-217.

Parrish, J.T., 1990, Gondwanan Paleogeography and Paleoclimatology, in Taylor, T.N., and Taylor, E.L., eds., Antarctic Paleobiology: Springer, New York, p. 15-26.

Parrish, J.T., 1993, Climate of the Supercontinent Pangea: The Journal of Geology, v. 101, p. 215-233.

Peterson, M.N.A., and Von Der Borch, C.C., 1965, Chert: modern inorganic deposition in a carbonate-precipitating locality: Science, v. 149, p. 1501-1503.

Pettijohn, F.J., 1975, Sedimentary Rocks: Harper and Row Publishers, New York, 628 p.

Pisciotto, K.A., 1981, Diagenetic trends in the siliceous facies of the Monterey Shale in the Santa Maria region, California: Sedimentology, v. 28, p. 547-571.

Plummer, F.B., 1946, Report on Maranhão and Piauí Geosyncline [Relatório 1M]: PETROBRÁS, DIREX/RENOR, 83 p.

Qui, Z., and Wang, QC., 2011, Geochemical evidence for submarine hydrothermal origin of the Middle-Upper Permian chert in Laibin of Guangxi, China: Science China Earth Sciences, v. 54, p. 1011–1023.

Rabelo, C.E.N., Ribeiro, A.C., Nogueira, A.C.R., Soares, J.L., and Góes, A.M., 2019, Genesis of poikilotopic zeolite in aeolianites: An example from the Parnaíba Basin, NE Brazil: Sedimentary Geology, v. 387, p. 61-78.

Renaut, R.W., and Gierlowski-Kordesch, E.H., 2010, Lakes, in James, N.P., and Darlymple, R.W., eds., Facies Models 4: St. John's Newfoundland, Geological Association of Canada, p. 541-575.

Rex, G.M., and Chaloner, W.G., 1983, The experimental formation of plant compression fossils: Palaeontology, v. 26, p. 231-252.

Riley, C.M., and Byrne, J.V., 1961, Genesis of primary structures in anhydrite: Journal of Sedimentary Research, v. 31, p. 553-559.

Robertson, A.H.F., 1977, The origin and diagenesis of cherts from Cyprus: Sedimentology, v. 24, p. 11-30

Röβler, R., and Galtier, J., 2002a, First Grammatopteris tree ferns from the Southern Hemisphere – new insights in the evolution of the Osmundaceae from the Permian of Brazil: Review of Palaeobotany and Palynology, v. 121, p. 205-230.

Röβler, R., and Galtier, J., 2002b, Dernbachia brasiliensis gen. nov. et sp. nov. – a new small tree fern from the Permian of NE Brazil: Review of Palaeobotany and Palynology, 122:239-263.

Röβler, R., and Galtier, J., 2003, The first evidence of the fern Botryopteris from the Permian of the Southern Hemisphere reflecting growth form diversity: Review of Palaeobotany and Palynology, v. 127, p. 99-124.

Röβler, R., 2006, Two remarkable Permian petrified forests: correlation, comparison and significance, in Lucas, S.G., Cassinis, G., and Schneider, J.W., eds., Non-Marine Permian Biostratigraphy and Biochronology: Geological Society of London, Special Publications, v. 265, p. 39-63.

Roedder, E., 1968, The non-colloidal origin of 'colloform' textures in sphalerite ores: Economic Geology, v. 63, p. 451–471.

Rooney, T.P., Jones, B.F., and Neal, J.T., 1969, Magadiite from Alkali Lake, Oregon: American Mineralogist, v.54, p. 1034–1043.

Rosen, M.R., 1994, The importance of groundwater in playas: A review of playa classifications and the sedimentology and hydrology of playas, in Rosen, M.R., ed., Paleoclimate and Basin Evolution of Playa Systems: Geological Society of America, Special paper, v. 289, p. 1-18.

Rossetti, D.D.F., 1999, Soft-sediment deformation structures in late Albian to Cenomanian deposits, São Luís Basin, northern Brazil: evidence for palaeoseismicity: Sedimentology, v. 46, p. 1065-1081.

Rubin, D.M., and Friedman, G.M., 1981, Origin of chert grains and a halite- silcrete bed in the Cambrian and Ordovician Whitehall Formation of eastern New York State: Journal of Sedimentary Petrology, v. 51, p. 69-72.

Santos, R.S., 1994, Paleoictiofaunula da Formação Pedra do Fogo, Bacia do Parnaíba, NE do Brasil: II. Eugeneodontida – Agassizodontidae: Anais da Academia Brasileira de Ciências, v. 66, p. 413-424.

Santos, M.E.C.M., and Carvalho, M.S.S., 2009, Paleontologia das Bacias do Parnaíba, São Luís e Grajaú: Reconstituições paleobiológicas, in Serviço Geológico do Brasil, DIEDIG/DEPAT, 215 p.

Scotese, C.R., Boucot, A.J., and McKerrow, W.S., 1999, Gondwanan palaeogeography and palaeoclimatology: Journal of African Earth Sciences, v. 28 p. 99-114.

Shearman, D.J., 1963, Recent anhydrite, gypsum, dolomite, and halite from the coastal flats of the Arabian shore of the Persian Gulf: Geological Society of London, Proceedings, v. 1, p. 63-65.

Schmidt, P., Slodczyk, A., Léa, V., Davidson, A., Puaud, S., and Sciau, P., 2013, A comparative study of the thermal behaviour of length-fast chalcedony, length-slow chalcedony (quartzine) and moganite: Physics and Chemistry of Minerals, v. 40, p. 331-340.

Schubel, K.A., and Lowenstein, T.K., 1997, Criteria for the recognition of shallow-perennial-saline-lake halites based on recent sediments from the Qaidam Basin, western China: Journal of Sedimentary Research, v. 67, p. 74-87.

Schubel, K.A., and Simonson, B.M., 1990, Petrography and diagenesis of cherts from Lake Magadi, Kenya: Journal of Sedimentary Research, v.60, p. 761-776.

Sebag, D., Verrecchia, E.P., Lee, S.J., and Durand, A., 2001, The natural hydrous sodium silicates from the northern bank of Lake Chad: occurrence, petrology and genesis: Sedimentary Geology, v. 139, p. 15-31.

Sheppard, R.A., and Gude, A.J., 1986, Magadi-type chert—A distinctive diagenetic variety from lacustrine deposits, in Mumpton, F.A., ed., Studies in diagenesis: U.S. Geological Survey Bulletin, Report, v. B1578, p. 335-345.

Siedlecka, A., 1972, Length-slow chalcedony and relicts of sulphates; evidences of evaporitic environments in the upper Carboniferous and Permian beds of Bear Island, Svalbard: Journal of Sedimentary Research, v. 42, p. 812-816.

Siedlecka, A., 1976, Silicified Precambrian evaporite nodules from Northern Norway: A preliminary report: Sedimentary Geology, v. 16, p. 161-175.

Siever, R., 1957, The Silica Budget in the Sedimentary Cycle: American Mineralogist, v. 42,

p. 821–841.

Siever, R., 1962, Silica Solubility, 0°-200° C., and the Diagenesis of Siliceous Sediments: The Journal of Geology, v. 70, p. 127-150.

Simonson, B.M., 1985, Sedimentology of cherts in the Early Proterozoic Wishart Formation, Quebec-Newfoundland, Canada: Sedimentology, v. 32, p. 23-40.

Souza, P.A., Matzembacher, L.T., Abelha, M., and Borghi, L., 2010, Palinologia da Formação Piauí, Pensilvaniano da bacia do Parnaíba: biocronoestratigrafia de intervalo selecionado do poço 1UN09Pi (Caxias, MA, Brasil): Revista Brasileira de Paleontologia, v. 13, p. 57-66.

Sugitani, K., Yamamoto, K., Adachi, M., Kawabe, I., and Sugisaki, R., 1998, Archean cherts derived from chemical, biogenic and clastic sedimentation in a shallow restricted basin: examples from the Gorge Creek Group in the Pilbara Block: Sedimentology, v. 45, p. 1045-1062.

Summerfield, M.A., 1983a, Silcrete as a palaeoclimatic indicator: evidence from southern Africa. Palaeogeography, Palaeoclimatology, Palaeoecology, v. 41, p. 65-79.

Summerfield, M.A., 1983b, Petrography and diagenesis of silcrete from the Kalahari Basin and Cape coastal zone, Southern Africa: Journal of Sedimentary Research, v. 53, p. 895–909.

Surdam, R.C., Eugster, H.P., and Mariner, R.H., 1972, Magadi-Type Chert in Jurassic and Eocene to Pleistocene Rocks, Wyoming: Geological Society of American, Bulletin, v. 83, p. 2261–2266.

Takiguchi, T., Sugitani, K., Yamamoto, K., and Suzuki, K., 2006, Biogeochemical signatures preserved in ancient siliceous sediments; new perspectives to Triassic radiolarian bedded chert compositions: Geochemical Journal, v. 40, p. 33-45.

Talbot, M.R., 1985, Major bounding surfaces in aeolian sandstones—a climatic model: Sedimentology, v. 32, p. 257-265.

Tooth, S.D., 1999, Floodouts in Central Australia, in Miller, A.J. and Gupta, A., eds., Varieties of Fluvial Form: John Wiley and Sons, Chichester, p. 219–247.

Toporski, J.K., Steele, A., Westall, F., Thomas-Keprta, K.L., and McKay, D.S., 2002, The simulated silicification of bacteria--new clues to the modes and timing of bacterial preservation and implications for the search for extraterrestrial microfossils: Astrobiology, v. 2, p. 1-26.

Truckenbrodt, W., 2019, Argilominerais nas Geociências: estruturas, propriedades, identificação e origem: Sociedade Brasileira de Geologia, Série Textos, 8, 124p.

Tucker, M.E., 2001, Sedimentary petrology: An Introduction to the origin Sedimentary Rocks: Blackwell Science, 262 p.

Tunbridge, I.P., 1984, Facies model for a sandy ephemeral stream and clay playa complex: The Middle Devonian Trentishoe Formation of North Devon, U.K: Sedimentology, v. 31, p. 697-715.

Vaz, P.T., Resende, N.G.A.M., Wanderley Filho, J.R., and Travassos, W.A., 2007, Bacia do Parnaíba: Boletim de Geociências Petrobrás, v. 15, p. 253-263.

Volpi, V., Camerlenghi, A., Hillenbrand, C.-D., Rebesco, M., and Ivaldi, R., 2003, Effects of biogenic silica on sediment compaction and slope stability on the Pacific margin of the Antarctic Peninsula: Basin Research, v. 15, p. 339-363.

Wagner, R.H., and Mayoral, E.J., 2007, The Early Permian of Valdeviar in Sevilla province, SW Spain: basin history and climatic/palaeogeographic implications: Journal of Iberian Geology, v. 33, p. 93-124

Walker, T.R., 1962, Reversible Nature of Chert-Carbonate Replacement in Sedimentary Rocks: Geological Society of American, Bulletin, v. 73, p. 237-242.

Walker, R.G., 1992, Facies, facies models and modern stratigraphic concepts, in Walker, R.G., and James, N.P., eds., Facies models: response to sea level change: St. John's Newfoundland, Geological Association of Canada, pp. 1-14.

Wang, J., Jiang, Z., and Zhang, Y., 2015, Subsurface lacustrine storm-seiche depositional model in the Eocene Lijin Sag of the Bohai Bay Basin, East China: Sedimentary Geology, v. 328, p. 55-72.

Walter, M.R., 1976, Chapter 3.3 Geyserites of Yellowstone National Park: An Example of Abiogenic "Stromatolites": Developments in Sedimentology, v. 20, p. 87-112.

Warren, J.K., and Kendall, C.G.C., 1985, Comparison of Sequences Formed in Marine Sabkha (Subaerial) and Salina (Subaqueous) Settings--Modern and Ancient: The American Association of Petroleum Geologist Bulletin, v. 69, p. 1013-1023.

Warren, J.K., 2006, Evaporites: Sediments, Resources and Hydrocarbons: Springer-Verlag Berlin Heidelberg, 1030 p.

Warren, J., 2016a, Silica mobility and replaced evaporites: 2 - Silicified anhydrite nodules: Salty Matters, Newslleter, p. 1-12.

Warren, J., 2016b, Silica mobility and replaced evaporites: 1 - Alkaline lakes: Salty Matters, Newslleter, p. 1-12.

Weibel, R., 1996, Petrified wood from an unconsolidated sediment, Voervadsbro, Denmark: Sedimentary Geology, v. 101, p. 31-41.

Wilson, R.C.L., 1996, Silica diagenesis in upper Jurassic limestones of southern England: Journal of Sedimentary Research, v. 36 p. 1036-1049.

Williams, L.A., Parks, G.A., and Crerar, D.A., 1985, Silica diagenesis, I. Solubility Controls: Journal of Sedimentary Research, v. 55, p. 301-311.

Williams, L.A., and Crerar, D.A., 1985, Silica diagenesis, II. General Mechanisms: Journal of Sedimentary Research, v. 55, p. 312-321.

White, J.F., and Corwin, J.F., 1961, Synthesis and origin of chalcedony: American Mineralogist, v. 46, p. 112–119.

White, D.E., Thompson, G.A., and Sandberg, C.H., 1964, Rocks, structure, and geologic history of Steamboat Springs thermal area, Washoe County, Nevada: U.S. Geological Survey, Professional Paper, v. 458-B, p. B1-B63.

Yamamoto, K., 1987, Geochemical characteristics and depositional environments of cherts and associated rocks in the Franciscan and Shimanto Terranes: Sedimentary Geology, v.2, p. 65-108.

Young, H.R., 1979, Evidence of former evaporites in the Cambro-Ordovician Durness Group, northwest Scotland: Sedimentary Geology, v. 22, p. 287-303.

Zharkov, M.A., and Chumakov, N.M., 2001, Paleogeography and Sedimentation Settings during Permian-Triassic Reorganizations in Biosphere: Stratigraphy and Geological Correlation, v. 9, p. 340–363.

7 CONCLUSÕES E CONSIDERAÇÕES FINAIS

O final do Carbonífero e início do Permiano foi caracterizado por eventos orogenéticos de grande amplitude que resultaram na formação do supercontinente Pangéia. Esta grande massa continental era subdividida em suas partes norte e sul e separada por um conjunto de elevados platôs e cadeias montanhosas que modificaram a circulação global dos ventos, levando extensas áreas do interior continental a um contínuo aumento da temperatura e aridez. Na Bacia do Parnaíba, esses eventos paleogeográficos e paleoclimáticos são registrados pela sucessão sedimentar do Grupo Balsas, que marca o início da continentalização e progressiva desertificação na bacia. A Formação Pedra de Fogo, datada no início do Permiano (Cisuraliano), registra a transição paleoclimática entre estágios mais úmidos e secos deste evento, marcada pela ciclicidade e multiplicidade lito-faciológica associada a um sistema lacustre desenvolvido durante sazonalidade climática, sob regime de megamonções que afetava o cinturão equatorial do Pangéia durante o início do Permiano. Sistemas lacustres são especialmente condicionados por fatores climáticos e tectônicos, e respondem de forma rápida à estas mudanças que são registrados independentemente do regime aberto ou fechado do lago. O controle tectônico condiciona mudanças na criação do espaço de acomodação, e na distribuição de energia física dentro dos lagos. A extensão do lago e a espessura da lâmina d'agua determina a estratificação, densidade e/ou mistura na coluna de água. A intensidade dos efeitos das ondas de tempo bom e tempestades, implica no potencial de preservação dos registros estratigráficos dos depósitos com esta influência. Além disso,mudanças relativas no nível de base em sistemas lacustres também exercem controle sobre a rede fluvial que os alimenta. Esta relação é análoga aos efeitos de variações relativas do nível do mar que afeta as porções distais de sistemas fluviais, que desaguam em bacias marinhas costeiras.

As análises de fácies, petrográfica e estratigráfica dos depósitos da Formação Pedra de Fogo nas bordas leste, sul e oeste da Bacia do Parnaíba permitiu demonstrar que os ambientes deposicionais do início do Permiano foram influenciados pela elevação no nível de base regional, provavelmente condicionada por subida do lençol freático. Este contexto paleoambiental foi desencadeado por condições climáticas sazonais associadas à crescente influência de um regime de megamonções. Como consequência, o extenso "Sistema Lacustre Pedra de Fogo" foi implantado sobre os depósitos flúvio-eólicos da Formação Piauí, e interrompeu um sistema desértico úmido instalado na borda leste da Bacia do Parnaíba desde o Pensilvaniano gerando uma supersuperfície que caracteriza uma discordância regional.

As associações de fácies e petrografia indicam que o Sistema Lacustre Pedra de Fogo foi permanentemente raso, e dinâmico, com constantes migrações de suas linhas de costa devido as expansões e contrações das massas de água em reposta a sazonalidade climática. Durante os períodos relativamente mais secos, a regressão da linha costa condicionava a periferia lacustre a precipitação química de evaporítos/carbonatos em ambiente de baixa energia, e sob delgada lâmina d'água, com intervalos de exposição subaérea que resultava em processos de dissecação com formação de gretas de contração, *tepees*, e nódulos evaporíticos. A baixa energia e ação mínima de correntes nesse subambiente e/ou em depressões efêmeras (*ponds*) preenchidas por água, e abandonas na planície lacustre durante a retração da linha de costa, propiciavam o desenvolvimento de microorganismos que através do aprisionamento e ligação de partículas sedimentares, resultavam na formação de estruturas organossedimentares. Durante os períodos relativamente mais úmidos, correntes de inundações efêmeras (*flash floods*), eram relativamente mais intensas propiciando fluxos de magnitudes variadas que desenvolviam principalmente fluxos hipopicnal (*overflows*), secundariamente hiperpicnal (*underflows*) e esporádicos homopicnais (*interflows*). Esses sistemas fluviais desenvolviam predominantemente fluxos não-confinados ou em lençol que depositavam sua carga sedimentar de forma espraiada por uma ampla área do substrato lacustre plano. Nos períodos de quiescência, esses depósitos eram recobertos por precipitação pelítica prevalescente no sistema lacustre, ou eram submetidos ao retrabalhamento por ondas de tempo bom, e frequentemente de tempestades. Esses regimes de tempestades desenvolviam ventos com energias suficientes para movimentar a superfície da água, arrastando sucessivamente camadas mais profundas e gerando movimentos orbitais das partículas da água na forma de ondas de tempestades que se propagavam movimentando o substrato lacustre por rápidos fluxos oscilatórios e relativamente mais lentos fluxos unidirecionais. As ocorrências comuns de depósitos de tempestades indicam que esses eventos eram frequentes e com intensidade suficiente para gerar os registros de suas ocorrências na forma da estratificação cruzada *hummocky*. Porções marginais descontínuas destes lagos eram colonizadas por uma pujante paleoflora formada principalmente por Samambaias e Gimnospermas. Esta paleoflora provavelmente minguava durante os períodos mais áridos, mantendo suas necessidades hídricas supridas pelo nível freático mais elevado nas periferias dos lagos, e proliferavam durante os períodos relativamente mais úmidos, o que sugere constante migração desta vegetação acompanhando os movimentos das linhas de costa lacustre. As porções superiores da sucessão estudada indicam extinção ou diminuição dos eventos de tempestades, e/ou da magnitude desses eventos, bem como redução na frequência

e energia dos eventos de rápida inundação. Esses registros sugerem condições menos sazonais e manutenção de condições climáticas permanentemente mais áridas.

A sobreposição da Formação Pedra de Fogo pela monótona ocorrência de pacotes de pelitos avermelhado e maciços com lentes evaporíticas, associadas da Formação Motuca, fortalecem esta interpretação.

Todo o conjunto de rochas da sucessão estudada é afetado por pervasiva silicificação, com tendência de redução para o topo. A análise petrográfica indica que o processo de silicificação ocorreu como múltiplos eventos, e foi inicialmente condicionada pelo clima. Durante os intervalos relativamente mais áridos, as altas taxas de evaporação aliada a reduzida precipitação pluviométrica com o consequente rebaixamento dos níveis dos lagos, condicionava essas bacias lacustres a altas concentrações em íons de Na^{+}, Ca^{2+}, Mg^{2+}, SO_4, HCO_3, com consequente precipitação evaporítica. Neste cenário, com pH potencialmente elevado (> 8), baixa proliferação de biomassa vegetal, a sílica proveniente do intemperismo continental e possivelmente fluídos freáticos, se mantinha em solução. O excesso de sílica possivelmente gerava gradual polimerização com formação de partículas coloidais pela agregação de microesferas de sílica amorfa que precipita no fundo dessas bacias. Através da evaporação da água da bacia, auxiliado por variações no pH associadas à possível atividade microbiana, e/ou pela adição de eletrólitos, esse colóide se tornava cada vez mais concentrado e era convertido para estado de gel. Durante esse estágio, edifícios microbiais, tecidos vegetais de caules caídos ou em posição de vida eram permeados e o processo de preservação dessas estruturas era iniciada por permineralização e preenchimento de vazios intracelulares.

Mudanças para condições climáticas mais úmidas ocasionavam maior influxo siliciclástico com consequente aumento nas taxas de deposição de pelito, que gradualmente recobria os níveis evaporíticos, que gradativamente nucleavam em pequenos nódulos. A progressiva subida no nível das águas, com consequente decréscimo na salinidade, possivelmente ocasionava diminuição no pH das águas superficiais e subterrâneas, que pode ter levado à dissolução parcial de alguns nódulos, e de sedimentos siliciclásticos circundantes, produzindo fluidos ricos em sílica, que somados ao acumulo de gel de sílica foram progressivamente substituindo esses nódulos evaporíticos e convertidos em nódulos de sílica. O efetivo do soterramento intensificou o processo de silicificação e completa substituição dos nódulos evaporíticos e dos tecidos vegetais, com cristalização subsequente que produziu mosaicos de microquartos. Cavidades posteriores foram progressivamente preenchidas por franjas e esferulitos de calcedônia, e por mosaicos de megaquartzo.

Este estudo faciológico, estratigráfico e petrográfico da sucessão cisuraliana associada a Formação Pedra de Fogo, constitui importante contribuição para o entendimento de sistemas deposicionais continentais sob intensas variações climáticas sazonais. Especialmente os sistemas lacustres, como mostrado neste trabalho, a sedimentação é fortemente condicionada pelas oscilações climáticas. No contexto paleoclimático e paleogeográfico da Bacia do Parnaíba durante o início do Permiano, este estudo registra a tendência geral de continentalização da bacia, com progressivo aumento da aridez compatível e progressiva elevação das temperaturas globais registras durante o Permiano. A intensa silicificação ao longo de toda a unidade, constitui importante evento de silicificação abiogênica continental.

REFERÊNCIAS

Abrantes Jr. F.R. & Nogueira A.C.R. 2013. Reconstituição paleoambiental das formações Motuca e Sambaíba, Permo-Triássico da Bacia do Parnaíba no sudoeste do Estado do Maranhão, Brasil. *Geologia USP, Série Científica*, **13**: 65-82.

Abrantes Jr. F.R., Nogueira A.C.R., Soares. J.L. 2016. Permian paleogeography of west-central Pangea: Reconstruction using sabkha-type gypsum-bearing deposits of Parnaíba Basin, Northern Brazil. *Sedimentary Geology*, **341**:175-188.

Aguiar G.A. 1964. Semi-detalhe da região de sudoeste de Balsas. *Relatório 21BM*, PETROBRÁS, DIREX/RENOR, 40 p.

Aguiar G.A. 1971. Revisão geológica da Bacia Paleozóica do Maranhão. *In*: SBG, 25º Congresso Brasileiro de Geologia. São Paulo, *Anais...*, v. 3, p. 113-122.

Andrade L.S. 2012. *Fácies e estratigrafia da parte superior da Formação Pedra de Fogo, Permiano da Bacia do Parnaíba, região de Filadélfia-TO*. MS Dissertation, Instituto de Geociências, Universidade Federal do Pará, Belém. 87 p.

Andrade L.S., Nogueira A.C.R., Silva Junior J.B.C. 2014. Evolução de um sistema lacustre árido Permiano, parte superior da Formação Pedra de Fogo, borda oeste da Bacia do Parnaíba. *Geologia USP, Série Científica*, **14**:39-60.

Araújo R.N., Nogueira A.C.R., Bandeira J., Angélica R.S. 2016. Shallow lacustrine system of the Permian Pedra de Fogo Formation, Western Gondwana, Parnaíba Basin, Brazil. *Journal of South American Earth Sciences*, **67**:57-70.

Arnot M.J., Good T.R., Lewis J.J.M. 1997. Photogeological and image-analysis techniques for colletcion of large-scale outcrop data: *Journal of Sedimentary Research*, **67**:984-987.

Barbosa E.N., Córdoba V.C., Souza D.C. 2016. Evolução Estratigráfica da Sequência Neocarbonífera-Eotriássica da Bacia do Parnaíba, Brasil. *Brazilian Journal of Geology*, **46**:181-198.

Barbosa O. & Gomes F. de A. 1957. Carvão mineral na Bacia do Tocantins-Araguaia. *Boletim*, Departamento Nacional de Produção Mineral, Divisão Geologia e Mineralogia, p. 1-34.

Benício J.R.W., Spiekermann R., Manfroi J., Uhl D., Pires E.F., Jasper A. 2015. Paleoclimatic inferences based on dendrological patterns of permineralized wood from the Permian of the northern Tocantins Petrified Forest, Parnaíba Basin, Brazil. *Palaeobiodiversity and Palaeoenvironments*, **96**:255-264.

Blakey R.C. 2008. Gondwana paleogeography from assembly to breakup - A 500 m.y. odyssey. In Fielding C.R., Frank T.D. & Isbell, J.L. (eds.) *Resolving the late Paleozoic ice age in time and space*. Geological Society of America, Special Paper, **441**:1-28.

Boucot A.J., Chen X., Scotese C.R., Morley R.J. 2013. *Phanerozoic Paleoclimate: An Atlas of Lithologic Indicators of Climate*. SEPM, Concepts in Sedimentology and Paleontology, **11**, 478 p.

Capretz R.L. 2010. *Paleoecologia e tafonomia da Floresta Petrificada do Tocantins Setentrional (Bacia do Parnaíba, Permiano)*. PhD Thesis, Instituto de Geociências e Ciências Exatas, Universidade Estadual de Paulista, 172 p.

Capretz R.L. & Rohn R. 2013. Lower Permian stems as fluvial paleocurrent indicators of the Parnaíba Basin, northern Brazil. *Journal of South American Earth Sciences*, **45**:69-82.

Caputo M.V., Reis D.E.S., Barata C.F., Pereira, L.C. 2006. Evolução tectônica da Bacia do Parnaíba: qual a influência das orogenias?. *In*: SBG, 6º Simpósio de Geologia da Amazônia, Manaus, *Anais*, 1CD-ROM..

Castro D.L. de, Fuck R.A., Phillips J.D., Vidotti R.M., Bezerra F.H.R., Dantas E.L. 2014. Crustal structure beneath the Paleozoic Parnaíba Basin revealed by airborne gravity and magnetic data, Brazil. *Tectonophysics*, **614**:128-145.

Catuneanu O. 2006. *Principles of sequence stratigraphy*. Elsevier, Amsterdam, 375 p.

Chumakov N.M. & Zharkov M.A. 2002. Climate during Permian–Triassic Biosphere Re-organizations, Article 1: Climate of the Early Permian. *Stratigraphy and Geological Correlation*, **10**:586–602.

Chumakov N.M. & Zharkov M.A. 2003. Climate during the Permian–Triassic Biosphere Reorganizations. Article 2. Climate of the Late Permian and Early Triassic: General Inferences. *Stratigraphy and Geological Correlation*, **11**:361–375.

Cisneros J.C., Abdala F., Rubidge B.S., Dentzien-Dias P.C., Bueno A.O. 2011. Dental Occlusion in a 260-Million-Year-Old Therapsid with Saber Canines from the Permian of Brazil. *Science*, **331:**1603-1605.

Cisneros J.C., Marsicano C., Angielczyk K.D., Smith R.M.H., Richter M., Fröbisch J., Kammerer C.F., Sadleir R.W. 2015. New Permian fauna from tropical Gondwana. *Nature Communications*, **6** , p. 8676.

Coimbra, A.M. & Mussa D. 1984. Associação lignitatoflorística na Formação Pedra de Fogo (Arenito Cacunda), bacia do Maranhão, Piauí, Brasil. *In*: SBG, 33º Congresso Brasileiro de Geologia, Rio de Janeiro, *Anais...*, v. 2, p. 591-605.

Conceição D.M., Andrade L.S., Cisneros J.C., Iannuzzi R., Pereira A.A., Machado F.C. 2016a. New petrified forest in Maranhão, Permian (Cisuralian) of the Parnaíba Basin, Brazil. *Journal of South American Earth Sciences*, **70**:308-323.

Conceição D.M., Cisneros J.C., Iannuzzi R. 2016b. Novo registro de floresta petrificada em Altos, Piauí; relevância e estratégias para geoconservação. *Pesquisas em Geociências*, **43**:311-324.

Cook P.J. 1970. Repeated diagenetic calcitization, phophatization, and silicification in the Phosphoria Formation. *Geological Society of America Bulletin*, **81**:2107-2116.

Cordani U.G., Brito Neves, B.B., Fuck R.A., Porto R., Thomaz Filho A., Cunha, F.M.B., 1984. Estudo preliminar de integração do Pré-Cambriano com os eventos tectônicos das bacias sedimentares brasileiras. *Ciência, Técnica, Petróleo*. Seção Exploração do Petróleo, **15**:20-27.

Courtillot V. & Renne P. 2003. On the ages of flood basalt events. *Comp. Rendus Geoscience*, **335:**113-140.

Cunha F.M.B. 1986. *Evolução paleozóica da Bacia do Parnaíba e seu arcabouço tectônico*. MS Dissertation, Instituto de Geociências, Universidade Federal do Rio de Janeiro, Rio de Janeiro, 107 p.

Day M.O., Ramezani J., Bowring S.A., Sadler P.M., Erwin D.H., Abdala F., Rubidge, B.S. 2015. When and how did the terrestrial mid-Permian mass extinction occur? Evidence from the tetrapod record of the Karoo Basin, South Africa. Royal Society of London, Philosophical Transactions, Series B, Biological Science, **282**:1-8.

Daly M.C., Andrade V., Barousse C.A., Costa R., McDowell K., Piggott N., Poole A.J. 2014. Brasiliano crustal structure and the tectonic setting of the Parnaíba basin of NE Brazil: Results of a deep seismic reflection profile. *Tectonics*, **33**:2102-2120.

Dias-Brito D., Rohn R., Castro J.C., Dias R.R., Röβler R. 2007. Floresta petrificada do Tocantins Setentrional - o mais exuberante e importante registro florístico tropical-subtropical permiano no Hemisfério Sul. *In:* Winge M., Schobbenhaus C., Berbet-Born M., Queiroz E.T., Campos D.A., Souza C.R.G., Fernanes A.C.S. (eds.) *Sítios geológicos e paleontológicos do Brasil*, p.1-16. Disponível em: http://www.unb.br/ig/sigep/sitio104/sitio104.pdf . Acesso em: 04/06/2011.

Dino R., Antonioli L., Braz S.M.N. 2002. Palynological data from the Trisidela member of upper Pedra de Fogo Formation ("Upper Permian") of the Parnaíba Basin, northeastern Brazil. *Revista Brasileira de Paleontologia*, **3**(1): 24-35.

Faria Jr L.E.C. 1979. *Estudo sedimentológico da Formação Pedra de Fogo – Permiano – Bacia do Maranhão*. MS Dissertation, Instituto de Geociências, Universidade Federal do Pará, Belém, 57 p.

Faria Jr. L.E.C. & Truckenbrodt W. 1980a. Estratigrafia e petrografia da Formação Pedra de Fogo – Permiano da Bacia do Maranhão. *In*: SBG, 31º Congresso Brasileiro de Geologia, Balneário Camboriú, *Anais...*, v. 2, p. 740-754.

Faria Jr. L.E.C. & Truckenbrodt W. 1980b. Estromatólitos na Formação Pedra de Fogo, Permiano, Bacia do Maranhão. *In:* SBG, 31º Congresso Brasileiro de Geologia, Balneário Camboriú, *Anais...*, v. 5, p. 3056-3067.

Fernandes Neto S. 2010. Contribuição da Catodoluminescência para o entendimento da Diagênese da Formação Jandaíra: Áreas do Campo de Petróleo da Fazenda Belém e Lajedo do Rosário. MS Dissertation, Centro de Ciências Exatas e da Terra, Universidade Federal do Rio Grande do Norte, 62 p.

Figueiredo A.M.F. & Raja Gabaglia G.P. 1986. Sistema Classificatório Aplicado às Bacias Sedimentares Brasileiras. *Revista Brasileira de Geociências*, **16**:350-369.

Figueroa R.T. & Gallo V. 2017. New chondrichthyan fin spines from the Pedra de Fogo Formation, Brazil. *Journal of South American Earth Sciences*, **76**:389-396.

Flügel E. 2004. *Microfacies analysis of limestones, analysis interpretation and application*. Berlin, Springer-Verlag, 976 p.

Folk R.L. 1974. *Petrology of sedimentary rocks*. Hamphill Publishing Company. Auxtin, TX, 190 p.

Góes A.M.O., Souza J.M.P., Teixeira L.B. 1990. Estágio exploratório e perspectivas petrolíferas da Bacia do Parnaíba. *Boletim de Geociências da Petrobrás*, **4**:55-64.

Góes A.M.O. & Feijó F.J. 1994. Bacia do Parnaíba. *Boletim de Geociências da Petrobrás*, **8**:57-67.

Góes A.M. 1995. A Formação Poti (Carbonífero Inferior) da Bacia do Parnaíba. PhD Thesis, Universidade de São Paulo, 171 p.

Kurzawe F., Iannuzzi R., Merlotti S., Röβler R., Noll R. 2013a. New gymnospermous woods from the Permian of the Parnaíba Basin, Northeastern Brazil, Part I: Ductoabietoxylon, Scleroabietoxylon and Parnaiboxylon. *Review of Palaeobotany and Palynology*, **195**:37-49.

Kurzawe F., Iannuzzi R., Merlotti S., Röβler R. 2013b. New gymnospermous woods from the Permian of the Parnaíba Basin, Northeastern Brazil, Part II: Damudoxylon, Kaokoxylon and Taeniopitys. *Review of Palaeobotany and Palynology*, **195**:50-64.

Kutzbach J.E. & Gallimore R.G. 1989. Pangaean climates: Megamonsoons of the megacontinent. *Journal Geophysical Research*, **94**:3341- 3357.

Lima E.A.M. & Leite J.F. 1978. Projeto estudo global dos recursos Minerais da Bacia Sedimentar do Parnaíba. *Integração geológico-metalogenética, Etapa III*, *Relatório Final* v. 16, 212 p.

Martins R.A. 2000. Fósseis de vegetais da Formação Pedra de Fogo: aspectos taxonômicos, mineralogia e composição química. MS Dissertation, Instituto de Geociências, Universidade Federal do Pará, 92 p.

Matysová P., Rössler R., Götze J., Leichmann J., Forbes G., Taylor E.L., Sakala J., Grygar T. 2010. Alluvial and volcanic pathways to silicified plant stems (Upper Carboniferous-Triassic) and their taphonomic and palaeoenvironmental meaning. *Palaeogeography, Palaeoclimatology, Palaeoecology*, **292**:127-143.

Moore B. 1964. Geological reconnaissance of the southern margin of the Maranhão Basin. *Relatório 216M*, PETROBRÁS, DIREX/RENOR, 46 p.

Neregato R., Röβler R., Iannuzzi R., Noll R., Rohn R. 2017. New petrified calamitaleans from the Permian of the Parnaíba Basin, central-north Brazil, part II, and phytogeographic implications for late Paleozoic floras. *Review of Palaeobotany and Palynology*, **237**:37-61.

Neregato R., Röβler R., Rohn R., Noll R. 2015. New petrified calamitaleans from the Permian of the Parnaíba Basin, central-north Brazil. Part I. *Review of Palaeobotany and Palynology*, **215**:23-45.

Parrish J.T. 1993. Climate of the Supercontinent Pangea. *The Journal of Geology*, **101**:215-233.

Pettijohn F.J. 1975. *Sedimentary rocks*. Harper and Row Publishers, New York, 628 p.

Pinto C.P. & Sad J.H.G. 1986. Revisão da estratigrafia da Formação Pedra de Fogo, borda sudoeste da Bacia do Parnaíba. *In:* SBP, 34º Congresso Brasileiro de Paleontologia, Goiás, *Anais...*, v. 1, p. 346-356.

Playford G. & Dino R. 2000a. Palynostratigraphy of upper Palaeozoic strata (Tapajós Group), Amazonas Basin, Brazil: part one. *Palaeontolographica Abteilung*, **255**:1-46.

Playford G. & Dino R. 2000b. Palynostratigraphy of upper Palaeozoic strata (Tapajós Group), Amazonas Basin, Brazil: part two. *Palaeontolographica Abteilung*, **255**:87-145.

Plummer F.B. 1946. Report on Maranhão and Piauí Geosyncline. *Relatório 1M*, PETROBRÁS, DIREX/RENOR, 83 p.

Price L.I. 1948. Um anfibio labirintodonte da Formação Pedra de Fogo, estado do Maranhão. *Boletim*, Departamento Nacional de Produção Mineral, Divisão Geologia e Mineralogia, **124**:1-32.

Rees P.M., Gibbs M.T., Ziegler A.M., Kutzbach J.E., Behling P.J. 1999. Permian climates; evaluating model predictions using global paleobotanical data. *Geology*, **27**:891-894.

Rees P.M, Ziegler A.M., Gibbs M.T., Kutzbach J.E., Behling P.J., Rowley D.B. 2002. Permian Phytogeographic Patterns and Climate Data/Model Comparisons. *The Journal of Geology,* **110**:1-31.

Rezende W.N. & Pamplona H.R.P. 1970. Estudo do desenvolvimento do Arco Ferrer-Urbano Santos. *Boletim Técnico da Petrobrás*, **13**:5-14.

Röβler R. & Galtier J. 2002a. First Grammatopteris tree ferns from the Southern Hemisphere – new insights in the evolution of the Osmundaceae from the Permian of Brazil. *Review of Palaeobotany and Palynology*, **121**:205-230.

Röβler R. & Galtier J. 2002b. Dernbachia brasiliensis gen. nov. et sp. nov. – a new small tree fern from the Permian of NE Brazil. *Review of Palaeobotany and Palynology*, **122**:239-263.

Röβler R. & Galtier J. 2003. The first evidence of the fern Botryopteris from the Permian of the Southern Hemisphere reflecting growth form diversity. *Review of Palaeobotany and Palynology*, **127**:99-124.

Röβler R. 2006. Two remarkable Permian petrified forests: correlation, comparison and significance. *In:* Lucas S.G., Cassinis G., Schneider J.W. (eds.). *Non-marine Permian biostratigraphy and biochronology*. Geological Society of London, Special Publications, **265**, p. 39-63.

Roscher M., Stordal F., Svensen H. 2011. The effect of global warming and global cooling on the distribution of the latest Permian climate zones. *Palaeogeography, Palaeoclimatology, Palaeoecology,* **309**:186-200.

Santos M.E.C.M. & Carvalho M.S.S. 2009. Paleontologia das Bacias do Parnaíba, São Luís e Grajaú: Reconstituições paleobiológicas. *In:* Serviço Geológico do Brasil, DIEDIG/DEPAT, 215 p.

Santos R.S. 1994. Paleoictiofáunula da Formação Pedra do Fogo, Bacia do Parnaíba, NE do Brasil: II. Eugeneodontida – Agassizodontidae. *Anais da Academia Brasileira de Ciências*, **66**:413-424.

Scotese C.R., Boucot A.J., McKerrow W.S. 1999. Gondwanan palaeogeography and palaeoclimatology. *Journal of African Earth Sciences*, **28**:99-114.

Shanley K.W. & McCabe P.J. 1993. Alluvial architecture in a sequence stratigraphic framework: a case study from the Upper Cretaceous of Southern Utah. U.S.A. *In:* Flint S.S., Bryant I.D. (eds.). *The geological modelling of hydrocarbon reservoirs and outcrop analogues*, International Association of Sedimentologists, **15**, p. 21-55.

Shanley K.W. & McCabe P.J. 1994. Perspectives on the sequence stratigraphy of continental strata. *American Association Petroleum Geological Bulletin*, **78**:544-568.

Schumm S.A. 1993. River response to base level change: implications for sequence stratigraphy. *The Journal of Geology*, **101**:279-294.

Tabor N.J. & Montañez I.P. 2002. Shifts in late Paleozoic atmospheric circulation over western equatorial Pangea: Insights from pedogenic mineral $\delta^{18}O$ compositions. *Geology*, **30**:1127-1130.

Tavares T.M.V., Rohn R., Röβler R., Noll R. 2014. Petrified Marattiales pinnae from the Lower Permian of North-Western Gondwana (Parnaíba Basin, Brazil). *Review of Palaeobotany and Palynology*, **201**:12-28.

Tucker M.E. 2001. *Sedimentary petrology*: an introduction to the origin sedimentary rocks. Oxford, Blackwell Science, 262 p.

Vaz P.T., Resende N.G.A.M., Wanderley Filho J.R., Travassos, W.A. 2007. Bacia do Parnaíba. *Boletim de Geociências Petrobrás*, **15**:253-263.

Walker R.G. 1992. Facies, facies models and modern stratigraphic concepts. *In*: Walker R.G. & James N.P. (eds.). *Facies models*: response to sea level change: St. John's Newfoundland, Geological Association of Canada, p. 1-14.

Witkowski F.W., Blundell D.J., Gutteridge P., Horbury A.D., Oxtoby N.H., Qing H. 2000. Video cathodoluminescence microscopy of diagenetic cements and its applications. *Marine and Petroleum Geology*, **17**:1085-1093.

Zharkov M.A. & Chumakov N.M. 2001. Paleogeography and Sedimentation Settings during Permian-Triassic Reorganizations in Biosphere. *Stratigraphy and Geological Correlation*, **9**:340–363.

UNIVERSIDADE FEDERAL DO PARÁ
INSTITUTO DE GEOCIÊNCIAS
PROGRAMA DE PÓS-GRADUAÇÃO EM GEOLOGIA E GEOQUÍMICA

UNIVERSIDADE FEDERAL DO PARÁ
PROGRAMA DE PÓS-GRADUAÇÃO EM GEOLOGIA E GEOQUÍMICA
TESE APROVADA COM DISTINÇÃO
INSTITUTO DE GEOCIÊNCIAS

PARECER

Sobre a Defesa Pública da Tese de Doutorado de LUIZ SATURNINO DE ANDRADE

A banca examinadora da Tese de Doutorado de **LUIZ SATURNINO DE ANDRADE** orientando do Prof. Dr. Afonso César Rodrigues Nogueira (UFPA), composta pelos professores doutores Ana Maria Goes (USP), Gelson Fambrini (UFPE), Werner Truckenbrodt (UFPA) e José Bandeira Cavalcante da Silva Júnior (UFPA), após apresentação da sua tese intitulada **"PALEOAMBIENTE E PALEOCLIMA DA FORMAÇÃO PEDRA DE FOGO DA BACIA DO PARNAÍBA E SUA CORRELAÇÃO COM OS EVENTOS GLOBAIS DE SILICIFICAÇÃO DO PERMINANO "**, emite o seguinte parecer:

O candidato realizou sua apresentação de forma clara, bem organizada e segura no tempo estipulado. Na arguição mostrou domínio da temática abordada e respondeu às perguntas formuladas pela banca. O trabalho escrito foi apresentado na forma de três artigos, dois internacionais e um nacional, e atende as exigências básicas para uma tese de doutorado.

Destacam-se as contribuições inéditas em relação à estratigrafia de alta resolução e novos dados que discutem a silicificação pervasiva do intervalo Pedra de Fogo.

Pelo exposto, a banca examinadora decidiu por unanimidade aprovar com distinção a tese de doutorado.

Belém, 02 de setembro de 2019.

Prof. Dr. Afonso César Rodrigues Nogueira (Orientador – UFPA)

Prof.ª Dr.ª Ana Maria Góes (USP)

Prof. Dr. Gelson Fambrini (UFPE)

Prof. Dr. Werner Truckenbrodt (UFPA)

Prof. Dr. José Bandeira Cavalcante da Silva Júnior (UFPA)